UNIVERSITY OF SOUTHAMPTON
FACULTY OF PHYSICAL AND APPLIED SCIENCES
SCHOOL OF ELECTRONICS AND COMPUTER SCIENCE

Cross-Layer Aided Routing Design for Ad Hoc Networks

by

Jing Zuo

A thesis submitted in the partial fulfilment of the requirements for the award of Doctor of Philosophy at the University of Southampton

June 2013

SUPERVISOR:
Prof. Lajos Hanzo and Dr. Soon Xin Ng

University of Southampton
Southampton SO17 1BJ
United Kingdom

UNIVERSITY OF SOUTHAMPTON

ABSTRACT

Faculty of Physical and Applied Sciences
School of Electronics and Computer Science

A thesis submitted in the partial fulfilment of the
requirements for the award of Doctor of Philosophy

Cross-Layer Aided Routing Design for Ad Hoc Networks

by Jing Zuo

In this thesis, we propose a series of cross-layer aided routing algorithms for *ad hoc* networks by jointly exploiting the characteristics of the physical layer, of the data link layer and of the network layer, for the sake of improving the network's throughput, while reducing the normalized energy consumption.

Since the node mobility in dynamic self-organizing *ad hoc* networks may render the routing information gathered during the route discovery process invalid and hence may disrupt the current data transmission, a fuzzy logic aided technique is incorporated into the routing algorithm for mitigating the influence of imprecise routing information. Both the expected route life-time and the number of hops are used as the input parameters of the Fuzzy Logic System (FLS), which outputs the 'stability' of a route. Hence, the specific route having the highest route 'stability' is finally selected for data transmission. The proposed fuzzy logic based routing outperforms the conventional Dynamic Source Routing (DSR) in terms of the attainable network throughput.

Moreover, since near-capacity channel coding aided Multiple-Input Multiple-Output (MIMO) schemes allow a single link to communicate using the lowest possible transmit power at a given Frame Error Rate (FER), multi-antenna aided routing was proposed for reducing the system's total energy consumption, which relied on a three-stage concatenated transceiver constituted by an Irregular Convolutional Code, Unity-Rate Code and Space-Time Trellis Code (IrCC-URC-STTC) equipped with two antennas. It is demonstrated that in a high-node-density scenario the average energy consumption per information bit and per node becomes about a factor two lower than that in the equivalent Single-Antenna Relay Nodes(SA-RNs) aided networks.

Finally, we further exploit the benefits of cross-layer information exchange, including the knowledge of the FER in the physical layer, the maximum number of retransmissions in the data link layer and the number of RNs in the network layer. Energy-consumption-based Objective Functions (OF) are invoked for calculating the end-to-end energy consumption of each potentially available route for both Traditional

Routing (TR) and for Opportunistic Routing (OR), respectively. We also improve the TR and the OR with the aid of efficient Power Allocation (PA) for further reducing the energy consumption. Moreover, two energy-efficient routing algorithms are designed based on Dijkstra's algorithm. The algorithms based on the energy-consumption OF provide the theoretical bounds, which are shown to be close to the bound found by exhaustive search, despite the significantly reduced complexity of the former. Finally, the end-to-end throughput and the end-to-end delay of this system are analyzed theoretically. The simulation results show that our energy-efficient OR outperforms the TR and that their theoretical analysis accurately matches the simulation results.

Declaration of Authorship

I, **Jing Zuo**, declare that the thesis entitled **Cross-Layer Aided Routing Design for Ad Hoc Networks** and the work presented in it are my own and has been generated by me as the result of my own original research. I confirm that:

- This work was done wholly or mainly while in candidature for a research degree at this University;
- Where any part of this thesis has previously been submitted for a degree or any other qualification at this University or any other institution, this has been clearly stated;
- Where I have consulted the published work of others, this is always clearly attributed;
- Where I have quoted from the work of others, the source is always given. With the exception of such quotations, this thesis is entirely my own work;
- I have acknowledged all main sources of help;
- Where the thesis is based on work done by myself jointly with others, I have made clear exactly what was done by others and what I have contributed myself;
- Parts of this work have been published.

Signed: .....

Date: .....

Acknowledgements

I would like to express my sincere gratitude to my supervisors, Professor Lajos Hanzo and Dr. Soon Xin Ng (Michael), for their invaluable guidance and inspiration throughout my research. Their utmost kindness and encouragement have greatly benefited me not only in work but also in life. Most importantly, I would like to thank them for their invaluable friendship.

Many thanks also to my colleagues and the staff of the Communications Group, both past and present, for their support, help and discussions throughout my research. Special thanks to my colleagues Prof. Lie-Liang Yang, Chen Dong and Hung Viet Nguyen for their technical support and collaborative work. I also appreciate the friendship and help from Mr. and Mrs. Robson, the former and present housemates and from all other incredible friends, who make my stay in Southampton joyful and colorful.

The financial support of the China-UK Scholarship Council and of the EU under the auspices of the Optimix project is gratefully acknowledged.

Finally, I would like to dedicate this thesis to my parents and my brother, who have provided me with tremendous love, support, understanding and lifelong encouragement.

Contents

List of Publications

Journal papers

1. C. Dong, L-L. Yang, **J. Zuo** and L. Hanzo, "Minimum Average End-to-End Packet Energy Consumption in a Buffer-Aided Three Nodes Networks with Opportunistic Routing", *(*to be submitted).
2. **J. Zuo**, C. Dong, H. V. Nguyen, S. X. Ng, L-L. Yang and L. Hanzo, "Cross-Layer Aided Energy-Efficient Opportunistic Routing in Ad Hoc Networks", *IEEE Transactions on Communications*, (under revision).
3. C. Lamy-Bergot, R. Fracchia, M. Mazzotti, S. Moretti, E. Piri, T. Sutinen, **J. Zuo**, J. Vehkaperä, G. Feher, G. Jeney, G. Panza and P. Amon, "Optimiztion of Multimedia over Wireless IP Links via X-Layer Design: An End-to-End Transmission Chain Simulator", *Multimedia Tools and Applications*, vol. 55, no. 2, pp. 261 - 288, November 2011.

Conference papers

1. **J. Zuo**, S. X. Ng and L. Hanzo, "Fuzzy Logic Aided Dynamic Source Routing in Cross-Layer Operation Assisted Ad Hoc Networks", in *Proceedings of the IEEE 72nd Vehicular Technology Conference Fall (VTC2010-Fall)*, Ottawa, Canada, 6-9 September 2010.
2. **J. Zuo**, H. V. Nguyen, S. X. Ng and L. Hanzo, "Energy-Efficient Relay Aided Ad Hoc Networks Using Iteratively Detected Irregular Convolutional Coded, Unity-Rate Coded and Space-Time Trellis Coded Transceivers", in *Proceedings of the 2011 IEEE Wireless Communications and Networking Conference (WCNC)*, Quintana-Roo, Mexico, 28-31 March 2011.
3. **J. Zuo**, C. Dong, S. X. Ng, L-L. Yang and L. Hanzo, "Energy-Efficient Routing in Ad Hoc Networks Relying on Channel State Information and Limited MAC Retransmissions", in *Proceedings of the 2011 IEEE 74th Vehicular Technology Conference (VTC2011-Fall)*, San Francisco, United States, 5-8 September 2011.

List of Symbols

$\underset{\sim}{A}$	The fuzzy set.
c	The speed of light in vacuum.
d	The distance between the transmitter and the receiver.
d_{max}	The transmission range.
d_{SD}	The distance between S and D.
D_{e2e}	The end-to-end delay.
D_f	The delay imposed on a packet's passage through the route, when it is dropped before reaching D.
$D_f(h)$	The delay experienced by a packet, which is dropped during the h-th hop.
$D_m(n_r)$	The delay experienced by a packet that is successfully delivered from S to R_m after $n_r - 1$ transmission attempts.
D_s	The delay required for delivering a packet successfully from S to D.
D_{total}	The total delay experienced by all data packets.
D_{R_mD}	The delay of a packet traversing from R_m to D.
E	The unit of energy dissipated by a packet in a single transmission attempt.
E_i	The energy dissipated by a packet in a single transmit attempt during the i-th hop.
E_f	The energy consumed by packet that is dropped before reaching D.
$E_f(h)$	The energy consumed by a packet that is dropped during the h-th hop.
$E_m(n_r)$	The energy dissipated by a packet which is successfully delivered from S to R_m after $n_r - 1$ transmission attempts.
E_s	The energy consumed by a packet which is successfully delivered from S to D.
E_{total}	The total energy consumed by all data packets.

$\overline{E}_{total}$	The total energy consumption, which is normalized by the end-to-end successful reception ratio.
$E_{R_m D}$	The total energy consumed by a packet transmitting from R_m to D.
f	The carrier frequency.
FER_i	The frame error ratio during the i-th hop.
h_c	The channel coefficient.
h_{nor}	The number of hops in a route which is normalized by the maximum number of hops allowed in a network.
H	The number of hops in an established route.
$\mathbf{H}$	The matrix of Channel Impulse Responses (CIRs).
l_{ij}	The life-time of link $i-j$.
L	The frame length.
M_l	The number of modulation level.
M	The number of relays.
n_r	The number of MAC retransmissions.
n_{MA}	The number of MA-Relays.
N	The total number of nodes in the network.
N_0	The thermal noise power spectral density.
N_d	The dimension of an additive noise vector.
N_r	The maximum number of MAC retransmissions, including the first transmission attempt.
p_i	The probability of a packet which is successfully delivered during the i-th hop.
p_f	The probability of a packet which is dropped before reaching D.
$p_f(h)$	The probability of a packet which is dropped during the h-th hop.
$p_m(n_r)$	The probability of a packet which is successfully delivered from S to R_m after $n_r - 1$ transmission attempts.
p_s	The probability of a packet which is successfully delivered from S to D.
$p_s(\tau)$	The probability of a packet which is successfully delivered all the way from S to D after a time duration of τ.
p_t	The life-time of an established route.
$p_{R_m D}$	The probability of a packet which is successfully delivered from R_m to D.
p_{SR_m}	The probability of a packet which is successfully delivered from S to R_m.
P_t	The transmit power.
P_{t_i}	The transmit power of the i-th node.

P_r	The Receive power.
P_r^*	The required minimum receive power.
R_{e2e}	The end-to-end throughput.
R_c	The code rate.
R_x	The number of receive antennas.
SNR_{dB}^*	The required minimum signal-to-noise ratio.
SNR_r	The receive SNR.
T	The time slot of a single transmission attempt across a given link.
T_x	The number of transmit antennas.
v	The node velocity.
v_{max}	The maximum mobile speed.
z^*	The output value after the defuzzification process.
γ	The channel SNR.
ζ	The probability of a packet which could not reach any relay after S does a single transmission attempt.
θ	The mobile direction.
λ	The carrier's wavelength.
$\mu_{\underset{\sim}{A}}(x)$	The membership value of the element x in the fuzzy set $\underset{\sim}{A}$.
ρ	The node density.

Chapter 1

Introduction

Since the commencement of the Defense Advanced Research Projects Agency (DARPA) project [1] developed by the American Defense Department in the 1970s, *ad hoc* networks have been widely applied in scenarios, including military applications, crisis response, medical care, conference meetings and space exploration. During the past few decades, *ad hoc* networks attracted substantial research attention as a benefit of their prompt set-up and their ability to self-organize their noncentrally-controlled dynamic topology. Each node of an *ad hoc* network plays the dual role of being both a terminal and a router under the assumption that not all nodes can directly communicate with each other [2]. Figure 1.1 and Figure 1.2 show the difference between the classic infrastructure based network and *ad hoc* network. Figure 1.1 shows that the nodes A, B and C communicate with each other under the control of Base Station (BS) 1 and that A communicates with E via BS 1 and BS 2. However, Figure 1.2 shows that A can only communicate with E by relying on B, C and D as its Relay Nodes (RNs). Each node has to discover its own neighbor list.

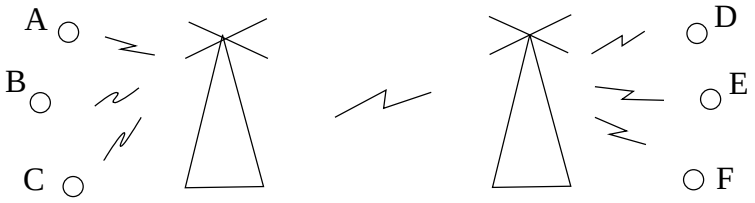

Figure 1.1: The infrastructure network.

The characteristics of *ad hoc* networks impose a number of open problems, which constitute challenges for the protocol design. For example, the scalability, the energy-efficiency, the Quality of Service (QoS) and the security are challenging problems to be solved and to be further improved. The problem of energy-efficiency also has to be considered. Hence the emphasis is on the design of routing protocols relying on

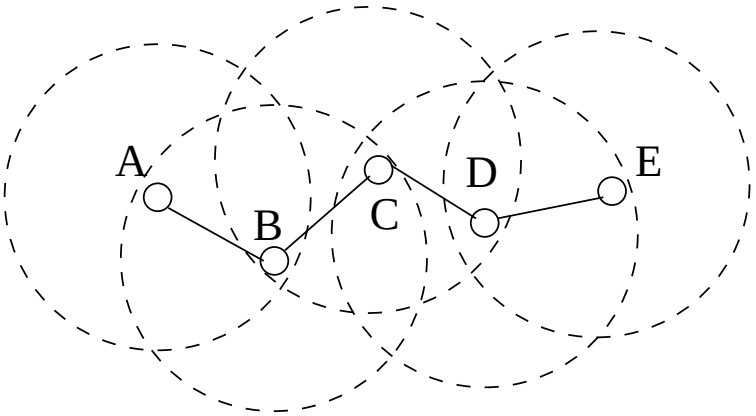

Figure 1.2: *Ad hoc* network.

cross-layer interaction for improving the attainable system performance, such as the normalized energy consumption, the end-to-end throughput and the end-to-end delay.

The organization of this chapter is as follows. Section 1.1 highlights the key techniques employed in the independent layers of the Open System Interconnection (OSI) Reference Model and introduces the general methods of cross-layer optimization, detailing their advantages and disadvantages compared to the conventional system operating without cross-layer interaction. Section 1.2 describes the classification of routing protocols employed in *ad hoc* networks and emphasizes the history of energy-efficient routing protocols. Section 1.3 introduces the channel models, as well as the coding and modulation schemes employed. Section 1.4 introduces the OMNeT++ simulator. Finally, Section 1.5 details the organization of this thesis and lists its novel contributions.

1.1 Cross-Layer Optimization

The International Standards Organization (ISO) created the SubCommittee 16 (SC16) in 1977 for developing an architecture, which could serve as a framework for the definition of standard protocols. At the end of 1979, the Reference Model of OSI was adopted by the parent of SC16, namely, Technical Committee (TC97). The OSI Reference Model was also recognized by the International Telegraph and Telephone Consultative Committee (CCITT) Rappporteur's Group on Public Data Network Services. The OSI Reference Model consists of seven layers, which are the physical layer, the data link layer, the network layer, the transport layer, the session layer, the presentation layer and the application layer. The benefit of this layering technique is to group the similar communication functions into these logical layers. A layer has to cooperate with the layer above it and the layer below it. However, when the Transmission Control Protocol (TCP) of the transport layer and the Internet Protocol

(IP) of the network layer were defined, the five-layer model (TCP/IP model) became the dominant one. More explicitly, the TCP/IP model consists of the application layer, the transport layer, the network layer, the data link layer and the physical layer [3–6]. Figure 1.3 illustrates the structure of the TCP/IP model and the main functions of each layer. The functions of these layers are briefly highlighted below:

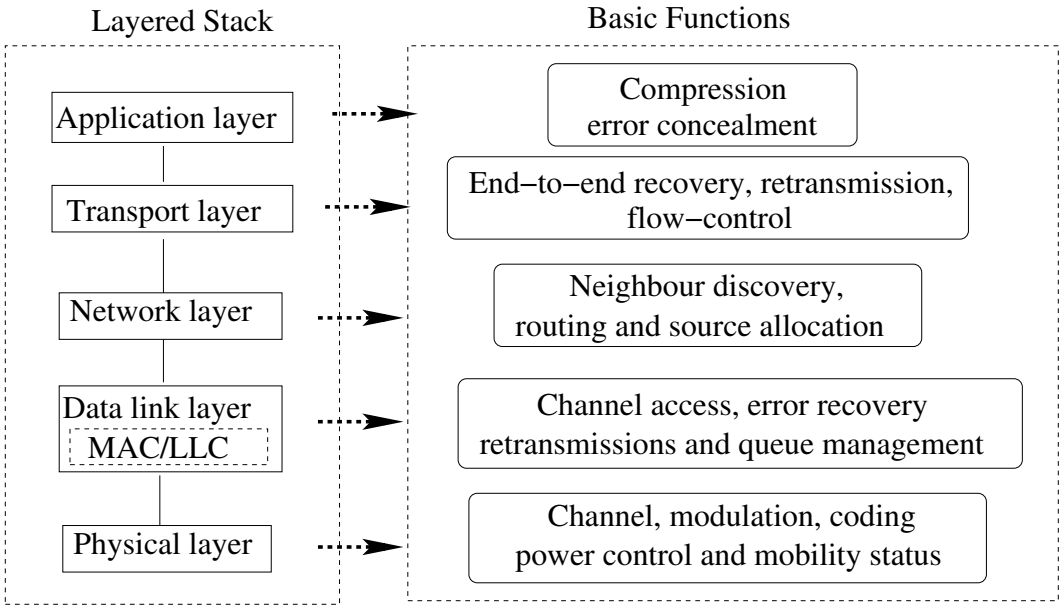

Figure 1.3: Layered stack and the main functions in each layer.

- **The physical layer**: The physical layer concentrates on both the physical devices and on the transmission media. Providing a diversity and/or multiplexing gain with the aid of multiple antennas is capable of improving the integrity and/or throughput of data transmission. Additionally, the adjustment of the transmit power, the design of the coding and modulation schemes as well as the effects of mobility and/or propagation effects constitute important design factors of the physical layer.
- **The data link layer**: The data link layer of Figure 1.3 is concerned with the media access, the error recovery, the retransmission and the queue management functions. It consists of two sub-layers, namely the Media Access Control (MAC) sublayer and the Logical Link Control (LLC) sublayer. In *ad hoc* networks, the MAC sublayer is responsible for the contention and channel allocation, including the random access functions. Carrier Sense Multiple Access combined with Collision Avoidance (CSMA/CA) constitutes one of the most commonly used MAC solutions in wireless networks. The transmission of a Request To Send (RTS) packet by the source and a Clear To Send (CTS) packet issued in response to it by the receiver, as proposed in the IEEE 802.11 RTS/CTS standard [7],

assists in eliminating the hidden and exposed terminal problems of conventional CSMA/CA. The LLC sublayer is above the MAC layer but under the network layer, acting as an interface between them and it is responsible for both the flow control and Automatic Repeat Request (ARQ) functions. The ARQ schemes assists in reducing the Packet Loss Ratio (PLR) by retransmitting the error-infested packets. The LLC sublayer of Figure 1.3 also provides both multiplexing mechanisms and queueing management, which assist in rendering the different network protocols compatible with each other. In recent years most functions of the LLC sublayer were assumed by the MAC layer. Therefore the MAC layer is used for representing the second layer of the five-layer TCP/IP model of Figure 1.3 in the rest of this thesis.

- **The network layer**: The network layer is responsible for the neighbor discovery, routing and resource allocation functions. Neighbor discovery is activated, when a node first joins a network for the sake of identifying the nodes, which are only a single hop away. Routing is the main function of the network layer, guiding a packet through the network from a source to the destination. The Internet Protocol version 4 (IPv4) [8] and the Internet Protocol version 6 (IPv6) [9] are widely used IP protocols, which attach both source and destination addresses to the logical message. Numerous routing protocols have been designed based on the IP protocol for satisfying the requirements of wireless *ad hoc* networks. Moreover, due to the coexistence of multiple source-destination pairs, multi-path routing and multicast routing may have to be employed for satisfying the fairness requirements during resource allocation, such as power- and bandwidth-allocation. The protocol design conceived for the network layer fundamentally predetermines the attainable performance in terms of the PLR, the end-to-end delay and the network's throughput.
- **The transport layer**: The transport layer is responsible for flow control, congestion control, error recovery, packet reordering and for the end-to-end connection setup. It assists the application layer of Figure 1.3 in allocating/mapping the flows to different routes, which are found in the network layer. It also assists by monitoring the end-to-end data transmission and in avoiding network congestion. Since the data packets may be transmitted via different routes and hence may experience different delays, the transport layer assumes responsibility for appropriately ordering the packets that arrived at the destination. Although the TCP [10] performs well in wired networks in terms of guaranteeing the reliability of end-to-end data transmission, it becomes inefficient in wireless *ad hoc* networks, since packets may be lost owing to hostile channel-effects and

node mobility. Hence, the User Datagram Protocol (UDP) [11] is widely used, because it does not rely on retransmissions from the source, therefore reducing the unnecessary waste of communications resources.

- **The application layer**: The application layer constitutes the interface to the end user in the TCP/IP model of Figure 1.3. By considering the requirements of the end user, it divides the user services into different categories, such as for example, real-time and non-real-time services, continuous and intermittent services, Constant Bit Rate (CBR) and Variable Bit Rate (VBR) multimedia services, etc. Most services require a certain guaranteed QoS, such as a certain maximum end-to-end delay, or end-to-end throughput and PLR, which has to be taken into consideration in this layer. Moreover, data compression is another important function of the application layer, which reduces the burden imposed on the network, but increases the packets' sensitivity to errors. These QoS metrics may be employed for characterizing the system's performance. The end-to-end delay, the delay jitter and Peak Signal-to-Noise Ratio (PSNR) are used for evaluating the performance of real-time services, such as voice, video and image applications. By contrast, the PLR and the end-to-end throughput are used for evaluating non-real-time services, such as file transfer [12].

Again, although the layered architecture has its own advantages and performs well in wired networks in terms of portability, flexibility and low design complexity, it is not suitable for wireless networks, especially in wireless *ad hoc* networks. The reason for its inadequacy in wireless scenarios is that the services offered by the layers to those above them in Figure 1.3 are realized by specifically tailored protocols for the different layers and that the architecture forbids direct communication between non-adjacent layers. The communication between adjacent layers is limited to procedure calls and to their responses. Moreover, the hostile wireless links impose several new problems on the associated protocol design that cannot be readily handled by the layered architecture [13]. More explicitly, having a strict layered design is not flexible enough to cope with the dynamics of Mobile *Ad hoc* NETwork (MANET) environments and will thus result in a low performance [14]. Thus, the mutual impact of the layers on each other cannot be ignored [15]. Hence the concept of cross-layer optimization has been proposed in an attempt to achieve a performance gain by exploiting the close interaction amongst the different layers. Srivastava and Motani [13] defined "Cross-Layer operation" as: "Protocol design by the violation of a reference layered communication architecture is cross-layer design with respect to the particular layered architecture", while R. Jurdak [15] define it as: "Cross-layer design with respect to a reference layered architecture is the design of algorithms,

protocols, or architectures that exploit or provide a set of inter-layer interactions that is a superset of the standard interfaces provided by the reference layered architecture". Therefore, cross-layer operation may be interpreted as the 'violation' of the layered architecture seen in Figure 1.3, which requires more interaction amongst the layers, beyond the interaction between the adjacent layers. Cross-layer design clearly requires information exchange between layers, as well as adaptivity to this information at each layer and a certain grade of diversity built into each layer for the sake of improving the achievable robustness [5].

There are two basic methods of information sharing in cross-layer design. One of them makes the variables of a specific layer visible to the other layers, which is referred to as a layer-centric solution [16]. The other relies on a shared middleware, which provides the service of storage/retrieval of information to all layers, which is termed as a centralized solution [16]. Figure 1.4 illustrates how these two cross-layer solutions operate.

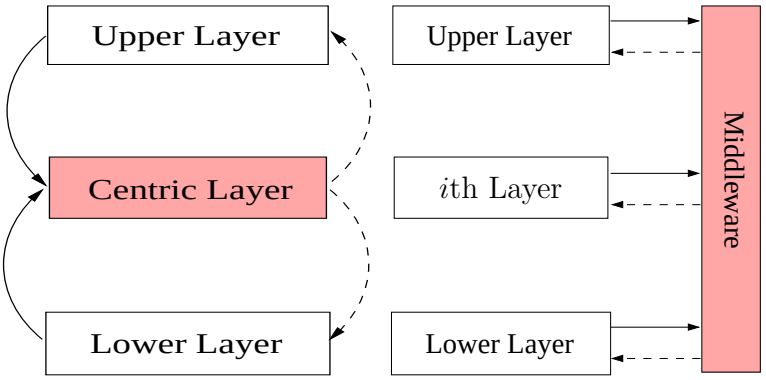

(a) Layer-centric solution (b) Centralized solution

Figure 1.4: Conceptual illustration of cross-layer optimization methods.

The basic principles of the above-mentioned pair of cross-layer solutions [16] are:

- **The layer-centric solution**: A certain layer is allowed to be the central layer, which controls the cross-layer adaptation by accessing the internal protocol parameters and algorithms of the other layers, as shown in Figure 1.4(a). Although this approach significantly improves the attainable system performance, it violates the layered architecture, since it requires access to the internal variables of other layers.
- **The centralized solution**: A middleware or a system-level monitor (centralized optimizer) is employed for estimating both the availability of resources and the environmental dynamics, for the sake of coordinating the allocation of resources across diverse applications as well as nodes, and for adapting the protocols' parameters within each layer based on the dynamics experienced,

as shown in Figure 1.4(b). This approach requires each layer to forward the complete information characterizing its protocol parameters and algorithms to the middleware or system monitor. It also requires each layer to carry out the actions requested by the central optimizer. This approach also violates the layered architecture. The so-called MobileMan [14] and CrossTalk [17] protocols constitute important centralized cross-layer solutions.

The cross-layer operation aided design of wireless *ad hoc* networks poses challenges mainly due to the time-variant characteristics of wireless channels. The signal is substantially more vulnerable to the effects of noise, fading and interference than in benign fixed networks, leading to potential performance degradations within the higher layers. For example, a packet has to be retransmitted in the data link layer or the transmit power has to be adjusted to guarantee its high-integrity transmission, which may impose interference on other nodes or promote aggressive contention for channel access. In the network layer, the current route may become invalid and hence route maintenance/repair has to be activated or even a new route discovery process has to be initiated. As a result, potentially more energy is consumed and the end-to-end delay is increased, while the end-to-end throughput is reduced. Therefore, careful adaptation of the protocol stack should be used at each layer in order to compensate for the variations at that layer, depending on the specific time scale of these variations [5]. Both the local adaptation of parameters within each layer and the adaptation based on the other layers have to be considered. For example, the transmit power, the signal processing hardware's power dissipation, the information transmit rate, the coding and modulation schemes, the Frame Error Ratio (FER) and the mobility in the physical layer constitute important parameters, which may be beneficially shared with other layers. The protocol design of the upper layers has to consider the information gleaned from the physical layer for minimizing the energy consumption, the resource allocation, scheduling and the queueing management, while maintaining a certain QoS guarantee. Meanwhile, the number of retransmissions, as well as both the routing and network topology related information received from the upper layers may be beneficially shared. Additionally, node cooperation also calls for cross-layer design [13].

As detailed above, cross-layer design has substantial benefits, but it has its own disadvantages as well. For example, the cross-layer interactions create dependencies amongst the layers, which will affect not only the layer concerned, but also the other layers. Hence, a complete redesign of the operational networks and protocols will lead to a high implementational cost [16]. Therefore, cross-layer design should be carefully crafted, because once the seven-layer OSI structure is violated, the benefits of independent, layer-specific protocol design will disappear [13, 18]. The effects of

any protocol chosen in every single layer on the overall system has to be carefully considered.

This thesis is mainly dedicated to cross-layer operation aided routing design in *ad hoc* networks, hence we list the major contributions to the literature of cross-layer aided routing protocols conceived for *ad hoc* networks in Table 1.1.

1.2 Routing Protocols

The network layer of Figure 1.3 plays a key role in *ad hoc* networks, which substantially influences the performance of the overall system. The network layer is responsible both for allocating IP addresses and for choosing the right route for communication between the source and destination. The routing protocols of *ad hoc* networks may be classified as proactive routing, reactive routing and hybrid routing [37], as shown in Figure 1.5.

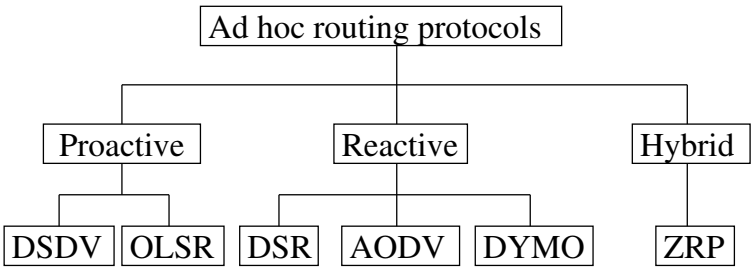

Figure 1.5: Categorization of *ad hoc* routing protocols (DSDV: Destination-Sequenced Distance Vector routing; OLSR: Optimized Link State Routing; DSR: Dynamic Source Routing; AODV: Ad-hoc On-demand Distance Vector routing; DYMO: DYnamic Manet On-demand routing; ZRP: Zone Routing Protocol).

The proactive routing periodically transmits "hello" packets for the sake of identifying all possible routes in the network. Hence every node has to maintain a routing table, which stores the route spanning from itself to all other available nodes. The advantage of this kind of routing protocol is that the route discovery time is low. By contrast, its disadvantage is that each node has to maintain a routing table. If the number of nodes in the network becomes high, then the routing table becomes large and hence requires a large memory. On the other hand, periodically sending "hello" packets increases the network control load imposed. The so-called Destination-Sequenced Distance Vector (DSDV) [38] protocol and the Optimized Link State Routing (OLSR) [39] protocol are typical proactive routing protocols, as seen in Figure 1.5.

The reactive routing protocols are source-driven, implying that they transmit route discovery packets to find a route to the destination, when there is sufficient data scheduled for transmission in the buffer, instead of periodically broadcasting the "hello" packets. As a benefit, not all nodes have to maintain a route table for storing the routes

Table 1.1: Major contributions of cross-layer aided routing protocols in *ad hoc* networks.

Year	Authors	Contribution
2002	Goldsmith [19] and Wicker	Reviewed each layer's protocol and emphasized the necessity of cross-layer design, particularly in energy-limited scenarios.
2005	Souryal *et al.* [20]	Proposed efficient channel-quality-aware adaptive routing relying on adaptive modulation.
	Lee *et al.* [21]	Combined power-aware routing with a MAC layer algorithm for minimizing the total consumed power.
2006	Johansson and Xiao [22]	Jointly optimized the end-to-end communication rates, routing, power allocation and transmission scheduling of a network.
	Mao *et al.* [23]	proposed a Genetic Algorithm (GA)-based application-centric cross-layer approach for minimizing video distortion.
	Abdrabou and Zhuang [24]	Presented a position-aware QoS routing scheme by considering its interactions with the MAC.
	Zhang *et al.* [25]	Addressed the topic of energy-efficient routing subject to both packet delay and multi-access interference constraints.
2007	Kompella *et al.* [26]	Optimized the performance of Multiple Description (MD) video subject to certain routing and link layer constraints.
	Chiang *et al.* [27]	Surveyed the functional modules, such as congestion control, routing, scheduling, random access, power control and channel coding.
2008	Phan *et al.* [28]	Presented a cross-layer optimization approach jointly considering the design of the MAC, routing and energy distribution.
	Liu *et al.* [29]	Jointly optimized the power and bandwidth allocation at each node and designed multihop/multipath routing for a MIMO-based wireless *ad hoc* network.
2009	Abdrabou and Zhuang [30]	Proposed a routing scheme based on a geographical on-demand routing protocol, which is capable of guaranteeing a certain maximum end-to-end delay.
	Li *et al.* [31]	Proposed a combined multi-rate power controlled MAC protocol and routing protocol relying on the effective transport capacity as the routing metric.
2010	Ding *et al.* [32]	Proposed a ROuting and dynamic Spectrum-Allocation (ROSA) algorithm aiming for maximizing the network's throughput by performing joint routing, dynamic spectrum allocation, scheduling and transmit power control.
	Lu *et al.* [33]	Presented Joint Channel Assignment and Cross-layer Routing (JCACR) by employing two metrics, namely the Channel Utilization Percentage (CUP) and the Channel Selection Metric (CSM).
2011	Ding and Leung [34]	Proposed cross-layer routing applying both cooperative transmission and path selection for striking a tradeoff between the transmit power consumption and the end-to-end reliability.
	Tavli and Heinzelman [35]	Presented real-time multicasting based routing
2012	Syue *et al.* [36]	Proposed a Relay-Aware Cooperative Routing (RACR) protocol relying on cross-layer design.

leading to all other nodes. Instead, they only store routes that were found during the process of route discovery. This technique reduces the network control load compared to the proactive routing protocols of Figure 1.5. The disadvantage of this routing protocol family is however that their delay is increased, because a route has to be found to the destination, when no routes leading to the destination exist in the route table. Additionally, the nodes' movement changes the network's topology, which hence requires the transmission of more control packets for the sake of maintaining the current communication session. As seen in Figure 1.5, the Dynamic Source Routing (DSR) [40], Ad-hoc On-demand Distance Vector (AODV) [41] and DYnamic Manet On-demand (DYMO) [42] routing protocols constitute typical reactive routing protocols.

Based on beneficially combining the advantages, whilst avoiding the disadvantages of the above-mentioned protocol families, hybrid routing protocols may also be conceived. We may divide the entire *ad hoc* network into several small areas and in each area proactive routing may be employed for establishing a link for all nodes. By contrast, between the areas, reactive routing protocols may be adopted for reducing the number of control packets required. Hybrid protocols are widely applied in large *ad hoc* networks. The so-called Zone Routing Protocol (ZRP) [43] is a typical hybrid routing protocol.

1.2.1 The Dynamic Source Routing Protocol

The DSR routing protocol [40] is a widely used reactive routing technique, which was proposed in 1996 [40]. It consists of two phases, namely the route discovery and route maintenance, which are implemented with the aid of a series of control packets, such as the Route REQuest (RREQ) packet, the Route REPly (RREP) packet, the Source Route (SR) packet, the Route ERRor (RERR) packet, the ACKnowledgement Request (ACK Req) packet and the ACKnowledgement (ACK) packet. Every data packet carries the description of the entire route, which covers all the hops spanning from the source node to the destination node. The route cache stores multiple alternative routes, which are found during the route discovery process, as seen in Figure 1.6.

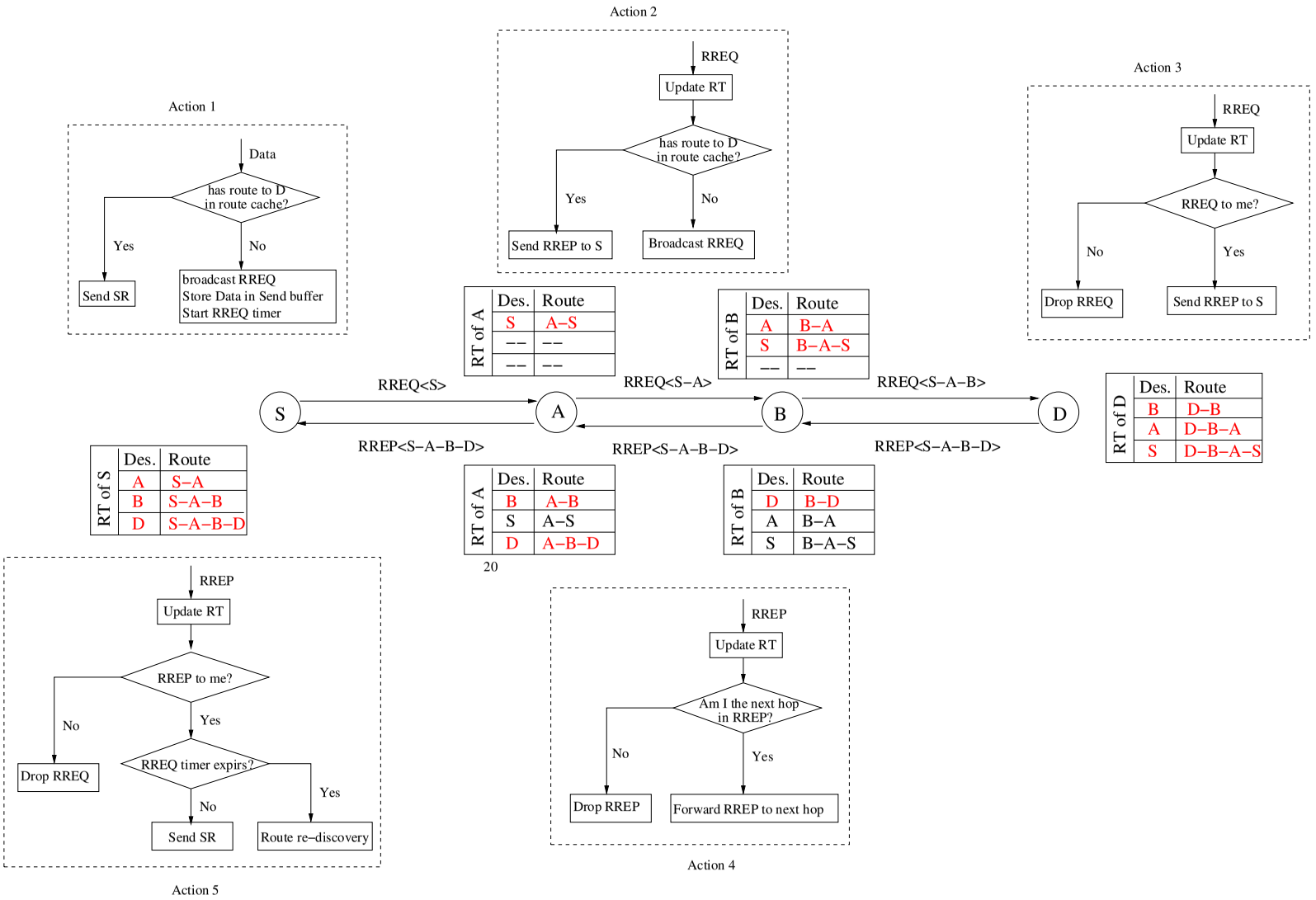

Figure 1.6: The route discovery process of the DSR protocol, including the actions and the routing table update at each node, which receives an RREQ/RREP packet. RT: Routing table; Des.: Destination; RREQ/RREP$\langle m-n-p-q\rangle$: RREQ/RREP packet carries the content of the route from the source m to the current node q via nodes n and p.

- **Route discovery**:
  - As seen in **Action 1** of Figure 1.6, when a data packet of the upper layers has to be transmitted to a certain destination D, it will first check the route cache of this specific node to ascertain as to whether a route leading to the desired destination D exists. If a route exists, then a SR packet is created, which consists of the data packet and the SR header. The SR packet carries the description of the entire route spanning from the source S to the destination D. If no route exists, then an RREQ packet is broadcast in order to find a route to the destination D. Meanwhile, the data is stored in the Send buffer and an RREQ timer is set, waiting for a route to be found.
  - Every time when an RREQ packet arrives at a node, such as nodes A or B of Figure 1.6, it triggers **Action 2**. More explicitly, it first checks, whether a cached route is available. If a cached route leading to the destination D exists, this node would immediately send back an RREP packet, otherwise it would broadcast the RREQ packet again, until it arrives at the destination D. The RREQ records the IP address of each node it traverses through, as exemplified by $RREQ\langle S-A\rangle$ or $RREQ\langle S-A-B\rangle$ in Figure 1.6. Meanwhile, the routing tables are updated. For example, node B updates its routing table by adding the following two route entries $B-A$ and $B-A-S$, as seen in Figure 1.6.
  - Finally, the destination becomes aware of the entire route $D-B-A-S$ after receiving the RREQ packet and copies the description of the entire route $D-B-A-S$ to an RREP packet. The RREP carrying the route entry $S-A-B-D$ is then sent back to the source S according to the route discovered, as seen in **Action 3** of Figure 1.6.
  - Whenever a node receives an RREQ (or RREP) packet, it extracts the route from the RREQ (or RREP) packet and stores it in its own route cache for its future use, as shown in **Action 2** - **Action 5** of Figure 1.6. At the same time, the node will search through the transmit buffer to check, if there is any data waiting to be transmitted to the destination. It there is, the data will be encapsulated in the SR packet and will be transmitted at once, as shown in **Action 5** of Figure 1.6. Several routes may be discovered during the same route discovery process. It is the source's responsibility to find the best route for transmitting the data.

- **Route maintenance**: For the sake of avoiding digressions, the process of route maintenance is not portrayed here, since we do not need these intricate details in the following chapters.
  - Once the source found the specific route, which has the lowest number of hops, a SR packet is created for signalling the description of the route as parts of its header.
  - Only those nodes that appear in the above-mentioned route would forward the SR packet, until it arrives at the destination.
  - For each pair of nodes, the SR packet requires an ACK Req packet and an ACK packet for confirming whether the link is available at that moment. Once the link is confirmed to be available, it will no longer require re-confirmation for a certain period of time. If the related timer expires without receiving an ACK packet after sending an ACK Req packet, then the transmit node of the link would regard this link as broken.
  - The data packet may be salvaged by the transmit node of this link, if the transmit node contains a valid and unexpired route in its route cache. Otherwise, an RERR packet is transmitted in order to inform the source of the broken link.
  - After receiving the RERR packet, the source node will choose another redundant route for sending the following packets, provided of course that a redundant route does exist in its route cache. If both the salvage and the route changing actions fail, a new route discovery process will be activated.
  - Every node that receives the RERR packet would check its own route cache and would consequently delete any route, which includes this broken link. The route cache is updated, whenever the node receives an RREQ, RREP, SR, ACK Req, ACK and RERR packet.

The DSR routing protocol has several beneficial features.

- Firstly, the route cache is updated dynamically, whenever the node receives or overhears an RREQ, RREP, SR, ACK and RERR packet, which keeps the contents of the route cache fresh, whilst mitigating the route control load potentially required for maintaining the route cache contents up-to-date.
- The second is that multiple routes are found during a single route discovery process, which reduces the end-to-end delay by immediately replacing an invalid route by a redundant route from the route cache.
- Thirdly, the complexity of the route selection is mitigated in the intermediate nodes, because the entire description of the route is carried in every data packet and the routing decision is made at the source node.

- Finally, the RERR packet may be superimposed on other types of packets, such as the SR packet, for the sake of informing as many as possible of the nodes, as to when these other types of packets are transmitted through the network. If any node, which receives the RERR packet stores an invalid link in its routing table, it will delete this broken link immediately. Hence the specific route, which includes this invalid link, must not be employed for future data transmission.

Naturally, DSR also has its own disadvantages.

- The multiple routes stored in the route cache would result in a high probability of employing some of the invalid routes, which results in reducing the end-to-end throughput, because a new route discovery process is only activated after all the routes in the route cache became invalid.
- Meanwhile, the route description carried by each data packet makes the routing decisions inflexible in the sense that they cannot be adjusted by the intermediate nodes based on the near-instantaneous availability of the route.

1.2.2 The Dynamic Manet On-demand Routing Protocol

The DYMO routing protocol [42] combines the benefits of both the AODV routing protocol [41] and of the DSR protocol [40], because it exploits the idea of the dynamic source routing inherited from the DSR protocol and the concept of using a routing table from the AODV protocol. It inherits the traditional routing table, which only records the destination identifier, the number of hops and the address of the next hop, while recording the routes only when required. The DYMO routing protocol is constituted by two main stages, namely the route discovery and route maintenance. During the route discovery, the RREQ and RREP packets are used for identifying a route spanning from the source to the destination, as seen in Figure 1.7. By contrast, during the route maintenance phase, an RERR packet is returned to the source, when a broken link is detected.

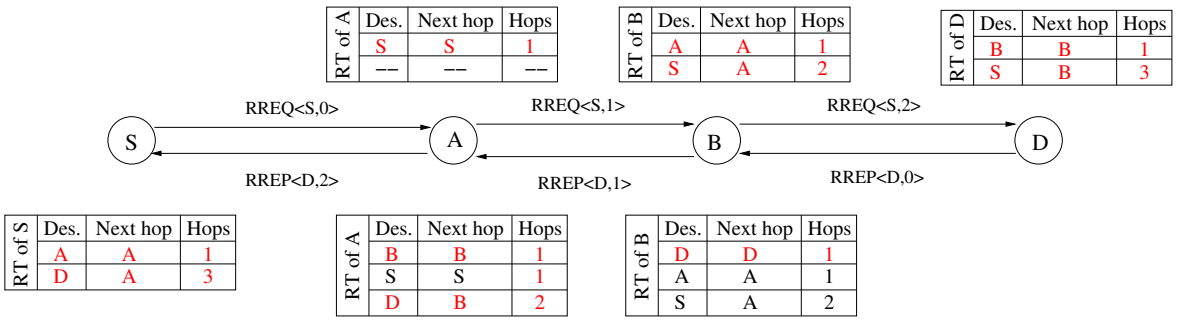

Figure 1.7: The route discovery process of DYMO protocol, including the routing table update at each node, which receives an RREQ/RREP packet. RT: Routing table; Des.: Destination; RREQ/RREP$\langle m, n\rangle$: RREQ/RREP packet carries the contents of its source address m and the distance n to the source m.

- **Route discovery**: The actions of this route discovery process are not plotted in Figure 1.7, because they are similar to those seen in Figure 1.6. Figure 1.7 draws our attention more to the routing table update, which is different from that of the DSR protocol.
  - When the source node S fails to find a route in the routing table leading to a certain destination D for transmitting a packet to D, the route discovery process is initiated. An RREQ packet is broadcast from the source node S and it is forwarded by other nodes, such as nodes A and B of Figure 1.7, until it arrives at the destination D or at an intermediate node, which has a valid route to the destination D and has the most fresh destination sequence number. The DYMO sequence numbers allow DYMO routers to judge the freshness of routing information and to avoid having loops in the route with the aid of the broadcast ID and the source's IP address. By contrast, DSR does not rely on this sequence number.
  - Then the destination D or an intermediate node, which has a cached route to the destination D, would respond by sending back an RREP packet to the source S, as shown in Figure 1.7.
  - At every node, the information of the reverse route leading to the source S is recorded in the RREQ packet, including the destination and the number of hops, when receiving an RREQ packet. Meanwhile, its routing table is updated by storing the destination (the source of the received RREQ packet), the next hop (the transmit node of the received RREQ packet) and the number of hops. For example in Figure 1.7, the RREQ packet arrives at node B from A, it carries the content of $RREQ\langle S, 1\rangle$, which tells the node B that a route leading to the source S via node A exists and the number of hops is 2. Hence, node B immediately updates its routing table by adding two route entries, which are: 1 hop to node A and 2 hops from the source S via A. Similarly, the forward route traversing through the nodes all the way to the destination is recorded, when receiving an RREP packet, which assists these intermediate nodes in learning the routes leading to the other nodes, instead of requiring explicit route discovery to find the specific routes leading to other nodes, as seen in Figure 1.7. After node B receives an RREP packet, it learns a new route, which is added into its routing table, indicating that it requires 1 hop to the destination D.
  - Finally, the source S obtains a route leading to the destination D after the RREP arrives at S. Hence the data packet is transmitted according to the

address of the next hop by checking the routing table on a hop-by-hop basis, which is different from the DSR packet.

- **Route maintenance**: The details of the route maintenance process will be portrayed in Figure 3.6, where we will critically appraise its similarities and dissimilarities with regard to the following methods may be employed at every node for maintaining specific link.
  - According to the first method, the node detects the availability of a link by receiving a packet transmitted by the next hop in the route.
  - The second one is that the network layer is informed of the link's failure by the link layer, when the number of retransmissions reaches its maximum value.
  - If a broken link is encountered, the transmission of an unsolicited RREP packet is activated by a node further 'up-stream' in the route to notify its predecessor nodes. The predecessor nodes will notify their own predecessor nodes, etc. All of them should erase the broken link from their routing tables. Then the source node would re-initialize the route discovery process.

The advantages of the DYMO routing protocol are as follows.

- The employment of the traditional routing table does not require the data transmission session to carry the description of the entire route spanning from the source node to the destination node. This is in contrast to the DSR protocol and it has the benefit of eliminating the potential overhead imposed by the packet header;
- In contrast to the DSR protocol, the periodic broadcast of the "hello" message updates the routing table frequently;

However, the DYMO routing protocol also has its own disadvantages.

- Only a single route is stored in the routing table for the destination node. This feature constitutes a disadvantage, because it is likely to increase the end-to-end delay and to decrease the end-to-end throughput due to the potential route re-discovery required in case of broken links. By contrast, redundant routes may exist in the DSR protocol.

1.3 Channel Model and Lookup Tables

The physical layer is located at the bottom of the OSI stack seen in Figure 1.3. Because of the time-varying and error-prone nature of the wireless channel, the Bit Error Ratio (BER) of wireless links is significantly higher than that of wired links. The potential node mobility in *ad hoc* networks further degrades the quality of the link. When the distance between a pair of mobile nodes changes, the communication session may be

aborted. Furthermore, the communication between a pair of nodes potentially imposes interference on the other nodes' communication. For the sake of guaranteeing the communication quality required, powerful modulation and coding schemes have been developed for diverse channel conditions. The BER and FER constitute a pair of important metrics characterizing the performance of the physical layer.

1.3.1 Channel Model

In wireless networks the information-bearing signal is radiated with the aid of an antenna [44], which is attenuated by the path-loss, shadow fading and Rayleigh fading as well as contaminated by the Additive White Gaussian Noise (AWGN). The co-channel interference is another factor contaminating the received signal, which is caused by the communication of other users in the same frequency-band.

- **Free-space path loss** [5]: The radio signal propagates along a straight line between the transmitter and receiver in the absence of obstacles between them, which is referred to as a Line-Of-Sight (LOS) channel. Assuming that the transmit power is P_t, the power P_r received at the receiver may be calculated as:

$$P_r = P_t \cdot \left(\frac{\sqrt{G_l} \cdot \lambda}{4 \cdot \pi \cdot d} \right)^2, \tag{1.1}$$

  where G_l is the product of the transmit and receive antenna gains in the LOS direction, λ is the carrier's wavelength and d is the distance between the transmitter and receiver.
- **Shadow fading**: Shadowing is usually caused by blocking objects in the signal's path, which results in random variations of the received power. Shadowing is related to the reflecting surfaces and scattering objects. Usually a statistical model is required for characterizing the shadowing model because of the unknown location and size of the reflecting surfaces and scattering objects.
- **Rayleigh fading**: Multipath propagation is encountered, when the radio signal is transmitted through multiple different-length paths. The resultant delay spread characterizes the delay between the last and first propagation path. If the delay spread is lower than the reciprocal of the signal's bandwidth, then the influence of the delay spread on the received signal remains modest.

1.3.2 BER/FER vs. SNR Lookup Tables

In order to avoid time-consuming bit-by-bit Monte-Carlo simulations in the physical layer, we characterize it with the aid of the system's BER/FER vs. Signal-to-Noise Ratio (SNR) lookup table. The format of a Turbo Trellis-Coded Modulation (TTCM)

Table 1.2: The format of the lookup table.

E_bN_0(dB)	SNR(dB)	BER	FER	Data Length (bits)
-5.00	-1.99	3.13×10^{-1}	1	100
-4.50	-1.49	3.01×10^{-1}	1	100
...	...	...	...	...
8.50	11.51	2.00×10^{-7}	1.00×10^{-5}	100
9.00	12.01	0	0	100
9.50	12.51	0	0	100
-5.00	-1.99	3.11×10^{-1}	1	200
-4.50	-1.49	3.01×10^{-1}	1	200
...	...	...	...	...
9.00	12.01	0	0	200
9.50	12.51	0	0	200
...	...	...	...	...

based 8 Phase-Shift Keying (8PSK) lookup table is exemplified in Table 1.2, which lists the BER and FER versus the Energy per bit to Noise power spectral density ratio (E_b/N_0) at the receiver. Whenever a node receives a packet at a specific channel condition, based on its receive SNR and the length of that packet, the related BER and FER may be found in the lookup table. Finally, these BER and FER values may be used for informing the upper layers of the physical layer's performance.

1.4 OMNeT++ Simulator

OMNeT++ is a modular, component-based C++ simulation library, relying on an Eclipse-based Integrated Development Environment (IDE) and a graphical runtime environment [45]. It has been publicly available since 1997. Domain-specific functionalities capable of supporting the simulation of communication networks, queuing networks, etc. are provided, which were developed by independent projects [13]. OMNeT++ may be operated under Linux, Mac OS/X or Windows systems, employing the GNU C Compiler (GCC) tool chain or the Microsoft Visual C++ compiler. Apart from academic research groups and individuals, numerous companies, such as IBM, Intel, Cisco, Thales and Broadcom also applied OMNeT++ successfully in commercial projects or in-house research [45].

OMNeT++ was designed for supporting large-scale network simulations. The adjacent modules communicate with each other by messages. The attributes of the modules are described by parameters, which are initialized in the so-called NEtwork Description (NED) file or the configuration file. The NED language is a special language defined in OMNeT++, which may describe the network topology. The OMNeT++ simulation model may be run either under a graphical interface or under

command-line control, by editing a configuration file. Scalar and vector results may be gathered and analyzed.

As mentioned above, the cross-layer design relies on the information shared among several OSI layers. OMNeT++ provides the functionalities of the so-called 'direct method calls between modules' and the 'NotificationBoard' for its information exchange [46].

1.5 Thesis Outline and Novel Contributions

1.5.1 Outline of the Thesis

Simultaneous energy efficiency and throughput maximization may be achieved by improving the procedures within a single OSI layer. However, as described in Section 1.1, cross-layer optimization is capable of providing substantial further benefits. Therefore, several cross-layer optimized routing protocols are proposed in this thesis for reducing the energy consumption, for improving the throughput and for striking a flexible tradeoff between them. Let us now highlight the outline of this thesis, which is portrayed in Figure 1.8.

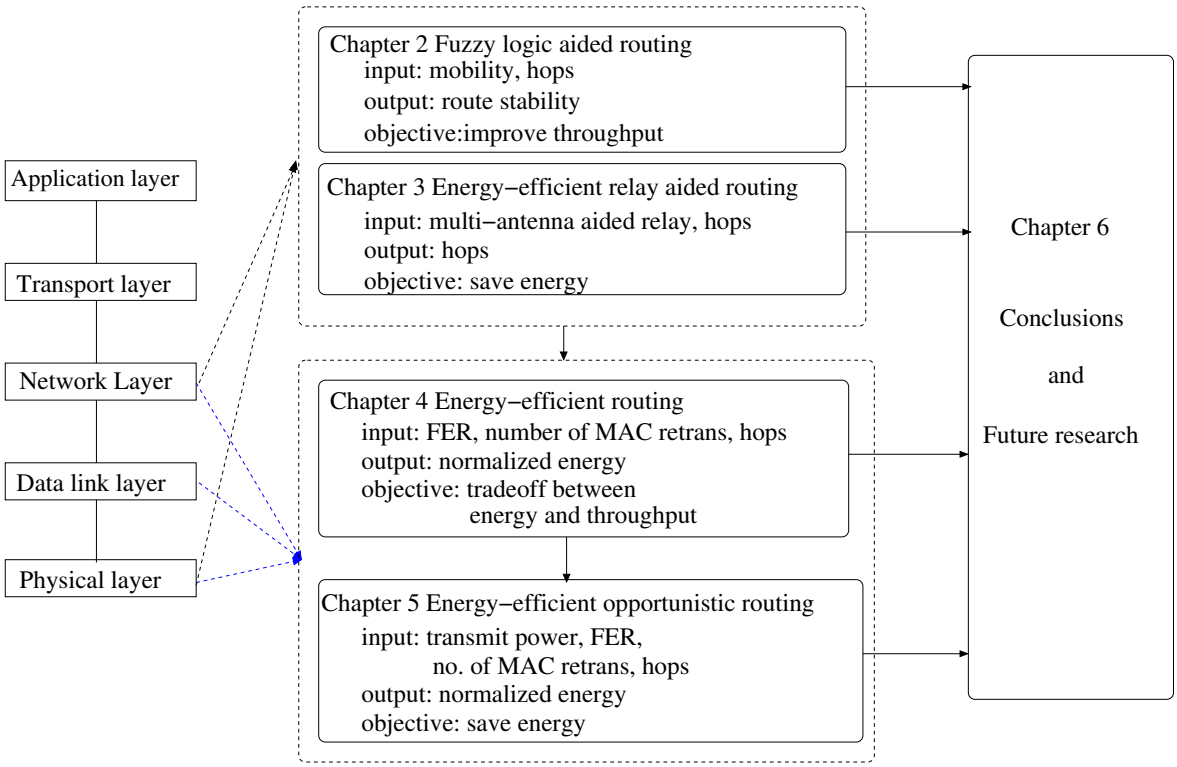

Figure 1.8: Organization of the thesis.

- Chapter 2 investigates the benefits of cross-layer operation between the physical layer and the network layer. It proposes a Fuzzy Logic (FL)-aided DSR routing protocol for improving the network's throughput, which jointly considers the

mobility status in the physical layer and the number of hops in the network layer, whilst relying on the so-called route stability as its routing metric. Section 2.1 presents the motivation behind this design. In Section 2.2, we highlight the basic concepts of fuzzy sets, fuzzy operations, fuzzy relations and membership functions and list the commonly used fuzzification, defuzzification and inference methods. Section 2.3 details several typical mobility models. In Section 2.4, a link life-time prediction model is conceived. Section 2.5 proposes the FL-based DSR routing protocol advocated and describe in detail how it operates. Section 2.6 constructs a random network in OMNeT++ for studying the network's attainable throughput. Section 2.7 concludes this chapter.

- Chapter 3 investigates the cross-layer operation between the physical layer and the network layer. It proposes a Multi Antenna (MA)-RN aided routing protocol using the number of hops as its routing metric, which is designed for reducing the system's total energy consumption. Section 3.1 presents the motivation of this chapter. In Section 3.2, we highlight the benefits of three-stage-concatenated Irregular Convolutional Coded, Unity-Rate Coded and Space-Time Trellis Coded (IrCC-URC-STTC) scheme and analyze its influence on the routing procedure. Section 3.3 constructs a random network for investigating the energy consumption versus both the number of MA-RNs and the node density. The conclusions of this chapter are provided in Section 3.4.
- Chapter 4 discovers the intricacies of cross-layer operation between the physical layer, the data link layer as well as the network layer. It proposes an energy-efficient routing algorithm for striking a tradeoff between the energy consumed and the throughput obtained. The normalized energy consumption is used as its routing metric. Section 4.1 indicates the motivation of this chapter. Section 4.2 theoretically analyzes and formulates the normalized energy consumption and the end-to-end throughput of a multi-hop route by considering both the successful and unsuccessful transmissions. Then a low-complexity routing algorithm is proposed, which employs the normalized energy consumption as its routing metric. Section 4.3 first constructs a single-hop route for investigating the influence of the FER, the number of maximum retransmissions and the number of hops on the normalized energy consumption and on the end-to-end throughput. Then a simple six-node network topology characterized by its FER matrix is employed for further investigating the benefits of the proposed energy-based Objective Function (OF). Section 4.4 offers our conclusions.
- Again, in Chapter 5 we focus our attention on the cross-layer operation between the physical layer, the data link layer as well as the network layer by proposing

an energy-efficient Opportunistic Routing (OR) algorithm relying on careful power allocation for the sake of reducing the energy consumption. It employs the normalized energy consumption as its routing metric. Section 5.1 outlines the motivation of this chapter. In Section 5.2, we first characterize the FER performance of the IrCC-URC-Quadrature Phase-Shift Keying (QPSK) scheme with the aid of a four-segment function. Then we derive analytical formulae for characterizing the power allocation, the normalized energy consumption, the end-to-end throughput and the delay distribution of a single-hop route. Then we extend this analysis both to a linear network relying on a Traditional Routing (TR) protocol and to a random network using the proposed OR protocol. In Section 5.3, a pair of routing algorithms based on the energy-dissipation OF is proposed and the associated complexity is discussed. In Section 5.4 we constructed a twin-RN aided network for investigating the performance of both the TR and OR protocols. Section 5.5 summaries the findings of this chapter.

- Chapter 6 summarizes the entire thesis. Section 6.2 provides design guidelines and finally we suggest future research ideas in Section 6.3.

1.5.2 Novel Contribution of the Thesis

The thesis is based on the publications [47–50]. The novel contributions of this thesis are listed as follows:

- In [47], a link life-time prediction model is proposed according to the position, speed and traveling direction of a pair of nodes, which is then further extended for the sake of estimating the maximum life-time of an entire route. The route's maximum life-time is determined by the minimum link life-time of the route. Based on the knowledge of the route's estimated life-time, which is also combined with the knowledge of the number of hops in the network layer, an FL-DSR protocol is proposed, which relies on the output of the FLS, namely on the route stability as its routing metric. The proposed FL-DSR protocol improves the network's achievable throughput without unduly increasing the network's control load in mobile scenarios.
- An MA-RN aided routing protocol is conceived in [48], which relies on employing the near-capacity IrCC-URC-STTC transceivers of Section 3.2, where the route is selected based on the lowest number of potentially longer hops. This routing protocol is shown to reduce both the network's control load and its total energy-consumption, especially in high-node-density scenarios.
- In [49] an accurate energy-consumption-based OF is used, which takes into account the FER in the physical layer, a limited number of retransmissions (including the first transmission attempt) in the link layer and the number of

hops in the network layer. By employing this energy-consumption-based OF as its routing metric, an energy-efficient routing algorithm is proposed, which is shown to strike an attractive compromise between the energy consumed and the throughput achieved.

- In [50] a pair of accurate energy-consumption-based OFs are employed, which are combined with beneficial power allocation for both the TR and the OR. This system takes into account both the FER within the physical layer as well as the number of retransmissions and the number of RNs in the network layer. Then a pair of routing algorithms is designed, which rely on the above-mentioned energy-consumption-based OFs as their routing metrics. The proposed OR is shown to outperform the TR and operates close to the theoretical bound obtained by an exhaustive search algorithm in terms of its normalized energy consumption. Both the end-to-end throughput and the delay distribution of the system are also analyzed theoretically.

Chapter 2

Fuzzy Logic Aided Dynamic Source Routing in Cross-Layer Operation Assisted Ad Hoc Networks

This chapter considers the coordination between the physical layer and the network layer of the Open System Interconnection (OSI) structure. As seen from the system model of Figure 2.1, the mobility information acquired from the physical layer is forwarded to the network layer and then the route's life-time is calculated based on the mobility information obtained. Combining the route life-time information with the number of hops, a so-called 'route stability' metric is obtained for each possible route by employing a novel fuzzy-logic-aided system [47]. Finally, the specific route which has the highest route stability is selected for transmitting data. Figure 2.1 also shows the different schemes employed in the different OSI layers. The physical layer employs either uncoded Quadrature Phase-Shift Keying (QPSK) or Turbo Trellis-Coded Modulation (TTCM) based 8 Phase-Shift Keying (8PSK) [51–56]. Moreover, as a benchmark, the routing performance is also considered, when assuming that no bit errors occur in the physical layer. The IEEE802.11b regime [7] is employed in the data link layer of Figure 2.1. In the network layer, the Dynamic Source Routing (DSR) protocol [40] and its fuzzy logic aided version are compared in terms of the achievable network throughput. The channel model considered in this system is the Additive White Gaussian Noise (AWGN) channel, which is also subjected to free-space path loss.

2.1 Introduction

Cross-layer optimization is indispensable in wireless network design. This chapter proposes a new routing protocol conceived by combining the physical layer and

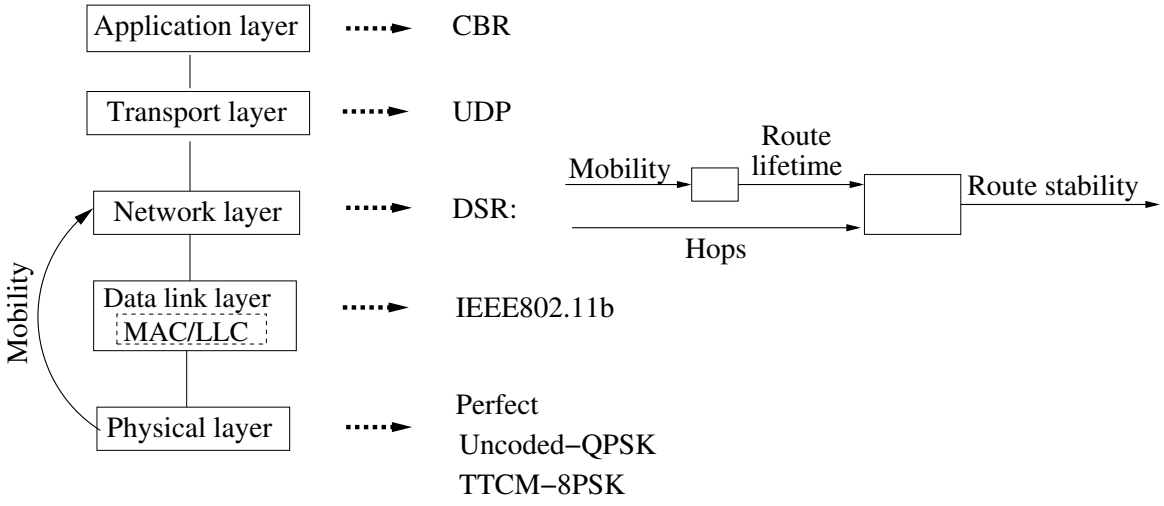

Figure 2.1: System model of our fuzzy logic aided *ad hoc* network, where the mobility status specifically indicates the nodes' position, speed and traveling direction.

network layer, in which the network layer exploits the knowledge of the mobility status gleaned from the physical layer. According to the mobility status, the link's life-time is predicted and then the estimated life-time of the entire route is calculated. Additionally, due to the node's mobility in wireless/mobile *ad hoc* networks, the network topology changes frequently, which requires the regular update of the routing information. Fuzzy Logic (FL) aided enhancements are invoked for processing the potentially unreliable routing information, since the FL was shown to be a powerful mathematical tool, which is widely used in the control industry and in artificial intelligence. We will demonstrate that our fuzzy logic aided DSR protocol is capable of finding the most stable route by jointly considering the route's life-time and the number of hops in the route.

The seven-layer OSI architecture was introduced before the emergence of wireless communications. However, wireless systems inherently rely on cross-layer operation for hand-overs, power control, packet scheduling, flow control, routing etc. Hence in the interest of efficiency, several OSI layers have to exchange information, rather than passing information only between adjacent layers [16, 57]. Maintaining a high network throughput is important, but achieving this objective is by no means straightforward, since it hinges on numerous aspects, including the quality of the wireless channel, the mobility status and the transmit power in the physical layer, the channel access and queueing management in the MAC layer, the routing algorithm employed in the network layer, the congestion control regime of the transport layer, and the flow control in the application layer, just to mention a few.

DSR is an appealingly simple routing protocol specifically designed for multi-hop wireless *ad hoc* networks [40]. Naturally, the network topology perpetually changes owing to node mobility, hence the currently used route may become broken, because the routing information stored in the route cache may become stale, especially in case of the high velocities encountered for example in vehicular *ad hoc* networks. Hence the routing information collected may become inaccurate even during the process of route discovery. Fuzzy logic based techniques have been widely applied in both the artificial intelligence [58] and the control research community [59], because they are capable of resolving complex decision problems based on potentially imprecise information and multiple inputs. Baldo and Zorzi [60] mitigated the link congestion problem in networks by deciding the size of the congestion window using a fuzzy logic based controller, whose inputs are the SNR and the Protocol Data Unit (PDU) drop ratio of the MAC layer. Xia *et al.* [61] also used a fuzzy logic system for adaptively adjusting the modulation and coding mode, the transmission power and the number of retransmissions by considering the node velocity in the physical layer, as well as the average packet delay and packet success ratio in the data link layer. El-Hajj *et al.* [62] employed a fuzzy routing controller based on the number of hops to be covered and the node's residual energy in order to choose the route having the highest route quality defined in terms of a specific objective function. In another paper [63], a fuzzy logic controller combining the residual node energy, the tele-traffic passing through a node expressed in bits/second and the average received signal power gradient was used to maximize the network's life-time, given its finite supply of energy. Rea and Pesch [64] employed a fuzzy logic aided system based on the link-quality, the available node energy and on the number of hops to be considered in order to decide wether to cache the newly discovered route in the face of the limited route cache capacity considered. In another contribution of Rea and Pesch [65], the current queue-length of the nodes was also incorporated as the fuzzy controller's input for the sake of adaptively setting the timeout of the route cache. All of the above-mentioned contributions adopted multiple-input fuzzy logic aided solutions in order to create efficient cross-layer designs by integrating the information available from several OSI layers. The contributions [62–65] considered the influence of mobility, when designing the routing protocol.

Against this background, in this chapter a link life-time prediction model is proposed by considering the nodes' mobility status, including the position, speed and traveling direction of the node, combined with a fuzzy logic aided controller in order to strike an attractive trade-off between the number of hops and route life-time in the face of node-mobility. The output of the fuzzy logic aided controller is a quantitative route stability metric, which is then used as the weight representing the desirability

of a specific route. The highest route-stability implies that the route is most reliable. At the same time, according to the route life-time, the timeout of the route recorded in the route cache is adjusted adaptively. We will demonstrate that the Fuzzy Logic based DSR (FL-DSR) protocol is suitable for diverse mobility models and characterize the achievable performance of the proposed FL-DSR compared to classic DSR in three different physical layer situations.

The rest of the chapter is organized as follows. Section 2.2 highlights the basic concepts and principles of fuzzy logic. Section 2.3 introduces the various mobility models relied upon. Section 2.4 describes our link life-time prediction model, while our FL-DSR technique is presented in Section 2.5. In Section 2.6, three different physical layer solutions are used for analyzing the attainable performance of the FL-DSR technique and that of the conventional DSR. Finally, Section 5.5 provides our conclusions.

2.2 Fuzzy Logic

Since fuzzy logic has the advantage of being capable of handling both imprecise information and multiple inputs, it is a more beneficial choice for improving the performance of routing schemes than its higher complexity counterparts [60–65]. some of the basic concepts of fuzzy logic will be discussed later in this section.

Fuzzy logic [66–68] is a technique which humans adopt for reasoning. By contrast, computers are unable to reason without requiring more detailed data. However, the real world is complex, where uncertainty and ambiguity exist. Natural language [66, Chapter 8] constitutes an example of creating uncertainty, because humans rely on approximate reasoning. Since Zadeh proposed the concepts of fuzzy sets in 1965 [69], diverse fuzzy logic aided solutions were developed. In Japan alone over 1000 patents were filed in the area of fuzzy logic aided products [66, Preface].

The incorporation of fuzzy set theory and fuzzy logic into computer models has shown tremendous benefits in areas, where intuition and judgement still play major roles in the model. Some of the basic concepts which have to be introduced are fuzzy sets, fuzzy operations, fuzzy relations, membership functions, fuzzifications, inference rules and defuzzifications [66–68].

- Fuzzy sets, fuzzy operations and fuzzy relations
  The boundary of the fuzzy sets [66, Chapter 2], [67, Chapter 2], [68, Chapter 1] is vague and ambiguous, which is described by a so-called membership function [66, Chapter 4], [67, Chapter 2], [68, Chapter 1] in a graphical form. The 'membership' value is used for characterizing the affiliation of an element belonging to a fuzzy set. Let us denote a fuzzy set by $\underset{\sim}{A}$, and the membership indicator of the element

x in the fuzzy set $\underset{\sim}{A}$ by $\mu_{\underset{\sim}{A}}(x)$, where we have $\mu_{\underset{\sim}{A}}(x) \in [0,1]$. Then the fuzzy set $\underset{\sim}{A}$ may be described as follows:

$$\underset{\sim}{A} = \left\{ \frac{\mu_A(x_1)}{x_1} + \frac{\mu_A(x_2)}{x_2} + \cdots \right\} = \left\{ \sum_i \frac{\mu_A(x_i)}{x_i} \right\} \quad \text{or} \tag{2.1}$$

$$\underset{\sim}{A} = \left\{ \int \frac{\mu_A(x)}{x} dx \right\}. \tag{2.2}$$

Almost all of the operations applied to the elements of classical sets remain valid for fuzzy sets, albeit there are some exceptions, as detailed in [66, Chapter 2]. Since fuzzy sets can overlap each other, a set and its complement set can also overlap. As a result, the union of $\underset{\sim}{A}$ and $\overline{\underset{\sim}{A}}$ may not cover the entire set X. The fuzzy relations [66, Chapter 3], [67, Chapter 3], [68, Chapter 5] map the elements of the universe X to another universe Y with the aid of the Cartesian product [66, Chapter 3] of the two universes. The Cartesian product may be defined as $\underset{\sim}{A} \times \underset{\sim}{B} = \underset{\sim}{R}$, where $\underset{\sim}{A}$ is the fuzzy set defined over the universe X, while $\underset{\sim}{B}$ is the fuzzy set over the universe Y. A fuzzy relation $\underset{\sim}{R}$ constitutes a mapping from the Cartesian space given by the Cartesian product of $(X \times Y)$ to the interval $[0,1]$, where the mapping is characterized by the membership function of the relation $\underset{\sim}{R}$ for ordered pairs of elements selected from the two universes as $\mu_{\underset{\sim}{R}}(x,y)$. The fuzzy relation $\underset{\sim}{R}$ obeys the membership function of

$$\mu_{\underset{\sim}{R}}(x,y) = \mu_{\underset{\sim}{A}\times\underset{\sim}{B}}(x,y) = \min[\mu_{\underset{\sim}{A}}(x), \mu_{\underset{\sim}{B}}(y)]. \tag{2.3}$$

The two most common forms of the composition operations are the max-min composition and max-product composition. Let us assume that $\underset{\sim}{R}$, $\underset{\sim}{S}$ and $\underset{\sim}{T}$ are the fuzzy relationships defined over the Cartesian space given by the Cartesian product of $(X \times Y)$, $(Y \times Z)$ and $(X \times Z)$, respectively. The max-min and the max-product compositions are defined by the membership-function-theoretic expressions of [66]

$$\mu_{\underset{\sim}{T}}(x,z) = \bigvee_{y \in Y} [\mu_{\underset{\sim}{R}}(x,y) \wedge \mu_{\underset{\sim}{S}}(y,z)] \tag{2.4}$$

$$\mu_{\underset{\sim}{T}}(x,z) = \bigvee_{y \in Y} [\mu_{\underset{\sim}{R}}(x,y) \cdot \mu_{\underset{\sim}{S}}(y,z)], \tag{2.5}$$

where $\wedge$, $\bigvee$ and $\cdot$ represent the min operation, the max operation and the algebraic product of two elements, respectively. Consider the max-min composition for example and let $X = \{x_1\}$, $Y = \{y_1, y_2\}$ and $Z = \{z_1, z_2, z_3\}$.

Then we have the following relations:

$$\underset{\sim}{R} = \begin{matrix} \\ x_1 \end{matrix} \begin{matrix} \begin{matrix} y_1 & y_2 \end{matrix} \\ \begin{bmatrix} 0.7 & 0.5 \end{bmatrix} \end{matrix} \quad \text{and} \quad \underset{\sim}{S} = \begin{matrix} \\ y_1 \\ y_2 \end{matrix} \begin{matrix} \begin{matrix} z_1 & z_2 & z_3 \end{matrix} \\ \begin{bmatrix} 0.9 & 0.6 & 0.2 \\ 0.1 & 0.7 & 0.5 \end{bmatrix} \end{matrix}. \tag{2.6}$$

According to Equation (2.4), we have

$$\mu_{\underset{\sim}{T}}(x_1, z_1) = \max[\min(0.7, 0.9), \min(0.5, 0.1)] = 0.7 \tag{2.7}$$

$$\mu_{\underset{\sim}{T}}(x_1, z_2) = \max[\min(0.7, 0.6), \min(0.5, 0.7)] = 0.6 \tag{2.8}$$

$$\mu_{\underset{\sim}{T}}(x_1, z_3) = \max[\min(0.7, 0.2), \min(0.5, 0.5)] = 0.5. \tag{2.9}$$

Then we arrive at the expression of the fuzzy relation $\underset{\sim}{T}$ from Equations (2.7) - (2.9):

$$\underset{\sim}{T} = \begin{matrix} \\ x_1 \end{matrix} \begin{matrix} \begin{matrix} z_1 & z_2 & z_3 \end{matrix} \\ \begin{bmatrix} 0.7 & 0.6 & 0.5 \end{bmatrix} \end{matrix}. \tag{2.10}$$

- Membership functions, fuzzification and defuzzification methods
  The membership function [66, Chapter 4], [67, Chapter 2], [68, Chapter 1] embodies the fuzziness of a particular fuzzy set. The membership functions are usually represented by different 'shapes', such as a triangle, trapezoid, sine, cosine, etc. Fuzzification is the process of making a crisp quantity fuzzy in terms of its membership function. There are numerous methods of assigning the values of the membership to the fuzzy variables, such as intuition [70], inference [66], neural networks [71], genetic algorithms [72, 73] and inductive reasoning [66, Chapter 4]. However, defuzzification [66, Chapter 5] is the conversion of a fuzzy quantity to a precise quantity. The output of a fuzzy process may be the logical union of two or more fuzzy membership functions defined over the universe of the output variable, where the logical union $\bigcup$ may be interpreted as the max operator. If assuming that the fuzzy output $\underset{\sim}{C}$ has 2 membership functions, we have $\underset{\sim}{C} = \underset{\sim}{C}_1 \bigcup \underset{\sim}{C}_2$. The most commonly employed defuzzification methods [66, Chapter 5] are the max-membership, the mean-max membership, the centroid and the weighted average

methods, which are characterized by

$$\text{Max-membership:} \quad \mu_{\underset{\sim}{C}}(z^*) \geq \mu_{\underset{\sim}{C}}(z) \tag{2.11}$$

$$\text{Mean-max membership:} \quad z^* = (z^{'} + z^{"})/2 \tag{2.12}$$

$$\text{Centroid:} \quad z^* = \int \mu_{\underset{\sim}{C}}(z) \cdot z dz / \int \mu_{\underset{\sim}{C}}(z) dz \tag{2.13}$$

$$\text{Weighted average:} \quad z^* = \sum \mu_{\underset{\sim}{C}}(\overline{z}) \cdot \overline{z} / \sum \mu_{\underset{\sim}{C}}(\overline{z}), \tag{2.14}$$

where z^* is the crisp output value after the defuzzification process. Their corresponding graphical interpretations are shown in Figure 2.2.

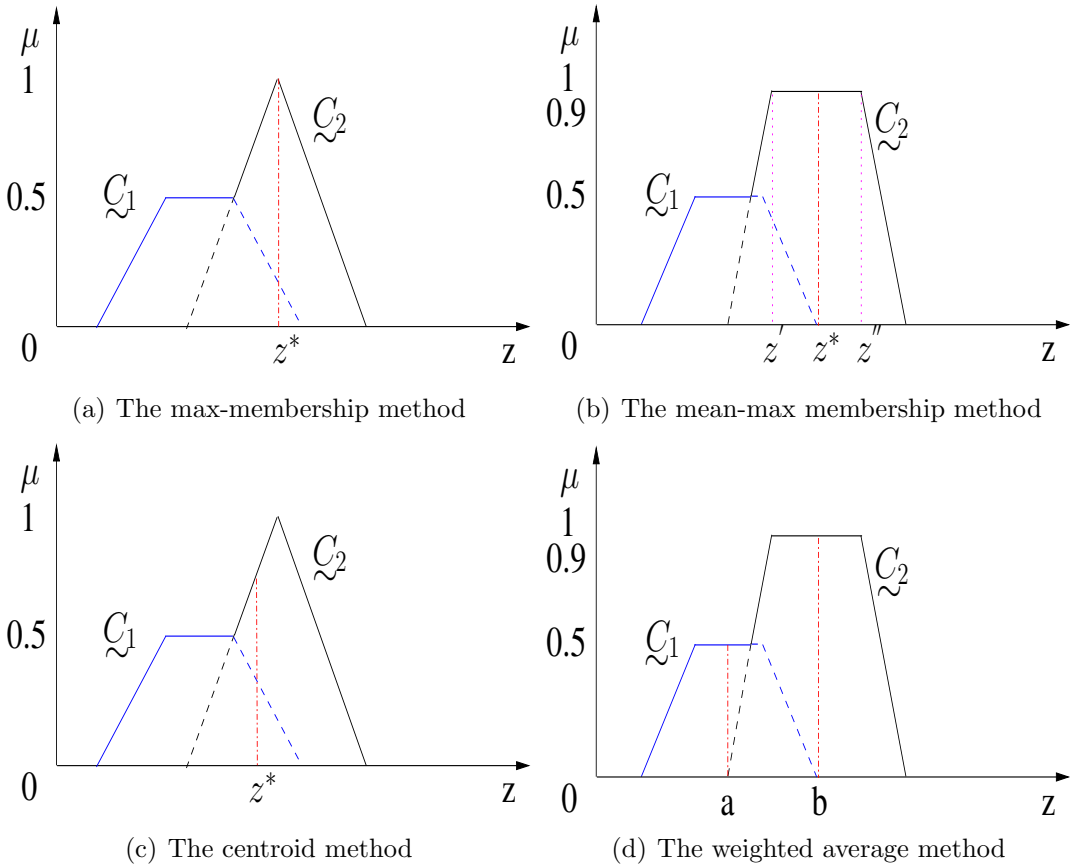

(a) The max-membership method (b) The mean-max membership method

(c) The centroid method (d) The weighted average method

Figure 2.2: The most common defuzzification methods.

- Inference rules

  Fuzzy logic [66, Chapter 7], [68, Chapter 8] may be deemed to be a method of reasoning 'approximately' and judging under uncertainty, where all truths are partial or approximate. Fuzzy logic constitutes an extension of classical logic, where partial truths are included to extend the classic set of true or false logical values to a multi-valued logic, implying that different degrees of truth between true and untrue exist [66]. Let us assume that the proposition $\underset{\sim}{P}$ is assigned to fuzzy set $\underset{\sim}{A}$ [74]. Then the truth value of a proposition, which is denoted by

$T(\underset{\sim}{P})$, is given by [66]

$$T(\underset{\sim}{P}) = \mu_{\underset{\sim}{A}}(x) \quad \text{where } 0 \leq \mu_{\underset{\sim}{A}} \leq 1. \tag{2.15}$$

Equation (2.15) indicates that the degree of truth for the proposition $\underset{\sim}{P} : x \in \underset{\sim}{A}$ is equal to the membership value of x in the fuzzy set $\underset{\sim}{A}$. Then the so-called logical connectives for proposition $\underset{\sim}{P}$ and proposition $\underset{\sim}{Q}$ are defined as

$$\begin{aligned}
&\text{Negation} && T(\overline{\underset{\sim}{P}}) = 1 - T(\underset{\sim}{P}) && (2.16)\\
&\text{Disjunction} && \underset{\sim}{P} \vee \underset{\sim}{Q} : x \text{ is } \underset{\sim}{A} \text{ or } \underset{\sim}{B}; \\
& && T(\underset{\sim}{P} \vee \underset{\sim}{Q}) = \max[T(\underset{\sim}{P}), T(\underset{\sim}{Q})] && (2.17)\\
&\text{Conjunction} && \underset{\sim}{P} \wedge \underset{\sim}{Q} : x \text{ is } \underset{\sim}{A} \text{ and } \underset{\sim}{B}; \\
& && T(\underset{\sim}{P} \wedge \underset{\sim}{Q}) = \min[T(\underset{\sim}{P}), T(\underset{\sim}{Q})] && (2.18)\\
&\text{Implication} && \underset{\sim}{P} \rightarrow \underset{\sim}{Q} : x \text{ is } \underset{\sim}{A}, \text{then } y \text{ is } \underset{\sim}{B}; \\
& && T(\underset{\sim}{P} \rightarrow \underset{\sim}{Q}) = T(\overline{\underset{\sim}{P}} \vee \underset{\sim}{Q}) = \max[T(\overline{\underset{\sim}{P}}), T(\underset{\sim}{Q})], && (2.19)
\end{aligned}$$

where proposition $\underset{\sim}{P}$ is defined over the fuzzy set $\underset{\sim}{A}$, while proposition $\underset{\sim}{Q}$ is defined over the fuzzy set $\underset{\sim}{B}$ and we have $y \in \underset{\sim}{B}$. Equation (2.19) [75] may be modeled in a so-called rule-based form: IF x is $\underset{\sim}{A}$, THEN y is $\underset{\sim}{B}$, which may be described by the set-theoretic fuzzy relation of $\underset{\sim}{R} = (\underset{\sim}{A} \times \underset{\sim}{B}) \cup (\overline{\underset{\sim}{A}} \times Y)$, where Y is the universe of the fuzzy set $\underset{\sim}{B}$. The membership function of $\underset{\sim}{R}$ is expressed as [66]:

$$\mu_{\underset{\sim}{R}(x,y)} = \max[(\mu_{\underset{\sim}{A}(x)} \wedge \mu_{\underset{\sim}{B}(y)}), (1 - \mu_{\underset{\sim}{A}(x)})], \tag{2.20}$$

which is a so-called rule-based antecedent-consequent form [66, chapter 8]. According to the approximate reasoning defined by Zadeh in 1976 [76], we can calculate the consequent $\underset{\sim}{B}'$ by the composition operation $\underset{\sim}{B}' = \underset{\sim}{A}' \circ \underset{\sim}{R}$, where $\underset{\sim}{R}$ is given by Equation (2.3) and the symbol $\circ$ denotes the composition operation. Since natural languages [66, Chapter 8], [67, Chapter 4] are often vague, imprecise, ambiguous and fuzzy, we tend to use rather subjective adjectives, such as 'slow', 'medium', 'young', etc. These phrases are then combined with certain linguistic connectors (such as 'and', 'or' and 'not') [66]. For example, assuming that the fuzzy sets $\underset{\sim}{A}$ and $\underset{\sim}{B}$ represent the linguistic variables of 'tomato is red' and 'tomato is ripe', respectively, then we may state that

$$IF \text{ the tomato is red} \quad THEN \text{ the tomato is ripe.}$$

Moreover, a complex fuzzy system may be characterized by a compound

rule structure, as exemplified in Table 2.1. The overall FL system may be

Table 2.1: The compound rule structure of a fuzzy rule-based system.

Rule 1:	IF condition C^1, THEN restriction R^1
Rule 2:	IF condition C^2, THEN restriction R^2
$\vdots$	$\vdots$
Rule r:	IF condition C^r, THEN restriction R^r

characterized by appropriately aggregating all rules. Two specific methods of aggregating the rules are listed here [66, 77]:

– **Conjunctive system of rules**. A system of rules must be jointly satisfied and connected by 'and' connectives. The aggregated output y is found by the fuzzy intersection of all individual rule consequents y^i, for $i = 1, 2, ...r$, which is formulated as

$$y = y^1 \text{ and } y^2 \text{ and } \cdots \text{ and } y^r \tag{2.21}$$

$$\text{or } \mu_y(y) = \min[\mu_{y^1}(y), \mu_{y^2}(y), \ldots, \mu_{y^r}(y)], \quad \text{for } y \in Y. \tag{2.22}$$

– **Disjunctive system of rules**. At least one rule is required for a disjunctive system of rules, where the rules are connected by 'or' connectives, which is expressed as:

$$y = y^1 \text{ or } y^2 \text{ or } \cdots \text{ or } y^r \tag{2.23}$$

$$\text{or } \mu_y(y) = \max[\mu_{y^1}(y), \mu_{y^2}(y), \ldots, \mu_{y^r}(y)], \quad \text{for } y \in Y. \tag{2.24}$$

Having highlighted all the basic concepts, let us now illustrate the design of a basic Fuzzy Logic System (FLS). The concept of FLS originates from fuzzy set theory, which has the benefit of resolving decision dilemmas, even when provided with inaccurate information generated by multiple inputs. A basic fuzzy logic control process consists of three parts: fuzzification, inference and defuzzification. In Figure 2.3 we present the structure of a basic FLS.

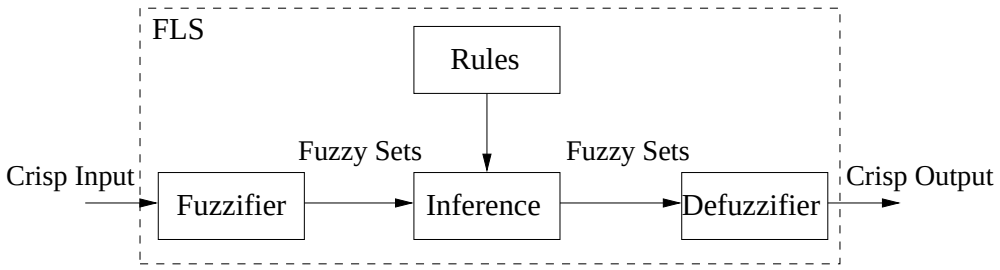

Figure 2.3: The structure of Fuzzy Logic System (FLS).

As detailed in [66], the key steps in designing a FLS are represented by the choice of the suitable antecedents, the membership function of the input and output, the fuzzy inference rule and the defuzzification method. The detailed steps are as follows:

- Identify the input and output variables;
- Partition the universe or the interval spanned by each variable into a number of fuzzy subsets, assigning each subset a linguistic label;
- Assign a membership function to each fuzzy subset;
- Assign the fuzzy relationship between the inputs' fuzzy subsets and the outputs' fuzzy subsets, which constitutes the required rule-base;
- Fuzzify the inputs;
- Employ fuzzy approximate reasoning to infer the fuzzy output according to each rule from the rule-base, individually;
- Aggregate the fuzzy outputs;
- Apply defuzzification to form a crisp output.

2.3 Mobility Models

In a real network, nodes usually move unpredictably. When analyzing the performance of complex networks, the unpredictable mobility pattern is usually decomposed into a set of regular mobility patterns, which are exploited by various network simulators, such as OPNET [78], NS3 [79] and OMNeT++ [45]. Based on the node velocity, direction of travel, acceleration and their update intervals, the mobility style may be divided into the following categories [80–87]:

- **Null mobility model**: This model is used by stationary nodes.
- **Linear mobility model**: This model considers the parameters of node velocity, mobile direction and acceleration. These three parameters remain constant, except that the mobile's direction of travel changes, when the moving node hits a wall. Whenever the moving node hits a wall, it is reflected by the wall with the same angle.
- **Circular mobility model**: Nodes move around in a circle according to this model.
- **Rectangular mobility model**: Nodes move along a rectangle in this model.
- **Constant speed mobility model**: This model defines a velocity and an update interval for each node. Initially, if a node's velocity is higher than zero, this model calculates a random target position for this node. Then, based on the velocity and on the update interval defined, we calculate the number of steps and the step-size, when aiming for reaching the destination. In each update interval, the

model calculates a new position, which is on its way to the target position. Once the target position is reached, the model calculates a new target position.

- **Random waypoint mobility model** [83, 84]: Nodes move following piecewise linear segments in this model. For each line segment, a random target position and a random speed is chosen. The speed may be defined as a set of speeds, from which a new value will be drawn for each line segment. It is customary to assume that it is uniformly distributed in the interval (v_{min}, v_{max}), where v_{min} is the minimum velocity of a node, while v_{max} is the maximum velocity of a node. When the node reaches the target position, it waits for a period of time t_{wait}. Then this model calculates a new random target position and chooses a new random speed, and their process is repeated continually.
- **Mass mobility model** [87]: This model is parameterized by the node velocity, mobile direction and the update interval. We denote node velocity as v, the mobile direction as θ and the update interval as t_{intv}, which are initialized as:

$$v = normal[v_{avg}, 0.01]\ (m/s) \tag{2.25}$$

$$\theta = normal[0, 30]\ (rad) \tag{2.26}$$

$$t_{intv} = normal[5, 0.1]\ (s), \tag{2.27}$$

where v_{avg} represents the average speed and $normal(a, b)$ is the normal distribution with the given mean a and standard deviation b. A node moves along a straight line at the speed of v and in the angular direction of θ for a period of t_{intv}, before it makes a turn. As defined in Equation (2.27), t_{intv} is a normally distributed random variable with an average of 5 s and a standard deviation of 0.1 s. When the node makes a turn, the new angle followed is a normally distributed random variable with an average, which is equal to the previous direction, whilst obeying an angular standard deviation of 30 degrees. Its speed v is also a normally distributed random number, with a controlled average of v_{avg}, ranging from 0.1 to 0.45 unit/s, and a standard deviation of 0.01 unit/s. A new corresponding random number is picked as its speed, when it makes a turn. This pattern of mobility is intended for modelling the node's movement, during which the nodes have a momentum and thus do not start, stop or turn abruptly. When a node hits a wall, it bounces off the wall at the same angle.

The node mobility has a significant influence on the achievable performance, because the radio-link may become inferior, hence potentially rendering the route invalid. Therefore, the family of routing algorithms considering the node mobility status attracted significant research attention for the sake of improving the network's

throughput. For example, Carofiglio *et al.* [88] developed mathematical expressions for characterizing the life-span of a route and for the availability of a link, taking into account the relative position, velocity and direction of the nodes. However, the expressions proposed in [88] were developed under the assumption of the specific spatial node distribution, which is only valid for the so-called 'random direction' mobility model[1]. Al-Akaidi and Alchaita [89] exploited the relative angle of direction of the nodes to select the next Relay Node (RN). Rubin and Liu [90] derived four link life-time distributions for four different movement patterns and developed four link-stability evaluation models. However, in [89] and [90], the link life-time distributions depend on the node velocity. Hence, if the environment is changed, the distributions have to be regenerated. Feng *et al.* [91] considered the relative velocity, angle of direction and position of the intermediate nodes and destination node in order to choose the optimal RN, instead of using the flooding technique of [92]. Although the Velocity-Aided Routing (VAR) protocol of [91] assumes that the source node has all the necessary location information, the velocity and the angle of direction for the destination, these information are usually unknown.

2.4 Link Life-Time Prediction Model

According to the system model of Figure 2.1, the mobility status information, including the nodes' position, speed and traveling direction, are provided by the physical layer for the network layer. Hence, for the sake of predicting the life-time of a certain route the life-time of its individual links is predicted first.

A direct consequence of node-mobility is that the network's topology is time-variant and when the nodes' communications fail to reach the destination, the route becomes invalid. Therefore, if the residual time of the link between two nodes can be predicted, then the reliability of the link can be estimated. Here a link life-time prediction model is proposed based on the node-mobility status, which includes the current position, the current speed and the current traveling direction of the node, which reflects the expected movement of the node in the near future. According to the relative node mobility status between two nodes, the achievable link life-time may also be calculated. In this system, mass mobility style is chosen due to its similarity character of the real environment. We assume that there are N nodes in the network. At time-instant t, the position of the ith node N_i is $(x_{i,t}, y_{i,t})$, its speed is $v_{i,t}$, and its direction is $\theta_{i,t}$. As a natural choice, the direction of the horizontal axis is assumed to be associated with the angle of 0. Similarly, the position of node N_j is $(x_{j,t}, y_{j,t})$, its speed is $v_{j,t}$, and its angular direction is $\theta_{j,t}$. As seen in Figure 2.4, the distance between node N_i and N_j is

[1]This model forces the mobile node to travel to the edge of the simulation area before changing its direction and speed.

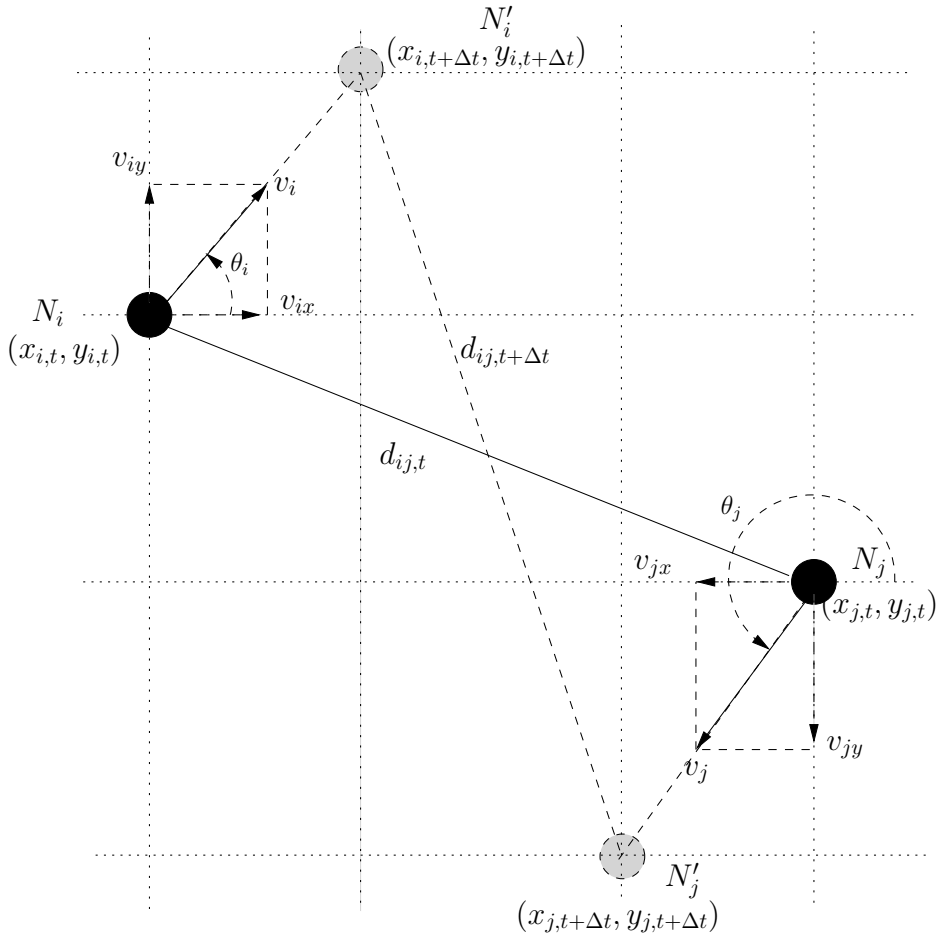

Figure 2.4: The relationship between N_i and N_j.

$d_{ij,t}$. After a time elapse of Δt, the position of node N_i becomes $(x_{i,t+\Delta t}, y_{i,t+\Delta t})$, while its speed is $v_{i,t+\Delta t}$ and its direction is $\theta_{i,t+\Delta t}$. Similarly, for node N_j, the future position becomes $(x_{j,t+\Delta t}, y_{j,t+\Delta t})$, while the corresponding speed is $v_{j,t+\Delta t}$, and the direction is $\theta_{j,t+\Delta t}$. When predicting a specific link's life-time, the simplest model is to consider the speed and the direction of the most recent hop only, although our future research will consider higher-order mobility predictions, as detailed in a speech prediction context in [93]. Therefore the speed and the direction of N_i and N_j at time-instant t based on this rudimentary first-order model are described as v_i, v_j, θ_i and θ_j.

$$x_{i,t+\Delta t} = x_{i,t} + v_i \cos(\theta_i)\ \Delta t, \tag{2.28}$$

$$y_{i,t+\Delta t} = y_{i,t} + v_i \sin(\theta_i)\ \Delta t, \tag{2.29}$$

$$x_{j,t+\Delta t} = x_{j,t} + v_j \cos(\theta_j)\ \Delta t, \tag{2.30}$$

$$y_{j,t+\Delta t} = y_{j,t} + v_j \sin(\theta_j)\ \Delta t. \tag{2.31}$$

The distance between node N_i and N_j at time-instant $(t + \Delta t)$ is calculated as:

$$d^2_{ij,t+\Delta t} \;=\; (x_{j,t+\Delta t} - x_{i,t+\Delta t})^2 \;+\; (y_{j,t+\Delta t} - y_{i,t+\Delta t})^2. \tag{2.32}$$

When the distance between any two nodes becomes higher than their reliable transmission range, the link between them will break and the related session will abort. The reliable transmission range is defined as the range, within which the receiver node becomes capable of receiving a transmitted packet with $FER < 10^{-5}$. Here assuming that every node has the same transmit power, thus the same transmission range, which is formulated as

$$d_{ij,t+\Delta t} \;\leq\; d_{max}, \tag{2.33}$$

where d_{max} is the reliable transmission range. Therefore, Equation (2.32) and (2.33) are combined to arrive at:

$$\begin{aligned}
&[(v_j \sin(\theta_j) - v_i \sin(\theta_i))^2 + \\
&(v_j \cos(\theta_j) - v_i \cos(\theta_i))^2](\Delta t)^2 + \\
&2[(y_{j,t+\Delta t} - y_{i,t+\Delta t})(v_j \sin(\theta_j) - v_i \sin(\theta_i)) + \\
&(x_{j,t+\Delta t} - x_{i,t+\Delta t})(v_j \cos(\theta_j) - v_i \cos(\theta_i))]\Delta t + \\
&[(y_{j,t+\Delta t} - y_{i,t+\Delta t})^2 + (x_{j,t+\Delta t} - x_{i,t+\Delta t})^2] - \\
&d^2_{max} \leq 0.
\end{aligned} \tag{2.34}$$

Observe that Equation (2.34) is a quadratic polynomial of the form $Ax^2 + Bx + C \leq 0$, where we have:

$$\begin{aligned}
A &= [v_j \sin(\theta_j) - v_i \sin(\theta_i)]^2 + [v_j \cos(\theta_j) - v_i \cos(\theta_i)]^2, \\
B &= 2[(y_{j,t+\Delta t} - y_{i,t+\Delta t})(v_j \sin(\theta_j) - v_i \sin(\theta_i)) \\
&\quad + (x_{j,t+\Delta t} - x_{i,t+\Delta t})(v_j \cos(\theta_j) - v_i \cos(\theta_i))], \\
C &= [(y_{j,t+\Delta t} - y_{i,t+\Delta t})^2 + (x_{j,t+\Delta t} - x_{i,t+\Delta t})^2] \;-\; d^2_{max}, \\
x &= \Delta t.
\end{aligned} \tag{2.35}$$

According to the characteristics of quadratic polynomials, the minimum real root represents the maximum link life-time as determined by the node's limited transmission range. Observe from Equation (2.35) that $A \geq 0, C \leq 0$ are obtained. If having $A = 0$, which implies that the two nodes considered have the same node mobility status, then the distance between them would never change, unless one of them changes its mobility

status. Thus the life-time of the link between them is infinite. By contrast, if having $A \neq 0$, and this is a relevant practical scenario, then Equation (2.34) must have one and only one real root, which satisfies $B^2 - 4AC \geq 0$. Then, according to the simple formula of $x = (-B + \sqrt{B^2 - 4AC})/(2A), A > 0$, the maximum link life-time may be determined.

For the sake of predicting the life-time of a certain link, the receiver node of the link has to be aware of the mobility status information of the corresponding transmitter node. Furthermore, for predicting the life-time of an entire route, the source node has to be aware of all the link life-time information of the entire route. Hence, the end-to-end exchange of the control packets in a routing protocol is required. Additionally, the route life-time information obtained may become invalid in a high-mobility scenario, after finishing the end-to-end exchange of the control packet between the source node and the destination node. Therefore, the pre-set expiration time of any route in the routing table has to be dynamically adjusted. Section 2.5 will discuss these two issues in detail.

2.5 Fuzzy Logic Based Dynamic Source Routing

Since DSR is a reactive routing protocol, it only commences its route discovery process when there is data to be transmitted. Following the route discovery process, several routes are identified and stored in the route cache of the source node. The metric employed for deciding, which route to choose for transmitting the source data is that of minimizing the number of hops. Further route rediscovery is triggered only, when a certain link in the currently used route breaks owing to node-mobility and no redundant route or route-repair is available. However, in mobile environments, opting for the lowest number of hops implies that we typically have a long distance between the individual nodes, which is likely to be associated with a low received power, a high BER and a potentially short route life-time. Additionally, if we opt for finding all the routes during the one and only initial route discovery process without frequent updates, this may render the route cache information stale, especially in the face of dynamic mobility. Once a node moves out of the transmission range of the other nodes, it may happen that not only the link considered, but all the other routes which include this link in the route cache become invalid at the same time. Therefore, the conventional DSR protocol may not perform well in mobile environments. A trade-off between opting for a 'few hops having a short route life-time' and 'many hops having a long route life-time' should be found.

To strike an attractive trade-off, a FL-DSR is proposed, which jointly considers the number of hops as well as the route life-time as its inputs, aiming for identifying

the right balance between them. The minimum route life-time reflects the grade of route stability to some degree. The longer the route life-time, the higher the route stability. At the same time, the fewer hops the route has, the less likely that the route breaks, hence the higher the route stability becomes. We assume that there are M hops in a route. The link life-time between node N_i and N_j is described as $l_{ij}, 0 \leq i, j \leq (M-1)$, which is calculated according to the link life-time prediction model introduced in Section 2.4. Naturally, the link having the shortest life-time constitutes the 'bottle-neck' of the route. Therefore, the shortest link life-time may be interpreted as the route life-time, as defined below:

$$p_t = \min(l_{ij}), 0 \leq i, j \leq M-1, \tag{2.36}$$

where p_t is the route life-time.

Based on its appealing simplicity and popularity, the so-called triangular membership function [66] is chosen to map the crisp input value into the fuzzy sets and vice versa. The output of the FLS is the route stability. We opt for using three fuzzy sets described by the loose terms 'Low', 'Medium' and 'High' for the number of hops and 'Short', 'Medium' and 'Long' for the route life-time. For the route stability, the terminology 'Low', 'Medium' and 'High' are used. The simple triangular membership functions of the number of hops and route life-time are shown in Figure 2.5 and Figure 2.6, where the normalized number of hops is defined as the number of hops in a route normalized by the maximum number of hops in the network. The membership function of the route stability has the same shape as that of the number of hops, thus it is not portrayed graphically here. Moreover, the universe of the number of hops and the route stability is normalized to the range of $[0, 1]$, while the universe of the route life-time to $[0, 300s]$, because the route cache expiry time-out is 300 s. For the triangular membership function of the route life-time, v_{max} denotes the maximum speed of all nodes.

As seen in Figure 2.5, the membership functions $F_{h_s}(x)$, $F_{h_m}(x)$ and $F_{h_l}(x)$ of the fuzzy sets 'Low', 'Medium' and 'High' defined for the normalized number of hops are

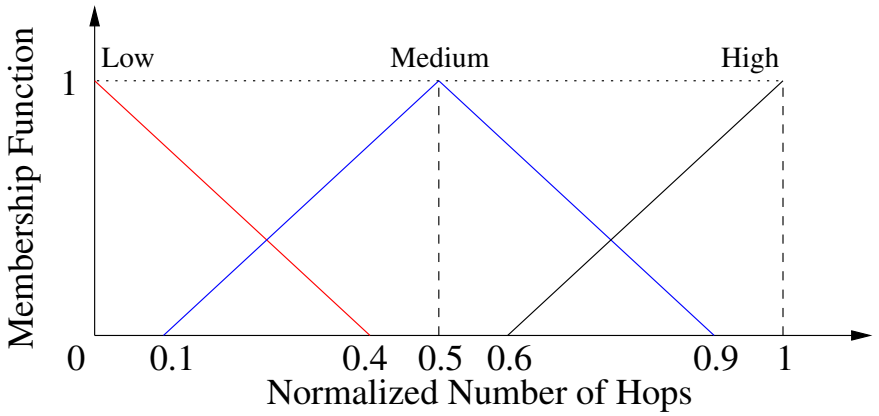

Figure 2.5: The triangular membership function versus the normalized number of hops.

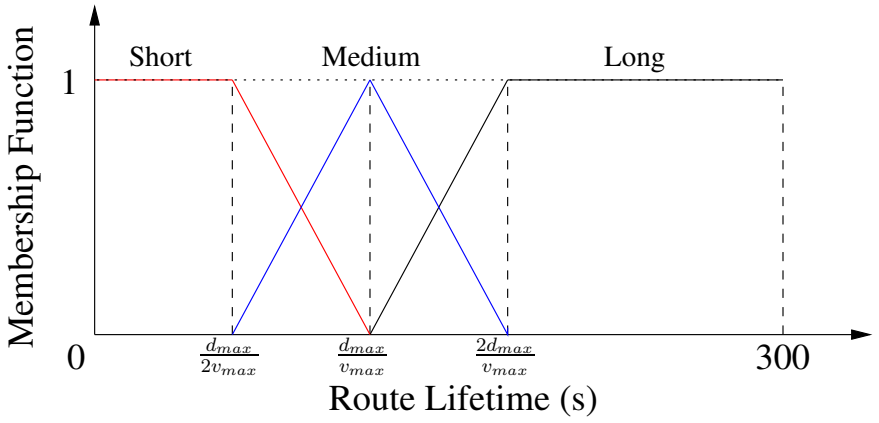

Figure 2.6: The triangular membership function versus the route life-time (s).

given by:

$$F_{h_s}(x) = \begin{cases} \dfrac{0.4 - x}{0.4}, & 0 \leq x \leq 0.4 \\ 0, & 0.4 < x \leq 1, \end{cases}$$

$$F_{h_m}(x) = \begin{cases} 0, & 0 \leq x \leq 0.1 \\ \dfrac{x - 0.1}{0.4}, & 0.1 < x \leq 0.5 \\ \dfrac{0.9 - x}{0.4}, & 0.5 < x \leq 0.9 \\ 0, & 0.9 < x \leq 1, \end{cases}$$

$$F_{h_l}(x) = \begin{cases} 0, & 0 \leq x \leq 0.6 \\ \dfrac{x - 0.6}{0.4}, & 0.6 < x \leq 1 \end{cases}. \tag{2.37}$$

Meanwhile, as seen in Figure 2.6, the membership functions $F_{t_s}(x)$, $F_{t_m}(x)$ and $F_{t_l}(x)$ of the fuzzy sets 'Short', 'Medium' and 'Long' of the route life-time are given by Equation (2.38):

$$
\begin{aligned}
F_{t_s}(x) &= \begin{cases} 1, & 0 \le x \le \dfrac{d_{max}}{2v_{max}} \\ \dfrac{\frac{d_{max}}{v_{max}} - x}{\frac{d_{max}}{2v_{max}}}, & \dfrac{d_{max}}{2v_{max}} < x \le \dfrac{d_{max}}{v_{max}} \\ 0, & \dfrac{d_{max}}{v_{max}} < x \le 300, \end{cases} \\
F_{t_m}(x) &= \begin{cases} 0, & 0 \le x \le \dfrac{d_{max}}{2v_{max}} \\ \dfrac{x - \frac{d_{max}}{2v_{max}}}{\frac{d_{max}}{2v_{max}}}, & \dfrac{d_{max}}{2v_{max}} < x \le \dfrac{d_{max}}{v_{max}} \\ \dfrac{\frac{2d_{max}}{v_{max}} - x}{\frac{d_{max}}{v_{max}}}, & \dfrac{d_{max}}{v_{max}} < x \le \dfrac{2d_{max}}{v_{max}} \\ 0, & \dfrac{2d_{max}}{v_{max}} < x \le 300, \end{cases} \\
F_{t_l}(x) &= \begin{cases} 0, & 0 \le x \le \dfrac{d_{max}}{v_{max}} \\ \dfrac{x - \frac{d_{max}}{v_{max}}}{\frac{d_{max}}{v_{max}}}, & \dfrac{d_{max}}{v_{max}} < x \le \dfrac{2d_{max}}{v_{max}} \\ 1, & \dfrac{2d_{max}}{v_{max}} < x \le 300 \end{cases} .
\end{aligned}
\tag{2.38}
$$

Again, the membership functions of the fuzzy sets 'Low', 'Medium' and 'High' defined for the route stability are not listed here, since their expressions are similar to those in Equation (2.37).

The classic 'IF-THEN' rule is chosen as the inference rule [66] for carrying out the mapping from the fuzzy input sets to the fuzzy output sets, where the max-min composition is employed in this chapter. The 'IF-THEN' rule is illustrated in Equation (2.20), while the max-min composition is formulated in Equation (2.4). The inference rule of the FLS adopted in this chapter is shown in Table 2.2 in detail. Consider the first line, for example, stating that IF the number of hops is 'Low' AND route life-time is 'short', THEN route stability is 'Medium'. The weighted averaging method [66] is selected as the defuzzification method, as shown in Equation (2.14).

The proposed FLS is incorporated in every node. The system model is shown in Figure 2.7. We characterize the FL-DSR from the two different perspectives, namely

Table 2.2: Inference rule of FLS.

No.	*NumHops*	*RouteLifetime*	*RouteStability*
1	Low	Short	Medium
2	Low	Medium	High
3	Low	Long	High
4	Medium	Short	Low
5	Medium	Medium	Medium
6	Medium	Long	High
7	High	Short	Low
8	High	Medium	Medium
9	High	Long	High

route discovery and route maintenance, where the routing metric is the route stability instead of the number of hops employed in the conventional DSR protocol.

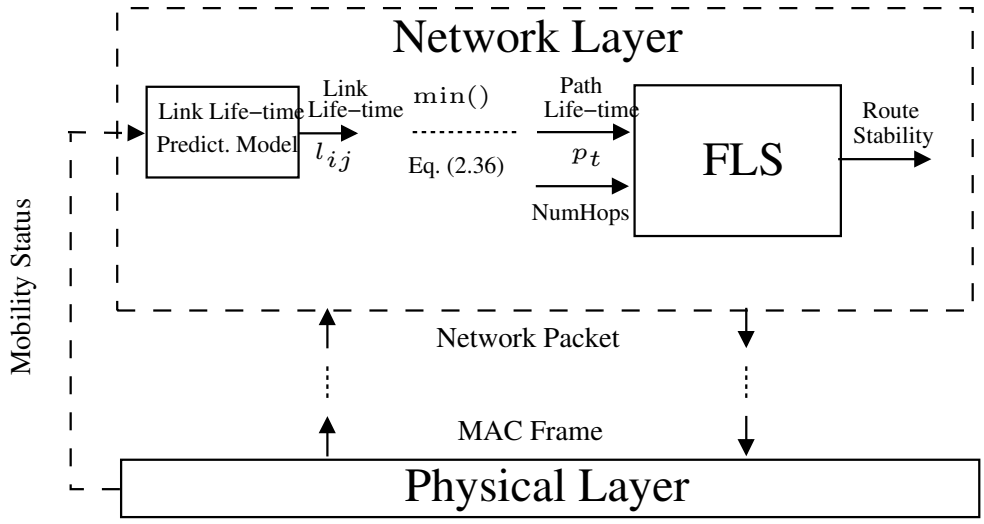

Figure 2.7: The system model of FL-DSR.

- **Route discovery**: Similar to the route discovery process of the DSR protocol described in Subsection 1.2.1, whenever an RREQ packet arrives at a node, it records the current mobility status and calculates the link life-time between this hop and the immediately preceding hop according to their relative mobility status, instead of taking into account the number of hops. When the RREQ packet arrives at the destination, the expected route life-time is calculated from Equation (2.36) and substituted into the RREP packet, which carries both the expected route life-time and the discovered route's identifier back to the source node. During a specific route discovery process, several viable routes may be found. Then, according to the FLS, the route exhibiting the highest route stability is chosen for transmitting the data from the source to the destination.

- **Route maintenance**: Similar to the route maintenance process of the classic DSR protocol described in Subsection 1.2.1, the SR packet is transmitted from the source node to the destination node. Whenever the SR packet arrives at a node during the transmission process, it records the current node's mobility status and updates the estimated link life-time for every pair of nodes, provided that there was a change in the mobility status. If any link of the selected routes breaks and if a redundant route exists, it will be activated in order to salvage the packet and ultimately the session. However, it is not known, whether the redundant route has become invalid in the meantime owing to node-mobility, which may cause a data transmission failure again. Hence, according to the residual route life-time, the expiry time-out of the route in the route cache is adjusted adaptively in order to update the route information in the route cache, instead of using a pre-defined route expiry time.

A detailed example is provided here for demonstrating how the route discovery process ensues and how the route is selected. The process of route discovery is shown in Figure 2.8 and Figure 2.9. The maximum number of hops is $H = 19$, the maximum transmission range is $d_{max} = 176.88$ m and the maximum mobile speed is $v_{max} = 10$ m/s. In Figure 2.8, the process of sending RREQ is detailed.

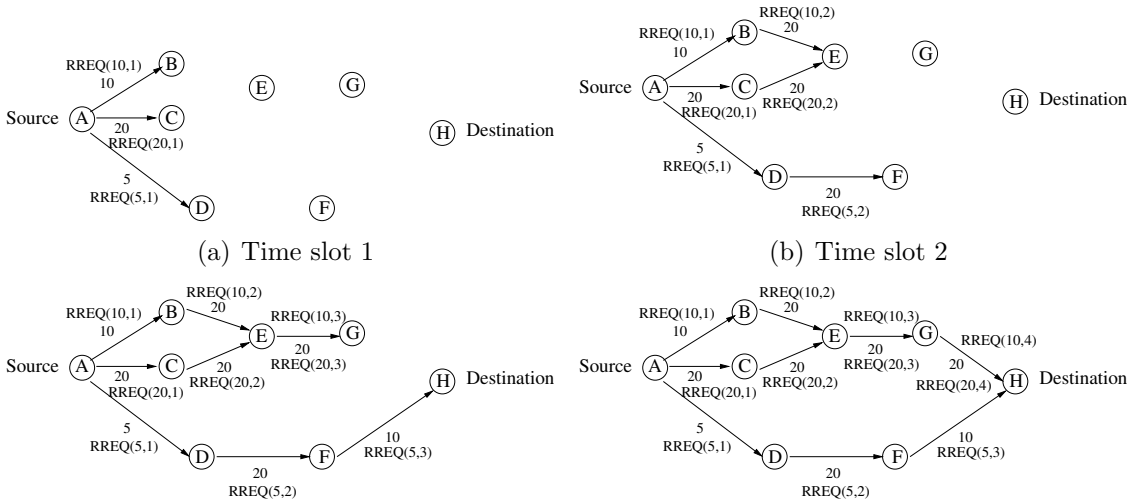

(a) Time slot 1 (b) Time slot 2

(c) Time slot 3 (d) Time slot 4

Figure 2.8: The process of sending RREQ: RREQ carries the $RREQ(a, b)$ forward to the destination H.

- **Time slot** 1 The source A broadcasts an RREQ packet to find a route to the destination H. When the RREQ packet arrives at node B, node B calculates the life-time of the link $(A - B)$, which is 10 s, as shown next to the link $(A - B)$. Meanwhile the life-time of the links $(A - C)$ and $(A - D)$ is calculated, when the

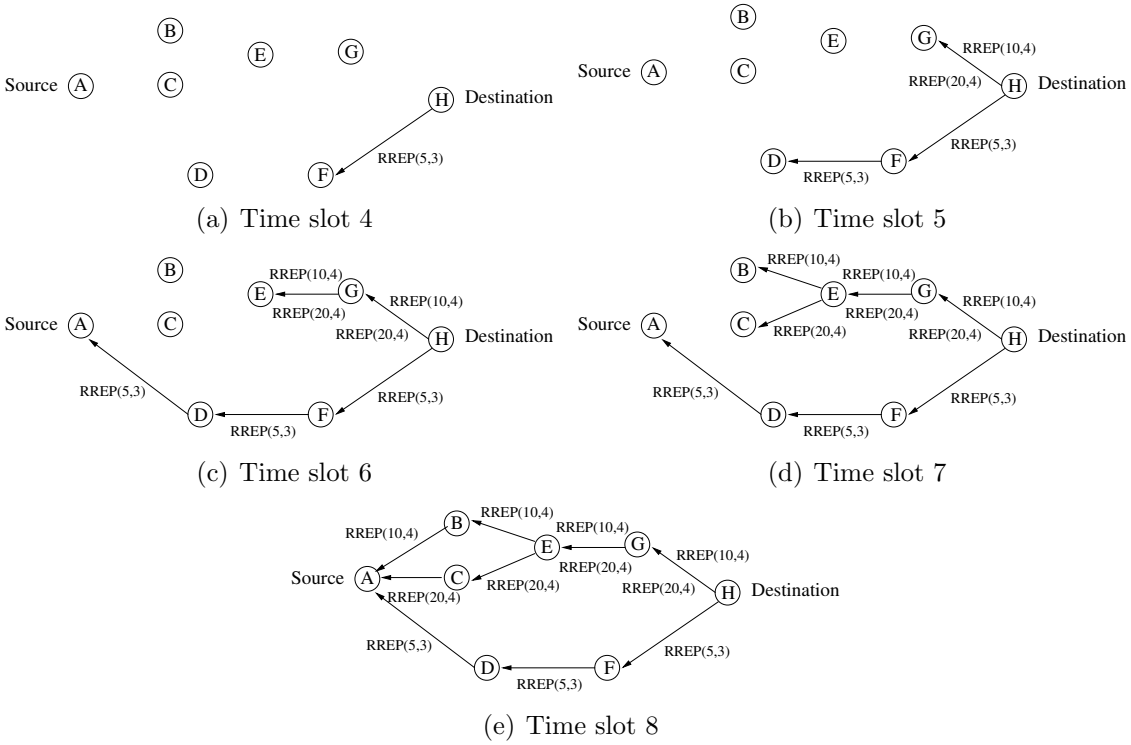

(a) Time slot 4

(b) Time slot 5

(c) Time slot 6

(d) Time slot 7

(e) Time slot 8

Figure 2.9: The process of sending RREP: RREP carries the $RREP(a, b)$ back to the source A.

RREQ packets arrive at the nodes C and D, which are 20 s and 5 s, respectively, as portrayed in Figure 2.8(a). At the same time, the number of hops at the nodes B, C and D increases by 1, respectively. Then, both the link life-time and the number of hops are stored in the RREQ packet header for future use. Hence, $RREQ(a, b)$ is used for indicating the current route life-time and the associated number of hops in the RREQ packet header, where a, b indicates the route life-time and the number of hops between the source A and the current node, respectively.

- **Time slot** 2 Afterwards, the nodes B, C and D of Figure 2.8(b) broadcast the received RREQ packet further. Then both node E and F receive the RREQ packets and calculate the predicted life-time of the links $(B - E)$, $(C - E)$ and $(D - F)$, all of which are 20 s, as seen in Figure 2.8(b). Hence, the route life-time should be updated according to Equation (2.36), which is 10 s for the route $(A - B - E)$, 20 s for the route $(A - C - E)$ and 5 s for the route $(A - D - F)$, as portrayed in Figure 2.8(b). Meanwhile, the number of hops should be updated by adding 1 as well. Then the associated contents of the RREQ packets are updated, which are $RREQ(10, 2)$, $RREQ(20, 2)$ and $RREQ(5, 2)$.
- **Time slot** 3 Then the nodes E and F broadcast the received RREQ packets further. Both node G and destination H receive the RREQ packets and calculate

the life-time of links $(E-G)$ and $(F-H)$, which are 20 s and 10 s, respectively, as seen in Figure 2.8(c). Again, the number of hops should be updated by adding 1 as well. Hence, the associated contents of the RREQ packets are updated to $RREQ(10,3)$, RREQ(20,3) and $RREQ(5,3)$. By now, the first RREQ packet has arrived at the destination H.

- **Time slot** 4 Node G broadcasts the received RREQ packets again. The destination H receives these RREQ packets and calculates the link life-time of $(G-H)$, which equals to 20 s. Then the associated contents of the received RREQ packets are updated to $RREQ(10,4)$ and $RREQ(20,4)$. By now, all RREQ packets have already arrived at the destination H, hence H will be in possession of all routing information (the route life-time and the number of hops) for each available route, as seen in Figure 2.8(d).

Observe in Figure 2.9 that for each received RREQ packet, the destination H generates an RREP packet. The route life-time and the number of hops obtained from the received RREQ packet are copied into the packet header of the newly generated RREP packet, which is denoted as $RREP(a,b)$, where a and b represent the route life-time and the number of hops spanning from the source A to the destination H in Figure 2.9. The process of sending RREQ is detailed as follows:

- **Time slot** 4 When the RREQ packet associated with the content of $RREQ(5,3)$ arrives at the destination H, H generates an RREP packet in Figure 2.9(a) for carrying $RREP(5,3)$.
- **Time slot** 5 When the RREQ packets associated with the contents of $RREQ(10,4)$ and $RREQ(20,4)$ arrive at the destination H, H generates two RREP packets in Figure 2.9(b) for carrying $RREP(10,4)$ and $RREP(20,4)$, respectively. Meanwhile, node F forwards the RREP packet to node D, which carries $RREP(5,3)$.
- **Time slot** 6 Node D forwards the received RREP packet carrying $RREP(5,3)$ to the source A. Now, source A has the knowledge of the route $A-D-F-H$ having a route life-time of 5 s, where the number of hops is $h=3$. Meanwhile, Node G forwards the received RREP packets carrying $RREP(10,4)$ and $RREP(20,4)$, respectively, to the node E, as seen in Figure 2.9(c).
- **Time slot** 7 Node E forwards the received RREP packets carrying $RREP(10,4)$ and $RREP(20,4)$ to the nodes B and C, respectively, as seen in Figure 2.9(d).
- **Time slot** 8 Nodes B and C forward the received RREP packets carrying $RREP(10,4)$ and $RREP(20,4)$ to the source A, respectively, as seen in Figure 2.9(e). Now, source A becomes aware of two routes, which are $A-B-E-G-D$ with the route life-time of 10 s, where the number of hops is $h=4$ and

$A-C-E-G-D$ with the route life-time of 20 s, where the number of hops is $h=4$. Hence, given these just generated RREP packets, both the route life-time and the number of hops is fed back to the source A along the specific route, which the RREQ packet just traversed through. Then by inputting the route life-time obtained and the number of hops extracted from the received RREP packets into the FLS, the source A becomes capable of determining which of the available routes has the highest route stability between the source A and the destination H.

Below, the processes of fuzzification, fuzzy inference and defuzzification will be discussed in more detail. Consider the route $A-C-E-G-H$ for example, where the number of hops is $h=4$. Hence the normalized number of hops is $h_{nor}=\frac{4}{19}=0.21$, where the maximum number of hops was set to $H=19$. The route life-time is $p_t=20\ s$. Then the membership functions are obtained from Equation (2.37) and Equation (2.38), which are shown in Figure 2.10 and Figure 2.11.

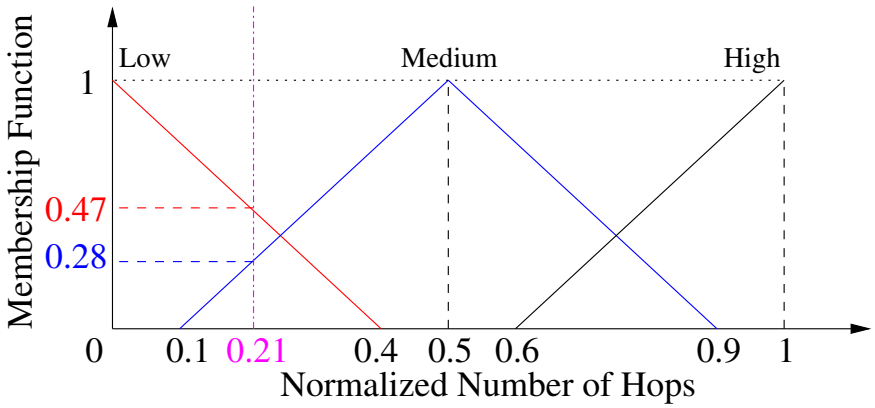

Figure 2.10: The membership function versus the normalized number of hops.

As seen in Figure 2.10, when the normalized number of hops is $h_{nor}=0.21$, the corresponding values of the membership function versus the normalized number of hops in the fuzzy sets 'Low', 'Medium' and 'High' are 0.47, 0.28 and 0, respectively. Meanwhile, as seen in Figure 2.11, when the route life-time is 20 s, the corresponding values of the membership function versus the route life-time in the fuzzy sets 'Short', 'Medium' and 'Long' are 0, 0.87 and 0.13, respectively. Then, according to the inference rules of the FLS, which are shown in Table 2.2, the output response value is calculated based on the Max-min method, which is described by Equation (2.20). Table 2.3 details how the 'IF-THEN' rules are executed. Take *Rule* 1 of the first line for example, where the number of hops input has the membership value of 0.47 as regards to belonging to the fuzzy set 'Low'. The input of the route life-time has the membership value of

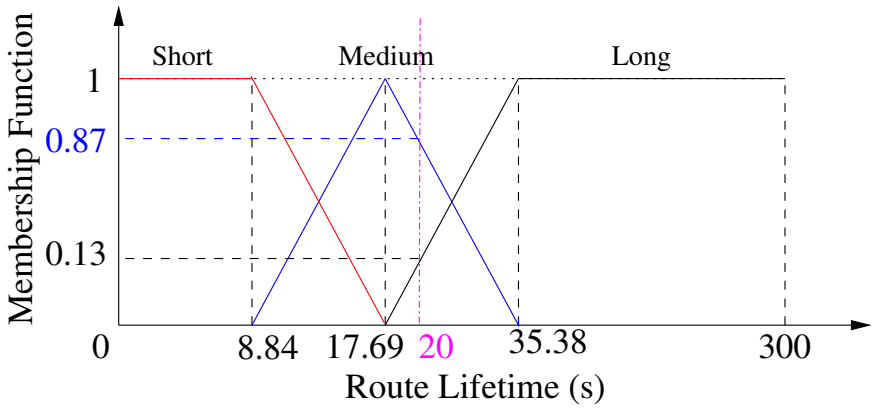

Figure 2.11: The membership function versus the route life-time (s).

Table 2.3: An example of the inference rule of Table 2.2.

No.	*NumHops*	*RouteLifetime*	*RouteStability*
1	0.47	0	$min(0.47, 0) = 0$
2	0.47	0.87	$min(0.47, 0.87) = 0.47$
3	0.47	0.13	$min(0.47, 0.13) = 0.13$
4	0.28	0	$min(0.28, 0) = 0$
5	0.28	0.87	$min(0.28, 0.87) = 0.28$
6	0.28	0.13	$min(0.28, 0.13) = 0.13$
7	0	0	$min(0, 0) = 0$
8	0	0.87	$min(0, 0.87) = 0$
9	0	0.13	$min(0, 0.13) = 0$

0 as regards to belonging to the fuzzy set 'Short', which also means that the route life-time is not 'short'. First, we execute the $\wedge$ operator of the Max-min method given in Equation (2.20) as $min(0.47, 0)$ and arrived at the route stability as 0. For *Rule* 2 of the second line in Table 2.3, the route stability is calculated as 0.47 by evaluating $min(0.47, 0.87)$, when the membership value of the number of hops is 0.47 and the membership value of the route life-time is 0.87.

Finally, according to the membership function versus the route stability, which has the same graphic shape as that versus the normalized number of hops seen in Figure 2.5, the output response value of the FLS may be categorized into its fuzzy sets of 'Low', 'Medium' and 'High'. According to the third column of Table 2.2, we know that for the route stability, both *Rule* 4 and *Rule* 7 obtain the fuzzy set of 'Low', *Rule* 1, *Rule* 5 and *Rule* 8 obtain the fuzzy set of 'Medium', whilst *Rule* 2, *Rule* 3, *Rule* 6 and *Rule* 9 obtain the fuzzy set of 'High' after the process of inference. Then, by executing the *max* operator of the Max-min method in Equation (2.20) we may arrive at:

- degree of 'Low' = $max(Rule\,4, Rule\,7) = max(0, 0) = 0$, which is defined as d^l;

Table 2.4: Route stability.

No.	*Hops*	*RouteLifetime*	*RouteStability*
1	4	10	0.42
2	4	20	0.81
3	3	5	0.40

- degree of 'Medium' $= max(Rule\,1, Rule\,5, Rule\,8) = max(0, 0.28, 0) = 0.28$, which is defined as d^m;
- degree of 'High' $= max(Rule\,2, Rule\,3, Rule\,6, Rule\,9) = max(0.47, 0.13, 0.13, 0) = 0.47$, which is defined as d^h;

As mentioned at the beginning of this section, the route stability is normalized to the range of $[0, 1]$. Then the center point c^l of the fuzzy set 'Low' is 0, the center point c^m of the fuzzy set 'Medium' is 0.5 and the center point c^h of the fuzzy set 'High' is 1. Then based on Equation (2.14), the defuzzification process is exemplified as:

$$\begin{aligned} z^* &= \frac{c^l \cdot d^l + c^m \cdot d^m + c^h \cdot d^h}{d^l + d^m + d^h} \\ &= \frac{0 \cdot 0 + 0.28 \cdot 0.5 + 0.47 \cdot 1}{0 + 0.28 + 0.47} \\ &= 0.81, \end{aligned} \tag{2.39}$$

where 0.81 is the stability of the route $A - C - E - G - H$. The stability of the route $A - B - E - G - H$ and of the route $A - D - F - H$ may be calculated in a similar way. Table 2.4 shows the stability of all routes, which were found during the route discovery.

Apparently, Route 2 ($A-C-E-G-H$) of Table 2.4 has the highest route stability, which is 0.81. Therefore Route 2 is selected by source A for transmitting its DATA packets, as seen in Figure 2.12.

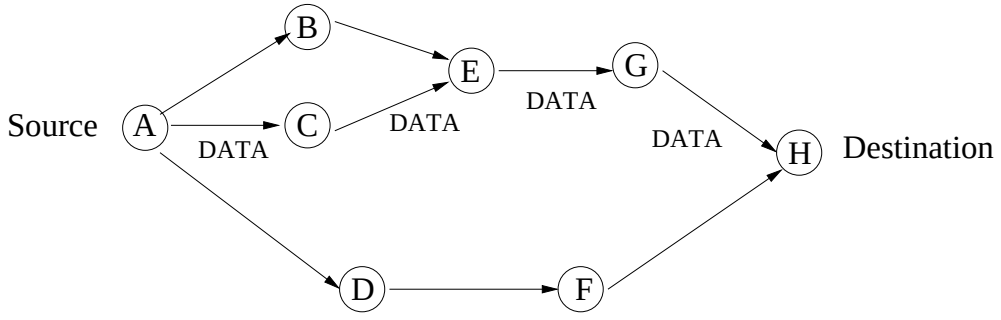

Figure 2.12: The process of sending DATA: DATA is forwarded according to the route 2 (A-C-E-G-H).

2.6 Performance Study

In this section, the achievable performance of the proposed FL-DSR and the conventional DSR for three different physical layer schemes are compared, namely for a perfect channel, for uncoded-QPSK and for TTCM-8PSK [51, 52, 94].

Strong coding and modulation schemes perform well in time-variant wireless channel scenarios in terms of the attainable BER or FER performance, which may influence the performance of the upper layers. Hence, first we employed OMNeT++ [45] for creating a simulation environment in order to compare the BER and FER performance of uncoded-QPSK and TTCM-8PSK. The two nodes considered were located in a 500×500 m^2 square-shaped field. The distance between them was 100 m. By appropriately adjusting the receive SNR, we recorded the BER and FER versus SNR relationship. The BER of uncoded-QPSK was calculated from the theoretical Q-function based formula [51], while for TTCM-8PSK we used a pre-computed lookup table for the Additive White Gaussian Noise (AWGN) channel in order to generate the BER based on both the SNR and on the length of the turbo-interleaved frame. The generator polynomial used by the TTCM constituent code was $[11\ 2\ 4]_8$ in octal representation. Four iterations were invoked in the TTCM decoder. The interleaved frame size of the physical layer was varied from 100 bits to 6000 bits. The simulation results suggested that for an SNR of about 7.5 dB, the BER of TTCM-8PSK was 10^{-5} and the FER was 10^{-2}, while uncoded-QPSK required an SNR of about 12.5 dB for a BER of 10^{-5} and an FER of 10^{-2}, as seen in Figure 2.13 and Figure 2.14. This implies that TTCM-8PSK has a nearly 5 dB gain compared to uncoded-QPSK at a BER of 10^{-5} and an approximately 5.5 dB gain compared to uncoded-QPSK at a FER of 10^{-2}, although naturally this gain is achieved at the cost of an increased implementational complexity.

Then we considered a complex simulation environment, where 20 nodes were located in a $(500m \times 500m)$ square-shaped field with 5 nodes allocated in each row and 4 nodes in each column. The source node was stationary at position $(499, 499)$, and the destination node was fixed at position $(0, 0)$. The other configurations are listed in Table 2.5.

For the sake of excluding the packet dropping events due to buffer overflow, the queue length in the data link layer is set to be infinite. We also assumed that no interference existed amongst the nodes and that both the control packets as well as the physical layer header were received without errors. Except for the source node and destination node, all other nodes obeyed the mass mobility model, where the speed and the direction of each node was chosen randomly. We compared the performance of the proposed FL-DSR and conventional DSR, when the thermal noise P_N was -92 dBm,

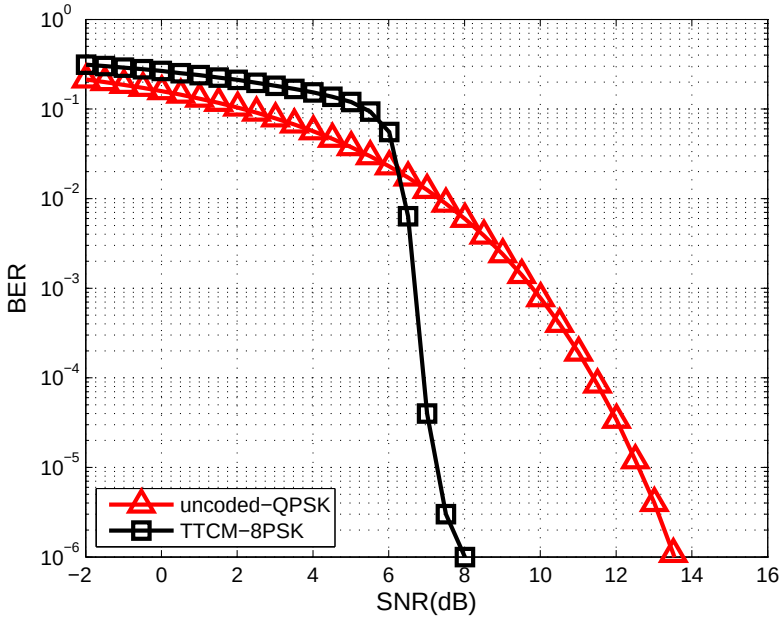

Figure 2.13: BER vs. SNR for transmission over an AWGN channel, when employing uncoded-QPSK and TTCM-8PSK.

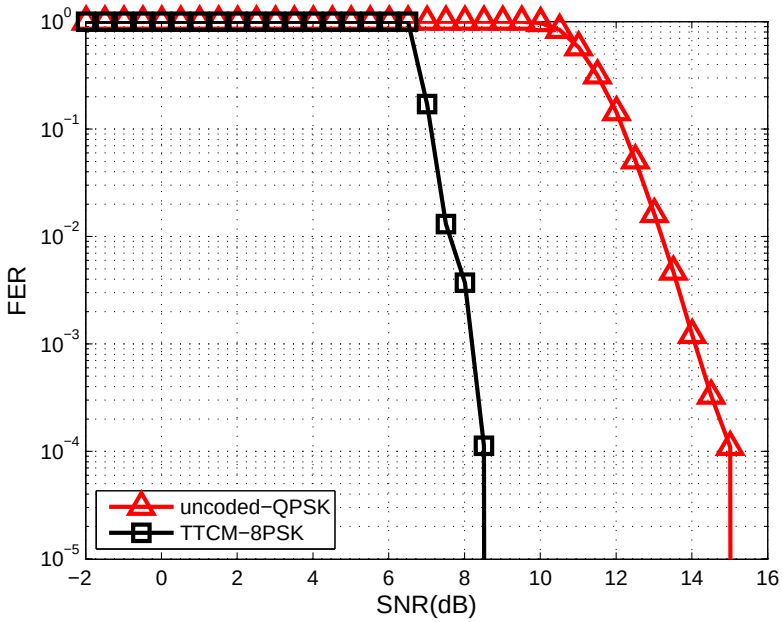

Figure 2.14: FER vs. SNR for transmission over an AWGN channel, when employing uncoded-QPSK and TTCM-8PSK.

Table 2.5: System parameters employed for generating the results of Figures 2.15, 2.16 and 2.17.

Network scenario	$500m \times 500m$
Application layer	5 packets/s with frame length of 512 Bytes
Transport layer	UDP
Network layer	IPv4, DSR
Data link layer	802.11b
Physical layer	'perfect', QPSK, TTCM-8PSK
Channel	AWGN + Free-space Path Loss
Transmit power	1 mW
Noise power	−92 dBm
Sensitivity threshold[a]	−85 dBm
SNR threshold	4 dB
Information rate	2 Mbits/s
Simulation time	40 seconds
Number of Simulation runs	100

[a] The receive sensitivity threshold is used to judge whether the received signal is deemed to be noise, because a signal with received power less than the sensitivity level is deemed to be noise.

and again, the uniformly distributed random mobile speed was $0 - 10$ m/s. The following performance metrics were compared as follows:

- Normalized Number of Route Breakage Events [95]: Every time when the data was not successfully forwarded to the next hop, the link between the two nodes was assumed to be broken and the number of route breakage events was increased by one. We normalized the number of route breakage events by the average number of hops;
- Network Throughput [96]: The number of data bits received at the destination per second in the network layer;
- The Reciprocal Network Control Load [96]: The number of data bits successfully delivered to the destination per the number of control bits transmitted, which may be viewed as the reciprocal of the number of control bits associated with the delivery of a data bit. The control bits include the bits of all routing packets and the header bits in all data packets. Each hop-based transmission of the control bits was counted.

Observe from Figure 2.15, 2.16, and 2.17 that upon increasing the mobile speed, both the FL-DSR and the conventional DSR relying on the three different physical layer schemes exhibit similar trends in terms of the number of route breakage events, network throughput and network control load. However in Figure 2.15, the number of route breakage events of uncoded-QPSK first decreases, then increases because the node mobility may allow the nodes to avoid idling in a deep fade, which is more clearly

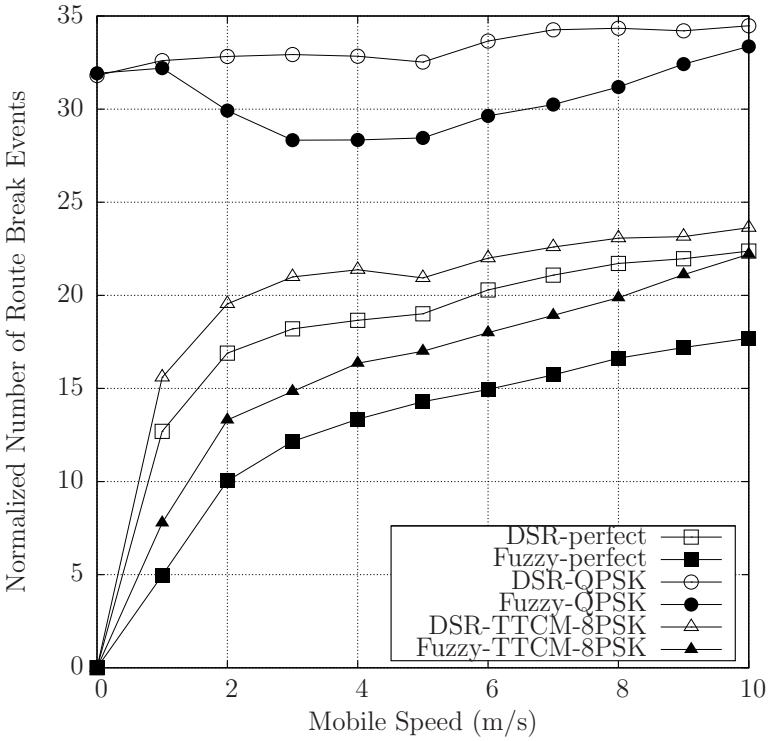

Figure 2.15: The normalized number of route breakage events versus node speed for 20 nodes.

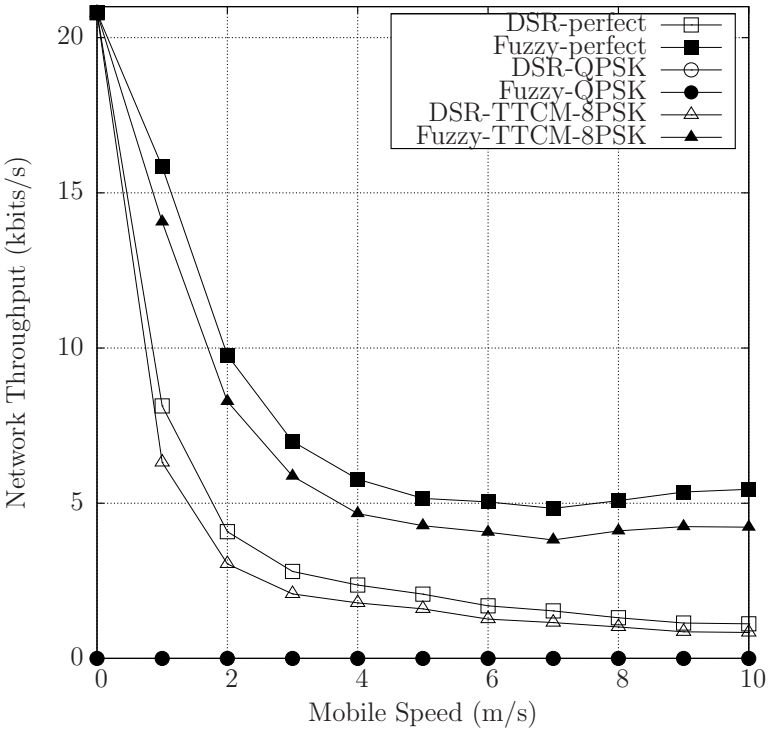

Figure 2.16: The achievable network throughput of different physical layer configurations for 20 nodes.

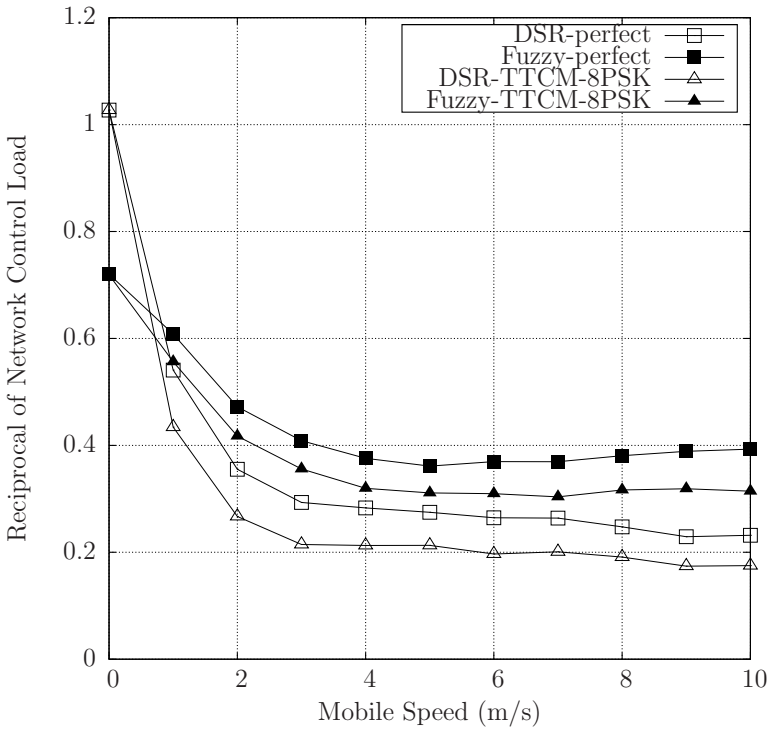

Figure 2.17: The comparison of the reciprocal of network control load.

visible for the FL-DSR scenario. FL-DSR scheme has a lower number of route breakage events and a higher overall network throughput.

As for the network control load characterized in Figure 2.17, it is observed that when the mobile speed is low, possibly 0 m/s, the FL-DSR imposes a higher network control load than the conventional DSR, because the former has to record the mobility status in the RREQ, RREP and SR packets, thus the number of control bits increases. By contrast, as seen in Figure 2.17, when the mobile speed is higher than 1 m/s, the negative impact of the extra control bits in the control packets and data packets has been mitigated by the increased node mobility, and as a result, the network control load of the FL-DSR becomes lower than that of conventional DSR. The reason for this phenomenon is that the FL-DSR always chooses the specific route having the highest route stability, which is loosely defined as the route having the highest resilience against any changes in the network's topology. If the number of route breakage events decreases, then naturally, the number of data packets delivered to the destination increases, thus the probability of activating new route discovery processes decreases, hence the number of control packets transmitted also decreases.

Naturally, TTCM-8PSK performs worse than an idealized perfect channel, since it requires an SNR of 7.5dB for maintaining a BER of 10^{-5}, hence the data packets may suffer from bit errors. Uncoded-QPSK performs even more poorly, since it necessitates an SNR of 12.5dB for maintaining a BER of 10^{-5}, as shown in Figure 2.13, hence

virtually, no data is delivered to the destination node successfully in the scenario considered. The number of route breakage events is high and the network throughput is close to zero, hence the reciprocal of the network control load is also close to zero. Therefore TTCM-8PSK outperforms uncoded-QPSK in terms of its network layer performance, which underlines that the suitable configuration of the physical layer is vitally important for achieving a desirable network layer performance.

2.7 Chapter Conclusions

In Section 2.2, we first introduced the basic concepts of fuzzy logic theory, such as fuzzy sets, fuzzy relations, membership functions, fuzzifications, inference rules and defuzzifications. Then we presented the structure of the basic FLS seen in Figure 2.3. Considering the detrimental influence of node mobility on the achievable system performance, Section 2.3 introduced various commonly used mobility models, such as the null mobility model, the linear mobility model, the circular mobility model, the rectangular mobility model, the constant speed mobility model, the random waypoint mobility model and finally, the mass mobility model. In Section 2.4 we proposed a link-life-time prediction model, which calculated the link-life-time of a pair of adjacent nodes based on their mobility status, which included their current position, current speed and current traveling direction. The link-life-time model enables us to predict the life-time of the entire route, as detailed in Section 2.5. More explicitly, Section 2.5 first discussed the conventional DSR protocol, which always made its routing decisions based on the number of hops within a route. Hence, the DSR protocol might not perform well in high-mobility environments. Therefore we exploited that a FLS has the advantage of resolving decision dilemmas, even when its inputs are constituted by inaccurate information. Hence, a FL-DSR protocol was proposed in Section 2.5, which jointly considered the number of hops as well as the route's life-time for the sake of striking a trade-off between them. Our FL-DSR protocol carried out its routing decisions based on the so-called 'route stability', which enables us to achieve performance improvements in mobile scenarios compared to the conventional DSR protocol, as demonstrated in Section 2.6.

To elaborate a little further, in Figures 2.13 and 2.14 of Section 2.6 we first discussed the BER and FER performance of uncoded-QPSK and TTCM-8PSK in an AWGN channel, which was additionally subjected to free-space path loss. It was demonstrated in Figures 2.13 and 2.14 that TTCM-8PSK has a nearly 5 dB gain compared to uncoded-QPSK at a BER of 10^{-5} and 5.5 dB gain at an FER of 10^{-2}. Then in Figures 2.15 - 2.17 we compared the performance of the FL-DSR protocol and of the conventional DSR protocol under the employment of uncoded-QPSK, TTCM-8PSK

and the idealized benchmark scheme relying on a perfect channel in the physical layer. It was demonstrated in Figures 2.15 - 2.17 that the FL-DSR protocol outperforms the conventional DSR protocol in terms of the normalized number of route breakage events, as well as in terms of the network throughput and network control load in mobile scenarios. However, the FL-DSR protocol imposed a higher network control load than the conventional DSR protocol in stationary scenarios, because the former has to record the mobility status in the RREQ, RREP and SR packets. Quantitatively, when the mobile speed is 4 m/s, it was shown that the FL-DSR protocol reduced the normalized number of route breakage events by 23.5%, the network control load by 42.9% and the network's throughput by 100%.

In the following chapters we will focus our attention on the energy consumption of *ad hoc* networks. Chapter 4 will also consider the trade-offs between the energy consumption and the achievable network throughput, while Chapter 3 will quantify the benefits of using multiple antennas and Chapter 5 will consider the benefits of the Opportunistic Routing (OR).

Chapter 3

Energy-Efficient Relay Node Aided Ad Hoc Networks Using Irregular Convolutional Coded, Unity-Rate Coded and Space-Time Trellis Coded Transceivers

The number of hops required for reaching the destination is a popular metric, which is commonly used in the network layer for making routing decisions [40–42]. However, maintaining a low number of hops cannot guarantee a good system performance, especially, when aiming for satisfying specific requirements, such as a high network throughput and a low energy consumption. This is even more of a challenge in high-mobility environments. Hence, in Section 2.5 we have employed the so-called 'route stability' as our routing metric, which was a specific feature of our Fuzzy Logic System (FLS) aided solution. The proposed Fuzzy-Logic-aided Dynamic Source Routing (FL-DSR) protocol of Section 2.5 was shown to be more efficient in terms of improving the network's throughput in Figure 2.16 than the conventional DSR protocol of Subsection 1.2.1. However, we have not considered the energy consumption in Chapter 2. Hence in this chapter we aim for minimizing the energy consumption by the joint optimization of both the physical and network layers with the assistance of Multiple-Antenna Aided Relay Nodes (MA-RN), as shown in the system model of Figure 3.1. Although our routing metric in this chapter is still the number of hops, the employment of MA-RNs assists in reducing the potential number of hops from the source to the destination, when dissipating a given transmit power at each node. Therefore MA-RNs are capable of reducing the entire system's energy consumption.

The influence of the number of MA-RNs in a system will be studied in Section 3.3. Both the perfect capacity-achieving coding abstraction and a realistic near-capacity coding scheme, namely a three-stage-concatenated Irregular Convolutional Coded, Unity-Rate Coded and Space-Time Trellis Coded (IrCC-URC-STTC) arrangement is employed in the physical layer. The IEEE802.11b regime [7] is used in the data link layer. In the network layer, the more efficient DYnamic Manet On-demand (DYMO) routing protocol [42] is employed, which replaces the DSR protocol [40] employed in Chapter 2, because the DYMO routing protocol imposes a lower network control load and it is more flexible in a high-mobility environment. However, the scenario considered in this chapter is still a stationary scenario. The investigation of high-mobility scenarios was set aside for future study. The User Datagram Protocol (UDP) [97] is employed in the transport layer and Constant Bit Rate (CBR) data streaming is used in the application layer. The channel model employed is an Additive White Gaussian Noise (AWGN) channel subjected to both inverse-second-power free-space path loss and to uncorrelated Rayleigh fading.

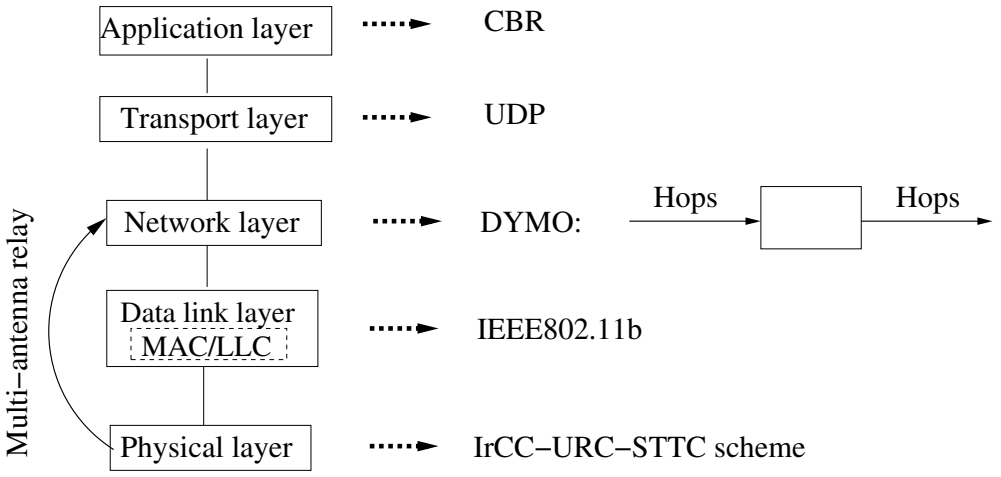

Figure 3.1: System model of the energy-efficient RN aided *ad hoc* networks considered.

3.1 Introduction

Energy-efficient wireless network design has recently attracted wide-spread research attention [98]. Diverse error-resilient Forward Error Correction (FEC) schemes were proposed in [99] for achieving a low Bit Error Ratio (BER) at near-capacity Signal-to-Noise Ratio (SNR) values. Therefore, the effective transmission range can be improved, when the required received signal power is reduced. Again, a novel DC-IrCC-URC-STTC scheme has been proposed for cooperative communications in [100]. Several

Single-Antenna RNs (SAs) were activated between the source and the destination. The RNs roaming closest to their optimal locations were activated based on a novel technique relying on EXtrinsic Information Transfer (EXIT) charts [101] in conjunction with near-capacity code design principles, which were detailed for example in [102].

Numerous power-aware routing protocols were proposed in [103] for improving the energy efficiency from a multiuser networking perspective. Moreover, cross-layer optimized power control has been widely exploited [104–109] for maintaining the required target-integrity at a low power in realistic propagation environments. A physical-layer-oriented routing protocol supported by sophisticated power control was proposed in [104] for a Line-Of-Sight (LOS) and shadow faded scenario, where the estimated end-to-end BER of a multi-hop path was used as the route selection metric. Furthermore, an adaptive relaying strategy switching between the Amplify-and-Forward (AF) and the Decode-and-Forward (DF) schemes was proposed in [105] for reducing both the energy consumption as well as the delay of the system. As a further design dilemma, the influence of the 'small number of long hops' versus the 'many short hops' philosophy on the energy consumption was studied in [106–108]. It was indicated in [106] that the 'small number of long hops' routing scheme was better than the 'many short hops' routing scheme provided that near-capacity coding strategies combined with a relatively short block length were employed, because a substantial SNR loss was exhibited by the 'many short hops' based routing scheme. Moreover, it was demonstrated in [107] that 'many short hops' perform well in energy-limited scenarios relying on spatial reuse, even in the absence of interference cancellation, while using a 'small number of long hops' is more suitable for bandwidth-limited scenarios. Therefore, the routing algorithms should be carefully designed, when jointly considering both the achievable energy-efficiency and the attainable bandwidth-efficiency. The tradeoffs between energy- and bandwidth-efficiency were studied in [108], where it was found that at high end-to-end data rates the routes associated with fewer hops minimize the energy consumption, while at lower end-to-end data rates the routes having more hops mitigate it.

Against this backdrop, *the novel contributions of this chapter are*

- *A near-capacity IrCC-URC-STTC transceiver is designed for multiple-antenna-relaying aided ad hoc networks, which is shown to reduce the network's total energy-consumption.*
- *This is achieved with the aid of sophisticated cross-layer-operation aided routing, where the routes are set up on the basis of using the lowest number of potentially longer hops, which become sufficiently reliable as a benefit of the powerful near-capacity IrCC-URC-STTC relay-transceivers.*

To elaborate a little further, the benefits of MA-RNs in *ad hoc* networks in terms of the attainable energy efficiency are characterized. The MA-RNs are assisted by the Quadrature Phase-Shift Keying (QPSK) based IrCC-URC-STTC scheme proposed in [100], while the SA-RNs employ an 8-ary Phase-Shift Keying (8PSK) based IrCC-URC scheme. The introduction of the MA-RNs influences the route selection. More specifically, MA-RNs allow to reduce the number of hops required as a benefit of their higher effective transmission range at a given transmit power compared to SA-RNs systems. Simulations are conducted for investigating the influence of both the number of MA-RNs and that of the node density on the energy consumption of the entire network. As the ultimate benchmark scheme, the Discrete-input Continuous-output Memoryless Channel's (DCMC) capacity [51] is considered.

The rest of the chapter is organized as follows. In Section 3.2, the IrCC-URC-STTC scheme and routing strategy are detailed. In Section 3.3, various practical scenarios are analyzed, leading to the conclusions in Section 3.4.

3.2 Theoretical Analysis

The influence of different coding and modulation schemes on the upper layer performance was investigated in Section 2.6, which shows that the beneficial configuration of the physical layer schemes would also improve the network layer performance. According to the system model of Figure 3.1, in this section we will further demonstrate how powerful near-capacity coding schemes affect the routing strategy and hence reduce the energy consumption of the entire system.

3.2.1 Near-Capacity Coding Schemes

Using a large constellation size has the potential of increasing the attainable throughput, while strong coding schemes are capable of reducing the transmit power required for achieving a given BER at the cost of a bandwidth expansion, which is proportional to the reciprocal of the coding rate. By contrast, joint coding and modulation schemes are capable of reducing the required transmit power even without a bandwidth expansion, which is achieved by expanding the modulated signal constellation for the sake of absorbing the parity bits of channel coding. Irregular Convolutional Codes (IrCCs) [110] are constituted by a family of convolutional codes, which use different code-rates for encoding the 'appropriately selected fractions' of the input stream. These IrCCs are employed as the outer code of the serial-concatenated transceiver scheme, since they are capable of approaching the channel capacity [110, 111]. The 'appropriately selected fractions' are determined using the procedures proposed in [112] and detailed in [102] by exploiting the fact that a low BER may be achieved by the IrCC at SNRs near the channel capacity, when its EXIT-chart exhibits an open but

narrow tunnel. Furthermore, as also detailed in [102], for the sake of guaranteeing a low BER and low Frame Error Ratio (FER), an infinite impulse response recursive Unity-Rate Code (URC) should be employed as an intermediate code in order to ensure that the three-stage concatenated scheme indeed becomes capable of reaching the $(1, 1)$ point of perfect convergence to a low BER in the EXIT chart [112]. The Space-Time Trellis Code (STTC) employed is a Multi-Input Multi-Output (MIMO) arrangement, which is capable of achieving both coding gain and spatial diversity gain [102, 113]. The multiplexing gain provides an increased data rate, while the diversity gain allows us to achieve a reduced BER in fading channels. As a result, the IrCC-URC-STTC coding scheme advocated is capable of approaching the DCMC capacity of the SA-RN aided cooperative system [100]. In this chapter, the pair of SA-RNs designed for the cooperative system of [100] is replaced with a single MA-RN and it is demonstrated that the IrCC-URC-STTC scheme is capable of approaching the DCMC link's capacity derived for MA-RN aided MIMO systems.

We assume that each MA-RN is equipped with two antennas. If more than one MA-RN exist in the multi-hop *ad hoc* network considered, then four different types of links may appear. Specifically, there exists the SA-RN to SA-RN, SA-RN to MA-RN, MA-RN to SA-RN and finally the MA-RN to MA-RN links. All the MA-RNs employ the above-mentioned QPSK-assisted IrCC-URC-STTC scheme, while all the SA-RNs employ the 8PSK-assisted IrCC-URC scheme.

First, the attainable FER performance of all the four links is analyzed, assuming that they are capable of approaching the FER recorded for an uncorrelated Rayleigh fading channel [51]. In contrast to the DCMC capacity, the capacity of the Continuous-input Continuous-output Memoryless Channel (CCMC) C_{CCMC} recorded for the uncorrelated Rayleigh fading channel [51] is given by:

$$C_{CCMC} = E\left[\frac{N_d}{2}\log_2(1 + |h_c|^2 SNR)\right], \tag{3.1}$$

where the expectation $E[\cdot]$ is computed by employing the Monte Carlo averaging method. Furthermore, N_d represents the dimension of the corresponding additive noise vector and h_c is the fading coefficient. However, the capacity of the DCMC depends on the number of modulation levels M_l. The Single-Input Single-Output (SISO) DCMC capacity C_{DCMC} is given by [114]:

$$C_{DCMC} = \log_2(M_l) - \frac{1}{M_l}\sum_{m=1}^{m=M_l} E\left[\log_2 \sum_{z=1}^{z=M_l} \exp(\psi_{m,z})|X_m\right], \tag{3.2}$$

where $E[A|X_m]$ is the expectation of A conditioned on the M_l-ary signals X_m. Note

that $\psi_{m,z}$ is a function of both the transmitted signal and of the channel as defined in [114], which is formulated as

$$\psi_{m,z} = \frac{-|h_c(x_m - x_z) + n_{c_m}|^2 + |n_{c_z}|^2}{N_0}, \tag{3.3}$$

where x and n_c are the transmitted signal and the AWGN, respectively, while N_0 is the thermal noise power spectral density. Hence the corresponding receive SNR value ($SNR_r|_{BPS}$) for a given Bits Per Symbol (BPS) throughput from the DCMC capacity curve computed using Equation (3.2) are readily found. The calculation of the DCMC capacity of the Single-Input Multi-Output (SIMO), Multi-Input Single-Output (MISO) and Multi-Input Multi-Output (MIMO) links can also be found in [114]. If the $SNR_r|_{BPS}$ is higher than the SNR threshold of the corresponding capacity curve, the FER tends to 0, otherwise it tends to 1. In this chapter, since the packet's length is varied from 100 to 10 000 bits, for the sake of comparing the DCMC capacity and IrCC-URC-STTC scheme under fair conditions, we define p^L_{DCMC} as the FER performance of an ideal/perfect coding scheme operating at the DCMC capacity associated with a certain frame length of L, which is formulated as:

$$p^L_{DCMC} = p_r(SNR_{average} > SNR_r), \tag{3.4}$$

where SNR_r represents the receiver's SNR, which is determined by finding the specific SNR value on the capacity curve corresponding to the DCMC of the SISO scheme considered in Equation (3.2) and those of the SIMO, MISO and MIMO arrangements characterized in [114]. Additionally, $SNR_{average}$ represents the average receive SNR of L channel fading samples, which is given by:

$$SNR_{average} = SNR_t + 10\log\left(\sum_{l=0}^{L-1}\sum_{i=0}^{T_x-1}\sum_{j=0}^{R_x-1}\frac{\parallel h_{c_{i,j}} \parallel^2}{L}\right), \tag{3.5}$$

where SNR_t indicates the transmit SNR [115][1] and ($\sum_{l=0}^{L-1}\sum_{i=0}^{T_x-1}\sum_{j=0}^{R_x-1}\frac{\|h_{c_{i,j}}\|^2}{L}$) is the average value computed from the channel coefficients $h_{c_{i,j}}$ representing the channel of the system employing T_x transmit antennas and R_x receive antennas. For example, the FER performance of all the four links at the frame length of 1500 bits characterized by the DCMC-capacity and that of the IrCC-URC-STTC scheme is portrayed in Figure 3.2. It can be observed that the IrCC-URC-STTC scheme performs close to the

[1]Transmit SNR is defined as the ratio of the transmit signal power to the thermal noise power, which is unconventional, since it relates two quantities to each other, which are measured at different points. However, it is convenient, because the receiver's SNR may vary due to the instant channel condition.

DCMC-capacity based scheme at a given SNR value. Meanwhile, the $IrCC_{2\times2}$ scheme has a 5 dB gain compared to $IrCC_{2\times1}$ or $IrCC_{1\times2}$ arrangements and has a nearly 10 dB gain compared to the $IrCC_{1\times1}$ scheme at an FER of 10^{-5}, where $IrCC_{T\times R}$ represents the IrCC-URC-STTC scheme and the subscript '$T \times R$' indicates having T transmit and R receive antennas. Hence, for the sake of guaranteeing the same FER performance, $IrCC_{2\times2}$ exhibits a larger transmit range at a given transmit power and may hence potentially reduce the number of hops required for conveying a message from the source to the destination, which can be explained by analyzing the calculation of the transmission range. More explicitly, the average maximum transmission range is defined as the range, over which the receiver node is capable of receiving a transmitted packet with $FER < 10^{-5}$.

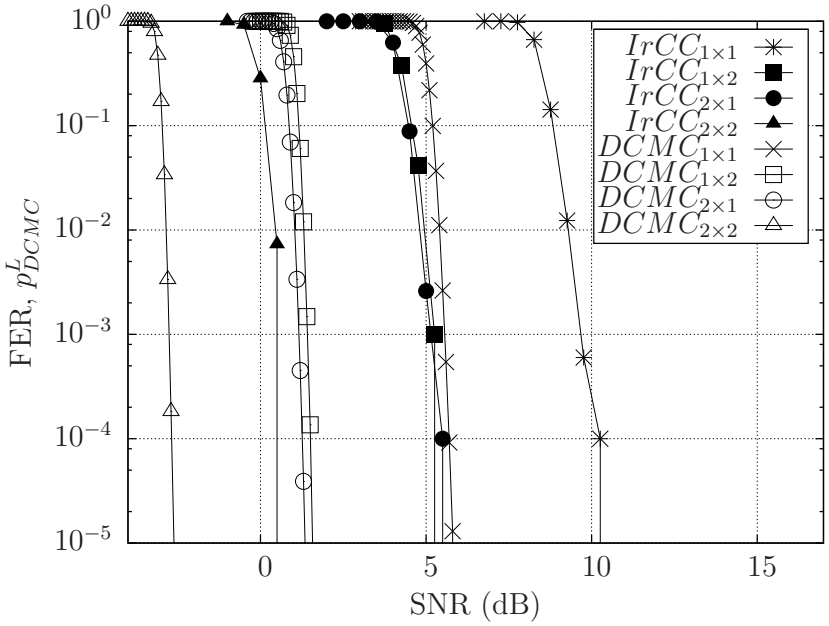

Figure 3.2: FER performance of the four types of links, for example at the frame length of 1500 bits, of the uncorrelated Rayleigh fading channel for DCMC-capacity-based scheme and the IrCC-URC-STTC scheme, where $DCMC_{T\times R}$ represents the DCMC-capacity-based scheme, and $IrCC_{T\times R}$ represents the IrCC-URC-STTC scheme. Additionally, the subscript '$T\times R$' represents having T transmit antennas and R receive antennas.

The inverse second-power free-space path loss law [5] and an uncorrelated Rayleigh fading channel model [116] are considered in this chapter. The received signal power P_r can be formulated as [5]

$$P_r = P_t \left(\frac{\sqrt{G_l}\lambda}{4\pi d} \right)^2 E\left[\| \mathbf{H} \|^2 \right], \tag{3.6}$$

where p_t is the transmitted power, $\sqrt{G_l}$ is the product of the transmit and receive antenna gains in the LOS direction, $\mathbf{H}$ is the matrix of Channel Impulse Responses (CIRs) having a dimension determined by the number of transmit and receive antennas, d is the average distance from the transmitter and λ is the carrier's wavelength. We assume $\sqrt{G_l} = 1$, $E\left[\| \mathbf{H} \|^2\right] = 1$ and $\lambda = c/f$, where c is the speed of light in vacuum and f is the carrier frequency. Hence, we have

$$d = \sqrt{\frac{P_t}{P_r}} \frac{\lambda}{4\pi}. \tag{3.7}$$

The receive signal-to-noise ratio is calculated in dB as

$$SNR_{dB} = 10 \log_{10} \left(\frac{P_r}{N_0} \right), \tag{3.8}$$

where N_0 is the thermal noise power and $N_{0dB} = 10 \log_{10} N_0$. Then the received signal power P_r may be expressed as

$$P_r = 10^{\frac{SNR_{dB} + N_{0dB}}{10}}. \tag{3.9}$$

According to Equation (3.8), we may calculate the required minimum signal-to-noise ratio SNR^*_{dB} from the minimum receive power P^*_r expressed in dBm as follows

$$SNR^*_{dB} = 10 \log_{10} \left(\frac{P^*_r}{N_0} \right). \tag{3.10}$$

Hence, given the above-mentioned parameters of P_t and SNR^*_{dB}, the average maximum distance d_{max} from the transmitter, where the SNR requirement SNR^*_{dB} may 'just' be satisfied to guarantee $FER < 10^{-5}$, is given by

$$d_{max} = \frac{\sqrt{P_t}\lambda}{4\pi 10^{\left(\frac{SNR^*_{dB} + N_{0dB}}{20} \right)}}. \tag{3.11}$$

Naturally, if the value of p_t and N_{0dB} are fixed, then it may be readily seen how the adequately 'illuminated' distance, where the required target-FER may be maintained, will vary as a function of the SNR value. As seen from Figure 3.2, the maximum adequately covered communication distance from MA-RN to MA-RN is the highest, while that from SA-RN to SA-RN is the lowest. Conversely, if p_t and d are fixed, then the FER is the lowest for the MA-RN to MA-RN link, while it is the highest for the SA-RN to SA-RN link.

3.2.2 Routing Algorithms

It was shown in [100] that the IrCC-URC-STTC scheme is capable of operating near the link's capacity, hence a substantial power saving may be attained. When this scheme is employed by the MA-RNs of the *ad hoc* network considered, the different error correction capability of the four different types of links will influence the routing strategy. Figure 3.3 provides an example on how the routing strategy is influenced, as detailed below.

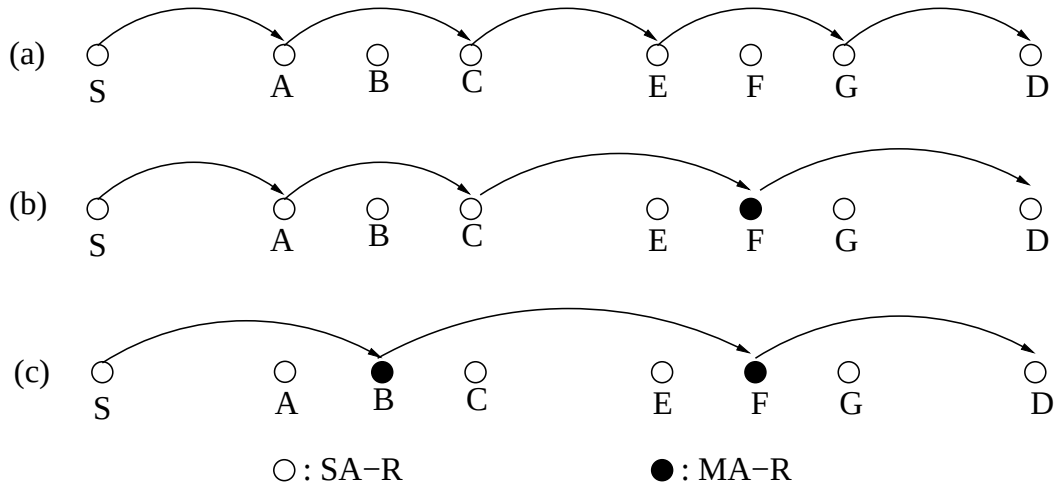

Figure 3.3: The influence of MA-RNs on the routing strategy: (a)$L_h = 5$ hops without MA-RNs; (b)$L_h = 4$ with 1 MA-RN at point F; (c)$L_h = 3$ with 2 MA-RNs at points B and F.

As seen from Figure 3.3, the network consists of $N = 8$ nodes, where S is the source and D is the destination. In Figure 3.3(a), all nodes are equipped with a single antenna, hence all links are SA-RN to SA-RN links, which yields $L_h = 5$ hops from S to D. A single MA-RN is employed at point F in Figure 3.3(b), where the packets arriving at node C are directly transmitted to node F. Then, node F will forward its received packets further to the destination D. More specifically, the C-to-F link is a SA-RN to MA-RN link, while the F-to-D link is an MA-RN to D link, where the $F - D$ distance is higher than that between the single-antenna nodes of Figure 3.3(a). Consequently, the number of hops from S to D is decreased to $L_h = 4$. In Figure 3.3(c), two MA-RNs, namely B and F, are employed. The number of hops is further decreased to $L_h = 3$ as a benefit of using MA-RNs for nodes B and F.

This chapter employs the DYMO routing protocol in the network layer, which combines most of the benefits of the Ad-hoc On-demand Distance Vector (AODV) [41] and DSR [40] protocols. The DYMO routing protocol always opts for the specific route having the lowest number of hops to the destination. When employing the MA-RN aided IrCC-URC-STTC scheme, it will be demonstrated that the route selected may

be expected to have a further reduced number of hops. The DYMO routing protocol is constituted by two main stages, namely the route discovery and route maintenance. During the route discovery, the Route REQuest (RREQ) and the Route REPly (RREP) packets are used for identifying a route from the source to the destination. By contrast, during the route maintenance phase, a Route ERRor (RERR) packet is returned to the source, when a broken link is detected. Figures 3.4, 3.6 and 3.5 show the process of route discovery and route maintenance for the DYMO routing protocol as well as for the data transmission process, which assisted us in analyzing the total energy consumption of the system. The topology considered in Figures 3.4, 3.6 and 3.5 has a source S, a destination D and the pair of RNs B and F. It is assumed that each node is only capable of communicating with its neighbour nodes. For example, node B can only communicate with node S and node F, while it cannot communicate with node D. The exchange of the control packets between the neighbour nodes, such as the exchange of the RREQ packet, RREP packet and RERR packet, and the associated data transmission process is detailed as follows:

- Route discovery process of Figure 3.4:

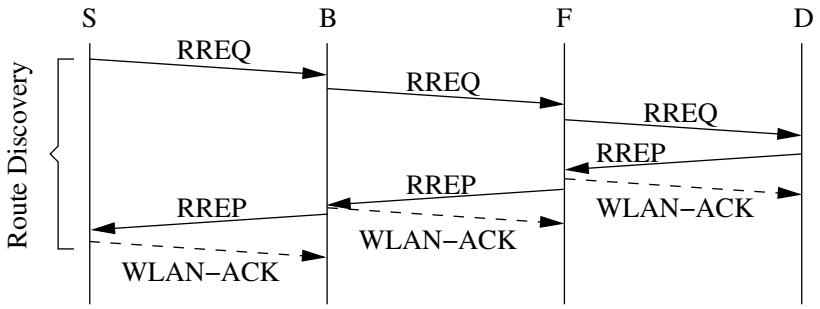

Figure 3.4: The process of **route discovery** in the DYMO routing algorithm.

As seen in Figure 3.4, first the source S broadcasts an RREQ packet and when node B receives this RREQ packet, it broadcasts it. Then node F receives the RREQ packet and broadcasts it again. Finally, the destination D receives the RREQ packet, which originated from the source S; The destination D responds to the RREQ packet with a newly generated RREP packet, which copies the routing information into its packet header from the received RREQ packet header. This information includes the number of hops, the IP address of the source S, the IP address of the destination D, the IP address of the next hop F and so on. This newly generated RREP packet is then transmitted to node F and node F forwards the RREP packet to node B. Finally, node B forwards the RREP packet to the source S. By now the source S has been informed about the specific route discovered all the way from itself to the destination D. The RREP packet

is then forwarded according to the routing table stored in each node. The routing information stored in the routing table of each node is refreshed, when ever an RREQ packet arrives at a node and it is also updated, when ever an RREP packet arrives at a node. Additionally, a Wireless Local Area Network-Acknowledgement (WLAN-ACK) packet[2] is required for confirming the successful reception of the RREP packet.

- Data Transmission process of Figure 3.5:

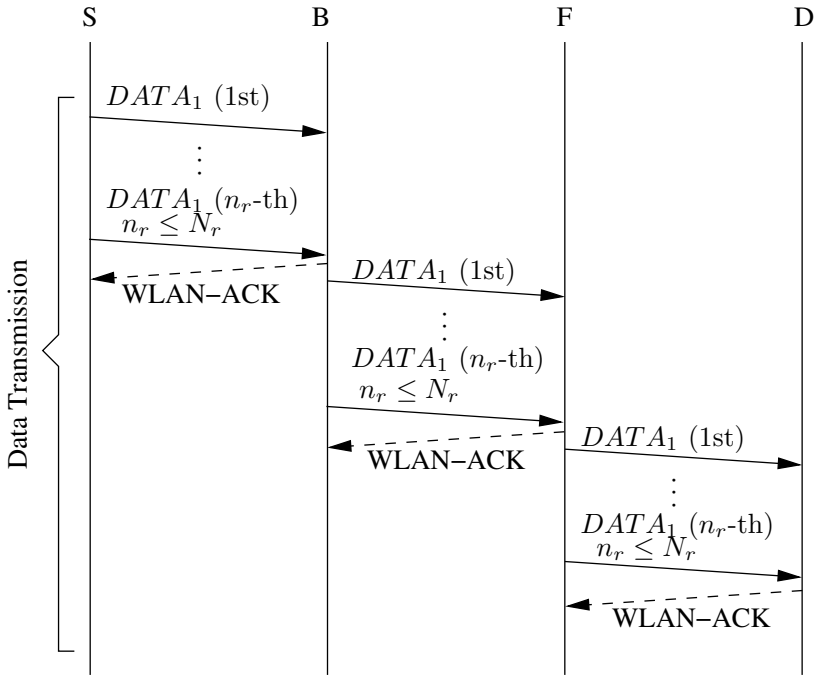

Figure 3.5: The process of **data transmission** after a route is found from source A to destination D.

When the RREP packet arrives at the source S during the process of route discovery, the source S is informed of a route spanning from the source S to the destination D, with node B being the next hop of this route. Hence, as seen in Figure 3.5, the buffered data packet $DATA_1$ is transmitted to node B according to the routing information stored in the routing table of source S. If the packet $DATA_1$ failed to reach node B, then node B has to retransmit the packet $DATA_1$ until the number of retransmission reaches its maximum of N_r. If and only if node B receives the packet $DATA_1$ successfully within n_r retransmissions, where $n_r \leq N_r$, it would respond to source S by sending back a WLAN-ACK packet. The WLAN-ACK is used for confirming the successful transmission of the packet

[2]The Acknowledgement packet is the one, which is returned to the transmitter as the acknowledgement of the correctly received data in the data link layer, hence it is referred to as WLAN-ACK in this chapter, where 'WLAN-ACK' represents the ACK packet employed in the IEEE802.11 standard. We assume that no Request-To-Send (RTS)/Clear-To-Send (CTS) mechanism is employed.

$DATA_1$. Meanwhile, node B forwards the packet $DATA_1$ to node F, since node F is its next hop *en route* to destination D. The routing information stored in node B's routing table is obtained during the route discovery process as well. In a similar way, if node F successfully receives the packet $DATA_1$, it respond with a WLAN-ACK to node B and forwards the packet $DATA_1$ to the destination D according to its own routing table. Finally, if the destination D successfully receives the packet $DATA_1$, it only has to respond with a WLAN-ACK packet to node F. Destination D does not forward the packet $DATA_1$, because it is the final destination of the packet $DATA_1$. Hence the packet from the source S to the destination D has been completed.

- Route Maintenance process of Figure 3.6:

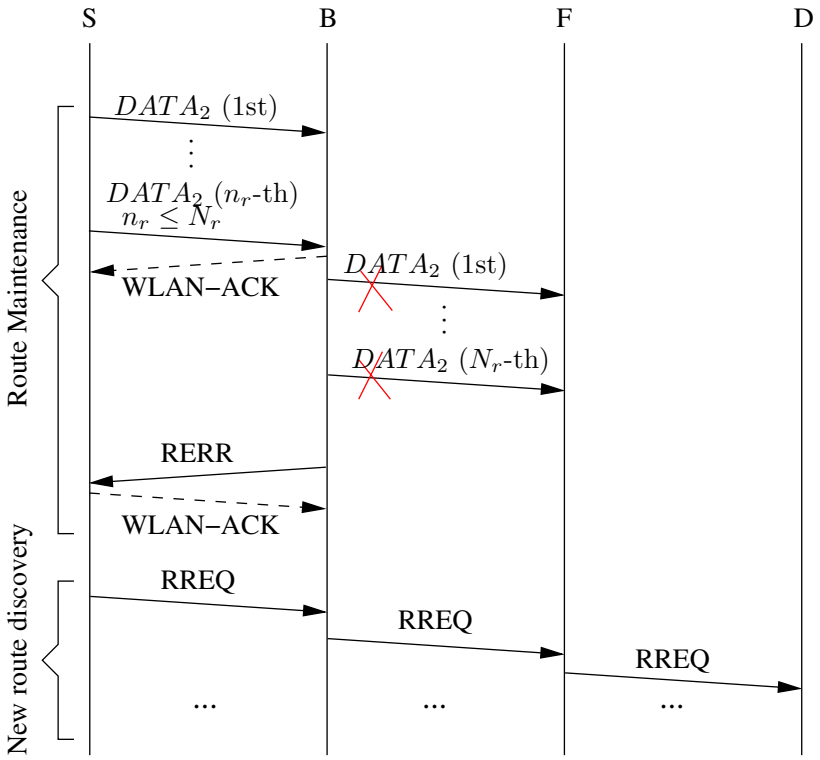

Figure 3.6: The process of **route maintenance** in the DYMO routing algorithm.

The process of route maintenance is graphically illustrated in Figure 3.6, where the transmission of the packet $DATA_2$ from the source S to the destination D is exemplified. First the packet $DATA_2$ is transmitted by the source S to node B. Node B receives the packet $DATA_2$ successfully during the n_r-th retransmission, where $1 \leq n_r \leq N_r$ and it responds with a WLAN-ACK packet to the source S for confirming the successful reception of the packet $DATA_2$. Then node B forwards the packet $DATA_2$ to node F. However, node F fails to receive the packet $DATA_2$ successfully after N_r retransmissions by node B. Therefore, no

response is sent from node F to node B. Once the pre-set timer expires at node B and node B has not received any WLAN-ACK packet from node F, then node B considers the link $B-F$ to be broken and actively sends an RERR packet to its adjacent-node, namely to the source S. Source S updates its own routing table by deleting all the routes, which include the link $B-F$. Therefore, the source S does not have a route to the destination D and a new route discovery process has to be activated. Hence, an RREQ packet is broadcast by the source S again, as shown in Figure 3.6.

We assume that every node has the same transmit power of P_t. Consequently, the sum of the energy E_T dissipated by all nodes in the network is given by

$$E_T = \sum E_{Route\_Discovery} + \sum E_{Data\_Transmission} + \sum E_{Route\_Maintenance}, \tag{3.12}$$

where E_T indicates the energy dissipated by a specific network topology. $\sum E_{Route\_Discovery}$ denotes the sum of energy dissipated by the RREQ, the RREP and the WLAN-ACK packets during the route discovery phase, which is shown in Figure 3.4. Furthermore, $\sum E_{Route\_Maintenance}$ includes all the energy during the route maintenance phase, except for $\sum E_{Data\_Transmission}$, which is the energy dissipated by the data packets and by the corresponding WLAN-ACK packets, as seen in Figure 3.6 and Figure 3.5. Hence, we may formulate $\sum E_{Data\_Transmission}$ as follows:

$$\sum E_{Data\_Transmission} = \sum \left(P_t \frac{L_{data}}{r_{data}} \right) + \sum \left(P_t \frac{L_{WLAN-ACK}}{r_{WLAN-ACK}} \right), \tag{3.13}$$

where L_{data} is the length of every packet arriving from the MAC layer, except for the WLAN-ACK packet. The length of the WLAN-ACK packet is $L_{WLAN-ACK}$. The information bit rate for transmitting data and WLAN-ACK packet is denoted by r_{data} and $r_{WLAN-ACK}$, respectively. We assume that the WLAN-ACK packet is protected by powerful, low-rate coding and modulation schemes and seldom has erroneous bits, hence $r_{WLAN-ACK}$ is different from r_{data}. Additionally, only the transmit power is considered in Equation (3.12). Substituting Equation (3.13) into Equation (3.12), we have

$$\begin{aligned} E_T = & \sum E_{Route\_Discovery} \\ & + \sum \left(P_t \frac{L_{data}}{r_{data}} \right) + \sum \left(P_t \frac{L_{WLAN-ACK}}{r_{WLAN-ACK}} \right) \\ & + \sum E_{Route\_Maintenance}. \end{aligned} \tag{3.14}$$

Furthermore, let BPS_{MA} and BPS_{SA} denote the bits per symbol throughput of the

MA and SA nodes, respectively. The IrCC, URC and STTC component codes have code rates of 0.5, 1.0 and 1.0, respectively. Since QPSK is used at the MA nodes and 8PSK at the SA nodes, then $BPS_{MA} = 2BPS_{SA}/3$ and $r_{MA} = 2r_{SA}/3$, where r_{MA} and r_{SA} are the bit rate at the MA-RNs and SA-RNs, respectively. Hence, Equation (3.14) may be simplified as:

$$\begin{aligned} E_T = & \sum E_{Route\_Discovery} \\ & + \frac{3P_t\ L_{data} - 1}{2r_{SA}} r_{ma} + \left(\frac{P_t\ L_{data}}{r_{SA}} + \frac{P_t\ L_{WLAN-ACK}}{r_{WLAN-ACK}} \right) L_h \\ & + \sum E_{Route\_Maintenance}, \end{aligned} \tag{3.15}$$

where again L_h is the number of hops of the selected route. First, the assumption that p_t, n_{data}, $n_{WLAN-ACK}$ and $r_{WLAN-ACK}$ are constant values is given. Then the shorthand of $A = \frac{3P_t\ L_{data} - 1}{2r_{SA}}$ and $B = \left(\frac{P_t\ L_{data}}{r_{SA}} + \frac{P_t\ L_{WLAN-ACK}}{r_{WLAN-ACK}} \right)$ are introduced. Furthermore, $\sum E_{Route\_Discovery}$ is replaced by $f_1(\rho, n_{MA}, \overrightarrow{v})$, and $\sum E_{Route\_Maintenance}$ is replaced by $f_2(\rho, n_{MA}, \overrightarrow{v})$, because they are influenced by the node density ρ, the number of MA-RNs n_{MA} and the mobile speed $\overrightarrow{v}$. Then, Equation (3.15) can be written as:

$$E_T = f_1(\rho, n_{MA}, \overrightarrow{v}) + An_{MA} + BL_h + f_2(\rho, n_{MA}, \overrightarrow{v}). \tag{3.16}$$

We further normalize E_T by the overall number of bits L_{app} received in the application layer of the destination and the number of nodes N of the entire network, where N is related to ρ and L_{app} is related to L_{data}. Finally, the overall energy consumption E_{NT} of the entire network can be expressed as:

$$E_{NT} = \frac{E_T}{NL_{app}} = F(\rho, n_{MA}, \overrightarrow{v}, L_h, BPS_{SA}, L_{app}). \tag{3.17}$$

3.3 Performance Study

As seen from Equation (3.17), the overall energy consumption of the entire network is dependent on numerous parameters, such as the node density, the number of MA-RNs, the mobile speed, the number of hops of the selected route, the BPS throughput and the amount of bits received in the application layer of the destination. In order to reduce the dimensionality of the investigations, some of the parameters are fixed when characterizing the benefits of MA-RNs on the node's achievable transmission range and FER performance. More explicitly, attention are mainly focused on the relationship between the number of MA-RNs and the energy consumption, as well as that between the node density and the energy consumption. The system parameters employed for the simulations of Figures 3.7, 3.8, 3.9, 3.10, 3.11 and 3.12 are listed in Table 3.1.

Table 3.1: System parameters employed for the simulations of Figures 3.7, 3.8, 3.9, 3.10, 3.11 and 3.12.

Network scenario	500m×500m
Application layer	5 packets/s with a frame length of 504 Bytes
Transport layer	UDP
Network layer	IPv4, DYMO
Data link layer	802.11b
Physical layer	IrCC-URC-8PSK for SA nodes IrCC-URC-STTC-QPSK for MA nodes
Channel	AWGN + Free-space Path Loss + Rayleigh Fading
Transmit power	1 mW
Sensitivity threshold[a], P_r^*	−85 dBm
Mobility	stationary(0 m/s)
Simulation time	30 second
Number of simulation runs	100

[a] The receive sensitivity threshold is used to judge whether the received signal is deemed to be noise, because a signal with received power less than the sensitivity level is deemed to be noise.

3.3.1 Energy Consumption versus the Number of MA-Relay nodes

Assuming that the node density ρ, the mobile speed $\overrightarrow{v}$, the BPS throughput BPS_{SA} and the number of bits L_{app} received in the application layer of the destination are constant, then Equation (3.17) can be simplified to:

$$E_{NT} = F(n_{MA}, L_h). \tag{3.18}$$

Four scenarios are considered in order to study the relationship between the number of MA-RNs and the energy consumption, where $N = 60$ stationary nodes are uniformly located in a 500m×500m field, hence the node density is $\rho = 240$ nodes per square kilometer. The source and the destination are located in the position $(499, 499)$ and $(0, 0)$, respectively. We increase the number of MA-RNs[3] from $n_{MA} = 0$ to $n_{MA} = 60$ in steps of 5. The receiver's sensitivity [47] is set to −85 dBm. Any signal received at a power lower than the sensitivity threshold is deemed to be undetectable. The energy consumption is quantified for both the IrCC-URC-STTC scenario[4] and the DCMC-capacity-based benchmark scenario at SNR_{dB}^* of 7 dB and 1 dB. We also quantify the Packet Loss Ratio (PLR) and the network control load in order to characterize the performance of the entire network. We define the PLR as the ratio of the data packets which are not delivered to the destinations to those generated by the sources.

[3]The number of MA-RNs also includes the source and the destination. Again, the multi-antenna aided nodes are denoted as MA-RNs and single-antenna nodes are denoted as SA-RNs.

[4]In the IrCC-URC-STTC scenario the network consists of QPSK-assisted IrCC-URC-STTC aided MA-RNs and 8PSK-assisted IrCC-URC aided SA-RNs.

Meanwhile, we define the network control load[5] as the number of routing control bits transmitted in the entire network divided by the number of data bits delivered to the destination [96].

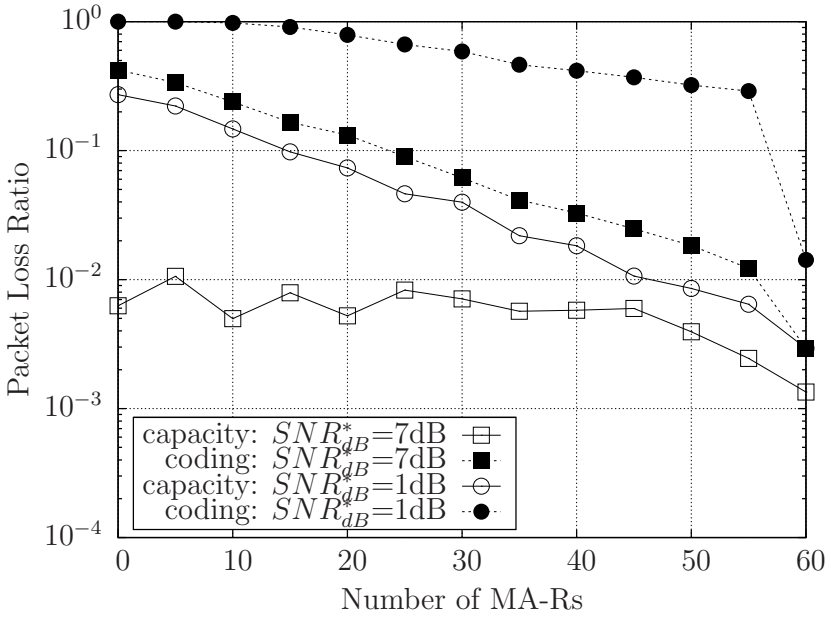

Figure 3.7: PLR versus the number of MA-RNs aiming for comparing the IrCC-URC-STTC scheme and the DCMC-capacity-based benchmark scheme at SNR^*_{dB} of 7 dB and 1 dB, where 'coding' denotes the IrCC-URC-STTC scheme and 'capacity' represents the DCMC-capacity-based benchmark scheme. All other system parameters are summarized in Table 3.1.

As seen from Figures 3.7, 3.8 and 3.9, the PLR, the network control load and the energy consumption of the IrCC-URC-STTC scheme and of the benchmark scheme decrease upon increasing the number of MA-RNs. As mentioned in Section 3.2.1, a low FER and a relatively high transmission range i.e. coverage area may be ensured by using the IrCC-URC-STTC scheme advocated. Furthermore, as justified in Section 3.2.2, the specific routes having the lowest number of hops tend to be activated in the MA-RNs aided network considered. Therefore, as expected, the PLR decreases, when the number of MA-RNs increases. Moreover, having a high physical-layer FER results in an increased number of retransmissions and hence may trigger route re-discovery, which results in more control packets being transmitted. Hence, more energy per payload bit is required for successfully delivering the source data to the destination, as demonstrated in Figure 3.9.

[5]In order to avoid the appearance of an infinite network control load, when no data are correctly received in the network layer, the reciprocal of the network control load is used instead of the control load itself.

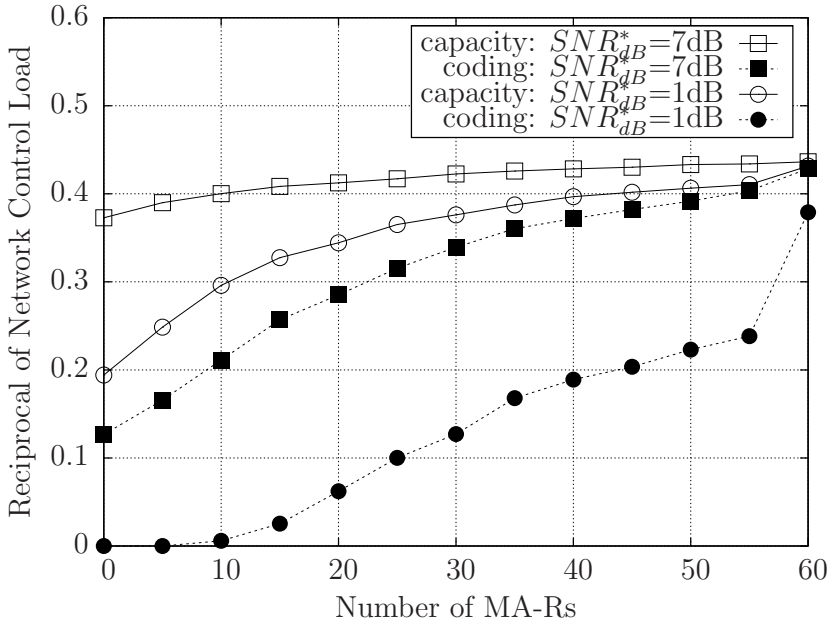

Figure 3.8: Reciprocal of the network control load versus the number of MA-RNs aiming for comparing the IrCC-URC-STTC scheme and the DCMC-capacity-based benchmark scheme at SNR^*_{dB} of 7 dB and 1 dB, where 'coding' denotes the IrCC-URC-STTC scheme and 'capacity' represents the DCMC-capacity-based benchmark scheme. All other system parameters are summarized in Table 3.1.

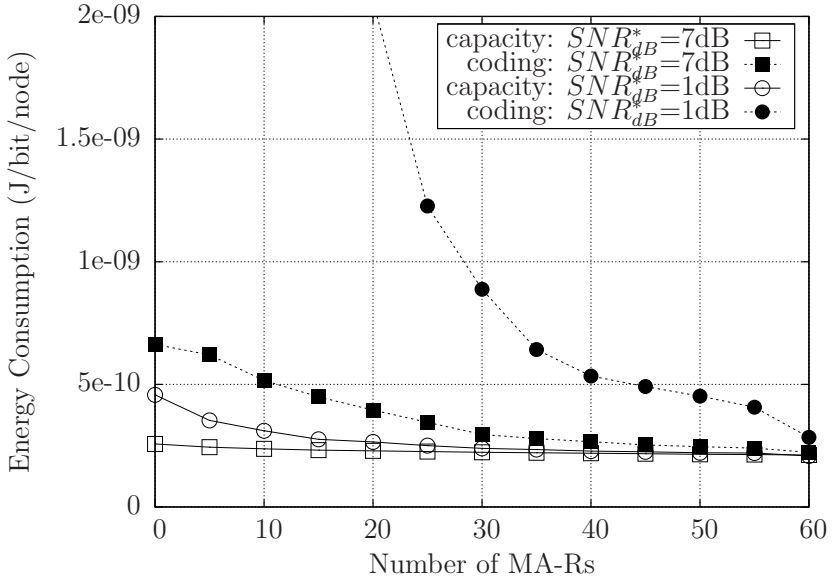

Figure 3.9: Energy consumption versus the number of MA-RNs aiming for comparing the IrCC-URC-STTC scheme and the DCMC-capacity-based benchmark scheme at SNR^*_{dB} of 7 dB and 1 dB, where 'coding' denotes the IrCC-URC-STTC scheme and 'capacity' represents the DCMC-capacity-based benchmark scheme. All other system parameters are summarized in Table 3.1.

3.3.2 Energy Consumption versus Node Density

Assuming that the number of MA-RNs n_{MA}, the mobile speed $\overrightarrow{v}$, the BPS throughput BPS_{SA} and the number of bits L_{app} received in the application layer of the destination are constant, Equation (3.17) can be simplified to:

$$E_{NT} = F(\rho, L_h). \tag{3.19}$$

Four scenarios are considered in order to study the relationship between the node density and the overall energy consumption of the entire network, where all the nodes are stationary and uniformly located in a 500m×500m field. The source and the destination are located in the position $(499, 499)$ and $(0, 0)$, respectively. We increase the node density from $\rho = 80$ to $\rho = 400$ in steps of 80. The receiver's sensitivity is set to -85 dBm, which corresponds to $SNR^*_{dB} = 7$ dB according to Equation (3.10). The energy consumption, the PLR and the network control load are quantified for both the IrCC-URC-STTC scheme and the benchmarker based on the DCMC capacity when $n_{MA} = 0$, 5, 10 and all nodes are equipped with two antennas in the *ad hoc* network considered.

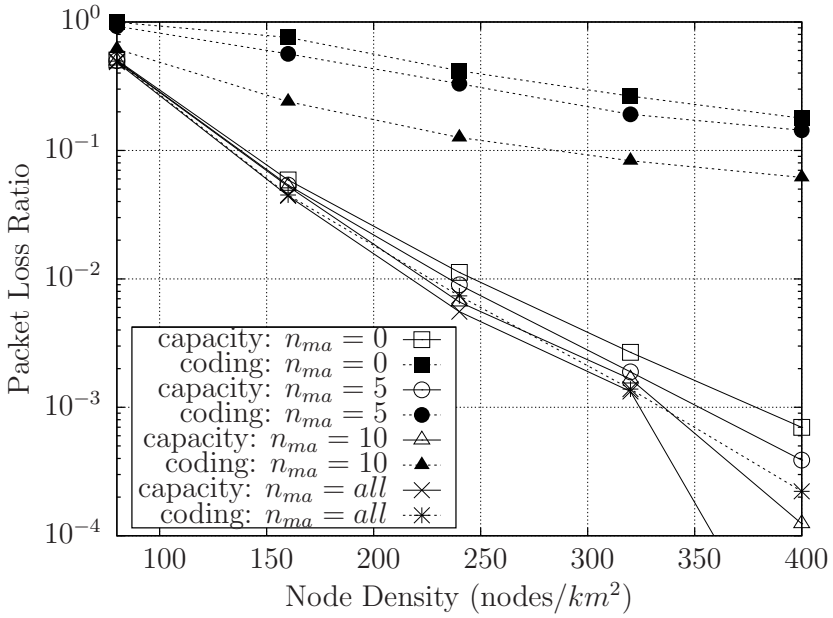

Figure 3.10: PLR versus node density aiming for comparing the IrCC-URC-STTC scheme and the DCMC-capacity-based benchmark scheme at SNR^*_{dB} of 7 dB when $n_{MA} = 0, 5, 10$ and *all*, where 'coding' denotes the IrCC-URC-STTC scheme and 'capacity' represents the DCMC-capacity-based benchmark scheme. All other system parameters are summarized in Table 3.1.

Figure 3.10 shows that the PLR decreases upon increasing the node density. A high node density implies having short average distances between the pairs of nodes, hence

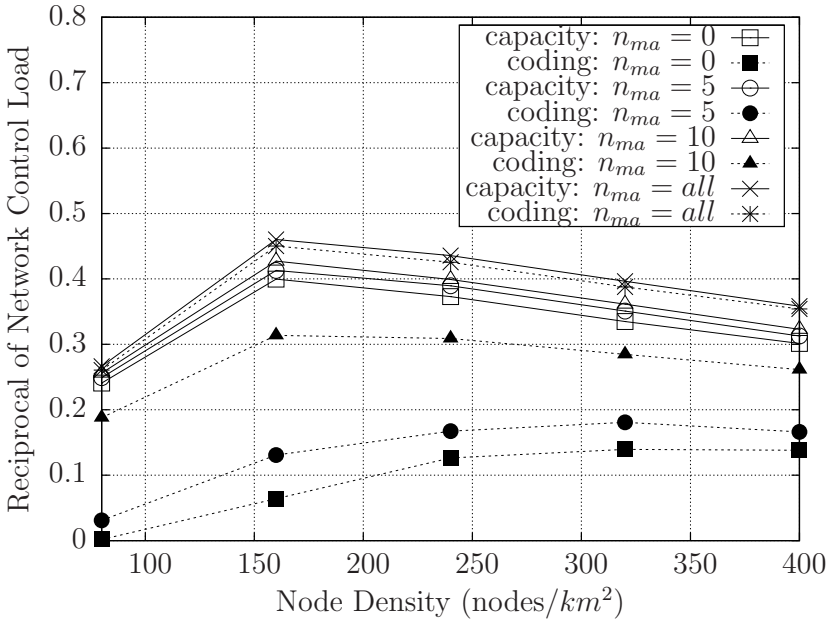

Figure 3.11: Reciprocal of the network control load versus node density aiming for comparing the IrCC-URC-STTC scheme and the DCMC-capacity-based benchmark scheme at SNR^*_{dB} of 7 dB when $n_{MA} = 0, 5, 10$ and *all*, where 'coding' denotes the IrCC-URC-STTC scheme and 'capacity' represents the DCMC-capacity-based benchmark scheme. All other system parameters are summarized in Table 3.1.

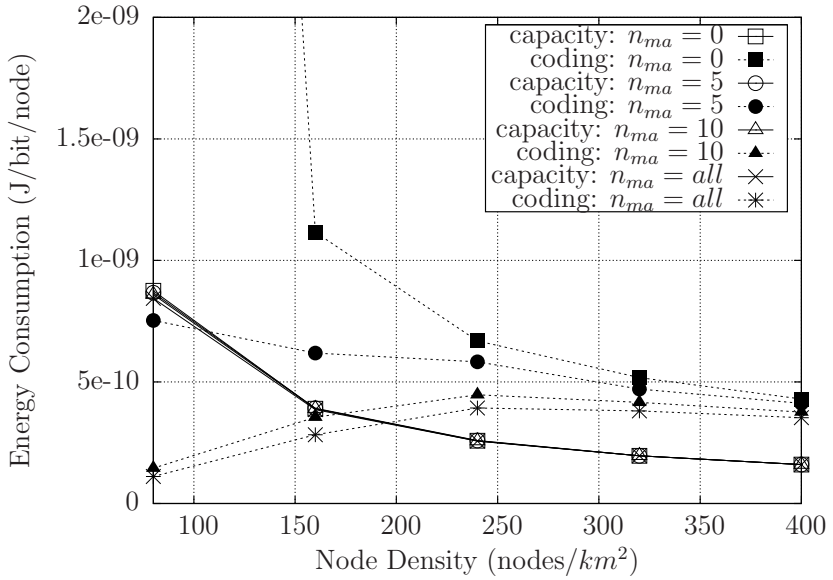

Figure 3.12: Energy consumption versus node density aiming for comparing the IrCC-URC-STTC scheme and the DCMC-capacity-based benchmark scheme at SNR^*_{dB} of 7 dB when $n_{MA} = 0, 5, 10$ and *all*, where 'coding' denotes the IrCC-URC-STTC scheme and 'capacity' represents the DCMC-capacity-based benchmark scheme. All other system parameters are summarized in Table 3.1.

a low PLR would be achieved as a benefit of having a high receive SNR. However, a high node density is also expected to impose a high interference on each node, which is expected to reduce the Signal-to-Interference Ratio (SIR). To explicitly characterize the underlying trends, Figure 3.11 shows that the network control load is reduced for the capacity-based bechmarker - i.e. its reciprocal is increased - upon increasing the node density to $\rho = 160$, since the benefits of the increased received signal power outweigh the detrimental effects of the degraded SIR. This trend was reversed above $\rho = 160$ for the DCMC-capacity-based benchmarker. By contrast, for the proposed IrCC-URC-STTC scheme, it is observed that in the presence of $n_{MA} = 0$ or 5 MA-RNs the network control load tends to gently decrease upon increasing the overall node density. Finally, the overall energy consumption expressed in Joule/bit/node is portrayed in Figure 3.12. The benchmarker based on the DCMC capacity could be deemed to represent the so-called 'perfect' coding scheme, which is capable of communicating at the capacity limit. Therefore, it may be readily seen from Figure 3.12 that near-capacity coding schemes benefit more substantially in high-node-density scenarios, when aiming for a high energy efficiency.

3.4 Chapter Conclusions

We have proposed the near-capacity three-stage concatenated IrCC-URC-STTC relay-transceiver scheme, where some RNs are equipped with two antennas for the *ad hoc* network considered. The system was shown to be capable of achieving a low FER at a low transmit power, as evidenced by Figure 3.2. The high effective transmission range of the IrCC-URC-STTC aided MA-RNs allows us to use cross-layer optimization for activating routes having the lowest number of longer hops. In Section 3.2, we theoretically analyzed the problem of normalized transmit energy consumption for the entire system. More specifically, we first characterized the benefits of a near-capacity IrCC-URC-STTC coding scheme in Figure 3.2 of Subsection 3.2.1. We considered single-antenna-aided SA-RNs for the 8PSK-assisted IrCC-URC scheme and twin-antenna-aided MA-RNs for the QPSK-assisted IrCC-URC-STTC scheme. Hence, four types of links might co-exist simultaneously in our system, which were the SA-RN to SA-RN link, the SA-RN to MA-RN link, the MA-RN to SA-RN link and the MA-RN to MA-RN link. As seen in Figure 3.2, the MA-RN to MA-RN link had a nearly 9 dB gain compared to the SA-RN to SA-RN link at an FER of 10^{-3} for both the IrCC-URC-STTC scheme and the DCMC-capacity-based benchmark scheme. Subsection 3.2.2 analyzed the beneficial influence of employing MA-RNs on the routing decisions. As suggested by Figure 3.3, the system might opt for the shortest route associated with a few potentially long hops, as a benefit of having more MA-RNs. This

subsection also introduced the process of route discovery, data transmission and route maintenance. During these processes, control packets were exchanged for the sake of guaranteeing the successful transmission of data packets. All the control packets and data packets also dissipated some of the nodes' residual energy. Therefore, the normalized transmit energy consumption of an entire system was formulated and the results were verified by simulations in Section 3.3. More specifically, Figure 3.9 of Subsection 3.3.1 quantified the energy consumption versus the number of MA-RNs and demonstrated that the normalized energy consumption was reduced by 25% when using the IrCC-URC-STTC scheme, as the number of MA-RNs increased from 10 to 20. Figure 3.12 of Subsection 3.3.2 characterized the energy consumption versus the node density and demonstrated that the normalized energy consumption was reduced by 25% for the IrCC-URC-STTC scenario, as the node density increased from 240 nodes/km^2 to 320 nodes/km^2, when the number of MA-RNs may set to 5. All the simulation results of Figures 3.9 and 3.12 confirmed that the energy consumption per bit and per node recorded for the MA-RN aided network was lower than that of the equivalent SA-RN aided network, especially in high-node-density scenarios.

In contrast to Chapter 2, this chapter aimed for reducing the entire system's energy consumption, instead of improving the network's throughput. We will further quantify the energy consumption in Chapter 4 and Chapter 5, where only the energy dissipated by the data packets is considered during the process of data transmission. Furthermore, Chapter 4 considers the trade-off between the energy consumption and the network's achievable throughput.

Chapter 4

Energy-Efficient Routing in Ad Hoc Networks Relying on Channel State Information and Limited Medium Access Control Retransmissions

Chapter 2 employed a so-called 'route stability' routing metric for improving the network's achievable throughput, while Chapter 3 exploited the benefits of Multi-Antenna aided Relay Nodes (MA-RNs) for reducing the entire system's energy consumption. Both chapters considered the coordination of the physical layer and the network layer with the aid of cross-layer operation. As a further evolution, this chapter considers the coordination of the physical layer, the data link layer and the network layer, as seen in the system model of Figure 4.1, which may be contrasted to the system model of Figure 3.1. We jointly exploit the Channel State Information (CSI) estimated in the physical layer, the number of retransmissions in the data link layer and the number of hops in the network layer for striking a trade-off between the energy consumption and the achievable network throughput in this chapter. The characteristics of the physical layer are represented by the Frame Error Ratio (FER), while the data link layer employs the IEEE802.11g standard [7]. In the network layer, an energy-efficient routing protocol is proposed for improving the energy dissipation, which constitutes our network-optimization Objective Function (OF). Here the channel model is the Additive White Gaussian Noise (AWGN) channel subjected to inverse second-power free-space path loss.

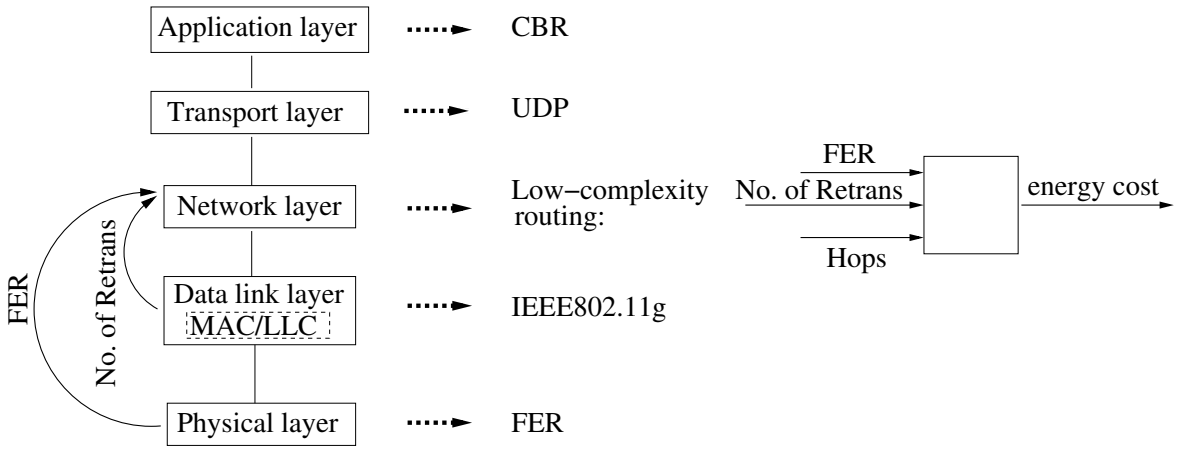

Figure 4.1: System model of our energy-efficient routing in *ad hoc* networks, which relies on the CSI and on a limited number of MAC retransmissions. This may be contrasted to the less sophisticated cross-layer regime of Figure 3.1.

4.1 Introduction

In recent years, numerous energy-efficient techniques have been proposed [107, 117–124]. However, simply minimizing the energy consumption results in deficient designs. It is more beneficial to strike a tradeoff between the energy consumed and other metrics, such as the attainable throughput. For example, a Minimum-Power Cooperative Routing (MPCR) algorithm was proposed in [117], which identifies and constructs the minimum-power route without unduly compromising the throughput. Multiple-Input and Multiple-Output (MIMO) schemes and near-capacity Space-Time Codes (STCs) were employed in [118] for optimizing the RN selection for the sake of maximizing the end-to-end throughput at a given total available power. While single-hop transmissions are more suitable for bandwidth-limited scenarios, multi-hop transmissions combined with spatial frequency-reuse tend to perform better in power-limited situations [107]. Spatial frequency-reuse employed in multi-hop scenarios may be beneficially combined with Interference Mitigation (IM) [107, 118] and transmit beamforming [118] for the sake of finding an attractive balance between energy minimization and throughput maximization in both single-hop and multi-hop schemes [107, 119, 120]. As a further advance, the authors of [119, 121] jointly considered both the transmit-energy and the signal-processing-related circuit-energy consumption. A beneficial tradeoff between the total energy consumption and throughput was found in [119] by considering both the transmission strategy of each node as well as the location of the RNs and the data rate of each node. In [121], a convex optimization technique was used for

tackling the cross-layer energy optimization problem. It combined single-hop and multi-hop transmissions, with the conclusion that circuit energy minimization favored transmissions relying on fewer hops.

The physical layer, data link layer, network layer and even the transport layer often cooperate with each other for the sake of energy minimization. For example, the impact of the link error rate on the route selection between a path associated with a large number of short-distance hops and another with a smaller number of long-distance hops was studied in [120]. In this paper, the link 'cost' was defined as a function of both the energy required for a single transmission attempt and the link error rate. This Objective Function (OF) captures the cumulative energy expended in reliable data transfer for both reliable and unreliable link layers. In [125], several routing algorithms were proposed, which opted for the route with minimum energy consumption in a mixed hop-by-hop and end-to-end retransmission mode. In the end-to-end retransmission mode, a single unreliable link may require retransmissions from the source, and hence may require more energy for successfully delivering packets. Consequently, routing protocols play an important role in saving energy. The authors of [126] took into account both the energy consumed by data packets as well as by control packets and MAC retransmissions, because ignoring the energy consumption of exchanging control packets might underestimate the actual energy consumption and thus may lead to inefficient designs. Furthermore, energy-efficient unicast and multicast routing protocols were proposed in [127], which relied on diverse power control techniques.

However, the energy OFs employed in [120, 125, 126] exploited the assumption of having access to a potentially infinite number of MAC retransmissions, which is unrealistic. Additionally, although the authors of [127] considered a limited number of MAC retransmissions, no specific OF was formulated. Against this backdrop, *the novel contributions of this chapter are*

- *We construct an accurate energy-consumption-based OF by considering the Frame Error Ratio (FER) in the physical layer, a limited number of MAC retransmissions (including the first transmission attempt) and the number of hops in the network layer. The achievable throughput is also treated as an important design factor.*
- *We design a routing algorithm, which employs the energy-consumption-based OF as the design metric. An attractive balance is attained between the energy consumed and the throughput achieved.*

The rest of the chapter is organized as follows. Our proposed energy-consumption-based OF is detailed in Section 4.2. In Section 4.3, the achievable performance is

analyzed. Finally, the conclusions are provided in Section 5.5.

4.2 Theoretical Analysis

Based on the system model of Figure 4.1, the impact of the lowest three layers of the OSI model on the total energy dissipated of the entire system is considered, which will be analyzed, whilst relying on an energy-consumption-based OF.

In this chapter the transmit energy consumed by the data packets during their transmission is considered, which are generated from the application layer. The energy consumed by other packets, such as routing and MAC control packets is not considered. In other words, the idealized simplifying assumption is that the energy consumed during the process of route discovery is negligible. The elimination of this simplification was set aside for the future work. The OF proposed is invoked for making routing-related decisions, which directly influence the energy consumed by future data packets. All nodes are assumed to be stationary. Only a single source-destination pair is supported in the network and only a single node has the chance of transmitting in a time slot, once the route was determined. The number of nodes in the network is denoted by N, while H indicates the number of hops in an established route. The transmit power of each node assigned to a single transmission attempt is P_{t_i} and the corresponding energy is E_i. We assume that all the data packets have the same length and all nodes have the same transmission rate. Hence, if P_{t_i} is the same at each node, then E_i is the same, which may hence be denoted by a constant E, while FER_i is the FER of the ith hop in a route that reflects the channel quality information. We opt for using p_i as the probability of successful transmission in the ith hop, which is given by:

$$p_i = 1 - FER_i. \tag{4.1}$$

The maximum number of MAC retransmission is N_r, which includes the first transmission attempt and $N_r = \infty$ implies having an infinite number of MAC retransmissions. The OF incorporates the total transmit energy normalized by the number of successfully delivered information bits. The total energy consumption is denoted by E_{total}, while its normalized version is denoted by $\overline{E}_{total}$. The throughput is defined as the number of information bits successfully delivered to the destination per second, which is R_{e2e}.

4.2.1 Objective Function

The employment of the OF proposed in [120, 125, 126] is feasible only when the affordable number of MAC retransmissions is infinite, which is formulated as

$$E_{total} = \sum_{1}^{H} \frac{E_i}{1 - FER_i}, \tag{4.2}$$

where $\frac{1}{1-FER_i}$ is the expected number of transmission attempts required for successfully delivering a packet across link i. As seen from Equation (4.2), the total energy of all hops is simply summed, which suggests that the success of the individual links in a route is deemed to be independent of each other, since the assumption that an infinite number of MAC retransmissions is affordable is given.

Naturally, having an infinite number of MAC retransmissions will impose a potentially infinite end-to-end delay at the destination, which is not realistic. In realistic environments, the wireless link may become broken owing to packet errors if the maximum number of MAC retransmissions has been exhausted. A broken link may trigger a route-repair or even route re-discovery for the sake of maintaining the current source-destination communications session. The route-repair is often required at the upper-node's broken link, while the route re-discovery should be initiated by the source. All these actions may consume more energy and naturally they reduce the attainable throughput. Additionally, the success of a specific hop emanating from a node relies on the success of all previous hops. If any of the previous links is broken, then no packet will be forwarded towards the destination. Naturally, any link is more likely to break if the number of MAC retransmissions is limited to N_r. We divide the energy consumption considered into two parts: the energy consumed by the data packets which succeed in reaching the destination and the energy consumed by the data packets which are dropped before reaching the destination. We define the time slot duration of a single transmission attempt across a given link as T. Given the same data packet length and the same transmission rate at each node, T is a constant value. Here, the energy-conscious OF of a two-hop route is detailed as an example. We use p_s and p_f to denote the probability of a packet being successfully delivered to the destination successfully and being dropped before reaching the destination, respectively. Furthermore, the notation $p_s(\tau)$ represents the probability that the packet is successfully delivered all the way from the source to the destination after a time duration of τ. First, the energy consumption analysis of a $2-$hop route is considered in Figure 4.2. The symbol $\surd$ indicates that the link's transmission is successful after $1 \leq \frac{\tau}{T} \leq N_r$ MAC retransmission attempts. Hence the time duration of the link's transmission is $T \leq \tau \leq N_r T$. Figure 4.2 shows that a packet's successful transmission

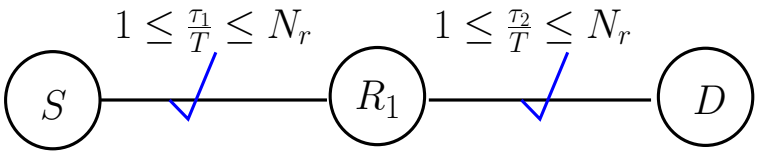

Figure 4.2: A packet is successfully delivered from S to D in a 2-hop route.

over the link $S-R_1$ requires a time duration of τ_1, while the successful transmission of a packet over the link R_1-D requires a time duration of τ_2. Hence the total time duration of a packet's passage between S and D is $(\tau_1+\tau_2)$, where we have $2T \leq \tau_1+\tau_2 \leq 2N_rT$.

Therefore, for each case we have:

$$p_s(2T) = p_1p_2, \tag{4.3}$$

$$p_s(3T) = (1-p_1)p_1p_2 + p_1(1-p_2)p_2, \tag{4.4}$$

$$\begin{aligned} p_s(4T) = &(1-p_1)^2p_1p_2 \\ &+ (1-p_1)p_1(1-p_2)p_2 + p_1(1-p_2)^2p_2, \end{aligned} \tag{4.5}$$

$$\vdots \qquad\qquad \vdots$$

$$p_s(2N_rT) = (1-p_1)^{N_r-1}p_1(1-p_2)^{N_r-1}p_2. \tag{4.6}$$

While p_s is given by

$$p_s = p_s(2T) + p_s(3T) + p_s(4T) + \cdots + p_s(2N_rT), \tag{4.7}$$

$$= \sum_{1}^{N_r}\sum_{1}^{N_r}(1-p_1)^{i_1-1}p_1(1-p_2)^{i_2-1}p_2. \tag{4.8}$$

Since during a single time slot T the nodes consume an energy of E, the estimated total energy E_s consumed by a successfully delivered packet in a two-hop route is

$$\begin{aligned} E_s = &[2p_s(2T) + 3p_s(3T) + 4p_s(4T) \\ &+ \cdots + 2N_rp_s(2N_rT)]E. \end{aligned} \tag{4.9}$$

In a similar way, the time D_s required for a packet, which is successfully delivered from the Source (S) to the Destination (D) is given by

$$\begin{aligned} D_s = &[2p_s(2T) + 3p_s(3T) + 4p_s(4T) \\ &+ \cdots + 2N_rp_s(2N_rT)]T. \end{aligned} \tag{4.10}$$

Additionally, the packets, which exhausted the maximum number N_r of MAC retransmissions and were finally dropped before reaching D due to poor channel

conditions also consume energy. This energy should also be taken into account in the total energy consumption. The energy dissipation analysis of a packet dropped before reaching the destination in a 2-hop route is portrayed in Figure 4.3. The symbol $\times$ indicates that the link's transmission fails after $\frac{\tau}{T} = N_r$ MAC retransmission attempts. As seen in Figure 4.3, a transmission failure may occur either in the $S - R_1$ link or in the $R_1 - D$ link of a 2-hop route. Hence, even when the data transmission in the $S - R_1$ link is successful within the time duration of $T \leq \tau_1 \leq N_r T$, the transmission might fail in the $R_1 - D$ link.

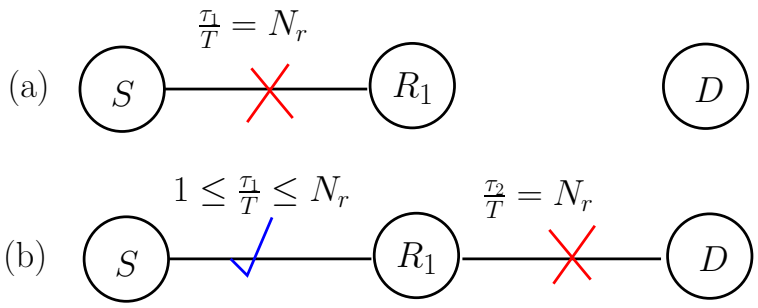

Figure 4.3: A packet is dropped before reaching D in a 2-hop route.

The probability of failure p_f of the two-hop route for a single packet is described as follows:

$$p_f(1) = (1 - p_1)^{N_r}, \tag{4.11}$$

$$p_f(2) = [(1 - p_f(1))](1 - p_2)^{N_r}, \tag{4.12}$$

$$p_f = p_f(1) + p_f(2), \tag{4.13}$$

where $p_f(h)$ represents the probability of the packet becoming dropped during the hth hop. Therefore, the energy E_f consumed by a dropped packet is quantified as follows:

$$E_f = \left[N_r p_f(1) + \sum_{1}^{N_r} (1 - p_1)^{i_1 - 1} p_1 (1 - p_2)^{N_r} (i_1 + N_r) \right] E. \tag{4.14}$$

Similarly, the average time D_f required by a packet to propagate from S up to the broken link is formulated as

$$D_f = \left[N_r p_f(1) + \sum_{1}^{N_r} (1 - p_1)^{i_1 - 1} p_1 (1 - p_2)^{N_r} (i_1 + N_r) \right] T. \tag{4.15}$$

The energy dissipation analysis of a packet's successful delivery to the destination and that of a packet dropped before reaching the destination in a H-hop route is characterized in Figure 4.4 and Figure 4.5, respectively. Figure 4.4 portrays the

scenario, where each link's transmission is successful after $1 \leq \frac{\tau}{T} \leq N_r$ MAC retransmission attempts. By contrast, Figure 4.5 shows that a transmission failure could take place within any of the links, where all the previous links' transmissions were successful. The time duration elapsed before reaching the failed link is $\tau = N_r T$, while that elapsing during all the previous link's transmission is $T \leq \tau \leq N_r T$.

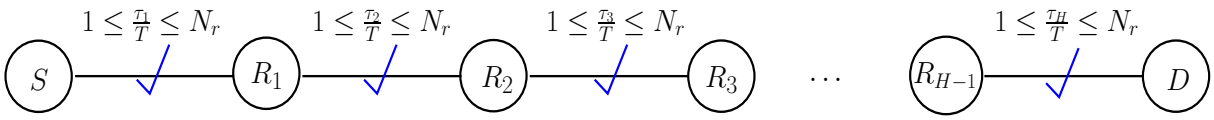

Figure 4.4: A packet is successfully delivered from S to D in a H-hop route.

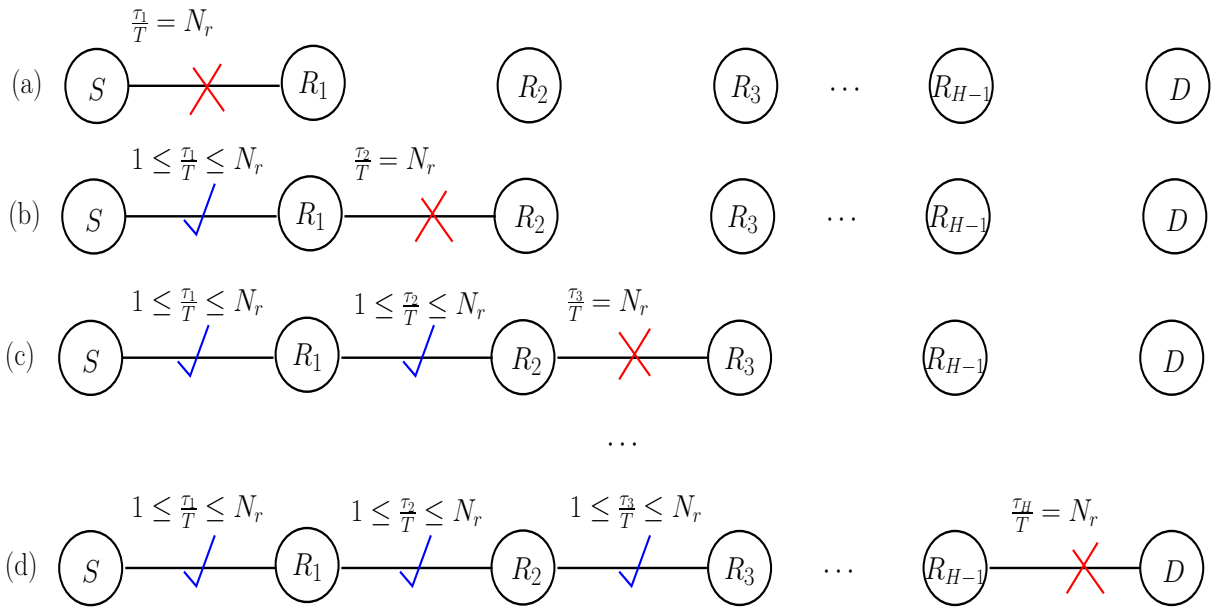

Figure 4.5: A packet is dropped before reaching D in a H-hop route.

Hence, the probability p_s and p_f for an H-hop route are given as follows:

$$p_s = \sum_{1}^{N_r} \cdots \sum_{1}^{N_r} (1-p_1)^{i_1-1} p_1 (1-p_2)^{i_2-1} p_2 \cdots (1-p_H)^{i_H-1} p_H, \tag{4.16}$$

$$p_f = p_f(1) + \sum_{2}^{H} p_f(h), h \neq 1, \tag{4.17}$$

where

$$p_f(h) = \sum_{1}^{N_r} \cdots \sum_{1}^{N_r} (1-p_1)^{i_1-1} p_1 \cdots (1-p_{h-1})^{i_{h-1}-1} p_{h-1} (1-p_h)^{N_r}, h \neq 1. \tag{4.18}$$

Therefore, the energy E_s consumed by a successfully delivered packet and the energy E_f consumed by a packet which is dropped before reaching the destination are formulated as:

$$E_s = \left[\sum_{1}^{N_r} \cdots \sum_{1}^{N_r} (1-p_1)^{i_1-1} p_1 (1-p_2)^{i_2-1} p_2 \cdots (1-p_H)^{i_H-1} p_H (i_1+i_2+\cdots+i_H) \right] E, \tag{4.19}$$

$$E_f = [N_r p_f(1)]\, E + \sum_{2}^{H} E_f(h), h \neq 1, \tag{4.20}$$

where

$$E_f(h) = \left[\sum_{1}^{N_r} \cdots \sum_{1}^{N_r} (1-p_1)^{i_1-1} p_1 \cdots (1-p_{h-1})^{i_{h-1}-1} p_{h-1} (1-p_h)^{N_r} (i_1+\cdots+i_{h-1}+N_r) \right] E, h \neq 1. \tag{4.21}$$

Similarly, the time D_s spent by a successfully delivered packet and the time D_f spent by a dropped packet throughout their passage can be derived, which is as follows:

$$D_s = \left[\sum_{1}^{N_r} \cdots \sum_{1}^{N_r} (1-p_1)^{i_1-1} p_1 (1-p_2)^{i_2-1} p_2 \cdots (1-p_H)^{i_H-1} p_H (i_1+i_2+\cdots+i_H) \right] T, \tag{4.22}$$

$$D_f = [N_r p_f(1)]\, T + \sum_{2}^{H} D_f(h), h \neq 1, \tag{4.23}$$

where

$$D_f(h) = \Bigg[\sum_{1}^{N_r} \cdots \sum_{1}^{N_r} (1-p_1)^{i_1-1} p_1 \cdots (1-p_{h-1})^{i_{h-1}-1} p_{h-1} \\ (1-p_h)^{N_r} (i_1 + \cdots + i_{h-1} + N_r) \Bigg] T, h \neq 1. \tag{4.24}$$

Therefore, the total normalized transmit energy consumption becomes:

$$\overline{E}_{total} = \frac{E_{total}}{p_s} = \frac{E_s + E_f}{p_s}. \tag{4.25}$$

Similarly, the end-to-end throughput R_{e2e} is given as

$$R_{e2e} = \frac{p_s}{D_s + D_f}. \tag{4.26}$$

For simplifying Equation (4.25) and Equation (5.36), the mathematical short-hand of $A(p_i) = \frac{1-(1-p_i)^{N_r}}{p_i} - N_r(1-p_i)^{N_r}$ and $B(p_i) = 1-(1-p_i)^{N_r}$ are defined, thus $p_s = \prod_1^H B(p_i)$ are obtained. The simplified normalized energy-conscious OF and end-to-end throughput are formulated in Equation (4.27) and Equation (4.28), respectively as:

$$\overline{E}_{total} = \frac{\left[N_r \left(1 - \prod_1^H B(p_i) \right) + \sum_1^{H-1} \left(\frac{A(p_i)}{B(p_i)} \prod_{j=1}^{i} B(p_j) \right) \right] E}{\prod_1^H B(p_i)}, \tag{4.27}$$

$$R_{e2e} = \frac{\prod_1^H B(p_i)}{\left[N_r \left(1 - \prod_1^H B(p_i) \right) + \sum_1^{H-1} \left(\frac{A(p_i)}{B(p_i)} \prod_{j=1}^{i} B(p_j) \right) \right] T}. \tag{4.28}$$

4.2.2 Routing Algorithm

A low-complexity routing algorithm was also designed in this chapter based on Dijkstra's shortest-path algorithm [128], which employs the OF of Equation (4.27) for making routing decisions. As seen from Equation (4.27) and Equation (4.28), the normalized energy consumption and the end-to-end throughput are inversely proportional to each other, which is formulated as:

$$\overline{E}_{total} \propto \frac{1}{R_{e2e}}. \tag{4.29}$$

Equation (4.29) shows that once the route having the lowest estimated normalized energy consumption is chosen to transmit data, the achieved end-to-end throughput would be maximized, if no route-repair and route re-discovery were allowed. Indeed,

the energy-conscious OF is capable of reflecting the probability of the route becoming broken because it considers both the FER, as well as the maximum number of MAC retransmission and the number of hops.

The process of route discovery is described in the pseudo-code given by Figure 4.6, where S represents the source and D represents the destination. In Figure 4.6 $E_{S\to n,t}$ denotes the estimated normalized energy consumption for the route spanning from S to node n at time instant t, while $E_{S\to n}$ is used for storing the minimum normalized energy consumption for every node in every time-slot of duration T. The symbol $\leftarrow$ implies assigning the Right-Hand-Side (RHS) value to the Left-Hand-Side (LHS) value, while H_{max} is the maximum number of hops in Figure 4.6. The Route REQuest (RREQ) message of Figure 4.6 is a broadcast packet, which is used for finding appropriate routes leading to D, while the Route REPly (RREP) message is used for returning all the route identifiers to S.

A flow chart is provided in Figure 4.7 for specifically highlighting the operations, when each node receives an RREQ packet. If S receives the RREQ packet, S will simply discard this RREQ packet. By contrast, if another node n ($n \neq S$) receives the RREQ packet, it calculates the normalized energy dissipation $E_{S\to n,t}$ and then compares $E_{S\to n,t}$ to $E_{S\to n}$. If we have $E_{S\to n,t} > E_{S\to n}$, then node n will discard the RREQ packet. Otherwise, if node n is D, then D will respond with a newly created RREP packet. However, if node n is not D, node n will broadcast the RREQ packet again.

Indeed, the RREP message carries the descriptors or identifiers of all the adequate routes to S. Once S receives the route-identifiers in the RREP message, it calculates the estimated normalized energy consumption of the routes using the energy-conscious OF. The route imposing the lowest estimated energy consumption will then be chosen to convey the data. If other RREP messages are also returned back to S, S repeats the process of route selection. When the RREP message propagates through the intermediate nodes back to S, all the intermediate nodes also update their routing tables for their potential future use. The energy-conscious OF can make the routing decisions more reliable than its conventional counterpart, which assumes having an infinite number of MAC retransmissions, since it considers the non-negligible probability of having broken links in the chosen route. Naturally, the cost of broken links would be very high, if the source had to opt for another route or carry out a new full-scale route re-discovery.

For interpreting how the proposed low-complexity routing algorithm operates, detailed examples are given by Figures 4.8 - 4.11 and 4.12, where S is the source,

```
for every node n ∈ N, n ≠ S do
    E_{S→n,0} ← 0, and E_{S→n} ← 0.
end for
S broadcasts RREQ.
t ← 1, E_{S→n} ← E_{S→n,1}.
while t ≤ H_max + 1 do
    for each node n which receives RREQ, n ≠ S do
        if E_{S→n,t} < E_{S→n} then
            E_{S→n} ← E_{S→n,t};
            if n ≠ D then
                broadcast RREQ further;
            else
                if D receives the first RREQ;
                    returns RREP at time t + 1;
                else
                    returns RREP if E_{S→D} is updated;
                end if
            end if
        end if
    end for
    t ← t + 1;
end while
```

Figure 4.6: The process of route discovery in the proposed low-complexity routing algorithm.

D is the destination and the other nodes are denoted by symbols A, B, C, E, F and G. The routing process may be divided into the following four steps:

- **Step 1** Node S broadcasts the RREQ packet;
- **Step 2** Every node carries out the operations detailed in Figure 4.7 upon receiving the RREQ packet;
- **Step 3** Node S receives the RREP packet and then updates the routing table;
- **Step 4** Then node S sends its data packet along the specific route having the lowest estimated $\overline{E}_{total}$.

At the very beginning, $E_{S\to n}$ of each node n is initialized to an infinite value. Moreover, as mentioned before, the time elapsed during the transmission of a packet is defined as a time slot, hence in each time slot we have the following:

During time slot 1, we do

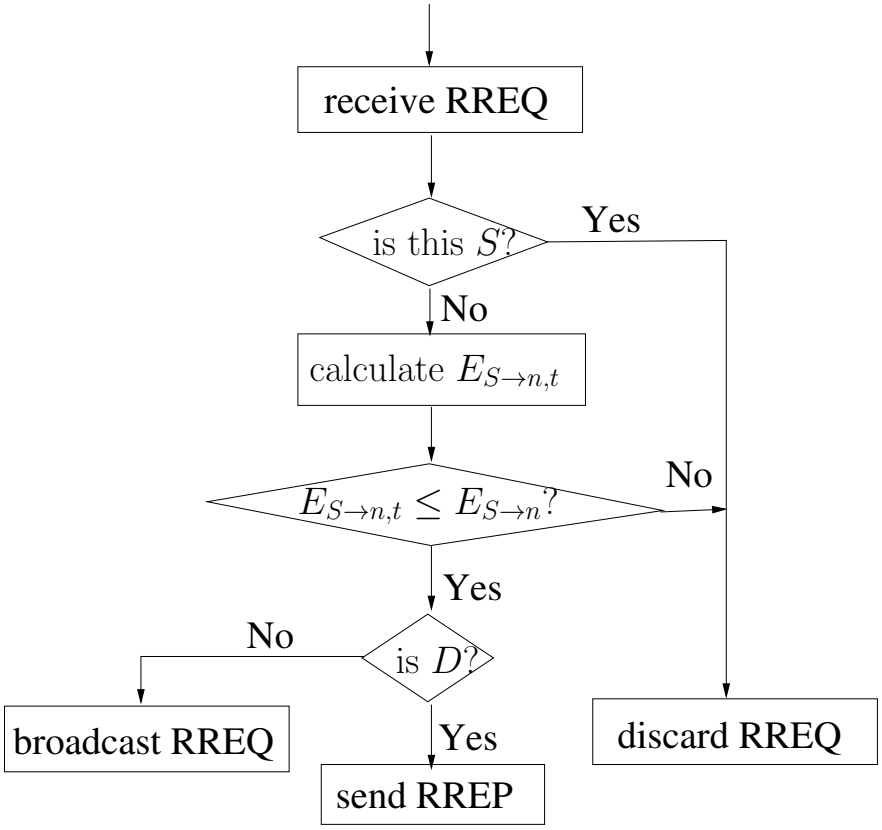

Figure 4.7: Operations when each node receives an RREQ packet.

- **Step 1** Node S broadcasts the RREQ packet;
- **Step 2** Nodes A, B and C receive the RREQ packet. According to the actions seen in Figure 4.7, nodes A, B and C first calculate $E_{S\to A,1}$, $E_{S\to B,1}$ and $E_{S\to C,1}$, respectively. Then they compare these newly calculated values with the aid of $E_{S\to A}$, $E_{S\to B}$ and $E_{S\to A}$, respectively. If $E_{S\to A,1} \leq E_{S\to A}$, then A will update $E_{S\to A}$ and will forward the RREQ packet during the next time slot, otherwise it will discard it. The same actions are carried out at node B and node C as well.

The actions carried out during time slot 1 are shown in Figure 4.8.

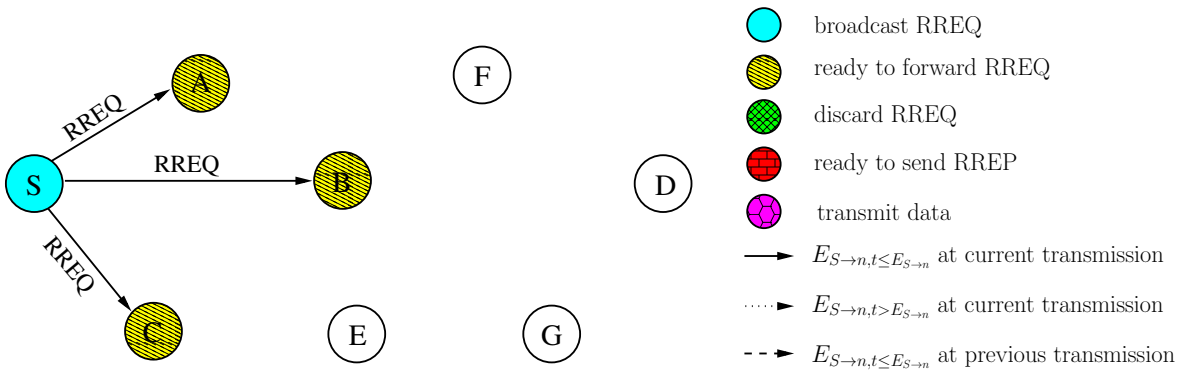

Figure 4.8: Actions during time slot 1.

Then during time slot 2, we do

- **Step** 2
  - Node A forwards the RREQ packet, then nodes S, B and F receive the RREQ packet. According to the actions seen in Figure 4.7, node S discards the RREQ packet directly. Node B discards the RREQ packet as well, since we have $E_{S\to B,2} > E_{S\to B}$. However, node F will forward the RREQ packet in the next time slot, since we have $E_{S\to F,2} \leq E_{S\to F}$;
  - Node C forwards the RREQ packet, then nodes S, B and E receive the RREQ packet. According to the actions observed in Figure 4.7, node S discards the RREQ packet directly, nodes B and E are ready to forward the RREQ packet, since we have $E_{S\to B,2} \leq E_{S\to B}$ and $E_{S\to E,2} \leq E_{S\to E}$;
  - Node B forwards the RREQ packet to nodes S, A, C, D, E, F and G. According to the actions seen in Figure 4.7, node S discards the RREQ directly, nodes A, C, E and F discard the RREQ packet as well, since the newly calculated $E_{S\to A,2}, E_{S\to C,2}, E_{S\to E,2}$ and $E_{S\to F,2}$ values are higher. Furthermore, node G will forward the RREQ packet, since we have $E_{S\to G,2} \leq E_{S\to G}$ and node D is ready to send back a newly created RREP packet in the next time slot, since node D is the destination and $E_{S\to D,2} \leq E_{S\to D}$.

The actions carried out during time slot 2 are shown in Figure 4.9. Afterwards, S will receive the RREP packet and updates its routing table with the route $S - B - D$ obtained, as indicated in **Step** 3. Finally, S will send the data packet along the route $S - B - D$, which is indicated in **Step** 4.

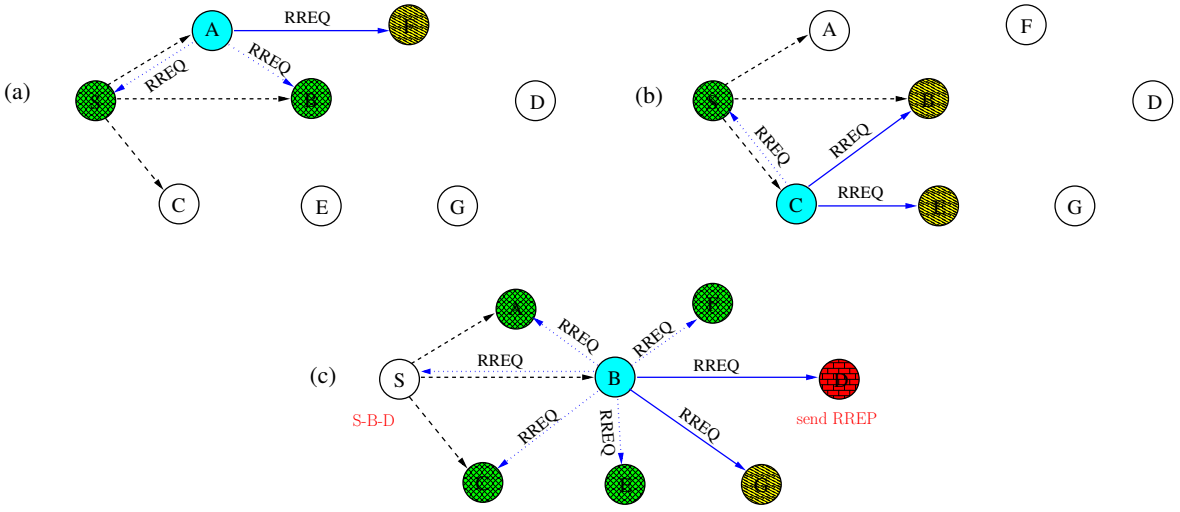

Figure 4.9: Actions during time slot 2 and node S updates its routing table with the route $S - B - D$.

During time slot 3, we do

- **Step** 2
  - Node F forwards the RREQ packet, then nodes A, B and D receive the RREQ packet and immediately discard it according to the actions seen in Figure 4.7, since we have $E_{S\to A,3} > E_{S\to A}$, $E_{S\to B,3} > E_{S\to B}$ and $E_{S\to D,3} > E_{S\to D}$;
  - Node E forwards the RREQ packet, then nodes B, C and G receive the RREQ packet and immediately discard it according to the actions observed in Figure 4.7, since we have $E_{S\to B,3} > E_{S\to B}$, $E_{S\to C,3} > E_{S\to C}$ and $E_{S\to G,3} > E_{S\to G}$;
  - Node B forwards the RREQ packet, then nodes S, A, C, D, E, F and G receive it. According to the actions portrayed in Figure 4.7, nodes S, A, C, E and F discard the RREQ packet, since node S is the source and we have $E_{S\to A,3} > E_{S\to A}$, $E_{S\to C,3} > E_{S\to C}$, $E_{S\to E,3} > E_{S\to E}$ and $E_{S\to F,3} > E_{S\to F}$. However, node G will forward the RREQ packet during the next time slot, since we have $E_{S\to G,3} \leq E_{S\to G}$. Node D will then send back a newly created RREP packet during the next time slot, since node D is the destination and we have $E_{S\to D,3} \leq E_{S\to D}$;
  - Node G forwards the RREQ packet, then nodes B, E and D receive the RREQ packet and immediately discard it according to the actions detailed in Figure 4.7, since we experience $E_{S\to B,3} > E_{S\to B}$, $E_{S\to E,3} > E_{S\to E}$ and $E_{S\to D,3} > E_{S\to D}$;

The actions during time slot 3 are shown in Figure 4.10. Afterwards, S will receive the second RREP packet and updates its routing table again with the route $S-C-B-D$ obtained, since the estimated normalized energy consumption of route $S-C-B-D$ is lower than that of route $S-B-D$, as indicated in **Step** 3. Finally, node S will send the next data packet along the updated route $S-C-B-D$, which is indicated in **Step** 4.

During time slot 4, we do

- **Step** 2
  - Node G forwards the RREQ packet, then nodes B, E and D receive it. According to the actions of Figure 4.7, nodes B and E discard the RREQ packet, since we have $E_{S\to B,4} > E_{S\to B}$ and $E_{S\to E,4} > E_{S\to E}$. Then D is ready to send back a newly created RREP packet during the next time slot, since node D is the destination and we have $E_{S\to D,4} \leq E_{S\to D}$;

The actions during time slot 4 are shown in Figure 4.11. Afterwards, S will receive the third RREP packet and updates its routing table again with the route $S-C-B-G-D$ obtained, since the estimated normalized energy dissipation of route $S-C-B-G-D$

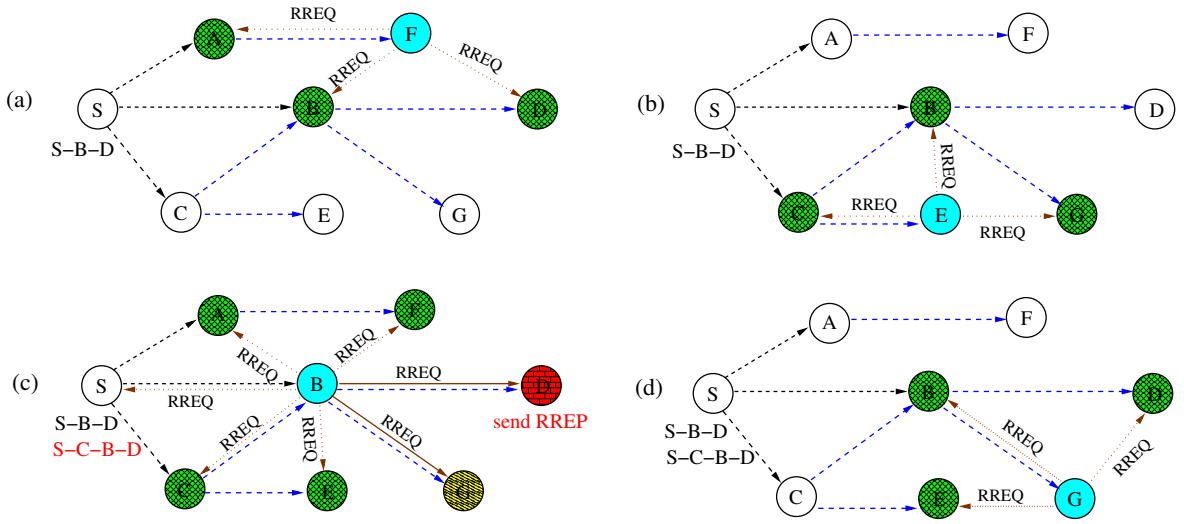

Figure 4.10: Actions during time slot 3 and node S updates its routing table with the route $S-C-B-D$ since the estimated normalized energy consumption of route $S-C-B-D$ is lower than that of route $S-B-D$.

is lower than that of route $S-C-B-D$, as indicated in **Step** 3. Finally, node S will send the next data packet along the updated route $S-C-B-G-D$, which is indicated in **Step** 4.

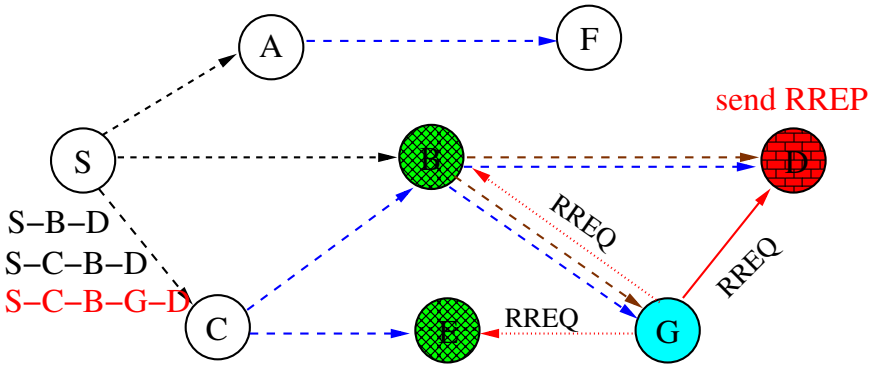

Figure 4.11: Actions during time slot 4 and node S updates its routing table with the route $S-C-B-G-D$, since the estimated normalized energy consumption of route $S-C-B-G-D$ is lower than that of route $S-C-B-D$.

Finally, after node S receives all the RREP packets, the route $S-C-B-G-D$ is selected as the best route, since it has the lowest estimated normalized energy consumption $\overline{E}_{total}$, which will be employed for transmitting the rest of the data packets. The process of data transmission is shown in Figure 4.12.

4.3 Performance Study

The analytically estimated normalized energy consumption associated both with an infinite and with N_r number of MAC retransmissions was calculated from Equation (4.2)

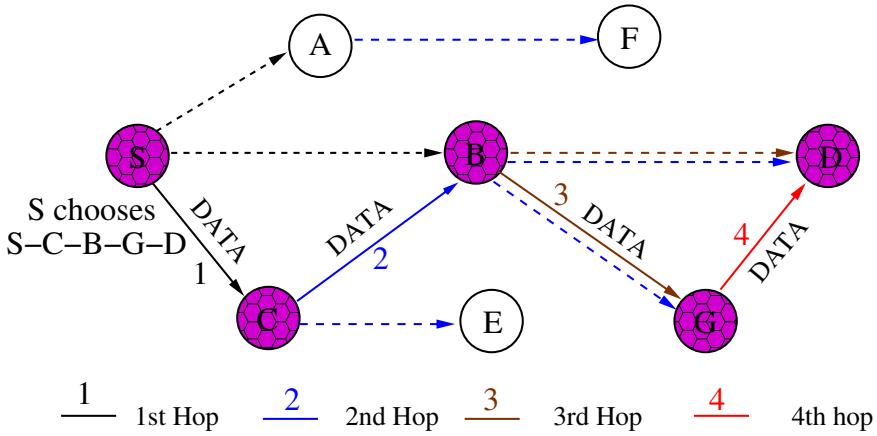

Figure 4.12: Node S transmits data along the route $S-C-B-G-D$ which has the lowest estimated $\overline{E}_{total}$.

and Equation (4.27), respectively. The network simulator OMNeT++ [45] was used for generating the simulation results. The analytical and simulation based results will be compared for the sake of quantifying the accuracy of the proposed OF and to quantify its influence on the routing decisions.

Two simple network topologies were studied. The system parameters employed for generating the simulation results of Figures 4.14, 4.15, 4.17 and Table 4.2 are listed in Table 4.1.

Table 4.1: System parameters employed for the simulations of Figures 4.14, 4.15, 4.17 and Table 4.2.

Application layer	5 packets/s with frame length of 1024 Bytes
Transport layer	UDP
Data link layer	802.11g
Channel	AWGN + Free-space Path Loss
Coding & modulation	IrCC-URC-STTC-QPSK
Transmit power	0.016 mW
Sensitivity threshold, P_r^*	-85 dBm
Mobility	stationary(0 m/s)
Simulation time	30 second
Number of simulation runs	100

In the first one all the nodes are equi-spaced along a line, as seen in Figure 4.13. The distance between S and D is d_{SD}. Then the distance between two adjacent nodes is $\frac{d_{SD}}{N-1}$. For the sake of fair comparisons, d_{SD} and varied the number of intermediate nodes between S and D are fixed. If the transmit power for a two-hop topology is 0.016 mW, which is denoted by P_{i_2}, then the transmit power for an $(N-1)$-hop topology

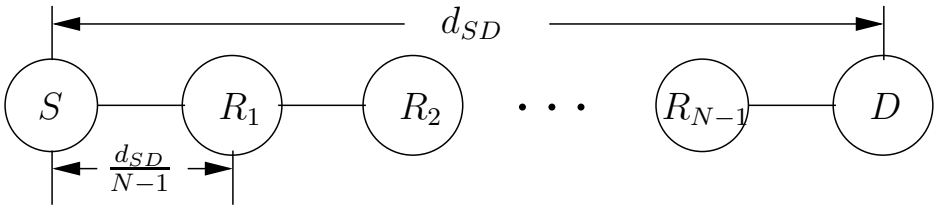

Figure 4.13: Test-topology relying on N nodes.

becomes:

$$P_{i_{N-1}} = P_{i_2} \left(\frac{2}{N-1} \right)^2. \tag{4.30}$$

The normalized energy consumption and the end-to-end throughput evaluated both from Equation (4.27) and Equation (4.28) as well as by simulations are portrayed in Figure 4.14 and Figure 4.15. Figure 4.14 displays three groups of performance curves recorded at $N_r = 1, 4$ and 7, respectively, for both the normalized energy consumption and for the end-to-end throughput, where N_r is the maximum number of MAC retransmissions. The performance figures recorded for the infinite number of MAC retransmissions scenario, namely for $N_r = \infty$ are identical for the theory evaluated from Equation (4.2) and for the simulations. All the analytical and the simulation based values recorded for the normalized energy consumption increase, when the FER increases. By contrast, the curves representing the end-to-end throughput decrease, when the FER increases. The reason for this observation is that a high FER in a link indicates a high breakage probability not only for the specific link and but also for the entire route, when retransmissions are required. However, if N_r is sufficiently high, then the success probability of a packet across a link or even the entire route becomes higher. This trend is presented in Figure 4.14, where the curve recorded for $N_r = 7$ is seen to be close to that of $N_r = \infty$. The discrepancy between the theoretical value and the simulation-based value becomes higher when N_r is reduced and simultaneously the FER is increased. Figure 4.14 also shows that the theoretical energy consumption of Equation (4.27) based on the energy-conscious OF is closer to the simulation based values than those based on the OF relying on an infinite number of MAC retransmissions. Naturally, the advantage of the proposed OF is more substantial for $N_r = 1$. Figure 4.15 also displays two groups of performance curves, one group for the normalized energy consumption and the other group for the end-to-end throughput, which are associated with $H = 2$ and 10, respectively. When H is increased, the normalized energy consumption is reduced and the end-to-end throughput is decreased, because the distance between a pair of adjacent nodes is reduced and therefore the

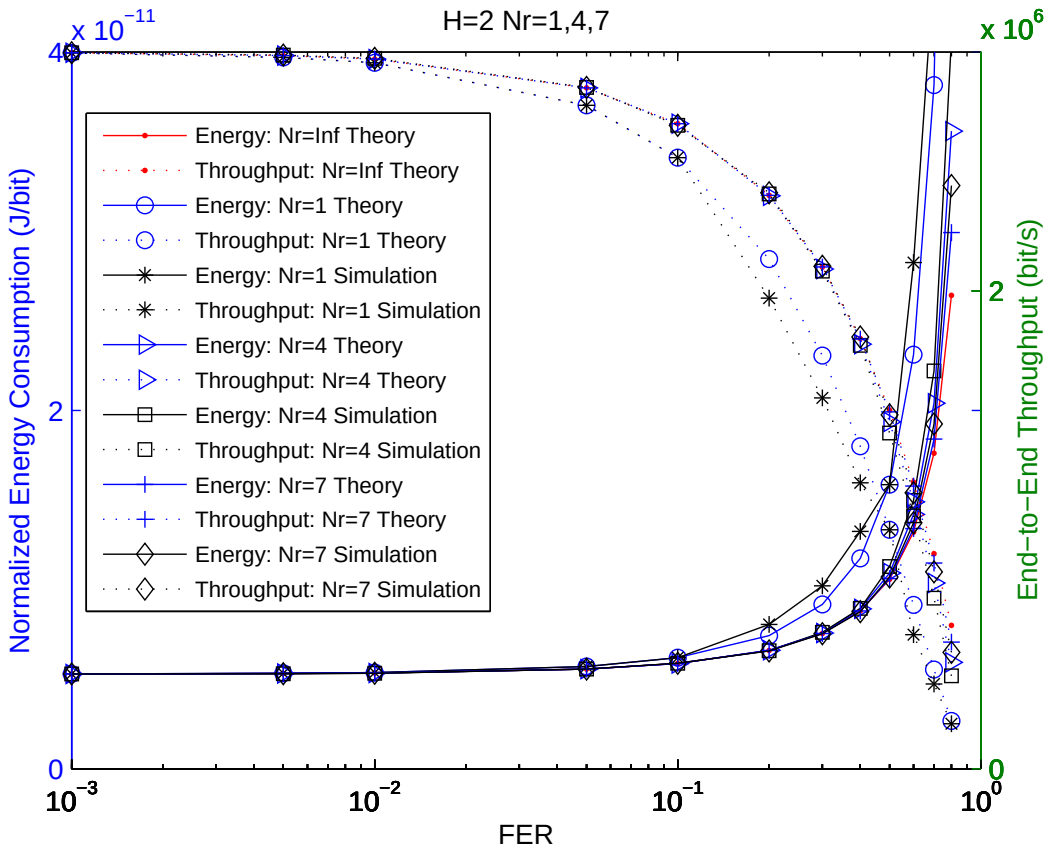

Figure 4.14: The normalized energy consumption and the end-to-end throughput versus FER ($10^{-3} \leq FER \leq 1$) and the maximum number of MAC retransmissions N_r ($N_r = 1, 4, 7$) with the number of hops $H = 2$ for comparing the theoretically analyzed values and simulation based values, which obeys the network topology of Figure 4.13. All other system parameters are summarized in Table 4.1.

transmit power required at each node for successfully delivering a packet is reduced, as suggested by Equation (4.30). Similarly, the theoretical values estimated based on the proposed OF are closer to the simulated values than to those estimated on the basis of an infinite number of MAC retransmissions, especially when both H and the FER are high. Hence from Figure 4.14 and Figure 4.15 the conclusion is reached that the proposed energy-conscious OF is more accurate than the one assuming an infinite number of MAC retransmissions at high FERs, or for a high number of hops at a low maximum number of MAC retransmissions.

Now the six-node topology of Figure 4.16 is considered. The line between each pair of nodes indicates that they are within the sensing range of each other. Node A is the source and F is the destination. The FER is assumed to be a random variable for each link which is generated by a random generator and uniformly distributed in [0,1]. All the other parameters are the same as in the linear topology of Figure 4.13.

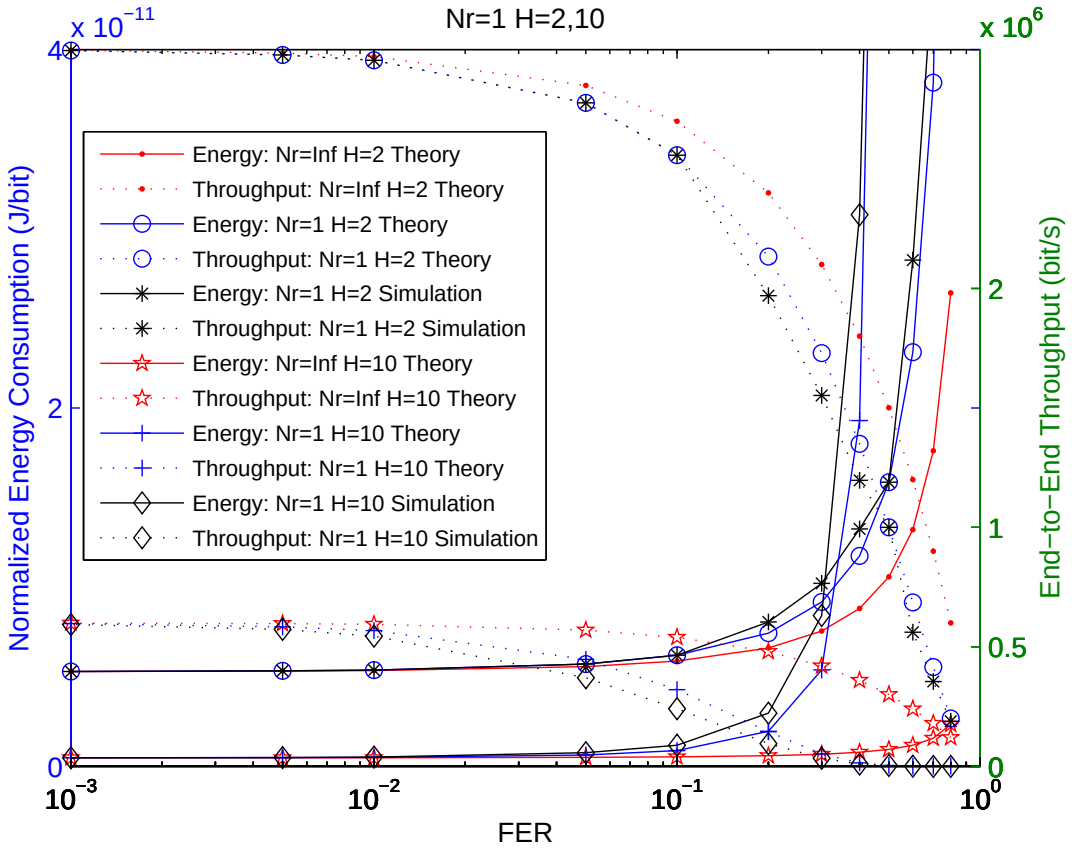

Figure 4.15: The normalized energy consumption and the end-to-end throughput versus FER ($10^{-3} \leq FER \leq 1$) and the number of hops H ($H = 2, 10$) with the maximum number of MAC retransmissions $N_r = 1$ for comparing the theoretically analyzed values and simulation based values, which obeys the network topology of Figure 4.13. All other system parameters are summarized in Table 4.1.

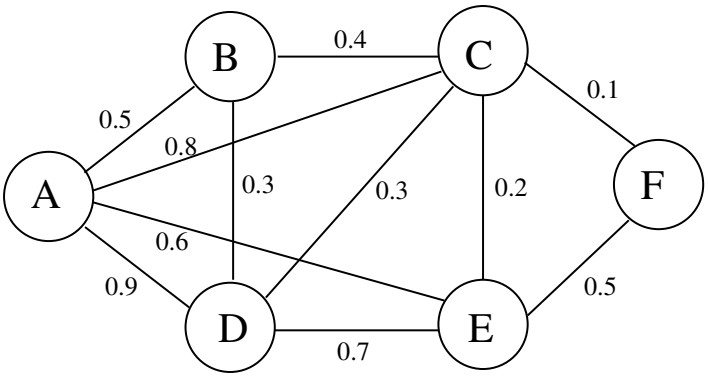

Figure 4.16: A simple six-node network topology.

Table 4.2: Route selection for the six-node topology of Figure 4.16 with $1 \leq N_r \leq 7$. Here, Columns '$N_r = \infty$ Theory' and 'Proposed Theory' denote the route decision based on the prediction of the theoretical normalized energy consumption. While Columns 'Energy1' and 'Energy2' represent the the simulation-based values of the normalized energy consumption, when choosing the routes 'A-E-F' and 'A-E-C-F', respectively. The matrix $\mathbf{M}_{FER}$ of FER is given by Equation (4.31). All other system parameters are summarized in Table 4.1.

N_r	$N_r = \infty$ Theory	Proposed Theory	Energy1(J/bit) A-E-F	Energy2(J/bit) A-E-C-F
1	A-E-F	A-E-C-F	2.10×10^{-11}	1.69×10^{-11}
2	A-E-F	A-E-C-F	1.54×10^{-11}	1.34×10^{-11}
3	A-E-F	A-E-F	1.37×10^{-11}	1.55×10^{-11}
...	...	...	...	...

Assuming a specific group of FERs between every pair of nodes for example, the matrix $\mathbf{M}_{FER}$ of FER is given by

$$\mathbf{M}_{FER} = \begin{bmatrix} 0 & 0.5 & 0.8 & 0.9 & 0.6 & 1.0 \\ 0.5 & 0 & 0.4 & 0.3 & 1.0 & 1.0 \\ 0.8 & 0.4 & 0 & 0.3 & 0.2 & 0.1 \\ 0.9 & 0.3 & 0.3 & 0 & 0.7 & 1.0 \\ 0.6 & 1.0 & 0.2 & 0.7 & 0 & 0.5 \\ 1.0 & 1.0 & 0.1 & 1.0 & 0.5 & 0 \end{bmatrix}, \tag{4.31}$$

where each row and column corresponds to a specific node. As seen from Figure 4.17, when N_r increases, the normalized energy consumption decreases and the end-to-end throughput increases. Table 4.2 portrays the routes selected when using either the conventional OF relying on an infinite number of MAC retransmissions or the proposed OF. Columns 'Energy1' and 'Energy2' show the simulation based values of the normalized energy consumption, when choosing the routes 'A-E-F' and 'A-E-C-F', respectively. We can see that the algorithm assuming an infinite number of MAC retransmissions always chooses the route 'A-E-F', while the proposed algorithm opts for 'A-E-C-F', when $N_r = 1, 2$ and chooses 'A-E-F' for $N_r = 3$ to 7. By observing the normalized energy consumptions listed in columns 'Energy1' and 'Energy2', the proposed algorithm is seen to make the right decisions, which saves energy and improves the throughput attained. By observing that the route 'A-E-C-F' is selected for $N_r = 1, 2$, the route associated with the minimum number of hops does not always perform well, when considering the attainable energy efficiency.

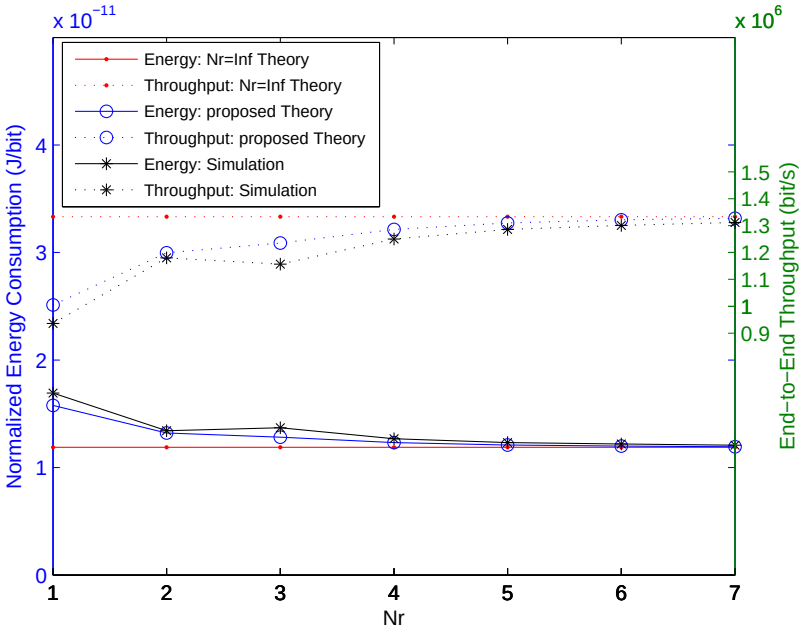

Figure 4.17: The normalized energy consumption and the end-to-end throughput with $1 \leq N_r \leq 7$ for comparing the theoretically analyzed values and simulation based values, which obeys the six-node topology of Figure 4.16. The matrix $\mathbf{M}_{FER}$ of FER is given by Equation (4.31). All other system parameters are summarized in Table 4.1.

4.4 Chapter Conclusions

In Subsection 4.2.1, an energy-conscious OF was proposed, which takes into account the FER of the physical layer, a finite number of N_r MAC retransmissions and the actual number of hops encountered in the network layer. Unlike the previously proposed OFs, which usually assume that the number of MAC retransmissions is infinite [120, 125, 126], the proposed OF of Equation (4.27) represents the real-world scenarios more closely, since it assumes a finite number of N_r MAC retransmissions. Moreover, the end-to-end throughput based OF of Equation (4.28) was also invoked. In Subsection 4.2.2, we found that the normalized energy consumption and the end-to-end throughput are inversely proportional to each other. Therefore, a low-complexity routing algorithm was designed for making reliable routing decisions purely based on the energy consumption using the energy-conscious OF of Equation (4.27). In Section 4.3, two scenarios were considered. The linear network of Figure 4.13 was set up to investigate the normalized energy consumption versus the FER, as well as the normalized energy versus the maximum number of MAC retransmissions N_r and the normalized energy versus the number of hops H. At the same time, the end-to-end throughput versus the FER, as well as the throughput versus the maximum number of MAC retransmissions N_r and the throughput versus the number of hops H was analyzed in Figures 4.14 and 4.15. All the simulation results of Figures 4.14 and 4.15 confirm the theoretical results

relying on the proposed OF, especially when the FER is high, the maximum number of MAC retransmissions N_r is low and the number of hops H is high. Furthermore, in Section 4.3 a simple six-node network topology was set up for demonstrating that the proposed low-complexity routing algorithm is capable of minimizing the normalized energy consumption without unduly compromising the end-to-end throughput, as evidenced by Figure 4.17. Compared to the routing protocol which employs the energy-conscious OF of Equation (4.2) based on an infinite number of MAC retransmissions, our routing algorithm achieved a 19.5% and 12.1% reduction of energy consumption for $N_r = 1$ and $N_r = 2$, respectively, as observed in Figure 4.17 and Table 4.2.

Our routing algorithm proposed in Section 4.2.2 is based on the more sophisticated energy-conscious OF of Equation (4.27). However, this energy-conscious OF of Equation (4.27) was formulated by assuming the same transmit power at each node. Although the proposed routing algorithm of Section 4.2.2 is capable of striking a trade-off between the normalized energy consumption and the end-to-end throughput, it still wastes some of the energy. When considering a practical random distributed network, the distance between each pair of nodes is different and hence appropriate power allocation control has to be employed for further reducing the energy consumption. Additionally, all the data are transmitted along a pre-selected route in this chapter, since neither mobility nor the instantaneous channel condition were considered. Once the pre-selected route becomes invalid for any reason, another redundant route will take over or a new route re-discovery process is activated, provided that no redundant routes exist, which may dissipate extra energy. Therefore, as a logical counter-measure, power allocation is introduced in Chapter 5 for the sake of conceiving a new energy-conscious OF. Moreover, an energy-efficient opportunistic routing algorithm was proposed in [129–131] by taking into account the effects of diverse time-variant channel conditions, where pre-selecting a route was unnecessary.

Chapter 5

Cross-Layer Aided Energy-Efficient Opportunistic Routing in Ad Hoc Networks

In Chapter 3 the sophisticated near-capacity Irregular Convolutional Coded, Unity-Rate Coded and Space-Time Trellis Coded (IrCC-URC-STTC) transceiver of Figure 3.2 was invoked, which relied on the cross-layer interaction of the physical- and network-layers, as portrayed in the system model of Figure 3.1. The scope of cross-layer interaction was then further extended to include not only the physical- and network-layers, but also the data link layer in Chapter 4, as seen in the system model of Figure 4.1. The operation of the physical layer was characterized in terms of the Frame Error Ratio (FER) vs. Channel Signal-to-Noise Ratio (SNR). Chapter 4 proposed a routing algorithm based on the energy-conscious Objective Function (OF) of Equation (4.27). Although this routing algorithm was capable of striking a trade-off between the normalized energy dissipation and the end-to-end throughput, it still wasted some energy, since it assumed that all nodes had the same transmit power. By contrast, in reality the distance amongst the nodes is different, hence they also require different powers for reaching the closest node during the next hop. Additionally, a pre-selected route was employed for data transmission, which may impose extra energy dissipation, if the pre-selected route becomes invalid. Hence, for the sake of solving these problems, in this chapter we introduce an appropriate power allocation scheme combined with an opportunistic scheme. The opportunistic scheme does not employ a pre-selected route, while it will fully utilize the time-variant characteristic of the hostile wireless channel, where any Relay Node (RN) has the chance to forward a packet as long as the packet arrives at this RN successfully. A pair of energy-consumption-based OFs are constructed for Traditional Routing (TR) and Opportunistic Routing

(OR) by exploiting the knowledge of both the corresponding FER within the physical layer, as well as that of the number of MAC retransmissions and of the number of RNs in the network layer, as seen in the system model of Figure 5.1. The above-mentioned traditional and opportunistic routing algorithms employ the corresponding energy-consumption-based OFs as their routing metrics, respectively. Apart from the normalized energy consumption, we evaluate the end-to-end throughput, the end-to-end delay and the delay distribution. We will demonstrate that the proposed algorithms are capable of operating close to the theoretical bound found by the exhaustive search of all routes. In Figure 5.1, the characteristics of the physical layer are represented with the aid of the FER, while the data link layer employs the IEEE802.11g standard. In the network layer, the above-mentioned TR and OR are employed, which make their decisions on the basis of the above energy-consumption-related OFs. The User Datagram Protocol (UDP) is employed in the transport layer and the data streaming relies on a Constant Bit Rate (CBR) service in the application layer. As in Chapter 3, the channel imposes both free-space path-loss and uncorrelated Rayleigh fading, plus the ubiquitous Additive White Gaussian Noise (AWGN).

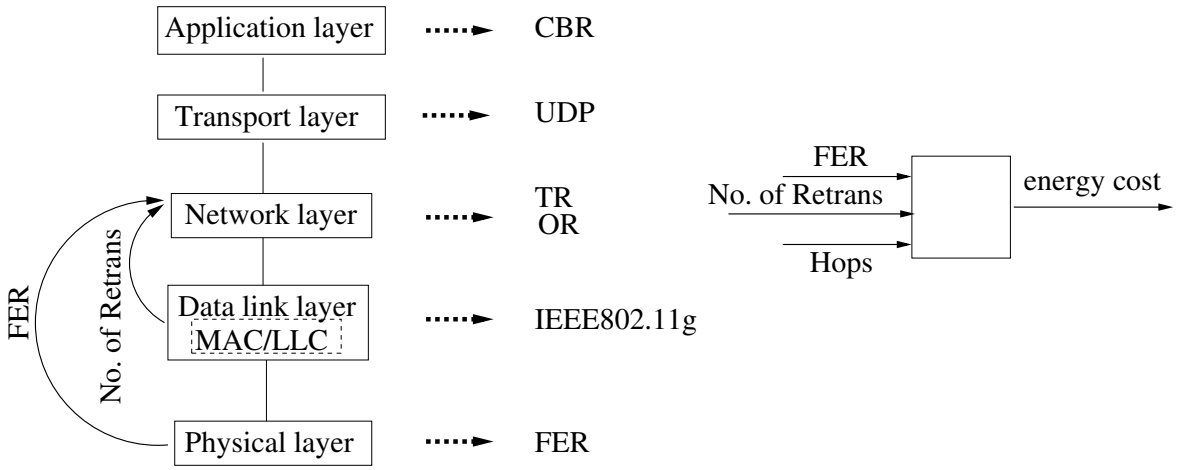

Figure 5.1: System model of our cross-layer aided energy-efficient routing in *ad hoc* networks, which may be contrasted to the regimes seen in Figures 3.1 and 4.1.

5.1 Introduction

Energy saving in wireless *ad hoc* networks is a salient problem, which mitigates the problem of limited battery supply at each node. Numerous energy-efficient algorithms have been proposed for reducing the energy consumption [127, 132–142]. The authors of [135, 136] have aimed for energy saving without considering the specifics of the

network layer, the data link layer or the physical layer. By contrast, the authors of [127, 130, 134, 137–140, 143–146] invoked cross-layer optimization, since the energy reduction is related to several layers. The authors of [132, 135] conceived energy-efficient routing concepts.

Traditional Routing (TR) relies on a route discovery process invoked for gleaning sufficient routing information for the source to make meritorious routing decisions, regardless, whether the routing protocol is proactive or reactive [96]. However, due to the rapid fluctuation of the channel conditions, the routing information estimated on the basis of the average Channel Quality Information (CQI) may become stale, resulting in suboptimum routing. Therefore, Opportunistic Routing (OR) [129–134, 138, 144, 147–150] has been proposed for avoiding this problem. In OR no pre-selected route is employed, instead a so-called forwarder RN set is used for forwarding the packets along a beneficial route. The near-instantaneously varying characteristics of wireless channels is beneficially exploited considered by OR. Liu *et al.* [129] illustrated the basic idea behind OR and categorized the potential design criteria, including the Estimated Transmission count (ETX), the geographic distance aided and the energy consumption based philosophies. Biswas and Morris [130] proposed an Extremely Opportunistic Routing (ExOR) scheme, which employed the ETX metric at the destination for deciding the priority order of selecting a RN from the potential forwarder set. The proposed routing regime integrated the routing protocol and the MAC protocol for the sake of increasing the attainable throughput of multi-hop wireless networks. Their solution [130] also exploited the less reliable long-distance links, which would have been ignored by traditional routing protocols. Moreover, Dubois-Ferrière *et al.* [147] conceived the Least-Cost Anypath Routing (LCAR) regime, which finds the optimal choice of candidate RNs relying on the expected ETX cost of forwarding a packet to the destination. This LCAR algorithm considers the coordination of the link layer protocols. Laufer *et al.* [150] proposed a 'polynomial-time multirate anypath' routing algorithm and provided the proof of its optimality. The proposed routing algorithm employed the Expected Anypath Transmission Time (EATT) as the routing metric, which is a generalization of the unidirectional ETX metric that takes into account that nodes transmit at multiple bit rates. The authors of [131, 132, 149] employed a geographic distance based metric for choosing the potential forwarder RN set. More specifically, Zorzi and Rao [131] proposed an OR scheme based on random forwarding, where the specific node, which is closest to the Destination (D) is chosen as the RN for the next hop. This chapter theoretically analyzed the achievable multi-hop performance. Furthermore, Zorzi and Rao [132] analyzed the achievable energy as well as latency performance and provided a detailed description

of a MAC scheme based on both opportunistic concepts and on collision avoidance. Zeng *et al.* [149] proposed a multirate OR by incorporating rate adaptation into their candidate-selection algorithm, which was shown to achieve a higher throughput and lower delay than the corresponding traditional single-rate routing and its opportunistic single-rate routing counterpart. The authors of [133, 134, 138] employed the energy consumption metric for choosing the potential forwarder RN set. More concretely, Mao *et al.* [133] presented an energy-efficient OR strategy relying on sophisticated power allocation, which prioritizes the forwarder RNs by directly minimizing the total energy consumption of all nodes. Dehghan *et al.* [134] developed a minimum-energy cooperative routing based on many-to-many cooperation and determines the optimal route with the aid of the Bellman-Ford algorithm [151]. Wei *et al.* [138] proposed an energy-conserving Assistant Opportunistic Routing (AsOR) protocol, which classified a sequence of nodes into three different node sets, namely, the frame node, the assistant node and the unselected node. The frame nodes were indispensable for decode-and-forward operation, while the assistant nodes provided protection against unsuccessful opportunistic transmissions. Although the authors of [133, 134, 138] employed the energy consumption as their routing metric, they have not provided any theoretical bounds in their performance analysis. Moreover, these authors assumed that the number of affordable MAC retransmissions was infinite. Against this background, *our novel contributions are:*

- *Two accurate energy-consumption-based OFs are constructed, which are used for the TR and the OR respectively. We exploit the knowledge of both the Frame Error Ratio (FER) within the physical layer, and of the number of MAC retransmissions as well as of the number of RNs in the network layer.*
- *A routing algorithm is designed for the TR, which employs our energy-consumption-based OF. Similarly, a routing algorithm is designed for OR, which employs our energy-consumption-based OF for ordering the RNs (from small to large) in the forwarder set. Theoretical bounds are derived for the Normalized Energy Consumption (NEC) of both the algorithms, which are shown to be close to the ultimate bound obtained with the aid of an exhaustive search.*
- *The achievable end-to-end throughput, the end-to-end delay and the delay distribution of the system are also evaluated theoretically.*

The rest of the chapter is organized as follows. Section 5.2 theoretically analyzes the performance of the system for the single-hop route, for the TR and for the OR. Section 5.3 describes our energy-efficient routing algorithms conceived for TR and OR, respectively. The delay distribution of OR is also analyzed. Finally,

Section 4.3 analyzes the overall performance of the system, while Section 5.5 provides our conclusions.

5.2 Theoretical Analysis

In this chapter, the transmit energy consumed by the data packets during their transmission is considered under the idealized simplifying assumption that the energy dissipated by other packets, such as the routing and MAC control packets, is negligible. Before defining the proposed energy-consumption-based OF, the symbols used are defined.

- H: the number of hops in an established route;
- P_{t_i}: the transmit power in the i-th node of the established route;
- FER_i: the FER of the i-th link in an established route;
- p_i: the successful probability of the i-th link, where $p_i = 1 - FER_i$;
- N_r: the maximum number of MAC retransmissions, including the first transmission attempt;
- E_{total}: the total energy consumption;
- $\overline{E}_{total}$: the total energy consumption E_{total} normalized by the end-to-end successful reception probability, which is the average energy consumption dissipated by the entire system during the successful delivery of a packet from the source to the destination.

5.2.1 FER and Power Allocation in a Single-Hop Route

In our previous work [49], an accurate energy-consumption-based OF was employed for estimating the normalized end-to-end energy consumption for a given route under the assumption that the FER, the maximum number of MAC retransmissions and the number of hops were known. Although the energy-consumption-based OF representing the real-world scenarios is beneficial, the resultant best route still wastes energy, since the distances between the different pairs of RNs are different. For the sake of ensuring that the total power-consumption is minimized, each node's transmit power should be different. Therefore, we invoke power control for further reducing the energy consumption by finding the optimum transmit power for each node.

Naturally, the channel conditions, the thermal noise level and the distance between the transmitter and the receiver jointly determine the FER of a link. We conducted simulations for characterizing the FER performance versus the Signal-to-Noise-Ratio (SNR) and followed the approach of [143] for fitting a polynomial to the FER versus SNR curve. The benefits of using curve-fitting is that this allows us to obtain a closed-form expression for representing the near-instantaneous channel conditions. The Forward Error Correction (FEC) scheme employed in this chapter is an Irregular

Convolutional Coded, Unity-Rate Coded and Quadrature Phase-Shift Keying (IrCC-URC-QPSK) [48, 152] scheme. The corresponding FER versus SNR curve was generated with the aid of bit-by-bit simulations. The overall FEC code rate was $R_c = 0.5$, the effective throughput was 1 bps (bits/symbol), the frame length was 8688 bits, the number of transmitted frames was 10 000. The IrCC had 17 component codes, associated with the weights [0.049, 0, 0, 0, 0, 0.24, 0.16, 0.12, 0.035, 0.102, 0, 0.071, 0.093, 0, 0.091, 0, 0.039][1]. We generated the FER curve for the AWGN channel model with the aid of simulation. According to the approach of [143], this will allow us to determine the average FER for arbitrary fading channels upon weighting the AWGN-FER by the Probability Distribution Function (PDF) of the fading channel and averaging it over the legitimate dynamic range. More specifically, the channel model considered is the uncorrelated, non-dispersive Rayleigh fading channel. The average FER expression $FER_{Rayleigh}$ is determined for the Rayleigh fading channel considered by integrating the specific FER_{AWGN} value of the AWGN channel experienced at a given SNR after weighting it by the probability of that specific SNR, which is given by:

$$FER_{Rayleigh} = \int_0^\infty e^{-\gamma} FER_{AWGN}(\gamma) d\gamma, \tag{5.1}$$

where γ is the channel SNR, $e^{-\gamma}$ represents the Rayleigh channel while the $FER_{AWGN}(\gamma)$ versus the SNR curve is approximated by the following four-segment FER vs. SNR model representing the AWGN channel:

$$FER_{AWGN}(\gamma) \approx \begin{cases} 1, & \text{if } 0 \leq \gamma < \eta_1, \\ 10a_1 \log(\gamma) + a_2, & \text{if } \eta_1 \leq \gamma < \eta_2, \\ 10a_3 \log(\gamma) + a_4, & \text{if } \eta_2 \leq \gamma < \eta_3, \\ a_5 e^{-10a_6 \log(\gamma)}, & \text{if } \gamma \geq \eta_3, \end{cases} \tag{5.2}$$

with η_1, η_2 and η_3 being the break-points of the four-segment FER versus SNR approximation $FER_{AWGN}(\gamma)$. Equation (5.1) and Equation (5.2) are suitable for approximating different FER curves by appropriately setting the corresponding parameter values invoked. Equation (5.1) may be readily extended to arbitrary channel models. Given $FER_{Rayleigh}$, we can calculate the successful reception probability of a link which is equal to $[1 - (FER_{Rayleigh})^{N_r}]$ if the maximum number of MAC

[1]The 17 coding coefficients α_i, $i = [1, 2, ..., 17]$, are the 17 coding fractions of the 17 corresponding component codes (subcode), the i^{th} of which having a code rate β_i encodes the fraction α_i of the input bit stream, where we have $[\beta_1 = 0.1, \beta_2 = 0.15, \beta_3 = 0.2, \beta_4 = 0.25, \beta_5 = 0.3, \beta_6 = 0.35, \beta_7 = 0.4, \beta_8 = 0.45, \beta_9 = 0.5, \beta_{10} = 0.55, \beta_{11} = 0.6, \beta_{12} = 0.65, \beta_{13} = 0.7, \beta_{14} = 0.75, \beta_{15} = 0.8, \beta_{16} = 0.85, \beta_{17} = 0.9]$. Hence, the constraint of $R_c = \sum_{i=1}^{17} \alpha_i \beta_i = 0.5$ is always satisfied.

retransmissions (including the first MAC retransmission attempt) is N_r. Specifically, for the IrCC-URC-QPSK scheme of Subsection 3.2.1 [48] employed, we have $a_1 = -0.5889$, $a_2 = 1.3341$, $a_3 = -3.705$, $a_4 = 3.5169$, $a_5 = 4.4669 \times 10^6$ and $a_6 = 18.9118$. Additionally, the values of the break-points η_1, η_2 and η_3 are determined for the SNR points of 0.6 dB, 0.7 dB and 0.9 dB, which are based on the curves seen in Figure 5.2. Figure 5.2 shows the FER performance versus the SNR, when the IrCC-URC-QPSK scheme of Subsection 3.2.1 is employed, relying on the average code rate of $R_c = 0.5$ in an AWGN channel. As seen from Figure 5.2, the corresponding horizontal points of the symbol '$\times$' are 0.6 dB, 0.7 dB and 0.9 dB.

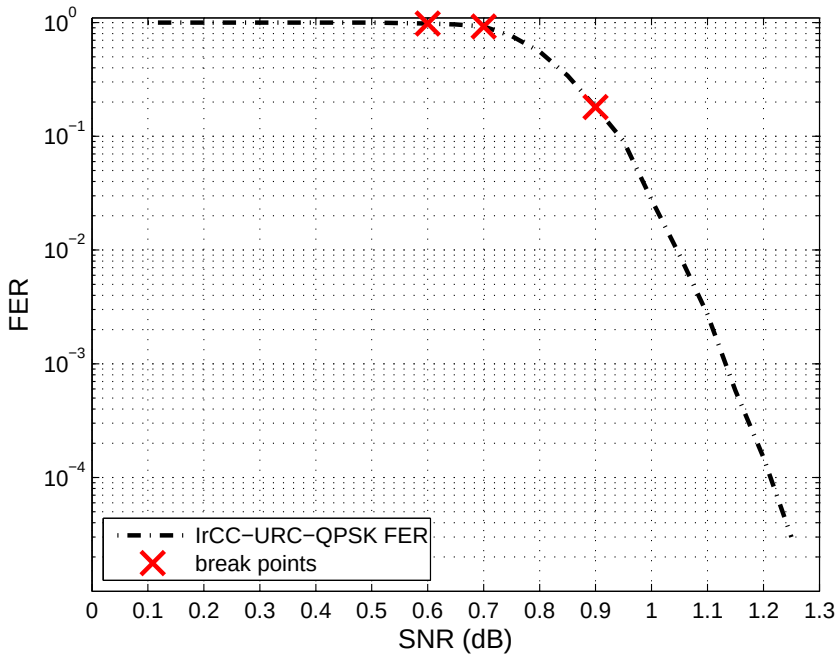

Figure 5.2: FER versus SNR for the IrCC-URC-QPSK scheme of Subsection 3.2.1 for the average code rate of $R_c = 0.5$ in an AWGN channel.

Their relationships are given by:

$$\eta_1 = \frac{10^{\frac{0.6}{10}} d^\alpha N_0 (4\pi)^2}{P_{t_1} \lambda^2} \tag{5.3}$$

$$\eta_2 = \frac{10^{\frac{0.7}{10}} d^\alpha N_0 (4\pi)^2}{P_{t_1} \lambda^2} \tag{5.4}$$

$$\eta_3 = \frac{10^{\frac{0.9}{10}} d^\alpha N_0 (4\pi)^2}{P_{t_1} \lambda^2}, \tag{5.5}$$

where λ is the wavelength of light, d is the distance between the transmitter and the receiver, N_0 is the thermal noise power and α is the path-loss exponent. In this chapter, we set $\alpha = 2$.

Substituting our FER versus SNR model of Equation (5.2) associated with the above-mentioned parameters into Equation (5.1), we have the following results:

- When $0 \leq \gamma < \eta_1$, we have

$$\begin{aligned} FER_I &= \int_0^{\eta_1} e^{-\gamma} d\gamma = 1 - e^{-\eta_1} \\ &= 1 - e^{-\frac{10^{\frac{0.6}{10}} d^\alpha N_0 (4\pi)^2}{P_{t_1} \lambda^2}}; \end{aligned} \tag{5.6}$$

- When $\eta_1 \leq \gamma < \eta_2$, we have

$$\begin{aligned} FER_{II} &= \int_{\eta_1}^{\eta_2} (10a_1 \log(\gamma) + a_2) e^{-\gamma} d\gamma \\ &= a_2(e^{-\eta_1} - e^{-\eta_2}) + a_1 \int_{\eta_1}^{\eta_2} \frac{10}{\ln 10} \ln\left(\frac{P_{t_1}\lambda^2}{(4\pi)^2 d^\alpha}\gamma\right) e^{-\gamma} d\gamma; \end{aligned} \tag{5.7}$$

  After carrying out the integration with the aid of the Euler function of $Ei(x) = \int_{-x}^{\infty} \frac{e^{-t}}{t} dt$ [153] (8.211.1), we arrive at:

$$FER_{II} = a_2(e^{-\eta_1} - e^{-\eta_2}) + 0.6a_1 e^{-\eta_1} - 0.7a_1 e^{-\eta_2} + a_1 \frac{10}{\ln 10} \left[Ei(-\eta_2) - Ei(-\eta_1)\right]; \tag{5.8}$$

- When $\eta_2 \leq \gamma < \eta_3$, we have an expression similar to Equation (5.8):

$$\begin{aligned} FER_{III} &= \int_{\eta_2}^{\eta_3} (10a_3 \log(\gamma) + a_4) e^{-\gamma} d\gamma \\ &= a_4(e^{-\eta_2} - e^{-\eta_3}) + 0.7a_3 e^{-\eta_2} - 0.9a_3 e^{-\eta_3} + a_3 \frac{10}{\ln 10} \left[Ei(-\eta_3) - Ei(-\eta_2)\right]; \end{aligned} \tag{5.9}$$

- Finally, for $\gamma \geq \eta_3$, we have

$$\begin{aligned} FER_{IV} &= \int_{\eta_3}^{\infty} a_5 e^{(-10a_6 \log(\gamma))} e^{-\gamma} d\gamma \\ &= a_5 \int_{\eta_3}^{\infty} \frac{e^{-\gamma}}{e^{\ln\left[\frac{P_{t_1}\lambda^2}{(4\pi)^2 d^\alpha}\gamma\right]^{\frac{10b}{\ln 10}}}} d\gamma \\ &= 10^{\frac{-0.9a_6}{\ln 10}} a_5 \eta_3 G_{1,2}^{2,0}\left[\eta_3 \left| \begin{matrix} \frac{10a_6}{\ln 10} \\ \frac{10a_6}{\ln 10} - 1, 0 \end{matrix} \right.\right], \end{aligned} \tag{5.10}$$

  where the Meijer-G function is defined in [153] (9.301) and we have $G_{1,2}^{2,0}\left[x \left| \begin{matrix} \nu \\ \nu - 1, 0 \end{matrix} \right.\right] = E_\nu(x) = \int_1^{\infty} \frac{e^{-xt}}{t^\nu} dt$ [154] (06.34.02.001.01).

However, the FER formula derived above does not consider the effects of retransmissions in the data link layer, neither does it take into account the number of hops in the network layer. In a realistic scenario, however, we have poor channel conditions, a high level of interference, the effects of node mobility, potential network congestions and so on, where the packets are often dropped before reaching the destination. However, the dropped packets consume a high amount of energy during their passage through the network. Therefore, we analyze the Normalized Energy Consumption (NEC) during a packet's passage from the source to the destination. We have to consider two scenarios, namely the energy consumption E_s when a packet is delivered successfully to the destination and that given by E_f when it is dropped before reaching the destination.

The performance of a single-hop route is analyzed first, where p_1 is the successful probability of the first hop. Then, the probability p_s that a packet is successfully delivered from the Source (S) to the destination (D) within the maximum N_r number of retransmissions is [49]

$$p_s = \sum_{i_1=1}^{N_r} (1-p_1)^{i_1-1} p_1, \tag{5.11}$$

By contrast, the probability p_f that a packet is dropped before reaching its destination is [49]

$$p_f = 1 - p_s = (1-p_1)^{N_r}. \tag{5.12}$$

Hence, the energy E_s required for the successful transmission of a packet and that dissipated during the transmission of a failed packet, namely E_f, are respectively given by

$$E_s = \sum_{i_1=1}^{N_r} (1-p_1)^{i_1-1} p_1 i_1 P_{t_1} T, \tag{5.13}$$

$$E_f == (1-p_1)^{N_r} N_r P_{t_1} T, \tag{5.14}$$

where T is the duration of a time slot.

Consequently, the average total energy E_{total} required for transmitting a packet is $E_{total} = E_s + E_f$. Regardless, whether the packet successfully arrives at D or not, if it dissipated the nodes' energy, it will be taken into account in E_{total}. Furthermore, the total energy E_{total} normalized by the successful probability p_s, which is the energy dissipated by the whole system during the successful delivery of a packet to D, can be

expressed as

$$\overline{E}_{total} = \frac{E_{total}}{p_s} = \frac{E_s + E_f}{p_s}. \tag{5.15}$$

When substituting Equations (5.11), (5.13) and (5.14) into Equation (5.15), we arrive at:

$$\overline{E}_{total} = \frac{P_{t_1}}{p_1} T, \tag{5.16}$$

which shows that $\overline{E}_{total}$ is independent of the number of retransmissions in a single-hop route. In this context, the NEC is the same as that of a transmitter operating without a transmission limit, i.e. when we have $N_r = \inf$. Moreover, Equations (5.6), (5.7), (5.9) and (5.10) illustrate the relationship between P_{t_1} and p_1. Then, $\overline{E}_{total}$ only depends on the distance between S and D. Therefore, optimizing the transmit power of the S may be formulated as a convex optimization problem.

Once we have the closed-form expression (Equation (5.16)) of the NEC $\overline{E}_{total}$ of a single hop, the optimized transmit power P_{t_1} may be calculated by setting the derivative of Equation (5.16) with respect to P_{t_1} to zero, which yields

$$\begin{aligned} \frac{1}{p_1} + \frac{P_{t_1}}{p_1^2} \frac{d(1-p_1)}{dP_{t_1}} &= 0 \\ \frac{p_1}{-P_{t_1}} &= \frac{d(1-p_1)}{dP_{t_1}}, \end{aligned} \tag{5.17}$$

where we have $\frac{d(1-p_1)}{dP_{t_1}} = \frac{d(FER_1)}{dP_{t_1}}$, since $p_1 = 1 - FER_1$. Upon manipulating Equation (5.17) further by setting the derivatives of the four parts of the four-segment approximated FER versus SNR curve detailed in Equations (5.6), (5.7), (5.9) and (5.10), we arrive at

$$\frac{p_1}{-P_{t_1}} = \frac{dFER_{1,I}}{dP_{t_1}} + \frac{dFER_{1,II}}{dP_{t_1}} + \frac{dFER_{1,III}}{dP_{t_1}} + \frac{dFER_{1,IV}}{dP_{t_1}}. \tag{5.18}$$

To elaborate a little further, based on Equation (5.6), we have

$$\begin{aligned} \frac{dFER_{1,I}}{dP_{t_1}} &= \frac{d(1-e^{-\eta_1})}{dP_{t_1}} \\ &= -\frac{10^{\frac{0.6}{10}}(4\pi)^2 d^\alpha N_0 e^{-\frac{10^{\frac{0.6}{10}}(4\pi)^2 d^\alpha N_0}{P_{t_1}\lambda^2}}}{P_{t_1}^2 \lambda^2}, \end{aligned} \tag{5.19}$$

While based on Equation (5.7), we arrive at Equation (5.20),

$$\begin{aligned}\frac{dFER_{1,II}}{dP_{t_1}} =& \frac{d\left[a_2(e^{-\eta_1}-e^{-\eta_2})\right]}{dP_{t_1}} + \frac{d\left[0.6a_1e^{-\eta_1}-0.7a_1e^{-\eta_2}+a_1\frac{10}{\ln 10}\left[Ei(-\eta_2)-Ei(-\eta_1)\right]\right]}{dP_{t_1}} \\ =& -(0.6a_1+a_2)\frac{10^{\frac{0.6}{10}}(4\pi)^2d^\alpha N_0 e^{-\frac{10^{\frac{0.6}{10}}(4\pi)^2d^\alpha N_0}{P_{t_1}\lambda^2}}}{P_{t_1}^2\lambda^2} \\ &+(a_2+0.7a_1)\frac{10^{\frac{0.7}{10}}(4\pi)^2d^\alpha N_0 e^{-\frac{10^{\frac{0.7}{10}}(4\pi)^2d^\alpha N_0}{P_{t_1}\lambda^2}}}{P_{t_1}^2\lambda^2} \\ &+\frac{10a_1}{P_{t_1}\ln 10}\left[e^{-\frac{10^{\frac{0.6}{10}}(4\pi)^2d^\alpha N_0}{P_{t_1}\lambda^2}}-e^{-\frac{10^{\frac{0.7}{10}}(4\pi)^2d^\alpha N_0}{P_{t_1}\lambda^2}}\right],\end{aligned} \tag{5.20}$$

where $\frac{dEi(x)}{dx}=\frac{e^x}{x}$ [153] (8.211.1). It can be readily shown that $\frac{dFER_{1,III}}{dP_{t_1}}$ obeys an expression similar to Equation (5.20), which is formulated in Equation (5.21).

$$\begin{aligned}\frac{dFER_{1,III}}{dP_{t_1}} =& \frac{d\left[a_4(e^{-\eta_2}-e^{-\eta_3})\right]}{dP_{t_1}} + \frac{d\left[0.7a_3e^{-\eta_2}-0.9a_3e^{-\eta_3}+a_3\frac{10}{\ln 10}\left[Ei(-\eta_3)-Ei(-\eta_2)\right]\right]}{dP_{t_1}} \\ =& -(0.7a_3+a_4)\frac{10^{\frac{0.7}{10}}(4\pi)^2d^\alpha N_0 e^{-\frac{10^{\frac{0.7}{10}}(4\pi)^2d^\alpha N_0}{P_{t_1}\lambda^2}}}{P_{t_1}^2\lambda^2} \\ &+(a_4+0.9a_3)\frac{10^{\frac{0.9}{10}}(4\pi)^2d^\alpha N_0 e^{-\frac{10^{\frac{0.9}{10}}(4\pi)^2d^\alpha N_0}{P_{t_1}\lambda^2}}}{P_{t_1}^2\lambda^2} \\ &+\frac{10a_3}{P_{t_1}\ln 10}\left[e^{-\frac{10^{\frac{0.7}{10}}(4\pi)^2d^\alpha N_0}{P_{t_1}\lambda^2}}-e^{-\frac{10^{\frac{0.9}{10}}(4\pi)^2d^\alpha N_0}{P_{t_1}\lambda^2}}\right].\end{aligned} \tag{5.21}$$

Finally, based on Equation (5.10), the 4th part at the righthand side of Equation (5.18) can be expressed as Equation (5.22),

$$\begin{aligned}\frac{dFER_{1,IV}}{dP_{t_1}} =& \frac{d\left[10^{\frac{-0.9a_6}{\ln 10}}a_5\eta_3E_{\frac{10a_6}{\ln 10}}(\eta_3)\right]}{dP_{t_1}} \\ =& -10^{\frac{-0.9a_6}{10}}a_5G_{2,3}^{2,1}\left[\frac{10^{\frac{0.9}{10}}(4\pi)^2d^\alpha N_0}{P_{t_1}\lambda^2}\,\middle|\,\begin{matrix}-1,\frac{10a_6}{\ln 10}\\ \frac{10a_6}{\ln 10}-1,0,0\end{matrix}\right]\frac{10^{\frac{0.9}{10}}(4\pi)^2d^\alpha N_0}{P_{t_1}^2\lambda^2},\end{aligned} \tag{5.22}$$

where the differentiation of Meijer's G function was taken from [154] (07.34.20.0005.01).

Finally, when substituting Equations (5.19), (5.20), (5.21) and (5.22) into Equation (5.18), the analytical expression of the optimized transmit power P_{t_1} can be found. The existence of the optimized transmit power at the source of a single-hop route is shown in Figure 5.6.

5.2.2 Analysis of Traditional Routing in a Linear-Topology Network

The energy consumption of an idealized multi-hop route arranged in a line is analyzed in this subsection. The network topology is shown in Figure 5.3.

In Figure 5.3, we have a single S, a single D and $(H-1)$ Rs. The $(H-1)$ Rs are located between S and D. Our previous contribution [49] analyzed both the probability and the total energy consumption of a packet, when it is delivered successfully to D or when it is dropped before reaching D of Figure 5.3. However, in [49] we assumed that the transmit power of all nodes is the same, which wasted some energy in the realistic scenario, when the distances between each pair of nodes was different. If the optimal distance-dependent transmit power is found, then the NEC may be further reduced.

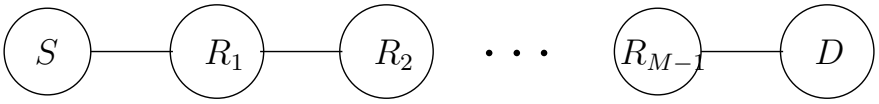

Figure 5.3: Test-topology having one source, one destination and $(H-1)$ RNs.

The probabilities p_s and p_f are the same as those in [49], namely

$$p_s = \sum_{i_1=1}^{N_r} \cdots \sum_{i_H=1}^{N_r} (1-p_1)^{i_1-1} p_1 (1-p_2)^{i_2-1} p_2 \cdots (1-p_H)^{i_H-1} p_H, \tag{5.23}$$

$$p_f = p_f(1) + \sum_{h=2}^{H} p_f(h), \tag{5.24}$$

where $p_f(1)$ is given by Equation (5.12) and $p_f(h)$ is the probability that a packet is dropped at the h-th hop, which is formulated as:

$$p_f(h) = \sum_{i_1=1}^{N_r} \cdots \sum_{i_{h-1}=1}^{N_r} (1-p_1)^{i_1-1} p_1 \cdots (1-p_{h-1})^{i_{h-1}-1} p_{h-1} (1-p_h)^{N_r}, h \neq 1. \tag{5.25}$$

Let E_i be the energy required by node i to send a packet, where $E_i = P_{t_i} T$. Then, we can show that E_s and E_f are formulated as:

$$\begin{aligned} E_s = & \sum_{i_1=1}^{N_r} \cdots \sum_{i_H=1}^{N_r} (1-p_1)^{i_1-1} p_1 (1-p_2)^{i_2-1} p_2 \\ & \cdots (1-p_H)^{i_H-1} p_H (i_1 E_1 + i_2 E_2 + \cdots + i_H E_H), \end{aligned} \tag{5.26}$$

$$\begin{aligned}E_f =& E_f(1) + \sum_{h=2}^{H} E_f(h) \\ =& N_r E_1 (1-p_1)^{N_r} + \sum_{h=2}^{H} \Bigg[\sum_{i_1=1}^{N_r} \cdots \sum_{i_{h-1}=1}^{N_r} (1-p_1)^{i_1-1} p_1 \\ & \cdots (1-p_{h-1})^{i_{h-1}-1} p_{h-1} (1-p_h)^{N_r} (i_1 E_1 + \cdots + i_{h-1} E_{h-1} + N_r E_h) \Bigg]. \end{aligned} \tag{5.27}$$

Let D_s denote the average time required for delivering a packet successfully to D, where the source of delay is assumed to be the Automatic Repeat reQuest (ARQ)-aided retransmissions. Explicitly, each new hop and new transmission attempt imposes a delay of unity, i.e. one Time-Slot (TS). Furthermore, let D_f be the average delay imposed on a packet's passage through the route, when it is dropped before reaching its destination. These average delays have been quantified in [49], which are

$$D_s = \Bigg[\sum_{i_1=1}^{N_r} \cdots \sum_{i_H=1}^{N_r} (1-p_1)^{i_1-1} p_1 (1-p_2)^{i_2-1} p_2 \cdots (1-p_H)^{i_H-1} p_H (i_1 + i_2 + \cdots + i_H) \Bigg] T, \tag{5.28}$$

$$D_f = p_f(1) N_r T + \sum_{h=2}^{H} D_f(h), \tag{5.29}$$

where $D_f(h)$ is the average delay experienced by a packet, which is dropped during the h-th hop, expressed as

$$\begin{aligned} D_f(h) =& \Bigg[\sum_{i_1=1}^{N_r} \cdots \sum_{i_{h-1}=1}^{N_r} (1-p_1)^{i_1-1} p_1 \cdots (1-p_{h-1})^{i_{h-1}-1} p_{h-1} (1-p_h)^{N_r} \\ & (i_1 + \cdots + i_{h-1} + N_r) \Bigg] T, h \neq 1. \end{aligned} \tag{5.30}$$

For the sake of simplifying Equation (5.26), (5.27), (5.28) and (5.29), we define $A(p_i) = (\frac{1-(1-p_i)^{N_r}}{p_i} - N_r(1-p_i)^{N_r}) E_i$ and $B(p_i) = 1-(1-p_i)^{N_r}$. Then, we have $p_s = \prod_1^H B(p_i)$. Furthermore, it may be readily shown that E_s and E_f can be formulated alternatively as:

$$E_s = \left[\prod_{i=1}^{H} B(p_i) \right] \left[\sum_{i=1}^{H} \frac{A(p_i)}{B(p_i)} \right], \tag{5.31}$$

$$E_f = \sum_{h=2}^{H} \left[\left[\prod_{i=1}^{h-1} B(p_i) \right] \left[\sum_{i=1}^{h-1} \frac{A(p_i)}{B(p_i)} \right] [1 - B(p_h)] + N_r E_h (1 - B(p_h)) \prod_{i=1}^{h-1} B(p_i) \right] + N_r E_1 [1 - B(p_1)]. \quad (5.32)$$

Similarly, upon defining $C(p_i) = (\frac{1-(1-p_i)^{N_r}}{p_i} - N_r(1-p_i)^{N_r})T$, we can express D_s and D_f as

$$D_s = \left[\prod_{i=1}^{H} B(p_i) \right] \left[\sum_{i=1}^{H} \frac{C(p_i)}{B(p_i)} \right], \quad (5.33)$$

$$D_f = \sum_{h=2}^{H} \left[\left[\prod_{i=1}^{h-1} B(p_i) \right] \left[\sum_{i=1}^{h-1} \frac{C(p_i)}{B(p_i)} \right] [1 - B(p_h)] + N_r T [1 - B(p_h)] \prod_{i=1}^{h-1} B(p_i) \right] + N_r T [1 - B(p_1)]. \quad (5.34)$$

Based on the above derivation, the NEC expressed as $\overline{E}_{total} = \frac{E_{total}}{p_s} = \frac{E_s + E_f}{p_s}$ can now be evaluated.

The end-to-end delay D_{e2e} is given by

$$D_{e2e} = D_s, \quad (5.35)$$

which represents the delay experienced by a packet that is successfully delivered to the destination. Moreover, the end-to-end throughput R_{e2e} is given by

$$R_{e2e} = \frac{p_s}{D_s + D_f}. \quad (5.36)$$

The objective function of the optimization is $\overline{E}_{total} = \frac{E_{total}}{p_s} = \frac{E_s + E_f}{p_s}$, where E_s, E_f, p_s can be found in Equations (5.31), (5.32) and (5.24). Note that E_s and E_f are a function of both p_i and E_i, $i = 1, 2, \cdots, H$, while p_s is the function of p_i, $i = 1, 2, \cdots, H$. As shown in Equations (5.18), (5.19), (5.20), (5.21) and (5.22), p_i is the function of P_{t_i} and $E_i = P_{t_i} T$, hence E_s, E_f and p_s are ultimately the function of P_{t_i}.

We set $\frac{\partial \overline{E}_{total}}{\partial P_{t_i}} = 0$, $i = 1, 2, \cdots, H$, giving us H equations, which allows us to find P_{t_i}, $i = 1, 2, \cdots, H$, since we have H unknowns. Therefore all the transmission powers P_{t_i} can be found theoretically.

However, the complexity of solving this set of equations is unacceptably high. Below, some of the relevant equations are listed. Note that only one of the H equations

is shown here:

$$\begin{aligned}\frac{\partial \overline{E}_{total}}{\partial P_{t_i}} &= \frac{\partial \frac{E_s+E_f}{p_s}}{\partial P_{t_i}} \\ &= \frac{\partial \frac{E_s}{p_s}}{\partial P_{t_i}} + \frac{\partial \frac{E_f}{p_s}}{\partial P_{t_i}}.\end{aligned} \tag{5.37}$$

There are two terms in Equation (5.37) and the first term is:

$$\begin{aligned}\frac{\partial \frac{E_s}{p_s}}{\partial P_{t_i}} &= \partial \sum_{i=1}^{H} \frac{A(p_i)}{B(p_i)} / \partial P_{t_i} \\ &= \partial \frac{A(p_i)}{B(p_i)} / \partial P_{t_i} \\ &= \partial \left((\frac{1}{p_i} - \frac{Nr(1-p_i)^N r}{1-(1-p_i)^N r}) T P_{t_i} \right) / \partial P_{t_i} \\ &= \left(\frac{1}{p_i} - \frac{Nr(1-p_i)^N r}{1-(1-p_i)^N r} \right) T + T P_{t_i} \left(\frac{-1}{p_i^2} + \frac{Nr^2(1-p_i)^{(Nr-1)} \frac{\partial p_i}{\partial P_{t_i}}}{(1-(1-p_i)^N r)^2} \right),\end{aligned} \tag{5.38}$$

where $\frac{\partial p_i}{\partial P_{t_i}}$ is shown in Equations (5.18), (5.19), (5.20), (5.21) and (5.22). The second term may be classified as $\partial \frac{E_f}{p_s} / \partial P_{t_1}$, $\partial \frac{E_f}{p_s} / \partial P_{t_H}$ and $\partial \frac{E_f}{p_s} / \partial P_{t_i}$, $i = 2, 3, \cdots, H-1$, yielding

$$\begin{aligned}\frac{\partial \frac{E_f}{p_s}}{\partial P_{t_1}} &= \frac{1}{\prod_{i=2}^{H} B(p_i)} \frac{\partial \frac{NrTP_{t_1}(1-p_1)^N r}{1-(1-p_1)^N r}}{\partial P_{t_1}} + \partial \left(\sum_{h=2}^{H} \left[\frac{1}{\prod_{i=h}^{H} B(p_i)}) \right] (1 - B(p_h)) \left[\sum_{i=1}^{h-1} \frac{A(p_i)}{B(p_i)} \right] \right) / \partial P_{t_1} \\ &= \frac{1}{\prod_{i=2}^{H} B(p_i)} \frac{\partial (-NrTP_{t_1} + \frac{NrTP_{t_1}}{1-(1-p_1)^N r})}{\partial P_{t_1}} + \sum_{h=2}^{H} \left[\frac{1 - B(p_h)}{\prod_{i=h}^{H} B(p_i)}) \right] \partial \frac{A(p_1)}{B(p_1)} / \partial P_{t_1} \\ &= \frac{NrT(1-p_1)^N r}{\prod_{i=2}^{H} B(p_i)} \frac{1 - p_1 - (1-p_1)^{(Nr+1)} - P_{t_1} \frac{\partial p_i}{\partial P_{t_i}}}{(1-(1-p_1)^N r)^2} \\ &+ \sum_{h=2}^{H} \left[\frac{1 - B(p_h)}{\prod_{i=h}^{H} B(p_i)} \right] (\frac{1}{p_1} - \frac{Nr(1-p_1)^N r}{1-(1-p_1)^N r}) T + T P_{t_1} (\frac{-1}{p_1^2} + \frac{Nr^2(1-p_1)^{(Nr-1)} \frac{\partial p_1}{\partial P_{t_1}}}{(1-(1-p_1)^N r)^2}).\end{aligned} \tag{5.39}$$

It is somewhat tedious, but not challenging to derive $\partial \frac{E_f}{p_s} / \partial P_{t_H}$ and $\partial \frac{E_f}{p_s} / \partial P_{t_i}$, $i = 2, 3, \cdots, H-1$, which we skip here. The above formulas already demonstrate that the complexity of the exact theoretical solution of finding the optimized transmit power for multiple hops becomes unacceptably high, hence this brute-force method is abandoned. Instead, this chapter is dedicated to the optimization of every single hop, which is implemented in Line 8 of **Algorithm 1** detailed in Subsection 5.3.1.

5.2.3 Analysis of Opportunistic Routing in a Random Network

The TR transmits the packet along the specific pre-selected route having the lowest estimated NEC. This pre-selected route is determined after the estimation and comparison of the NEC of each potential candidate route. The information invoked for routing decisions is gleaned during the process of route discovery, but this information may become stale owing to node-mobility. Instead, OR considers the potential chances of success for each candidate RN, bearing in mind their time-variant channel conditions. Regardless of which particular RN receives the packet from the source successfully, if this RN has the highest priority in the forwarder RN list, it will forward the packet to the next RN. Naturally, the challenge in the design of the OR procedure is the beneficial selection of the forwarder RN set, the specific priority order of the potential forwarders and the avoidance of duplicate transmissions [129]. We assume that all the nodes in a node's neighbor list belong to this node's forwarder R-list. The metric used for determining the priority order is the normalized energy required by this particular RN for reaching D. Acknowledgement (ACK) packets are employed for avoiding the duplicate transmissions. The particular RN in the forwarder R-set, which has the highest priority owing to requiring the lowest energy will send the ACK first. The other RNs, which overhear the ACK will withdraw from the competition [155, 156].

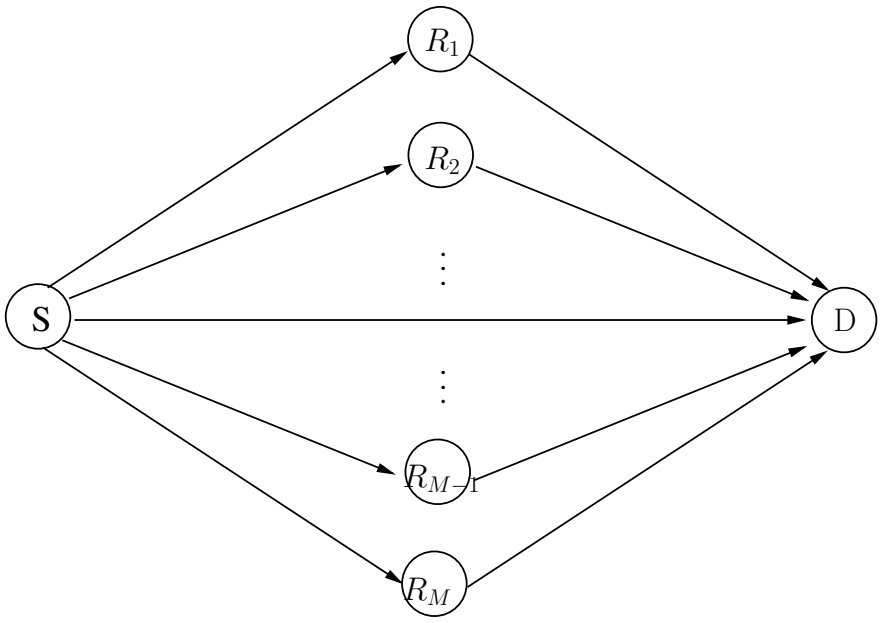

Figure 5.4: A two-hop network assisted by a number of RNs.

A two-hop network is shown in Figure 5.4, which has a single source S, a single destination D and M RNs $R_1, R_2, \cdots, R_{M-1}, R_M$. S and D are capable of communicating with all the RNs, as well as with each other. By contrast, the M RNs are unable to communicate with each other. We stipulate the idealized simplifying assumption furthermore that each node knows the position of all other nodes. For

each RN $R_m, m = 1...M$, the total average energy consumption E_{R_mD} required for transmission from R_m to D is given by $E_{R_mD} = E^s_{R_mD} + E^f_{R_mD}$, where $E^s_{R_mD}$ and $E^f_{R_mD}$ are given in Equation (5.13) and (5.14). Let E_S denote the energy dissipated while sending a packet from the source S to any of the RNs R_m, which is $E_S = P_{t_S}T$. We assume that $E_{R_1D} < E_{R_2D} < \cdots < E_{R_MD}$. Furthermore, for convenience, we represent the destination node D as R_0 and define $\prod_{m=0}^{M}(1 - p_{SR_m}) = \zeta$.

If the source successfully sends a packet to the m-th RN, $m = 0, 1, \ldots, M$, with the aid of n_r transmissions, the probability of this event is

$$p_0(n_r) = \zeta^{n_r-1} p_{SR_0}, if\ m = 0 \tag{5.40}$$

$$p_m(n_r) = \zeta^{n_r-1} \prod_{i=0}^{m-1}(1 - p_{SR_i}) p_{SR_m}, if\ 1 \le m \le M. \tag{5.41}$$

Correspondingly, the energy dissipated becomes

$$E_0(n_r) = n_r E_S, if\ m = 0 \tag{5.42}$$

$$E_m(n_r) = n_r E_S + E_{R_mD}, if\ 1 \le m \le M. \tag{5.43}$$

Let D_{R_mD} denote the average delay of a packet traversing from R_m, $m = 1, \ldots, M$, to D, including the delay $D^s_{R_mD}$ encountered by a packet that is successfully delivered to D and the delay $D^f_{R_mD}$ experienced when a packet is dropped before reaching D. We then have $D_{R_mD} = D^s_{R_mD} + D^f_{R_mD}$, where $D^s_{R_mD}$ represents D_s expressed by Equation (5.33) and $D^f_{R_mD}$ corresponds to D_f expressed by Equation (5.34), provided that the number of hops is 1. Consequently, we have:

$$D_0(n_r) = n_r D_S, if\ m = 0 \tag{5.44}$$

$$\begin{aligned} D_m(n_r) &= n_r D_S + D_{R_mD} \\ &= n_r D_S + (D^s_{R_mD} + D^f_{R_mD}), if\ 1 \le m \le M, \end{aligned} \tag{5.45}$$

where D_S is T, which denotes the duration of a TS.

Consequently, when taking into account all the possible events, the total energy consumption is

$$E_{total} = \sum_{n_r=1}^{N_r} p_0(n_r)E_0(n_r) + \sum_{n_r=1}^{N_r}\sum_{m=1}^{M} p_m(n_r)E_m(n_r) + \zeta^{N_r}(N_r E_S), \tag{5.46}$$

while the total delay becomes:

$$D_{total} = \sum_{n_r=1}^{N_r} p_0(n_r) D_0(n_r) + \sum_{n_r=1}^{N_r} \sum_{m=1}^{M} p_m(n_r) D_m(n_r) + \zeta^{N_r}(N_r D_S), \tag{5.47}$$

where the final term in Equation (5.46) and Equation (5.47) is contributed by the event that the packet was not delivered by the source S even after N_r attempts. Upon substituting Equation (5.41) and Equation (5.43) into Equation (5.46), we obtain

$$\begin{aligned} E_{total} = &\sum_{n_r=1}^{N_r} \zeta^{n_r-1} p_{SR_0}(n_r E_S) \\ &+ \sum_{n_r=1}^{N_r} \sum_{m=1}^{M} \zeta^{n_r-1} \prod_{i=0}^{m-1} (1 - p_{SR_i}) p_{SR_m}(n_r E_S + E_{R_m D}) + \zeta^{N_r}(N_r E_S). \end{aligned} \tag{5.48}$$

After substituting Equation (5.41) and Equation (5.45) into Equation (5.47), we arrive at Equation (5.49),

$$\begin{aligned} D_{total} = &\sum_{n_r=1}^{N_r} \zeta^{n_r-1} p_{SR_0}(n_r D_S) \\ &+ \sum_{n_r=1}^{N_r} \sum_{m=1}^{M} \zeta^{n_r-1} \prod_{i=0}^{m-1} (1 - p_{SR_i}) p_{SR_m}(n_r D_S + D^s_{R_m D} + D^f_{R_m D}) + \zeta^{N_r}(N_r D_S) \\ = &\sum_{n_r=1}^{N_r} \zeta^{n_r-1} p_{SR_0}(n_r D_S) + \sum_{n_r=1}^{N_r} \sum_{m=1}^{M} \zeta^{n_r-1} \prod_{i=0}^{m-1} (1 - p_{SR_i}) p_{SR_m}(n_r D_S + D^s_{R_m D}) \\ &+ \sum_{n_r=1}^{N_r} \sum_{m=1}^{M} \zeta^{n_r-1} \prod_{i=0}^{m-1} (1 - p_{SR_i}) p_{SR_m}(n_r D_S + D^f_{R_m D}) + \zeta^{N_r}(N_r D_S), \end{aligned} \tag{5.49}$$

where the second term is contributed by the event that a packet is successfully delivered from the source S to the destination D, while the third term by the event that a packet is successfully delivered from the source S to the RN R_m, $m = 1, \ldots, M$, but it is dropped during its passage from the RN R_m, $m = 1, \ldots, M$, to the destination D.

After further simplifications, Equation (5.46) and Equation (5.47) may be written as Equation (5.50) and Equation (5.51).

$$E_{total} = E_S \left(\frac{1 - \zeta^{N_r}}{1 - \zeta} - N_r \zeta^{N_r} \right) + \frac{1 - \zeta^{N_r}}{1 - \zeta} \sum_{m=1}^{M} \left[E_{R_m D} p_{SR_m} \left[\prod_{j=0}^{m-1} (1 - p_{SR_j}) \right] \right] + N_r E_S \zeta^{N_r} \tag{5.50}$$

$$D_{total} = D_S\left(\frac{1-\zeta^{N_r}}{1-\zeta} - N_r\zeta^{N_r}\right) + \frac{1-\zeta^{N_r}}{1-\zeta}\sum_{m=1}^{M}\left[D^s_{R_mD}p_{SR_m}\left[\prod_{j=0}^{m-1}(1-p_{SR_j})\right]\right] + \frac{1-\zeta^{N_r}}{1-\zeta}\sum_{m=1}^{M}\left[D^f_{R_mD}p_{SR_m}\left[\prod_{j=0}^{m-1}(1-p_{SR_j})\right]\right] + N_rD_S\zeta^{N_r}. \quad (5.51)$$

Then, the end-to-end delay D_{e2e} is given by the first two terms of Equation (5.51), formulated as Equation (5.52).

$$D_{e2e} = D_s = D_S\left(\frac{1-\zeta^{N_r}}{1-\zeta} - N_r\zeta^{N_r}\right) + \frac{1-\zeta^{N_r}}{1-\zeta}\sum_{m=1}^{M}\left[D^s_{R_mD}p_{SR_m}\left[\prod_{j=0}^{m-1}(1-p_{SR_j})\right]\right]. \quad (5.52)$$

Meanwhile, the packet transmitted from S may be dropped in the $S-D$, $S-R_m$ or R_m-D link, where we have $m=1,...,M$ and again, the destination can be replaced by R_0 . The probabilities of these events are given by

$$p_{f,S-R_m} = \zeta^{N_r}, m = 0,\ldots,M \quad (5.53)$$

$$p_{f,R_m-D} = \sum_{n_r=1}^{N_r}\sum_{m=1}^{M}\zeta^{n_r-1}\left[\prod_{j=0}^{m-1}(1-p_{SR_j})\right]p_{SR_m}(1-p_{R_mD}), m = 1,\ldots,M, \quad (5.54)$$

where p_{R_mD} is the probability that a packet is successfully delivered from R_m, $m = 1,\ldots,M$, to the destination D.

Then we may formulate the end-to-end outage probability p_f as

$$p_f = p_{f,S-R_0} + p_{f,S-R_m} + p_{f,R_m-D}, m = 1,\ldots,M. \quad (5.55)$$

Upon substituting Equation (5.54) into Equation (5.55), we arrive at:

$$\begin{aligned} p_f &= \zeta^{N_r} + \sum_{n_r=1}^{N_r}\sum_{m=1}^{M}\zeta^{n_r-1}\left[\prod_{j=0}^{m-1}(1-p_{SR_j})\right]P_{SR_m}(1-p_{R_mD}) \\ &= \zeta^{N_r} + \frac{1-\zeta^{N_r}}{1-\zeta}\sum_{m=1}^{M}\left[\prod_{j=0}^{m-1}(1-p_{SR_j})\right]P_{SR_m}(1-p_{R_mD}). \end{aligned} \quad (5.56)$$

Furthermore, we may formulate the NEC $\overline{E}_{total}$ as

$$\overline{E}_{total} = \frac{E_{total}}{1-p_f}, \quad (5.57)$$

while the end-to-end throughput R_{e2e} is given by

$$R_{e2e} = \frac{1 - p_f}{D_{total}}. \tag{5.58}$$

Let us now introduce a new low-complexity algorithm in the next section for calculating both the delay D_{e2e} and the throughput R_{e2e} in a simpler way. Moreover, we will demonstrate that our analysis of the energy consumption can be extended to a large network synthesized by numerous two-hop networks, as shown in Figure 5.4. The corresponding details are provided in Section 5.3.1. The way of finding the exact theoretical solution of the optimized transmit power for multiple hops in OR is the same as for TR, which was provided in Subsection 5.2.2.

5.3 Routing Algorithms

5.3.1 Traditional Routing Algorithm

The performance of the single-hop route and of an idealized linear-topology network was characterized in Subsections 5.2.1 and 5.2.2, which may be readily extended to existing routing protocols, such as the (Dynamic Source Routing)DSR, (Ad hoc On-demand Distance Vector) AODV and (DYnamic Manet On-demand) DYMO routing protocols. During the route discovery process, the routing packets are used for gathering the necessary information and for feeding it back to the source. Then the source makes the final decision required for sending the data packets. The most important feature of traditional routing is that the route is selected first, then the packets are always delivered along this particular route, until it is broken, for example due to node-mobility. At that moment, a sub-optimal candidate route is chosen by route-repair, or the route re-discovery process will be re-activated for finding a totally new route.

The idealized linear-topology multi-hop network of Figure 5.3 may be extended to a more realistic random network relying on Dijkstra's routing algorithm [157] and invoking the NEC $\overline{E}_{total}$ for route selection. The routing algorithm is described in **Algorithm 1**. We assume that $\mathcal{V}$ is the vertex set, v is a node in the set $\mathcal{V}$, $\mathcal{F}(v)$ denotes the predecessor set of nodes in the route before the node v, while $\overline{E}(v), \overline{E}(S, v)$ denote the NEC and $p_s(v), p_s(S, v)$ represent the successful probability of a packet from the source S to the node v. Furthermore, $D_s(v)$ and $D_s(S, v)$ denote the delay encountered by a packet delivered successfully from the source S to the node v, while $D_f(v)$ and $D_f(S, v)$ represent the delay of a packet that was dropped before reaching the node v. Specifically, $\overline{E}(S, v)$, $p_s(S, v)$, $D_s(S, v)$ and $D_f(S, v)$ are the intermediate values of $\overline{E}(v)$, $p_s(v)$, $D_s(v)$ and $D_f(v)$, respectively. Moreover, $\mathcal{S}$ represents the set of selected nodes, while $P_t^{opt}(u, v)$ denotes the optimal transmit power of node u assigned for transmission to node v.

Algorithm 1: TR

1 **for** *every node* $v \in \mathcal{V}$ **do**
2 $\quad \mathcal{F}(v) \leftarrow \varnothing$, and $\overline{E}(v) = \infty$.
3 **end**
4 $\overline{E}(S) \leftarrow 0$, $D_s(S) \leftarrow 0$, $D_f(S) \leftarrow 0$, $p_s(S) \leftarrow 0$, $\mathcal{S} \leftarrow S$ and $u \leftarrow S$.
5 **while** $\mathcal{S} \neq \mathcal{V}$ **do**
6 $\quad temp \leftarrow \infty$;
7 $\quad$ **for** *each node* $v \notin \mathcal{S}$ **do**
8 $\quad\quad$ Find the optimal transmit power $P_t^{opt}(u, v)$ that minimizes $\overline{E}(S, v)$ among all possible power assignments from S to v by Equation (5.15). Meanwhile, calculate the time $D_s(S, v)$, $D_f(S, v)$ and the successful probability $p_s(S, v)$.
9 $\quad\quad$ **if** $\overline{E}(S, v) < \overline{E}(v)$ **then**
10 $\quad\quad\quad$ $\mathcal{F}(v) \leftarrow u$, $\overline{E}(v) \leftarrow \overline{E}(S, v)$, $D_s(v) \leftarrow D_s(S, v)$, $D_f(v) \leftarrow D_f(S, v)$ and $p_s(v) \leftarrow p_s(S, v)$;
11 $\quad\quad$ **end**
12 $\quad\quad$ **if** $\overline{E}(v) < temp$ **then**
13 $\quad\quad\quad$ $temp \leftarrow \overline{E}(v)$, and $u^{'} \leftarrow v$;
14 $\quad\quad$ **end**
15 $\quad$ **end**
16 $\quad u \leftarrow u^{'}$, and $\mathcal{S} \leftarrow \mathcal{S} \bigcup \{u\}$;
17 **end**

Lines 1-3 initialize the predecessor set $\mathcal{F}(v)$ of each node and the NEC between S and each other node. In line 4, the NEC, the delay and the successful delivery probability are set to zero and S is selected for inclusion into $\mathcal{S}$. In line 8, the notation u represents the specific node, which has just been incorporated into $\mathcal{S}$ in the previous loop. Initially, only S belongs to $\mathcal{S}$. Therefore, S is u. S has a neighbor node set. For each node v, which belongs to the neighbor set of S, we can calculate the NEC $\overline{E}(S, v)$ between S and v, given that S employs the optimal transmit power. The optimal transmit power $P_t^{opt}(u, v)$ of node u in the link 'u-v' is found by identifying the lowest NEC between S and v, which is obtained by setting the derivative of Equation (5.15) with respect to P_{t_u} to zero. Meanwhile, lines 9-11 show that if the NEC $\overline{E}(S, v)$ from S to v via u becomes lower than the stored $\overline{E}(v)$, then the NEC $\overline{E}(v)$ and the corresponding delay from S to v are updated. In lines 12-14, the specific node, which has the lowest $\overline{E}_{S,v}$ amongst all u's neighbor set, would be incorporated into $\mathcal{S}$ and becomes the new u in the next loop, as seen in line 16. Again, u has a new neighbor set and the next new u will be selected from the neighbor set. When we have $\mathcal{S} = \mathcal{V}$, **Algorithm 1** converges, as shown in line 5. Moreover, this algorithm is

a locally - rather than globally - optimal algorithm, which is in fact optimal for every single hop. This is justified by the calculation of the optimal transmit power $P_t^{opt}(u, v)$ in line 8. Therefore, the source S employs **Algorithm** 1 for identifying that particular route, which has the lowest NEC $\overline{E}_{total}$. At the same time, it also determines the delay $D_s(S)$, namely, the end-to-end delay D_{e2e} of the selected route. Finally, the end-to-end throughput R_{e2e} may be calculated by Equation (5.36) based on $D_s(S)$, $D_f(S)$ and $p_s(S)$.

The computational complexity has three main contributing factors: a) the calculation of a single NEC in a specific case; b) the number of NEC calculations; c) and finally, finding the minimum NEC in each round. Let us denote the complexity of E_s in Equation (5.31), E_f in Equation (5.32) and p_s, where $p_s = \prod_1^H B(p_i)$, by $\mathcal{C}(E_s)$, $\mathcal{C}(E_f)$ and $\mathcal{C}(p_s)$. The complexity of evaluating D_s and D_f is the same as that of E_s and E_f, apart from a multiplicative constant. The number of NEC calculations is given by the number of node pairs, which is $\mathcal{V}(\mathcal{V}-1)/2$ (see line 5 and line 7 in **Algorithm 1**). The minimum NEC can be found based on the Fibonacci heap approach of [158], which has a complexity on the order of $\mathrm{O}(\log \mathcal{V})$. Therefore, the complexity imposed by **Algorithm 1** is $\mathrm{O}[\mathcal{V}^2[\mathcal{C}(E_s) + \mathcal{C}(E_f) + \mathcal{C}(p_s)] + \mathcal{V} \log \mathcal{V}]$.

5.3.2 Opportunistic Routing Algorithm

In Section 5.2.3, the minimum NEC is obtained by finding the optimal power allocation. Although the network topology in Figure 5.4 has only two hops, this algorithm may be extended to a large network, where the OR principle is employed for each hop. Meanwhile, the optimal transmit power of each node is found for the sake of minimizing the NEC required for the successful passage of a packet from that node to the destination. Therefore, **Algorithm** 2 is conceived for calculating the minimum NEC by carrying out optimum distance-dependent power allocation at each node, hop-by-hop. As a by-product, the delay distribution $\mathbf{D}_s(S)$ of a packet being successfully delivered to the destination and the delay distribution $\mathbf{D}_f(S)$ of a packet being dropped before reaching the destination are also delivered by **Algorithm** 2, where $\mathbf{D}_s(S)$ is the end-to-end delay distribution, which allows us to calculate the average end-to-end delay. Moreover, the end-to-end throughput may also be calculated based on $\mathbf{D}_s(S)$, $\mathbf{D}_f(S)$ and $p_f(S)$. Here, for any node v in a given vertex set $\mathcal{V}$, $\overline{E}(v), \overline{E}(v, D)$ denotes the NEC $\overline{E}_{total}$ necessitated for transmission from node v to the destination D, where we denote the potential set of receiver nodes by $\mathcal{R}$. Furthermore, $P_t^{opt}(v)$ is the optimal transmit power, which minimizes the NEC required for transmission from node v to the destination D, while $\mathbf{D}_s(v), \mathbf{D}_s(v, D)$ denotes the vector of probabilities for each particular integer delay in terms of TSs, when a packet is delivered successfully from node v to the destination D. For example, a single-hop route has the vector

of delay probabilities given by $\mathbf{D}_s(S, D)$, where the number of elements is N_r. The elements of $\mathbf{D}_s(S, D)$ are given by $(1 - p_s)^{n_r} p_s$, where p_S is the probability of a packet being successfully delivered to the destination D and $n_r = 1, ..., N_r$ is the number of MAC retransmissions. Furthermore, $\mathbf{D}_s^{n_r}(v)$ denotes the delay probability vector of a packet, which is delivered from node v to the destination D, when the number of MAC retransmissions is n_r. By contrast, $\mathbf{D}_f(v), \mathbf{D}_f(v, D)$ denotes the delay probability vector of a packet, which is dropped before reaching the destination D. Let us denote the probability of a packet being successfully delivered from node v to node n by $p_s(v, n)$ and the probability of a packet, which is dropped before reaching the destination by $p_f(v), p_f(v, D)$. $\gg n_r$ implies that the vector elements are shifted to the right by n_r positions and the left positions are filled with zeros.

In **Algorithm 2**, Lines 1-3 initialize the NEC between each node and the destination. Line 4 shows that D is incorporated into the receiver set $\mathcal{R}$ and the probability vectors of delay $D_s(D)$ and $D_f(D)$ from D to itself are set to unity. Initially, only D belongs to $\mathcal{R}$ and D has a neighbor node set. In line 8, the notation u represents the specific node, where $u \notin \mathcal{R}$ belongs to the neighbor set of D at each loop. The optimal transmit power $P_t^{opt}(u)$ of node u can be obtained by setting the derivative of Equation (5.57) with respect to P_{t_u} to zero, which minimizes $\overline{E}(u, D)$. Meanwhile, the probability $p_f(u, D)$ is calculated by Equation (5.56). Lines 23-25 show that if the NEC $\overline{E}(u, D)$ from node u to D via the receiver set $\mathcal{R}$ is lower than the stored NEC $\overline{E}(u)$, then $\overline{E}(u)$, the probability vector of delay $D_s(u)$, $D_f(u)$ and the delivery failure probability $p_f(u)$ are updated. Lines 26-28 show that if a node u has the lowest NEC $\overline{E}(u, D)$ in each loop, then it will be represented as u' and be incorporated into $\mathcal{R}$, as seen in line 30. Again, in the next loop, any node, which belongs to the neighbor set of u' and does not belong to $\mathcal{R}$, will become a new u. The new u and $\mathcal{R}$ will contain a new opportunistic relaying sub-network, where the new sub-network topology is similar as the one in Figure 5.4 and the optimal transmit power of each RN has already been obtained in the previous loops. **Algorithm 2** would converge, when we have $\mathcal{R} = \mathcal{V}$, as seen in line 5. Like TR, **Algorithm** 2 is also a locally optimal algorithm, which is in fact optimal for every single hop. This can also be explained by the calculation of the optimal transmit power $P_t^{opt}(u)$ in line 8. The technique of determining the optimal transmit power and the specific choice of the next RN together at each single opportunistic-RN-aided hop will be elaborated on as follows.

The process of finding the optimized transmit power is activated during the initialization stage before data transmission, which is only dependent on the position of each node. During this process, the forwarder set of each node is also determined. Following the initialization stage, the source node starts to transmit data and

Algorithm 2: OR

for *every node* $v \in \mathcal{V}$ **do**
  $\overline{E}(v) \leftarrow \infty$.
end
$\mathcal{R} \leftarrow \{D\}$, $\mathbf{D}_s(D) \leftarrow [1]$ and $\mathbf{D}_f(D) \leftarrow [1]$.
while $\mathcal{R} \neq \mathcal{V}$ **do**
  $temp \leftarrow \infty$
  for *every node* $u \notin \mathcal{R}$ **do**
    Find the optimal transmit power $P_t^{opt}(u)$ that minimizes $\overline{E}(u, D)$ among all possible power assignments from u to D by Equation (5.57). Meanwhile, calculate the probability $p_f(u, D)$ by Equation (5.56).
    $\mathbf{D}_s(u, D) \leftarrow [0]$ and $\mathbf{D}_f(u, D) \leftarrow [0]$.
    for *every node* $v \in \mathcal{R}$, *v is the m-th element of* $\mathcal{R}$ **do**
      for $(n_r = 1; n_r \leq N_r; n_r++)$ **do**
        if *node v is the destination D* **then**
          $\mathbf{D}_s^{n_r}(u, D) \leftarrow \mathbb{Q}^{n_r-1} p_s(u, D)\mathbf{D}_s(v)$, $\mathbf{D}_s^{n_r}(u, D) \gg n_r$.
          if $n_r == N_r$ **then**
            $\mathbf{D}_f^{N_r}(u, D) \leftarrow \mathbb{Q}^{N_r}\mathbf{D}_f(v)$, $\mathbf{D}_f^{N_f}(u, D) \gg N_r$.
          end
        else
          $\mathbf{D}_s^{n_r}(u, D) \leftarrow \mathbb{Q}^{n_r-1} \prod_{i=1}^{m-1}(1 - p_s(u, i))p_s(u, v)\mathbf{D}_s(v)$,
          $\mathbf{D}_f^{n_r}(u, D) \leftarrow \mathbb{Q}^{n_r-1} \prod_{i=1}^{m-1}(1 - p_s(u, i))p_s(u, v)\mathbf{D}_f(v)$, $\mathbf{D}_s^{n_r}(u, D) \gg n_r$,
          $\mathbf{D}_f^{n_r}(u, D) \gg n_r$.
        end
      end
      $\mathbf{D}_s(u, D) \leftarrow \mathbf{D}_s(u, D) + \sum_1^{N_r} \mathbf{D}_s^{n_r}(u, D)$, $\mathbf{D}_f(u, D) \leftarrow \mathbf{D}_f(u, D) + \sum_1^{N_r} \mathbf{D}_f^{n_r}(u, D)$.
    end
    if $\overline{E}(u, D) < \overline{E}(u)$ **then**
      $\overline{E}(u) \leftarrow \overline{E}(u, D)$, $\mathbf{D}_s(u) \leftarrow \mathbf{D}_s(u, D)$, $\mathbf{D}_f(u) \leftarrow \mathbf{D}_f(u, D)$ and $p_f(u) \leftarrow p_f(u, D)$;
    end
    if $\overline{E}(u) < temp$ **then**
      $temp \leftarrow \overline{E}(u)$ and $u' \leftarrow u$;
    end
  end
  $\mathcal{R} = \mathcal{R} \bigcup \{u'\}$;
end

the potential RN will forward the data. Since the channel conditions vary near-instantaneously, any node j (that belongs to the forwarder set of node i), which correctly decoded the data packet and has the lowest NEC, will forward the data packets further. The corresponding timeline of events may explain the associated procedure explicitly, which is listed below:

Each node is assumed to know the positions of all other nodes.

- Initialization stage:
  - **Algorithm 2** finds the optimized transmit power and forwarder set for each node.
- Data transmission stage:
  - Node i transmits its data packet at the current time instant.
  - The specific node, which simultaneously satisfies the conditions of a), b) and c) listed below, is selected as the RN, where the three conditions are:
    a) It correctly decodes the data packet;
    b) It is an element of node i's forwarder set;
    c) It has the lowest NEC required for reaching the destination compared to all the other elements of node i's forwarder set[2].
    We note that the selected RN may be different, whenever the same node, i.e. node i transmits its data packet, owing to the fading channel's near-instantaneous fluctuation. All the required operations may be implemented by the MAC layer protocol detailed in [155, 156].
  - The data packets finally reach the destination.

Moreover, lines 9-22 explain how to generate the delay distribution for the path spanning from node u to D. In each loop, node u and the receiver set $\mathcal{R}$ constitute a sub-network. The delay distribution of every node v in $\mathcal{R}$ has been obtained in the previous loops. As described above, the delay distribution of node v is a N_r-element vector $D_s(v)$, where the value of each element is the probability of a particular integer delay quantified in terms of TSs. Lines 13-16 calculate the delay distribution $D_s(u, D)$ if D receives the packet from u, while line 18 calculates the delay distribution $D_s(u, D)$ if node v in $\mathcal{R}$ - except for D - receives the packet from u. The *for loop* in line 11 considers all conditions when the number of MAC retransmissions from u to $\mathcal{R}$ is $1 \leq N_r \leq N_r$, where the sum is calculated in line 21. Finally, when **Algorithm 2** converges, we obtain the end-to-end delay distribution, which is $D_s(S)$.

The complexity of finding the transmit power and the forwarder set also depends on three contributing factors, just like for the TR scenario. In **Algorithm 2**, the

[2]A retransmission is requested from node i, when no node in its forwarder set satisfies the conditions of a), b) and c).

delay distribution **D** does not affect the complexity of finding the transmit power and the forwarder set. Let us denote the complexity of E_{total} in Equation (5.50) and of p_f in Equation (5.56) by $\mathcal{C}(E_{total})$ and $\mathcal{C}(p_f)$, respectively. Then line 5 in **Algorithm 2** has to be invoked $\mathcal{V}$ times, adding a further node into $\mathcal{R}$ in each round (in line 30 of **Algorithm 2**). Line 7 suggests that the optimal transmit power of any node in $(\mathcal{V}-\mathcal{R})$ is calculated in a specific round and the complexity of this calculation is given by $\mathcal{C}(E_{total})+\mathcal{C}(p_f)$. Again, the complexity of finding the optimal transmit power can be calculated by Fibonacci heap [158] which has a complexity on the order of $\mathrm{O}(\log \mathcal{V})$. Therefore, the complexity of **Algorithm 2** is $\mathrm{O}[\mathcal{V}^2[\mathcal{C}(E_{total})+\mathcal{C}(p_f)]+\mathcal{V}\log\mathcal{V}]$.

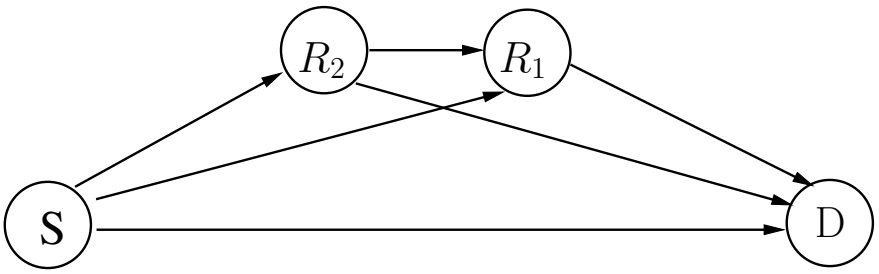

Figure 5.5: A twin-RN assisted network.

Figure 5.5 shows a twin-RN assisted network, which we use to exemplify **Algorithm 2**. We assume that each node is aware of the other nodes' position, hence also of their distance. In a compact form, we have $\mathcal{V}=\{S,R_1,R_2,D\}$ and $\mathcal{R}=\{D\}$. First, S, R_1 and R_2 calculate their transmit power optimized for minimizing the NEC $\overline{E}_{SD}$, $\overline{E}_{R_1D}$, $\overline{E}_{R_2D}$ for transmission to D by Equation (5.57), as seen in line 8. If the element $\overline{E}_{R_1D}$ is the lowest in the set of three energies, we update $\mathcal{R}$ to $\{R_1,D\}$, as shown in line 26 and line 30. In the second step, S and R_2 update their NEC for transmission to node D by considering $\{R_1,D\}$ as their forwarder RN set, as shown in line 23. Then, if $\overline{E}_{R_2D}$ is less than $\overline{E}_{SD}$, $\mathcal{R}$ is updated to $\{R_2,R_1,D\}$, as shown in line 26 and line 30. Finally, S adjusts its own transmit power to the optimal one, which minimizes $\overline{E}_{SD}$, where $\{R_2,R_1,D\}$ is the resultant forwarder R-set, as shown in line 8. At this stage, **Algorithm 2** may be deemed to have converged. In this algorithm, every node has to find its own forwarder R-set by itself upon exploiting the knowledge of the other nodes' positions. If more than one node in a node's forwarder R-list receives the packet from that node successfully, then that particular one, which requires the lowest NEC for transmission to the destination has the highest priority for forwarding this packet. The nodes of the forwarder R-set communicate with each other similarly to the technique of [155] and again, the NEC required for successful transmission to D is invoked for deciding the priority order of the forwarders.

Table 5.1: The common simulation configuration.

Packet Length	8688 bits
coding & modulation	IrCC-URC-QPSK
Channel model	uncorrelated and non-dispersive Rayleigh channel
Path-loss exponent	2
Information transmission rate	6 Mbits/s
Thermal noise power	−110 dBm

5.4 Performance Study

Having defined the energy-consumption-based OF and the optimal transmit power of both the TR and of the OR, let us now characterize the attainable system performance in terms of:

- Normalized energy consumption (mJ/bit): The total energy consumed by all the data packets transmitted through the network is normalized by the successful end-to-end reception probability. However, we do not consider the energy consumed by the control packets and the energy dissipated at the receiver nodes by signal processing.
- End-to-end throughput (bit/s): The number of data bits successfully delivered to the destination in a second, while neglecting the bits of the control packets.
- delay PDF: The probability distribution of the end-to-end delay.

The common parameters of the following simulations are listed in Tab 5.1.

Example 1: Let us first analyze the performance of a single-hop route. The maximum number of MAC retransmissions is $N_r = 7$. The distance between S and D is 1000 m. The other simulation configurations are listed in Tab 5.1. The NEC $\overline{E}_{total}$ and the end-to-end throughput R_{e2e} of the TR and the OR are compared both in terms of simulation and theoretical results in Figure 5.6.

The NEC is formulated in Equation (5.15) and simplified to Equation (5.16) in the case of a single-hop route. If the transmit power is low, then the successful reception probability is also low. By contrast, if the transmit power is high, then the successful reception probability is high. By setting the derivative of Equation (5.16) with respect to P_{t_1} to zero, the optimal transmit power of the source is found to be 0.12 mW, which may be obtained from Equation (5.17). When the source assigns the optimal transmit power to transmit its data, the NEC will reach its lowest value, as shown in Figure 5.6. Figure 5.6 shows that the NEC initially decreases and then increases slowly beyond the transmit power of 0.12 mW. The end-to-end throughput increases upon increasing the transmit power at S. Observe in Figure 5.6 that the simulation results closely match the theoretical curve.

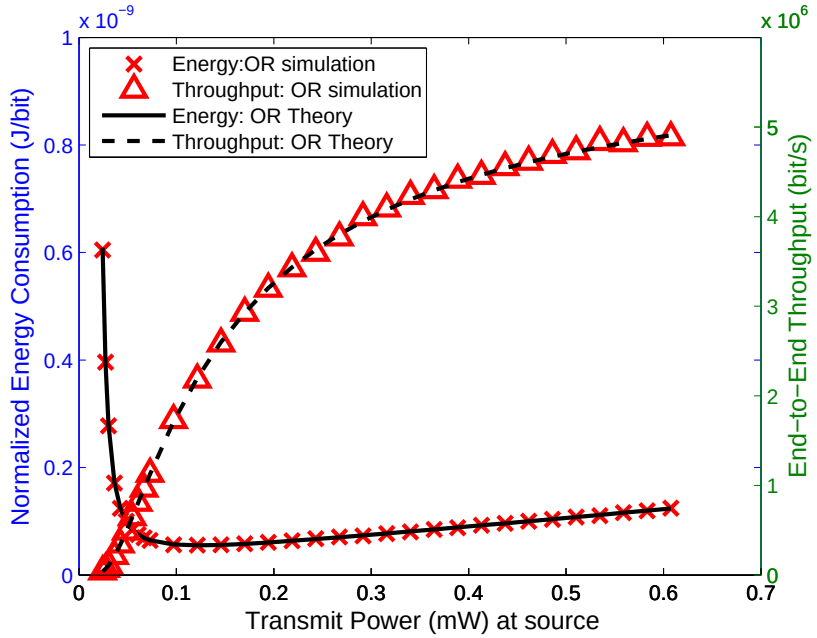

Figure 5.6: The NEC $\overline{E}_{total}$ and the end-to-end throughput R_{e2e} versus the transmit power P_{t_S}.

Example 2: Let us now analyze the performance of the two-RN assisted network seen in Figure 5.5. The positions of S, D, R_1 and R_2 are $(100, 100)$, $(900, 100)$, $(500, 500)$ and $(300, 400)$, respectively. The other simulation configurations are listed in Tab 5.1.

Since all the references [133, 134, 138] considered Opportunistic Routing (OR) algorithms, we will focus on discussing the differences and similarities between the OR proposed in this chapter and those in [133, 134, 138].

The schemes in [134, 138] are significantly different from that proposed in this chapter. More specifically, reference [134] developed a minimum-energy cooperative routing protocol based on many-to-many cooperation. The opportunistic routing of [134] is designed with the aid of cooperative routing, which hence introduced the many-to-many cooperation scheme. Additionally, the optimum power allocation of the forwarder nodes in the forwarder list is carried out under assuming a given outage probability constraint p_ϵ at each link. However, we only consider one-to-many cooperation, assuming furthermore that no outage probability constraint is imposed in this chapter. On the other hand, reference [138] proposed an energy-conserving regime referred to as the Assistant Opportunistic Routing (AsOR) protocol, which forwarded the data stream through a sequence of nodes. These nodes were classified as three different node sets, namely the frame node, the assistant node and the unselected node. Both the frame nodes and the assistant nodes belonged to a predetermined shortest route, which was selected by the traditional algorithm. The unselected nodes

did not join the data transmission at all. Each predetermined route can be divided into several disjoint segments, where each segment was constituted by a pair of frame nodes and the corresponding N^* assistant nodes between them. Within each segment opportunistic transmission was activated. Hence, the frame nodes were indispensable for decode-and-forward operation, while the assistant nodes provided protection against unsuccessful opportunistic transmissions. However, this chapter only considered the forwarder nodes and the unselected nodes. Therefore, we do not benchmark our OR against the algorithms of [134, 138].

To elaborate a little further, reference [133] presented an energy-efficient OR strategy relying on a different power allocation method, which prioritizes the forwarder RNs by directly minimizing the total energy consumption of all nodes. Our scheme is similar to that of [133]. However, although [133] employed the normalized energy consumption as the routing metric, it has not provided any theoretical bounds concerning its performance. Moreover, it did not consider the maximum number of affordable MAC retransmissions, it rather assumed it to be infinite. For example, in the two-hop network of Figure 5.4 the system's Normalized Energy Consumption (NEC) was the sum of the normalized energy consumed by S plus that of all forwarder nodes $R_i, i = 1, 2, ..., M$, both of which were normalized by the successful transmission probability of a packet from S to R_i. Using an infinite number of MAC retransmissions implied that the data transmission would never fail. By contrast, in this chapter the maximum number of MAC retransmissions is finite, which may render the links' transmission attempts unsuccessful. Moreover, the success or failure of each future link's transmission depends on the successful reception of all the previous links, instead of having an independent relationship amongst the consecutive links, albeit the latter assumption was stipulated in [133]. Again, when considering the two-hop network of Figure 5.4 for example, if the transmissions from S to R_i failed, then no transmissions took place from R_i to D and hence no energy was consumed by R_i. Furthermore, unsuccessful receptions may occur also during the transmission from R_i to D. Therefore, the total energy consumption is constituted by two contributions:

- The energy dissipated by a packet's transmission, which was successfully delivered to the destination;
- The energy consumed by a packet, which is dropped before reaching its destination.

The total energy consumption is appropriately weighted by the successful end-to-end delivery probability instead of the successful transmission probability of a packet from S to R_i, as assumed in [133]. Hence, instead of the simplistic additive relationship

used in [133] the energy dissipation relationship of the links considered in this chapter is more complex, as explicitly explained by Equations 5.50, 5.56 and 5.57.

Therefore, we opted for comparing the Adjustable power allocation aided Energy-Efficient Opportunistic Routing (A-EEOR) algorithm of [133] (which is referred to as **Algorithm 3**) to our OR algorithm (which is referred to as **Algorithm 2**) in this chapter.

The NEC $\overline{E}_{total}$ and the end-to-end throughput R_{e2e} are shown in Figure 5.7 and Figure 5.8 as a function of the maximum number of MAC retransmissions N_r. We also investigate the theoretical NEC bound of both TR and OR, which is found by the exhaustive search of all the routes spanning from S to D. Figure 5.7 shows that the performance of the energy-consumption OF based algorithm is close to the theoretical bound, especially in the case of a large N_r. Both Figures 5.7 and 5.8 show that our energy-efficient OR outperforms both the Adjustable Energy-Efficient Opportunistic Routing (A-EEOR) algorithm defined in [133] and the energy-efficient TR. More specifically, compared to A-EEOR algorithm our OR algorithm has a lower normalized energy consumption for $N_r < 4$, as seen in Figure 5.7, while exhibiting a higher end-to-end throughput for $N_r < 6$, as shown in Figure 5.8. Moreover, both our OR and TR simulation results closely match the theoretical curves. Note that the NEC $\overline{E}_{total}$ decreases upon increasing N_r. However, the end-to-end throughput R_{e2e} of OR is more stable. When we have $N_r = 1$ or 2, both the exhaustive search, labeled by "TR bound" and our proposed TR algorithm, labeled by "TR theory", selected the route 'S-D', hence, the NEC is the same for both. When we have $2 < N_r < 8$, the exhaustive search and our proposed TR algorithm choose different routes, since the exhaustive search is the globally optimal algorithm, while our proposed TR algorithm is a locally optimal algorithm, which is optimal for every single hop. Moreover, the simulation results corresponding to the 'TR simulation' label match the theoretical value represented by the label 'TR theory'. Therefore, the 'TR simulation/theory' and 'TR bound' scenarios have a performance gap, when we have $2 < N_r < 8$, as seen in Figure 5.7. Additionally, the end-to-end throughput for TR is in fact higher than that of OR for $N_r = 1$ and 2, but it is lower for $N_r \geq 4$, as seen in Figure 5.8. This is because in case of a low number of MAC retransmissions, the direct near-line-of-light route from S to D in the TR has a more dominant priority than the other routes.

There is no linear relationship between the number of hops and the NEC or the end-to-end throughput. Their relationships are characterized by Equations (5.15) and (5.36) for TR and by Equations (5.57) and (5.58) for OR in this chapter. In fact, Figure 4.15 of Chapter 4 analyzed the impact of the number of hops on both the NEC and on the end-to-end throughput, which shows that both the NEC as well as the

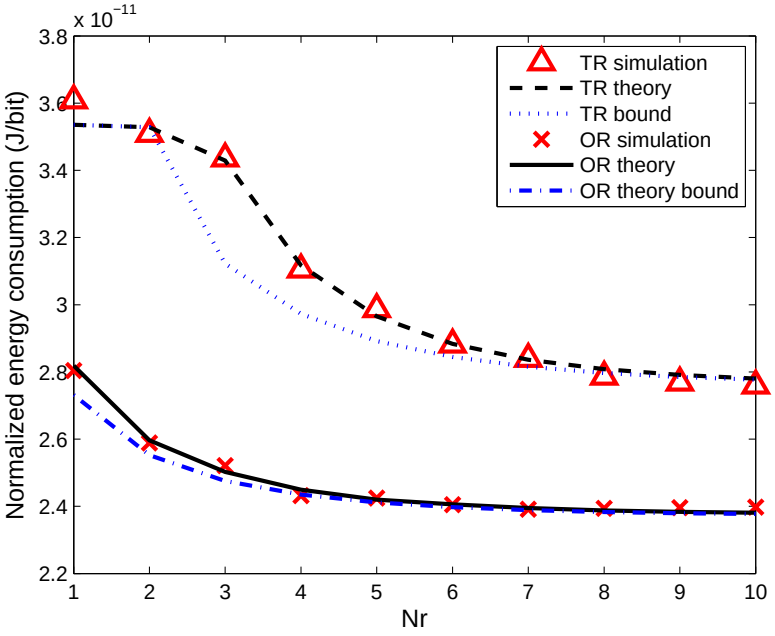

Figure 5.7: The NEC $\overline{E}_{total}$ versus the maximum number of MAC retransmissions N_r.

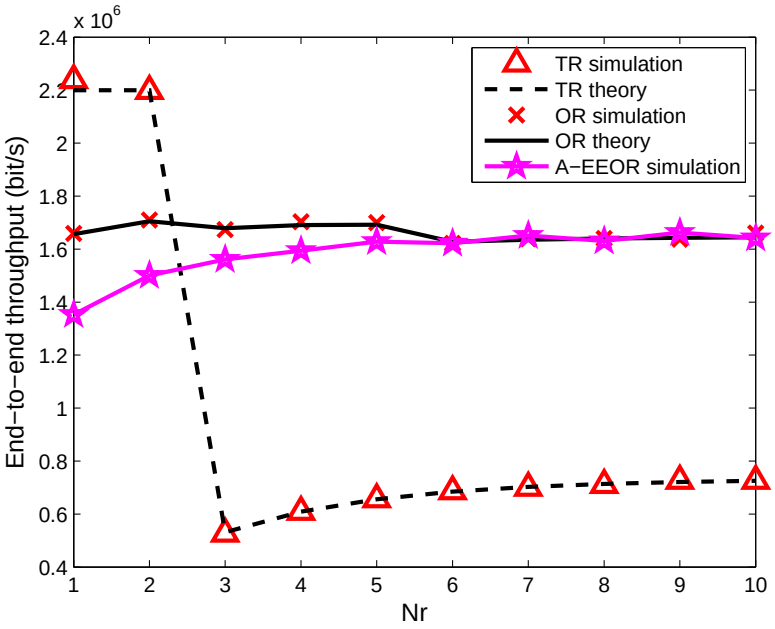

Figure 5.8: The end-to-end throughput R_{e2e} versus the maximum number of MAC retransmissions N_r.

end-to-end throughput are decreased, when the number of hops is increased. However, since the transmit power is assumed to be the same at each node in Figure 4.15, the relationships between them are no longer suitable in the context of this chapter.

We then continued by investigating the delay-PDF of the system in Figure 5.9 versus the end-to-end delay D_{e2e}, which was quantified in terms of the number of transmit TSs. Each TS has a duration of T and a packet is forwarded by a node during T. The two-RN assisted network seen in Figure 5.5 traverses at most through three hops from S to D. Therefore, the maximum delay is $D_{e2e} = 3N_r$. If after a period of $3N_r$ the packet is still not received by D successfully, it will be discarded, hence its delay contribution is not counted towards the end-to-end delay D_{e2e}. Figure 5.9 shows that

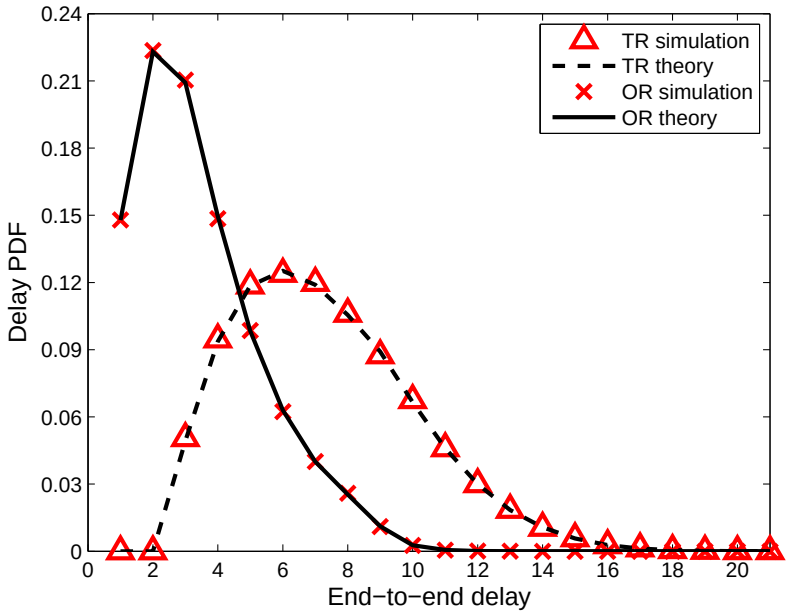

Figure 5.9: The delay distribution.

the proposed energy-efficient OR algorithm has a lower end-to-end delay than the TR algorithm, since the delay PDF curve of the OR algorithm reaches its peak probability at the delay of about 2 TSs, while that of the TR algorithm at 6 TSs.

Figure 5.10 illustrates that the optimal transmit power set $\mathcal{P}$ found by our proposed energy-efficient OR algorithm is close the optimal one generated by the exhaustive search. The optimal transmit group $\mathcal{P}$ is defined as the optimal power set of the node S, R_1 and R_2, which is $\{P_{S_{opt}}, P_{R_{1opt}}, P_{R_{2opt}}\}$. If we increase or decrease the transmit power by a sub-optimum multiplicative factor k yielding $\{kP_{S_{opt}}, kP_{R_{1opt}}, kP_{R_{2opt}}\}$, then the NEC $\overline{E}_{total}$ becomes higher than that associated with the optimal transmit power, as seen in Figure 5.10. The dashed line in Figure 5.10 indicates the theoretical minimum NEC $\overline{E}_{total}$ for the TR algorithm, which should be a single point in the figure for $k = 1$. However, we extend this point to a dashed line to show the advantage of our

OR algorithm. As seen in Figure 5.10, the curve characterizing the OR algorithm is below the curve of the TR algorithm for $0.6 < k < 2.2$, which means that our OR algorithm still outperforms the TR algorithm, although the OR does not achieve its own best performance. The OR algorithm improves the NEC by 15.57% compared to the TR algorithm at the optimal point for $k = 1$.

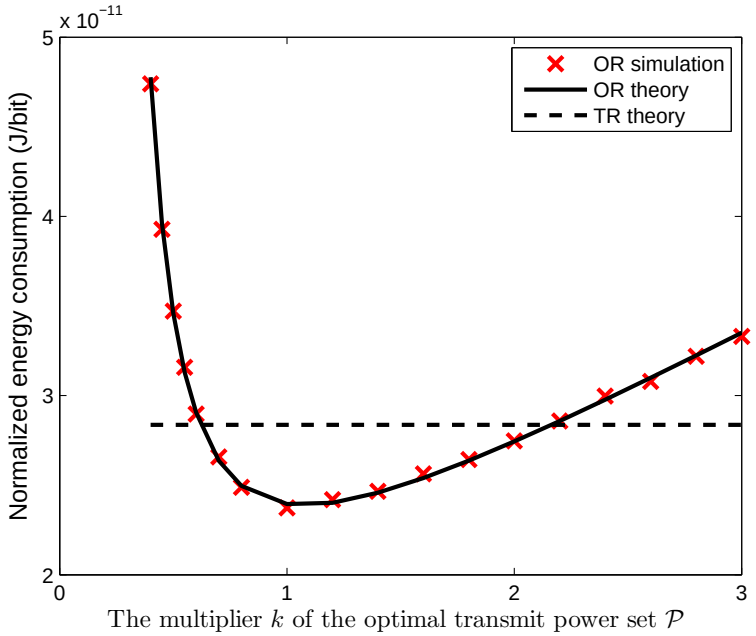

Figure 5.10: The NEC $\overline{E}_{total}$ versus the multiplier k of the optimal transmit power set $\mathcal{P}$.

5.5 Chapter Conclusions

In Section 5.1 we detailed the benefits of OR in terms of the achievable energy saving and stated the main contributions of this chapter. In Section 5.2, we theoretically analyzed both the normalized energy consumption, as well as the end-to-end delay and the delay distribution for a single-hop route, followed by the analysis of the TR in the context of an idealized linear-topology network and the OR in a random network. Moreover, a beneficial power allocation scheme was employed for finding the optimal transmit power for the sake of minimizing the normalized energy consumption. In Section 5.3, we invoked the energy-consumption-based OFs formulated in Section 5.2, which was followed by the conception of an energy-efficient TR algorithm in Subsection 5.3.1 and of an energy-efficient OR algorithm in Subsection 5.3.2. Both of the algorithms were designed based on Dijkstra's algorithm. They were locally optimal algorithms, since the optimal transmit power to be assigned to each node was found step-by-step for each consecutive hop. Additionally, the delay distribution was also derived. Furthermore, the computational complexity of these two

algorithms was also discussed in Section 5.3. In Section 4.3, we continued by analyzing the influence of the transmit power on both the normalized energy consumption and on the end-to-end throughput of a single-hop route in **Example 1**, which showed that the optimal transmit power can be found for the sake of minimizing the normalized energy consumption. Then, in **Example 2** we compared the performances of the TR, of the OR and of the A-EEOR proposed in [133]. The simulation results of **Example 2** were portrayed in Figures 5.7 - 5.10, which demonstrated that our proposed OR algorithm had a lower normalized energy consumption, higher end-to-end throughput and lower end-to-end delay than the TR algorithm and the A-EEOR algorithm, as portrayed in Figures 5.7, 5.8 and 5.9. Finally, in Section 4.3 the simulation results of both the TR algorithm and of the OR algorithm were used for verifying the theoretical analysis of Section 5.2, which were found to be close to the bounds provided by the exhaustive search algorithm.

Chapter 6

Conclusions and Future Research

In this chapter, we will provide our overall conclusions in Section 6.1. The design guidelines are presented in Section 6.2 and our potential future research ideas will be presented in Section 6.3.

6.1 Conclusions

In this thesis, we have provided detailed cross-layer aided routing designs for enhancing the achievable system performance. More specifically, we proposed diverse routing schemes, investigating the impact of node mobility, the benefits of multi-antenna aided RNs, the FER, the number of MAC retransmissions and the number of hops on the performance of the network's throughput and energy consumption. Table 6.1 summaries the basic characteristics of all the cross-layer aided routing algorithms proposed in this thesis, chapter by chapter, including the channel model employed, the parameters in the lower three layers of the OSI architecture and the routing metric. Basic performance comparisons between our proposed cross-layer aided routing algorithms and the conventional algorithms are provided as well.

- **Chapter 1**: In Chapter 1, we provided a generic overview of cross-layer optimization, highlighted the common routing protocols and a range of advanced coding and modulation schemes invoked for our *ad hoc* networks.
  More specifically, in Section 1.1 we described the main functions of the OSI model layer by layer, then we highlighted the common design methods of cross-layer optimization. The historical development of cross-layer aided routing protocol designs was portrayed in Table 1.1. In Section 1.2, we categorized the family of *ad hoc* routing protocols and detailed both the DSR and DYMO routing protocols, which were improved in the following chapters. Section 1.3 presented our basic channel model. Additionally, a lookup table was introduced for reducing the complexity imposed, which is given in Table 1.2. Section 1.4 introduced the

Table 6.1: Summary of the cross-layer aided routing design in this thesis.

Cross-layer	PHY & Link Layer				PHY & Link & NET Layer					
Chapter No.	**Chapter 2**		**Chapter 3**		**Chapter 4**		**Chapter 5**			
Schematic[a]	FL-Routing, Fig. 2.1		MA-Routing, Fig. 3.1		Energy-Routing, Fig. 4.1		Energy-OR, Fig. 5.1			
Objective	Throughput		Energy		Energy & Throughput		Energy			
Channel	AWGN +path loss		AWGN +path loss +Rayleigh fading		AWGN +path loss		AWGN +path loss +Rayleigh fading			
Parameters PHY	TTCM-8PSK		IrCC-URC-STTC		FER		IrCC-URC-QPSK			
Parameters MAC	-		-		No. of retrans, N_r		No. of retrans, N_r			
Parameters NET	No. of hops		No. of hops		No. of hops		No. of hops			
Routing metric	Route stability		No. of hops		NEC		NEC			
Performance Compared scheme[b]	DSR		SA-Routing		Routing ($N_r = \infty$)		Energy-TR		A-EEOR [133]	
	$v = 2$ m/s	$v = 10$ m/s	No. of MA ($0 \rightarrow 60$)		$N_r = 1$	$N_r = 2$	$N_r = 1$	$N_r = 3$	$N_r = 1$	$N_r = 3$
Performance Throughput	166.7% ↑	300% ↑	-		24.3% ↑	14.9% ↑	26.7% ↓	22.2% ↑	200% ↑	6.5% ↑
Performance Energy	-	-	62.7% ↓		19.5% ↓	12.1% ↓	22.2% ↓	3.7% ↓	26.6% ↓	9.4×10^{-4} ↓

[a] Schematic indicates the proposed cross-layer aided routing algorithm.

[b] Compared scheme represents the conventional scheme proposed by other authors, which are used to compare with our corresponding routing algorithms proposed in this thesis.

operational principles of the network simulator OMNeT++. In Section 1.5, the outline and the novel contributions of the thesis were highlighted. Specifically, Figure 1.8 presented the structure of this thesis.

- **Chapter 2** [47]: In Chapter 2, a novel FL-DSR protocol was proposed in order to process multiple inputs potentially providing imprecise information, which jointly considered the number of hops and the route life-time, when choosing the specific route having the highest route stability.

  Section 2.1 briefly reviewed the fuzzy-logic aided system, highlighting its benefits in terms of solving problems in the presence of potentially imprecise information. The effects of node mobility were shown to be a significant factor in predetermining the system's performance, such as for example the network's throughput. In Section 2.2, we first introduced the basic FL concepts before detailing the structure of an FLS, which were fuzzy sets, fuzzy operations, fuzzy relations, membership functions, fuzzfications, inference rules and defuzzifications. Then we depicted the basic structure of FLS in Figure 2.3, which consists of three parts: fuzzification, inference and deffuzification. The three parts corresponded to the key steps of designing an FLS system, which were the suitable antecedents selection, the membership function design of the inputs and outputs, the design of the fuzzy inference and the selection of the defuzzification method.

  In Section 2.3, we introduced seven different mobility models according to the values of node velocity, mobile direction, acceleration and their update interval, which were implemented in various network simulators, such as OPNET, NS, OMNeT++ and so on. In Section 2.4, we proposed a link life-time prediction model, which was capable of estimating the maximum link life-time between any pair of moving nodes. In this chapter, the linear mobility model was employed.

  In Section 2.5, we proposed an FL-DSR routing protocol, which was depicted in Figure 2.7. The mobility status received from the physical layer, including the position, speed and traveling direction of each node, was input to the link life-time prediction model in the network layer, where the model helped to predict the link life-time of each pair of nodes and hence to calculate the entire route's life-time. In fact, the route's life-time is given by the minimum link life-time of the whole route. Afterwards, both the route's life-time and the number of hops were input to the FLS and then an output metric, namely the route stability was defined. The so-called triangular membership functions were selected for mapping the input values (the values of the route life-time and the number of hops) into two fuzzy sets, respectively. The 'IF-THEN' rules were designed as

the inference rules, as shown in Table 2.2 and Table 2.3.

To elaborate on the FLS a little further, an example was provided in Figures 2.8, 2.9 and 2.12, for detailing how the FL-DSR protocol operated during the process of route discovery and route maintenance. Finally, in Section 2.6, we first plotted Figures 2.13 and 2.14 for illustrating the advantage of the TTCM-8PSK scheme in terms of both the attainable BER and FER performance for transmission over an AWGN channel and compared it to that of the uncoded-QPSK scheme.

Then we employed the OMNeT++ simulator for characterizing a random network scenario, where the DSR and the FL-DSR, a perfect idealized channel, the uncoded-QPSK and the TTCM-8PSK were employed. The simulation results confirmed that the FL-DSR outperformed the conventional DSR protocol, since it reduced the number of route breakage events, improved the network's throughput, while reducing the network control load imposed, as seen in Figures. 2.15 - 2.17. At the same time, the impact of different physical layer schemes on the achievable performance was quantified for uncoded-QPSK and TTCM-8PSK, which indicated that error-resilient coding and modulation substantially improved the performance of the upper layers. A pre-stored BER vs. SNR lookup table was employed by TTCM-8PSK for emulating the physical layer instead of using time-consuming bit-by-bit Monte-Carlo simulations, which substantially reduced the simulation time imposed.

- **Chapter 3** [48]: Again, in Chapter 2, we focused our attention on the achievable network throughput improvement attained with the aid of the FL-DSR routing protocol, which combined the mobility status in the physical layer and the number of hops in the network layer. By contrast, the emphasis in Chapter 3 was shifted to the reduction of the energy consumption by exploiting the benefits of the coordination between the physical layer and the network layer. Specifically, the advantages of near-capacity coding schemes were quantified in terms of their energy saving. A near-capacity three-stage concatenated IrCC-URC-STTC relay-transceiver equipped with two transmit antennas was proposed for the *ad hoc* network considered, since it achieved a low FER at a low transmit power. The high effective transmission range of the IrCC-URC-STTC aided MA-RNs facilitated cross-layer optimization for activating beneficial routes having the lowest number of longer hops.

  Section 3.1 briefly reviewed the family of power-aware routing protocols and described the novel contributions of this chapter. In Section 3.2, we first analyzed the FER performance of four different types of links subjected to uncorrelated Rayleigh fading. Both a 'perfect' capacity-achieving code operating exactly at the

DCMC-capacity and the practical IrCC-URC-STTC scheme of Subsection 3.2.1 were investigated in Figure 3.2. Then, we analyzed the beneficial influence of MA-RNs on the routing strategy, as characterized in Figure 3.3, where the source tended to transmit data along the route having the lowest number of relatively long hops with the aid of MA-RNs. In Subsection 3.2.2, we also detailed the processes of route discovery, the data transmission and route maintenance in the context of the DYMO routing algorithm.

According to the above-mentioned route discovery, data transmission and route maintenance processes the total energy consumption of this system was divided into three parts. For the sake of fair comparison, we normalized the total energy consumption by the total number of bits received in the application layer and by the number of nodes. It was demonstrated that the overall energy consumption depended on a number of parameters, namely on the node density, on the number of MA-RNs, the mobile speed, the number of hops, the BPS throughput and on the total number of bits received in the application layer. In Section 3.3, we invoked OMNeT++ for simulating four scenarios and further studied both the energy consumption versus the number of MA-RNs and the energy consumption versus the node density. The simulation configurations were summarized in Table 3.1. The simulation results of Figures 3.7 - 3.12 confirmed that the energy consumption per bit and per node invoked for the MA-RN aided network became lower than that in the equivalent SA-RN aided network, especially in high-node-density scenarios.

- **Chapter 4** [49]: Again, Chapter 3 exploited the benefits of a near-capacity MA assisted transceiver in terms of reducing the system's total energy consumption, which was designed relying on cross-layer operation across both the physical layer and the network layer. By contrast, Chapter 4 was specifically dedicated to minimizing the energy consumed by the data packets during the process of data transmission, where the normalized energy consumption was quantified by considering both the physical layer as well as the MAC layer and the network layer.

  Section 4.1 briefly reviewed the state-of-the-art in cross-layer routing techniques, striking a tradeoff between the energy consumed as well as the attainable throughput and described the novel contributions of this chapter. In Section 4.2, we proposed an energy-conscious OF, which took into account the FER experienced in the physical layer, as well as a finite number of N_r MAC retransmissions in the MAC layer and the actual number of hops encountered in the network layer. Unlike the previously proposed OFs, which usually assumed that the number of

MAC retransmissions was infinite, the OF proposed in Section 4.2 represented the practical real-world scenarios more closely, since it assumed a finite number of N_r MAC retransmissions.

More specifically, in Section 4.2 we first analyzed the energy consumed by a packet successfully delivered from the source to the destination or dropped before reaching the destination in a 2-hop route and its corresponding total delivery-duration, as shown in Figures 4.2 as well as 4.3 and formulated in Eqs. (4.9), (4.14), (4.10) and (4.15). Then in Section 4.2 we analyzed the energy consumed by a packet successfully delivered from the source to the destination or dropped before reaching the destination in a H-hop route and its corresponding total delivery-duration , as shown in Figures 4.4 as well as 4.5 and formulated in Eqs. (4.19), (4.20), (4.22) and (4.23). Finally, we obtained the total energy normalized by the successful packet reception probability in Eq. (4.27) and the end-to-end throughput in Eq. (4.28). In Section 4.2.2, a low-complexity routing algorithm was designed for making reliable routing decisions based on the energy consumption, i.e. using the energy-conscious OF of Section 4.2. We detailed the routing algorithm in Figure 4.6, which was based on the Dijkstra's algorithm. The corresponding flow-chart was depicted in Figure 4.7 for highlighting the operations of each node, when it received the RREQ packet. More specifically, we described our new routing algorithm step by step in Figures 4.8 - 4.12. In Table 4.1 of Section 4.3, we listed the simulation parameters.

In Section 4.3 a test-topology relying on N nodes was constructed for studying both the normalized energy consumption and the end-to-end throughput versus the FER, versus the maximum number of MAC retransmissions and versus the number of hops. Still referring to Section 4.3, a simple six-node network topology was constructed, which was characterized by the corresponding FER matrix. The simulation results of Figures 4.14 and 4.15 confirmed the theoretical results of Equation (4.27) relying on the OF of Section 4.2. The match between the theory and simulations was particularly good, when the FER was high, the number of maximum MAC retransmissions was low and the number of hops was high. As suggested by Figure 4.17 and Table 4.2, our new routing algorithm successfully reduced the normalized energy consumption without unduly compromising the end-to-end throughput and had a high probability of making beneficial routing decisions in realistic scenarios.

- **Chapter 5** [50]: As discussed above, Chapter 4 assumed that the transmit power of each node was the same and each node employed a pre-selected route to transmit its data, which would waste some energy in a random network. Hence

in Chapter 5, we proposed a cross-layer operation aided energy-efficient OR algorithm for *ad hoc* networks and an energy-consumption-based OF combined with power allocation, which was employed both for finding a theoretical bound and for conveying the packets through the network.

Section 5.1 briefly reviewed the family of opportunistic routing algorithms and listed the novel contributions of this chapter. In Section 5.2, we first derived the FER distribution expression of the Rayleigh fading channel by integrating the specific FER value of the AWGN channel experienced at a given SNR after weighting it by the probability of that specific SNR. The FER versus SNR curve of the AWGN channel was generated with the aid of bit-by-bit simulations for the IrCC-URC-QPSK scheme of Section 3.2. Then the FER expression of the Rayleigh channel was represented by a four-segment function, as shown in Eqs. (5.6), (5.8), (5.9) and (5.10). The normalized energy consumption was formulated in Eq. (5.15), which was the sum of the energy consumed by both the successful and unsuccessful receptions, normalized by the successful reception probability. By setting the derivative of the normalized energy consumption with respect to the transmit power, the optimized transmit power was found. Secondly, in Subsection 5.2.2 we analyzed the normalized energy consumption, the end-to-end throughput and the end-to-end delay for TR in an idealized network relying on nodes arranged along a straight line. The corresponding expressions were formulated in Eqs. (5.31), (5.36) and (5.35). Thirdly, in Subsection 5.2.3 we analyzed the normalized energy consumption, the end-to-end throughput and the end-to-end delay for OR in a random network, which were given by Eqs. (5.57), (5.58) and (5.52). The OR regime was capable of fully exploiting the variance of the wireless channel and considered the potential chances of success for each candidate RN. In Section 5.3, two energy-efficient routing algorithms were proposed for TR and OR, respectively, which were detailed in **Algorithm 1** and **Algorithm 2**.

The energy-consumption-based OFs of Section 5.2 are applicable to both TR and to our OR. More specifically, **Algorithm 1** of Subsection 5.3.1 carried out its routing decisions according to the minimum normalized energy consumption, where the specific route having the minimum normalized energy consumption would be deemed as the pre-selected route and hence would transmit its data packets. The transmit power of each node was optimized step by step upon minimizing the normalized energy consumption during delivering the packets from the source to itself.

Algorithm 2 of Subsection 5.3.2 did not decide on a pre-selected route spanning

from the source to the destination. However, each node had to select the optimized forwarder set, which was found step by step. The optimal transmit power was also found before deciding the optimal forwarder set, where the normalized energy consumption associated with the reception from that node to the destination via the selected forwarder set was the minimum. Both of the two algorithms were locally optimum and their complexity was analyzed in Section 5.3.

In Section 5.4, the simulation configuration was detailed, as listed in Table 5.1. We first analyzed both the normalized energy consumption and the end-to-end throughput versus the transmit power for a single-hop route in Figure 5.6, where the normalized energy consumption was shown to decrease first and then increase, hence exhibiting a minimum value. Then we set up a twin-RN assisted network for studying the normalized energy consumption versus the maximum number of MAC retransmissions, as shown in Figures 5.7. Both of the algorithms performed close to the respective bounds found by an exhaustive search and their analytical performance matched the simulation results quite closely. The end-to-end throughput, the end-to-end delay and the delay distribution of the system were also analyzed theoretically, as seen in Figures 5.8 and 5.9. In conclusion, the OR outperformed the TR.

In a nutshell, the cross-layer aided routing design is capable of providing significant benefits, when aiming for saving energy, maximizing the end-to-end throughput or for striking a balance between them.

6.2 Design Guidelines

In general, three basic steps may be identified, when designing routing algorithms in *ad hoc* networks, which are:

1) Determining the design targets, such as the network's throughput and/or energy consumption;

2) Determining the key factors, which influence the design targets most crucially. These key factors may be related to different layers, including the mobility status, the channel categories, the protocol parameters and so on;

3) Determining the routing metrics used for making routing decisions, such as the number of hops, the route stability and/or the normalized end-to-end energy consumption.

Let us now detail these three design steps as follows:

- Throughput and energy consumption constitute a pair of important specifications in analyzing a network's performance, which critically depend on the parameters

of the different OSI layers. Hence, combining the functions of multiple layers with the aid of cross-layer operation is beneficial in terms of improving the attainable performance, as demonstrated in this thesis with the assistance of several cross-layer aided routing algorithms designed for *ad hoc* networks.

- The number of hops is one of the most popular routing metrics in routing design, as we demonstrated in the context of two classic routing algorithms, namely the DSR and DYMO protocols.
- One of the most important factors we have to consider in the physical layer is constituted by the specific characteristics of the time-variant wireless channel, which inflict bit/symbol errors and even packet loss events at the receiver node. Hence, strong and robust channel coding schemes have to be employed for mitigating the channel-induced degradations. The BER and FER are the two representative parameters, which are capable of characterizing the influence of both the time-variant wireless channel and of the FEC coding schemes, hence representing the overall performance of the physical layer. For the sake of reducing the simulation time, the corresponding BER/FER vs. SNR lookup table may be used for emulating the entire physical layer. We employed such a lookup table in our simulations presented in Sections 2.6, 3.3 and 5.4, which indeed proved to be efficient.
- If a mobile scenario is considered, then the specific character of mobility has to be considered as an important factor, regardless of the specific design target. The mobility-related characteristics are usually divided into the following three aspects: the nodes' position, speed and travelling direction, which determine the style of mobility. The link-lifetime between a pair of nodes and even an entire route's lifetime may be predicted according to the mobility-related characteristics. Naturally, the node mobility would render all the routing information stored during the route discovery process invalid. Therefore, at least the mobility characteristics and the number of hops should be born in mind during the cross-layer aided routing design of mobile *ad hoc* networks. The family of FLSs is recognized as being capable of beneficially processing multiple inaccurate input parameters in the interest of obtaining a single output. Section 2.5 designed an FL aided DSR protocol and introduced the concept of 'route stability' as the routing metric, where a link-lifetime prediction model was also designed for predicting the maximum lifetime of any potential route. The inputs of the designed FLS are the entire route's predicted lifetime and the number of hops in the network layer. As a design example, the proposed FL-aided DSR protocol was demonstrated to improve the network's throughput in Section 2.6.

- For the sake of reducing the system's total transmit energy consumption, a near-capacity coding scheme, such as the IrCC-URC-STTC scheme of Subsection 3.2.1 is the most appropriate choice, since it requires a reduced transmit power at a given BER/FER value, which may also be viewed as reducing the BER/FER at a given transmit power. This is the reason, why the IrCC-URC-STTC aided MA transceivers operate close to the achievable capacity and this is, why they are capable of reducing the number of hops spanning from the source to the destination. Requiring less hops implies that less nodes are involved, hence reducing the energy dissipation. An energy-efficient routing algorithm relying on the employment of IrCC-URC-STTC aided MA transceivers was proposed in Section 3.2. This scheme was then characterized in Section 3.3, showing that the system's total transmit energy consumption was reduced, especially in a high-node-density scenario.
- Furthermore, having considered the factors influencing the design of both the physical layer and of the network layer, we have to proceed by characterizing the influence of the MAC layer in our cross-layer aided routing design, with the goal of aiming both for a throughput improvement and for energy reduction. One of the representative factors in the MAC layer is constituted by the number of maximum MAC retransmissions. The larger the number of maximum MAC retransmissions, the more energy will be consumed and the higher the delay becomes. As a benefit, the successful packet reception probability is improved. Hence, we have to find the most appropriate number of maximum MAC retransmissions for the sake of striking an attractive compromise.
- Additionally, we emphasize that the energy assigned to the data packets plays a dominant role in determining the system's total energy dissipation, which hence has to be optimized. For the sake of achieving an improved network throughput and a reduced energy consumption, the joint influence of the FER in the physical layer, of the maximum number of retransmissions in the MAC layer and of the number of hops in the network layer has to be carefully considered. Additionally, opting for the normalized energy consumption as the routing metric instead of the number of hops is more beneficial in terms of reducing energy consumption. Hence, an accurate energy-consumption-based OF is required for combining all the three factors corresponding to the lower three layers of the seven-layer OSI architecture, as indicated in Subsection 4.2.1 of the thesis. The routing algorithm proposed in Subsection 4.2.2 strikes an attractive tradeoff between the normalized energy consumption and the end-to-end throughput in the context of real-world scenarios, as exemplified in Section 4.3.

- A hop-length-dependent power allocation has to be considered in further reducing the energy consumption. If the transmit power of each node is assumed to be the same, a certain amount of extra energy will be dissipated, since the distance between each pair of nodes is different, which would necessitate a different amount of transmit energy. An energy-efficient TR algorithm was designed with the aid of the hop-length-dependent power allocation of Section 5.3.1, which also jointly considered the FER in the physical layer, the maximum number of retransmissions in the MAC layer and the number of hops in the network layer. A reliable routing metric is constituted by the normalized energy consumption quantified in terms of the energy-based OF formulated in Section 5.2.2.
- Additionally, the violently time-varying fading channel will impose extra energy dissipation as well, because it may render a pre-selected route inadequate for reliable data transmission. This led to the concept of OR, which is capable of reducing the energy consumption. Hence an energy-efficient OR regime was designed with the aid of hop-length-dependent power allocation in Section 5.3.2, which also relied on cross-layer operation across the lower three layers of the TCP/IP model. Again, a reliable routing metric is constituted by the normalized energy consumption quantified in terms of the energy-based OF formulated in Section 5.2.3.
- The end-to-end delay is another important design target for near-real-time services, such as lip-synchronized video-telephony, where a high end-to-end delay may become intolerable. Hence the packet delay distribution was also analyzed in Chapter 5. Furthermore, the network control load also constitutes an important parameter in terms of characterizing a routing algorithm, since a higher network control load may result in dissipating some extra energy, hence reducing the network's normalized throughput. As a design-example, we characterized the network control load of the proposed routing protocols in Sections 2.6 and 3.3.

6.3 Future Work

In this section, we briefly discuss a number of future research ideas.

6.3.1 Energy-Efficient Routing Algorithm Design for Mobile Ad Hoc Networks

In Chapter 2, we introduced various mobility models [80–87] and employed the linear mobility model for estimating both the link's life-time between a pair of nodes and the route's life-time, as a function of both the node velocity and of the specific mobility model considered. However, Chapters 3, 4 and 5 investigated the system's

performance only in stationary scenarios. More specifically, the energy-consumption-based OFs of Equation (4.27) and of Equations (5.16) as well as of (5.57) may become inefficient in mobile scenarios, since the position of each node varies according to the specific mobility model concerned. Node-mobility might cause the following problems:

- In TR, both the pre-selected route and the pre-stored backup routes become invalid, which will activate route re-discovery and hence may deplete the residual energy of each node;
- In OR, both the pre-computed optimal transmit power and forwarder set might become invalid, which requires the re-computation of these two parameters. Hence, the effects of the route life-time have to be considered for estimating the energy consumption in a mobile scenario [159–162].

6.3.2 The Energy Dissipated by the Control Packets

In Chapters 2 and 3, we discussed the influence of our proposed routing schemes on the performance of the network control load, as quantified in Figures 2.17, 3.8 and 3.11. Chapters 4 and 5 have not considered these issues, because our focus was more on the energy dissipated by data packets during the process of data transmission. However, the control packets also play an important role in determining the system's total energy consumption, especially in mobile scenarios where the control packets maintain the current communications [160], as mentioned in Section 6.3.1. Additionally, a plethora of control packets are required for both route discovery and for route maintenance. Hence, the energy-consumption-based OFs of Equation (4.27) and of Equations (5.16) as well as of Equation (5.57) may require further adjustments, if the energy dissipated by the control packets is also considered. Additionally, it may be promising to employ bio-inspired algorithms, such as the ant colony algorithm [163], for accommodating a dynamically changing topology.

6.3.3 Energy vs. Throughput and Energy vs. Delay Trade-off

Chapter 2 discussed the improvement of the network's throughput, while Chapter 3 aimed for reducing the system's total energy consumption. By contrast, Chapter 4 stroke a trade-off between the end-to-end throughput and the normalized energy consumption, while Chapter 5 aimed for reducing the normalized energy consumption, although it also analyzed the end-to-end throughput and the delay distribution. However, the energy versus throughput and energy versus delay trade-offs experienced in throughput-sensitive or delay-sensitive services would also require urgent research-attention. Hence, a joint design of the application layer, the network layer, the MAC layer and even the physical layer holds the promise of combining their beneficial characteristics [164–168].

6.3.4 MAC Design for Supporting the Forwarder Set Selection

The OR regime of Chapter 5 was proposed for exploiting the time-variant characteristics of the fading channel. The optimal forwarder set of each node was selected before starting the transmission of the first data packet. However, during the process of data transmission any node belonging to the forwarder set may receive the data packet, which was broadcast from its predecessor node. Once a node in the forwarder set receives this data packet and it has the minimum estimated normalized energy for its transmission from itself to the destination, it has the highest priority of forwarding this data packet. Therefore, finding the most beneficial technique of informing the other nodes in the forwarder set that the above-mentioned RN has been given the highest transmission-priority also has to be considered in the future. Specifically, a novel MAC layer protocol has to be designed for implementing this scheme [169]. For example, a control packet may be broadcast from the specific node, which has the promise of the minimum estimated normalized energy consumption. Then the other nodes in the forwarder set will remain silent, despite the fact that they may have received this control packet correctly as well. Additionally, since the MAC layer protocol to be designed employs new control packets, it will inevitably impose extra energy consumption, extra delay and even a potential throughput reduction.

Glossary

8PSK	8-level Phase-Shift Keying.
A-EEOR	Adjustable Energy-Efficient Opportunistic Routing.
ACK	ACKnowledgement.
ACK Req	ACKnowledgement Request.
AF	Amplify-and-Forward.
AODV	Ad-hoc On-demand Distance Vector.
ARQ	Automatic Repeat Request.
AsOR	Assistant Opportunistic Routing.
AWGN	Additive White Gaussian Noise.
BER	Bit Error Ratio.
BPS	Bits Per Symbol.
BS	Base Station.
CBR	Constant Bit Rate.
CCITT	International Telegraph and Telephone Consultative Committee.
CCMC	Continuous-input Continuous-output Memoryless Channel.
CIR	Channel Impulse Response.
CQI	Channel Quality Information.
CSI	Channel State Information.
CSMA/CA	Carrier Sense Multiple Access with Collision Avoidance.
CTS	Clear To Send.
DARPA	Defense Advanced Research Projects Agency.

DCMC	Discrete-input Continuous-output Memoryless Channel.
DF	Decode-and-Forward.
DSDV	Destination-Sequenced Distance Vector.
DSR	Dynamic Source Routing.
DYMO	DYnamic Manet On-demand.
EATT	Expected Anypath Transmission Time.
ETX	Estimated Transmission count.
EXIT	EXtrinsic Information Transfer.
ExOR	Extremely Opportunistic Routing.
FEC	Forward Error Correction.
FER	Frame Error Ratio.
FL	Fuzzy Logic.
FL-DSR	Fuzzy Logic based DSR.
IDE	Integrated Development Environment.
IEEE	Institute of Electrical and Electronics Engineers.
IM	Interference Mitigation.
IP	Internet Protocol.
IPv4	Internet Protocol version 4.
IPv6	Internet Protocol version 6.
IrCC	Irregular Convolutional Code.
IrCC-URC-STTC	Irregular Convolutional Coded, Unity-Rate Coded and Space-Time Trellis Coded.
ISO	International Standards Organization.
LCAR	Least-Cost Anypath Routing.
LHS	Left-Hand-Side.
LLC	Logical Link Control.
LOS	Line-Of-Sight.
MA	Multiple Antenna.
MAC	Media Access Control.
MANET	Mobile Ad hoc NETwork.
MIMO	Multiple-Input Multiple-Output.
MISO	Multi-Input Single-Output.
MPCR	Minimum-Power Cooperative Routing.

NEC	Normalized Energy Consumption.
NED	NEtwork Description.
OF	Objective Function.
OLSR	Optimized Link State Routing.
OR	Opportunistic Routing.
OSI	Open System Interconnection.
PDF	Probability Distribution Function.
PDU	Protocol Data Unit.
PLR	Packet Loss Ratio.
PSNR	Peak Signal-to-Noise Ratio.
QoS	Quality of Service.
QPSK	Quadrature Phase-Shift Keying.
RERR	Route ERRor.
RHS	Right-Hand-Side.
RN	Relay Node.
RREP	Route REPly.
RREQ	Route REQuest.
RTS	Request To Send.
SA	Single Antenna.
SIMO	Single-Input Multi-Output.
SIR	Signal-to-Inference Ratio.
SISO	Single-Input Single-Output.
SNR	Signal-to-Noise Ratio.
SR	Source Route.
STC	Space-Time Code.
STTC	Space-Time Trellis Code.
TCP	Transmission Control Protocol.
TR	Traditional Routing.
TS	Time-Slot.
TTCM	Turbo Trellis Coded Modulation.
UDP	User Datagram Protocol.

URC Unity-Rate Code.

VAR Velocity-Aided Routing.
VBR Variable Bit Rate.

WLAN Wireless Local Area Network.

ZRP Zone Routing Protocol.

Bibliography

[1] H. Labiod, ed., *Wireless Ad Hoc and Sensor Networks*. John Wiley & Sons, Inc., 2008.

[2] R. Ramanathan and J. Redi, "A brief overview of ad hoc networks: Challenges and directions," *IEEE Communications Magazine*, vol. 40, pp. 20–22, May 2002.

[3] H. Zimmermann, "OSI reference model–the ISO model of architecture for open systems interconnection," *IEEE Transactions on Communications*, vol. 28, pp. 425–432, April 1980.

[4] "Reference model of open systems interconnection," 1979.

[5] A. Goldsmith, *Wireless Communications*. New York: Cambridge University Press, 2005.

[6] W. Stallings, *Wireless Communications & Networks, Second Edition*. Pearson Prentice Hall, 2005.

[7] "Information technology-telecommunications and information exchange between systems-local and metropolitan area networks-specific requirements," 2007.

[8] "Internet protocol." IETF Draft, 1981.

[9] S. Deering and R. Hinden, "Internet protocol, version 6 (IPv6) specification." IETF Draft, 1998.

[10] "Transmission control protocol." IETF Draft, 1981.

[11] "User datagram protocol." IETF Draft, 1980.

[12] "Definitions of terms related to quality of service." ITU-T E.800, 2008.

[13] V. Srivastava and M. Motani, "Cross-layer design: a survey and the road ahead," *IEEE Communications Magazine*, vol. 43, no. 12, pp. 112–119, 2005.

[14] M. Conti, G. Maselli, G. Turi, and S. Giordano, "Cross-layering in mobile ad hoc network design," *Computer*, vol. 37, no. 2, pp. 48–51, 2004.

[15] R. Jurdak, *Wireless Ad Hoc and Sensor Networks: A Cross-layer Design Perspective*. Springer, 2010.

[16] F. Fu and M. V. D. Schaar, "A new systematic framework for autonomous cross-layer optimization," *IEEE Transactions on Vehicular Technology*, vol. 58, no. 4, pp. 1887–1903, 2009.

[17] R. Winter, J. H. Schiller, N. Nikaein, and C. Bonnet, "Crosstalk: cross-layer decision support based on global knowledge," *IEEE Communications Magazine*, vol. 44, no. 1, pp. 93–99, 2006.

[18] V. Kawadia and P. R. Kumar, "A cautionary perspective on cross-layer design," *IEEE Wireless Communications*, vol. 12, no. 1, pp. 3–11, 2005.

[19] A. Goldsmith and S. B. Wicker, "Design challenges for energy-constrained ad hoc wireless networks," *IEEE Wireless Communications*, vol. 9, no. 4, pp. 8–27, 2002.

[20] M. R. Souryal, B. R. Vojcic, and R. L. Pickholtz, "Information efficiency of multihop packet radio networks with channel-adaptive routing," *IEEE Journal on Selected Areas in Communications*, vol. 23, no. 1, pp. 40–50, 2005.

[21] S.-H. Lee, E. Choi, and D.-H. Cho, "Timer-based broadcasting for power-aware routing in power-controlled wireless ad hoc networks," *IEEE Communications Letters*, vol. 9, no. 3, pp. 222–224, 2005.

[22] M. Johansson and L. Xiao, "Cross-layer optimization of wireless networks using nonlinear column generation," *IEEE Transactions on Wireless Communications*, vol. 5, no. 2, pp. 435–445, 2006.

[23] S. Mao, Y. T. Hou, X. Cheng, H. D. Sherali, S. F. Midkiff, and Y.-Q. Zhang, "On routing for multiple description video over wireless ad hoc networks," *IEEE Transactions on Multimedia*, vol. 8, no. 5, pp. 1063–1074, 2006.

[24] A. Abdrabou and W. H. Zhuang, "A position-based QoS routing scheme for UWB mobile ad hoc networks," *IEEE Journal on Selected Areas in Communications*, vol. 24, no. 4, pp. 850–856, 2006.

[25] J. Zhang, Q. Zhang, B. Li, X. Luo, and W. Zhu, "Energy-efficient routing in mobile ad hoc networks: mobility-assisted case," *IEEE Transactions on Vehicular Technology*, vol. 55, no. 1, pp. 369–379, 2006.

[26] S. Kompella, S. Mao, Y. T. Hou, and H. D. Sherali, "Cross-layer optimized multipath routing for video communications in wireless networks," *IEEE Journal on Selected Areas in Communications*, vol. 25, no. 4, pp. 831–840, 2007.

[27] M. Chiang, S. H. Low, A. R. Calderbank, and J. C. Doyle, "Layering as optimization decomposition: A mathematical theory of network architectures," *Proceedings of the IEEE*, vol. 95, no. 1, pp. 255–312, 2007.

[28] K. T. Phan, H. Jiang, C. Tellambura, S. A. Vorobyov, and R. Fan, "Joint medium access control, routing and energy distribution in multi-hop wireless networks," *IEEE Transactions on Wireless Communications*, vol. 7, no. 12, pp. 5244–5249, 2008.

[29] J. Liu, Y. T. Hou, Y. Shi, and H. D. Sherali, "Cross-layer optimization for MIMO-based wireless ad hoc networks: Routing, power allocation, and bandwidth allocation," *IEEE Journal on Selected Areas in Communications*, vol. 26, no. 6, pp. 913–926, 2008.

[30] A. Abdrabou and W. H. Zhuang, "Statistical QoS routing for IEEE 802.11 multihop ad hoc networks," *IEEE Transactions on Wireless Communications*, vol. 8, no. 3, pp. 1542–1552, 2009.

[31] P. Li, Q. Shen, Y. Fang, and H. Zhang, "Power controlled network protocols for multi-rate ad hoc networks," *IEEE Transactions on Wireless Communications*, vol. 8, no. 4, pp. 2142–2149, 2009.

[32] L. Ding, T. Melodia, S. N. Batalama, J. D. Matyjas, and M. J. Medley, "Cross-layer routing and dynamic spectrum allocation in cognitive radio ad hoc networks," *IEEE Transactions on Vehicular Technology*, vol. 59, no. 4, pp. 1969–1979, 2010.

[33] Y. Lu, J. Guan, Z. Wei, and Q. Wu, "Joint channel assignment and cross-layer routing protocol for multi-radio multi-channel ad hoc networks," *Journal of Systems Engineering and Electronics*, vol. 21, no. 6, pp. 1095–1102, 2010.

[34] Z. Ding and K. K. Leung, "Cross-layer routing using cooperative transmission in vehicular ad-hoc networks," *IEEE Journal on Selected Areas in Communications*, vol. 29, no. 3, pp. 571–581, 2011.

[35] B. Tavli and W. B. Heinzelman, "Energy-efficient real-time multicast routing in mobile ad hoc networks," *IEEE Transactions on Computers*, vol. 60, no. 5, pp. 707–722, 2011.

[36] S.-J. Syue, C.-L. Wang, T. Aguilar, V. Gauthier, and H. Afifi, "Cooperative geographic routing with radio coverage extension for SER-constrained wireless relay networks," *IEEE Journal on Selected Areas in Communications*, vol. 30, no. 2, pp. 271–279, 2012.

[37] E. M. Royer and C.-K. Toh, "A review of current routing protocols for ad hoc mobile wireless networks," *IEEE Personal Communications*, vol. 6, pp. 46–55, apr 1999.

[38] C. E. Perkins and P. Bhagwat, "Highly dynamic destination-sequenced distance vector (DSDV) for mobile computers," in *Proc. of the ACM SIGCOMM 1994 Conference on Communications Architectures, Protocols and Applications*, pp. 234–244, 31 Aug.-2 Sept. 1994.

[39] T. Clausen and P. Jacquet, "Optimized link state routing protocol (OLSR) (RFC 3626)." IETF Draft, 2003.

[40] "The Dynamic Source Routing Protocol (DSR) for Mobile Ad Hoc Networks for IPv4." Downloadable at http://tools.ietf.org/html/rfc4728.

[41] "Ad hoc On-Demand Distance Vector (AODV) Routing." Downloadable at http://tools.ietf.org/html/rfc3561.

[42] "Dynamic MANET On-demand (DYMO) Routing Routing." Downloadable at http://tools.ietf.org/html/draft-ietf-manet-dymo-19.

[43] "The zone routing protocol (ZRP) for ad hoc networks." Downloadable at http://tools.ietf.org/html/draft-ietf-manet-zone-zrp-04.

[44] J. G. Proakis, *Digital Communications, Fourth Edition.* The McGraw - Hill Companies, Inc., 2001.

[45] A. Varga and R. Hornig, "An overview of the OMNeT++ simulation environment," in *Proceeding of the 1st international conference on Simulation tools and techniques for communications, networks and systems & workshops (Simutools '08)*, pp. 1–10, 3-7 March 2008.

[46] A. Varga, "OMNeT++ discrete event simulation system version 3.2 user manual," 2005.

[47] J. Zuo, S. X. Ng, and L. Hanzo, "Fuzzy logic aided dynamic source routing in cross-layer operation assisted ad hoc networks," in *2010 IEEE 72nd Vehicular Technology Conference (VTC2010-Fall)*, (Ottawa, Canada), pp. 1–5, 6-9 Sept. 2010.

[48] J. Zuo, H. V. Nguyen, S. X. Ng, and L. Hanzo, "Energy-efficient relay aided ad hoc networks using iteratively detected irregular convolutional coded, unity-rate coded and space-time trellis coded transceivers," in *2011 IEEE Wireless Communications and Networking Conference (WCNC 2011)*, (Quintana-Roo, Mexico), pp. 1179–1184, 28-31 March 2011.

[49] J. Zuo, C. Dong, S. X. Ng, L.-L. Yang, and L. Hanzo, "Energy-efficient routing in ad hoc networks relying on channel state information and limited mac retransmissions," in *2011 IEEE Vehicular Technology Conference (VTC2011-Fall)*, (San Francisco, United States), pp. 1–5, 5-8 Sept. 2011.

[50] J. Zuo, C. Dong, S. X. Ng, L.-L. Yang, and L. Hanzo, "Cross-layer aided energy-efficient opportunistic routing in ad hoc networks," Downloadable at http://eprints.soton.ac.uk/id/eprint/349450.

[51] L. Hanzo, S.-X. Ng, T. Keller, and W. Webb, *Quadrature Amplitude Modulation: From Basics to Adaptive Trellis-Coded, Turbo-Equalised and Space-Time Coded OFDM, CDMA and MC-CDMA Systems.* Wiley-IEEE Press, 2nd ed., 2004.

[52] L. Hanzo, T. H. Liew, B. L. Yeap, and R. Y. S. Tee, *Turbo Coding, turbo equalisation and space-time coding: EXIT-chart aided near-capacity designs for wireless channels.* John Wiley and Sons, Ltd, 2010.

[53] G. Ungerboeck, "Channel coding with multilevel/phase signals," *IEEE Transactions on Infromation Theory*, vol. IT-28, pp. 55–67, January 1982.

[54] S. X. Ng, *Coded Modulation Schemes for Wireless Channels.* PhD thesis, ECS school, University of Southampton, 2002.

[55] G. Ungerboeck, "Trellis-coded modulation with redundant signal sets Part I: Introduction," *IEEE Communications Magazine*, vol. 25, pp. 5–11, feb 1987.

[56] G. Ungerboeck, "Trellis-coded modulation with redundant signal sets Part II: State of the art," *IEEE Communications Magazine*, vol. 25, pp. 12–21, feb 1987.

[57] Q. Zhang and Y.-Q. Zhang, "Cross-layer design for QoS support in multihop wireless networks," *Proceedings of the IEEE*, vol. 96, no. 1, pp. 64–76, 2008.

[58] E. P. Klement and W. Slany, "Fuzzy logic in artificial intelligence," in *8th Austrian Artificial Intelligence conference (FLAI'93)*, 28-30 June 1993.

[59] C.-C. Lee, "Fuzzy logic in control systems: fuzzy logic controller, Parts I and II," *IEEE Transactions on Systems, Man and Cybernetics*, vol. 20, pp. 404–418, Mar./Apr. 1990.

[60] N. Baldo and M. Zorzi, "Fuzzy logic for cross-layer optimization in cognitive radio networks," *IEEE Communications Magazine*, vol. 46, pp. 64–71, April 2008.

[61] X.-S. Xia, Q.-C. Ren, and Q.-L. Liang, "Cross-layer design for mobile ad hoc networks: energy, throughput and delay-aware approach," in *IEEE Wireless Communications and Networking Conference (WCNC 2006)*, vol. 2, (Las Vegas, NV USA), pp. 770–775, 3-6 April 2006.

[62] W. El-Hajj, A. Al-Fuqaha, M. Guizani, and H.-H. Chen, "On efficient network planning and routing in large-scale MANETs," *IEEE Transactions on Vehicular Technology*, vol. 58, pp. 3796–3801, Sept. 2009.

[63] W. El-Hajj, D. Kountanis, A. Al-Fuqaha, and M. Guizani, "A fuzzy-based hierarchical energy efficient routing protocol for large scale mobile ad hoc networks (FEER)," in *IEEE International Conference on Communications (ICC 2006)*, vol. 8, (Istanbul, Turkey), pp. 3585–3590, 11-15 June 2006.

[64] S. Rea and D. Pesch, "Multi-metric routing decisions for ad hoc networks using fuzzy logic," in *1st International Symposium on Wireless Communication Systems (ISWCS 2004)*, pp. 403–407, 20-22 Sept. 2004.

[65] S. Rea and D. Pesch, "Fuzzy logic routing with load-balancing using a realistic mobility model," in *IEEE 61st Semiannual Vehicular Technology Conference (VTC2005-Spring)*, vol. 4, (Stockholm, Sweden), pp. 2611–2615, 30 May-1 June 2005.

[66] T. J. Ross, *Fuzzy Logic With Engineering Applications*. New York: McGraw-Hill, Inc., 1995.

[67] H. Bandemer and S. Gottwald, *Fuzzy Sets, Fuzzy Logic, Fuzzy Methods with Applications*. Baffins Lane, Chichester, West Sussex PO19 1UD, England: Jhon Wiley & Sons Ltd, 1996.

[68] G. J. Klir and B. Yuan, *Fuzzy Sets and Fuzzy Logic: Theory and Applications*. Upper Saddle River, New Jersey 07458: Prentice Hall PTR, 1995.

[69] L. A. Zadeh, "Fuzzy Sets," *Information and Control*, vol. 8, pp. 338–353, 1965.

[70] L. A. Zadeh, "A rationale for fuzzy control," *Journal of Dynamic Systems, Measurement and Control*, vol. 94, pp. 3–4, 1972.

[71] T. Yamakawa, "A fuzzy logic controller," *Journal of Biotechnology*, vol. 24, pp. 1–32, 1992.

[72] S. Forrest, "Genetic algorithms: principes of natural selection applied to computation," *Science*, vol. 261, pp. 872–878, 1993.

[73] D. E. Goldberg, *Genetic algorithms*. New York: Addison-Wesley, 1989.

[74] I. M. Copi, *Introduction to logic, 12th edition*. Pearson, 2004.

[75] L. A. Zadeh, "Outline of a new approach to the analysis of complex systems and decision processes," *IEEE Transactions on Systems, Man and Cybernetics*, vol. 3, pp. 28–44, Jan. 1973.

[76] L. A. Zadeh, "The concept of a linguistic variable and its applications to approximate reasoning, Part 3," *Information Sciences*, vol. 9, pp. 43–80, 1976.

[77] M. Jamshidi, N. Vadiee, and T. J. Ross, *Fuzzy logic and control: Software and hardware applications*. PTR Prentice-Hall, 1993.

[78] "OPNET Homepage ." Downloadable at http://www.opnet.com/.

[79] "NS Documentation." Downloadable at http://www.nsnam.org/.

[80] T. Camp, J. Boleng, and V. Davies, "A survey of mobility models for ad hoc network research," *Wireless Communications And Mobile Computing (WCMC): Specail Issue On Mobile Ad Hoc Networking: Research, Trends And Applications*, vol. 2, pp. 483–502, 2002.

[81] V. Davies, *Evaluating Mobility Models Within An Ad Hoc Network*. Colorado School of Mines, 2000.

[82] R. Nagel and S. Eichler, "Efficient and realistic mobility and channel modeling for VANET scenarios using OMNeT++ and INET-framework," 2008.

[83] G. Lutz, "Efficient model for radio links in 4G networks for OMNeT++." diploma thesis, Institute for Telematics, University Karlsruhe, Germany, 2005.

[84] C. Bettstetter, G. Resta, and P. Santi, "The node distribution of the random waypoint mobility model for wireless ad hoc networks," *IEEE Transactions on Mobile Computing*, vol. 2, no. 3, pp. 257–269, 2003.

[85] "Mobility framework for OMNeT++ website." http://mobility-fw.sourceforge.net/.

[86] "FraSiMo: Simulation of mobility with OMNeT++." Downloadable at http://home.snafu.de/kirschd/TKN_Projekt01.pdf.

[87] C. E. Perkins and K.-Y. Wang, "Optimized smooth handoffs in mobile IP," in *Proceeding of the 4th IEEE Symposium on Computers and Communications (ISCC 1999)*, pp. 340–346, 6-8 July 1999.

[88] G. Carofiglio, C.-F. Chiasserini, M. Garetto, and E. Leonardi, "Route stability in MANETs under the random direction mobility model," *IEEE Transactions on Mobile Computing*, vol. 8, pp. 1167–1179, Sept. 2009.

[89] M. Al-Akaidi and M. Alchaita, "Link stability and mobility in ad hoc wireless networks," *IET Communications*, vol. 1, pp. 173–178, April 2007.

[90] I. Rubin and Y.-C. Liu, "Link stability models for QoS ad hoc routing algorithms," in *2003 IEEE 58th Vehicular Technology Conference (VTC2003-Fall)*, vol. 5, (Orlando, Florida, USA), pp. 3084–3088, 6-9 Oct. 2003.

[91] K.-T. Feng, C.-H. Hsu, and T.-E. Lu, "Velocity-assisted predictive mobility and location-aware routing protocols for mobile ad hoc networks," *IEEE Transactions on Vehicular Technology*, vol. 57, pp. 448–464, Jan. 2008.

[92] S.-Y. Ni, Y.-C. Tseng, Y.-S. Chen, and J.-P. Sheu, "The broadcast storm problem in a mobile ad hoc network," in *Proceedings of the 5th Annual ACM/IEEE International Conference on Mobile computing and networking (MobiCom '99)*, pp. 151–162, ACM, 15-20 Aug. 1999.

[93] L. Hanzo, P. Cherriman, and J. Streit, *Video Compression and Communications: From Basics to H.261, H.263, H.264, MPEG4 for DVB and HSDPA-Style Adaptive Turbo-Transceivers*. Chichester, England: John Wiley & Sons Ltd, 2007.

[94] P. Robertson and T. Worz, "Bandwidth-efficient turbo trellis-coded modulation using punctured component codes," *IEEE Journal on Selected Areas in Communications*, vol. 16, pp. 206–218, February 1998.

[95] Z.-G. Hu, R. Hu, and H. Ma, "A route reliability algorithm for mobile ad hoc networks," in *International Conference on Wireless Communications, Networking and Mobile Computing (WCNM 2005)*, vol. 2, pp. 787–790, 23–26 Sept. 2005.

[96] C.-E. Perkins, E.-M. Royer, S.-R. Das, and M.-K. Marina, "Performance comparison of two on-demand routing protocols for ad hoc networks," *IEEE Personal Communications*, vol. 8, pp. 16–28, Feb. 2001.

[97] "User Datagram Protocol." Downloadable at http : //tools.ietf.org/html/rfc768.

[98] D. Feng, C. Jiang, G. Lim, L. J. Cimini, G. Feng, and G. Y. Li, "A survey of energy-efficient wireless communications," *IEEE Communications Surveys Tutorials*, vol. 15, no. 1, pp. 167–178, 2013.

[99] M. C. Vuran and I. F. Akyildiz, "Error control in wireless sensor networks: A cross layer analysis," *IEEE/ACM Transactions on Networking*, vol. 17, pp. 1186–1199, Aug. 2009.

[100] H. V. Nguyen, S. X. Ng, and L. Hanzo, "Distributed three-stage concatenated irregular convolutional, unity-rate and space-time trellis coding for single-antenna aided cooperative communications," in *2010 IEEE 72nd Vehicular Technology Conference Fall (VTC 2010-Fall)*, (Ottawa, Canada), pp. 1–5, 6-9 Sept. 2010.

[101] S. T. Brink, "Convergence behavior of iteratively decoded parallel concatenated codes," *IEEE Transactions on Communications*, vol. 49, no. 10, pp. 1727–1737, 2001.

[102] L. Hanzo, O. Alamri, M. El-Hajjar, and N. Wu, *Near-Capacity Multi-Functional MIMO Systems*. New York, USA: John Wiley and Sons, 2009.

[103] J. G. Li, D. Cordes, and J. Y. Zhang, "Power-aware routing protocols in ad hoc wireless networks," *IEEE Wireless Communications*, vol. 12, pp. 69–81, Dec. 2005.

[104] G. Ferrari, S. A. Malvassori, and O. K. Tonguz, "On physical layer-oriented routing with power control in ad hoc wireless networks," *IET Communications*, vol. 2, pp. 306–319, Feb. 2008.

[105] J. C. Fricke, M. M. Butt, and P. A. Hoeher, "Quality-oriented adaptive forwarding for wireless relaying," *IEEE Communications Letters*, vol. 12, pp. 200–202, March 2008.

[106] M. Haenggi and D. Puccinelli, "Routing in ad hoc networks: a case for long hops," *IEEE Communications Magazine*, vol. 43, pp. 93–101, Oct. 2005.

[107] M. Sikora, J. N. Laneman, M. Haenggi, D. J. Costello, and T. E. Fuja, "Bandwidth- and power-efficient routing in linear wireless networks," *IEEE Transactions on Information Theory*, vol. 52, pp. 2624–2633, June 2006.

[108] C. Bae and W. E. Stark, "End-to-end energy and bandwidth tradeoff in multihop wireless networks," *IEEE Transactions on Information Theory*, vol. 55, pp. 4051–4066, Sept. 2009.

[109] J. Niu, L. Cheng, Y. Gu, L. Shu, and S. K. Das, "R3E: Reliable reactive routing enhancement for wireless sensor networks," *IEEE Transactions on Industrial Informatics*, vol. PP, no. 99, pp. 1–1, 2013.

[110] M. Tuchler and J. Hagenauer, "EXIT charts of irregular codes," in *Proceedings of the 36th Annual Conference on Information Sciences and Systems (CISS 2002)*, pp. 748–753, March 2002.

[111] M. Tuchler, "Design of serially concatenated systems depending on the block length," *IEEE Transactions on Communications*, vol. 52, pp. 209–218, Feb. 2004.

[112] S. X. Ng, J. Wang, M. X. Tao, L. L. Yang, and L. Hanzo, "Iteratively decoded variable length space-time coded modulation: Code construction and convergence analysis," *IEEE Transactions on Wireless Communications*, vol. 6, pp. 1953–1963, May. 2007.

[113] C. Oestges and B. Clerckx, *MIMO Wireless Communications : From Real-world Propagation to Space-time Code Design*. Academic Press, 2007.

[114] S. X. Ng and L. Hanzo, "On the MIMO channel capacity of multidimensional signal sets," *IEEE Transactions on Vehicular Technology*, vol. 55, pp. 528–536, March 2006.

[115] B. Zhao and M. C. Valenti, "Practical relay networks: a generalization of hybrid-ARQ," *IEEE Journal on Selected Areas in Communications*, vol. 23, no. 1, pp. 7–18, 2005.

[116] D. Tse and P. Viswanath, *Fundamentals of Wireless Communication.* Cambridge University Press, 2005.

[117] A. Ibrahim, H. Zhu, and K. J. R. Liu, "Distributed energy-efficient cooperative routing in wireless networks," *IEEE Transactions on Wireless Communications*, vol. 7, pp. 3930–3941, Oct. 2008.

[118] E. Baccarelli, M. Biagi, C. Pelizzoni, and N. Cordeschi, "Maximum-rate node selection for power-limited multiantenna relay backbones," *IEEE Transactions on Mobile Computing*, vol. 8, pp. 807–820, June 2009.

[119] C. Bae and W. E. Stark, "End-to-end energy-bandwidth tradeoff in multihop wireless networks," *IEEE Transactions on Information Theory*, vol. 55, pp. 4051–4066, Sept. 2009.

[120] S. Banerjee and A. Misra, "Minimum energy paths for reliable communication in multi-hop wireless networks," in *Proceedings of the 3rd ACM international symposium on mobile ad hoc networking and computing (MobiHoc '02)*, (Lausanne, Switzerland), pp. 146–156, 9-11 June 2002.

[121] S. Cui, R. Madan, A. Goldsmith, and S. Lall, "Cross-layer energy and delay optimization in small-scale sensor networks," *IEEE Transactions on Wireless Communications*, vol. 6, pp. 3688–3699, Oct. 2007.

[122] T. Lu and J. Zhu, "Genetic algorithm for energy-efficient QoS multicast routing," *IEEE Communications Letters*, vol. 17, no. 1, pp. 31–34, 2013.

[123] J. Vazifehdan, R. Prasad, and I. Niemegeers, "Energy-efficient reliable routing considering residual energy in wireless ad hoc networks," *IEEE Transactions on Mobile Computing*, vol. PP, no. 99, pp. 1–1, 2013.

[124] H. Alwan and A. Agarwal, "Multi-objective QoS routing for wireless sensor networks," in *International Conference on Computing, Networking and Communications (ICNC 2013)*, pp. 1074–1079, 28-31 Jan. 2013.

[125] Q. F. Dong and S. Banerjee, "Minimum energy reliable paths using unreliable wireless links," in *Proceedings of the 6th ACM international symposium on mobile ad hoc networking and computing (MobiHoc '05)*, (Urbana-Champaign, IL, USA), pp. 449–459, 25-28 May 2005.

[126] J. Zhu, C. Qiao, and X. Wang, "On accurate energy consumption models for wireless ad hoc networks," *IEEE Transactions on Wireless Communications*, vol. 5, pp. 3077–3086, November 2006.

[127] X.-Y. Li, Y. Wang, H. Chen, X. Chu, Y. Wu, and Y. Qi, "Reliable and energy-efficient routing for static wireless ad hoc networks with unreliable links," *IEEE Transactions on Parallel and Distributed Systems*, vol. 20, pp. 1408–1421, Oct. 2009.

[128] D. Bertsekas and R. Gallager, *Data Networks*. Upper Saddle River, New Jersey, USA: Prentice Hall, 1992.

[129] H. Liu, B. Zhang, H. Mouftah, X. Shen, and J. Ma, "Opportunistic routing for wireless ad hoc and sensor networks: Present and future directions," *IEEE Communications Magazine*, vol. 47, pp. 103–109, dec. 2009.

[130] S. Biswas and R. Morris, "Opportunistic routing in multi-hop wireless networks," *ACM SIGCOMM Computer Communication Review*, vol. 34, pp. 69–74, Jan. 2004.

[131] M. Zorzi and R. R. Rao, "Geographic random forwarding (GeRaF) for ad hoc and sensor networks: Multihop performance," *IEEE Transactions on Mobile Computing*, vol. 2, pp. 337–348, Oct.-Dec. 2003.

[132] M. Zorzi and R. R. Rao, "Geographic random forwarding (GeRaF) for ad hoc and sensor networks: Energy and latency performance," *IEEE Transactions on Mobile Computing*, vol. 2, pp. 349–365, Oct.-Dec. 2003.

[133] X. Mao, S. Tang, X. Xu, X.-Y. Li, and H. Ma, "Energy-efficient opportunistic routing in wireless sensor networks," *IEEE Transactions on Parallel and Distributed Systems*, vol. 22, pp. 1934–1942, Nov. 2011.

[134] M. Dehghan, M. Ghaderi, and D. Goeckel, "Minimum-energy cooperative routing in wireless networks with channel variations," *IEEE Transactions on Wireless Communications*, vol. 10, pp. 3813–3823, Nov. 2011.

[135] J. Zhu and X. Wang, "Model and protocol for energy-efficient routing over mobile ad hoc networks," *IEEE Transactions on Mobile Computing*, vol. 10, pp. 1546–1557, Nov. 2011.

[136] T. Luo, M. Motani, and V. Srinivasan, "Energy-efficient strategies for cooperative multichannel MAC protocols," *IEEE Transactions on Mobile Computing*, vol. 11, pp. 553–566, Apr. 2012.

[137] S. Kwon and N. B. Shroff, "Energy-efficient SINR-based routing for multihop wireless networks," *IEEE Transactions on Mobile Computing*, vol. 8, pp. 668–681, May 2009.

[138] C. Wei, C. Zhi, P. Fan, and K. B. Letaief, "AsOR: an energy efficient multi-hop opportunistic routing protocol for wireless sensor networks over Rayleigh fading channels," *IEEE Transactions on Wireless Communications*, vol. 8, pp. 2452–2463, May 2009.

[139] M. C. Vuran and I. F. Akyildiz, "XLP: A cross-layer protocol for efficient communication in wireless sensor networks," *IEEE Transactions on Mobile Computing*, vol. 9, pp. 1578–1591, Nov. 2010.

[140] H. Kwon, T. H. Kim, S. Choi, and B. G. Lee, "A cross-layer strategy for energy-efficient reliable delivery in wireless sensor networks," *IEEE Transactions on Wireless Communications*, vol. 5, pp. 3689–3699, Dec. 2006.

[141] A. N. Pantazis, S. A. Nikolidakis, and D. D. Vergados, "Energy-efficient routing protocols in wireless sensor networks: A survey," *IEEE Communications Surveys Tutorials*, vol. 15, no. 2, pp. 551–591, 2013.

[142] M. A. Rahman, S. Anwar, M. I. Pramanik, and M. F. Rahman, "A survey on energy efficient routing techniques in wireless sensor network," in *The 15th International Conference on Advanced Communication Technology (ICACT 2013)*, pp. 200–205, 27-30 Jan. 2013.

[143] Q. W. Liu, S. L. Zhou, and G. B. Giannakis, "Cross-layer combining of adaptive modulation and coding with truncated ARQ over wireless links," *IEEE Transactions on Wireless Communications*, vol. 3, pp. 1746–1755, Sept. 2004.

[144] Z. Wang, Y. Chen, and C. Li, "CORMAN: A novel cooperative opportunistic routing scheme in mobile ad hoc networks," *IEEE Journal on Selected Areas in Communications*, vol. 30, pp. 289–296, Feb. 2012.

[145] A. M. Akhtar, M. R. Nakhai, and A. H. Aghvami, "On the use of cooperative physical layer network coding for energy efficient routing," *IEEE Transactions on Communications*, vol. 61, no. 4, pp. 1498–1509, 2013.

[146] M. F. Uddin, C. Rosenberg, W. Zhuang, P. Mitran, and A. Girard, "Joint routing and medium access control in fixed random access wireless multihop networks," 2013.

[147] H. Dubois-Ferrière, M. Grossglauser, and M. Vetterli, "Valuable detours: Least-cost anypath routing," *IEEE/ACM Transactions on Networking*, vol. 19, pp. 333–346, Apr. 2011.

[148] A. A. Bhorkar, M. Naghshvar, T. Javidi, and B. D. Rao, "Adaptive opportunistic routing for wireless ad hoc networks," *IEEE/ACM Transactions on Networking*, vol. 20, pp. 243–256, Feb. 2012.

[149] K. Zeng, Z. Yang, and W. Lou, "Location-aided opportunistic forwarding in multirate and multihop wireless networks," *IEEE Transactions on Vehicular Technology*, vol. 58, pp. 3032–3040, July 2009.

[150] R. Laufer, H. Dubois-Ferrière, and L. Kleinrock, "Polynomial-time algorithms for multirate anypath routing in wireless multihop networks," *IEEE/ACM Transactions on Networking*, vol. 20, pp. 742–755, June 2012.

[151] T. H. Cormen, C. E. Leiserson, R. L. Rivest, and C. Stein, *Introduction to Algorithms, third edition.* Upper Saddle River, New Jersey, USA: MIT Press, 2009.

[152] H. V. Nguyen, S. X. Ng, J. L. Rebelatto, Y. Li, and L. Hanzo, "Near-capacity network coding for cooperative multi-user communications," in *2011 IEEE Vehicular Technology Conference (VTC2011-Fall)*, (San Francisco, United States), pp. 1–5, 5-8 Sept. 2011.

[153] I. S. Gradshteyn and I. M. Ryzhik, *Table of Integrals, Series, and Products, Seventh Edition*. Elsevier Pte Ltd., 2007.

[154] "Wolfram website." Downloadable at http://functions.wolfram.com/.

[155] C. Dong, L.-L. Yang, and L. Hanzo, "Performance analysis of multi-hop diversity aided multi-hop links over Nakagami-m fading channels with adaptive modulation," Downloadable at http://eprints.soton.ac.uk/343477/.

[156] C. Dong, L.-L. Yang, and L. Hanzo, "Performance analysis of multihop-diversity-aided multihop links," *IEEE Transactions on Vehicular Technology*, vol. 61, pp. 2504–2516, July 2012.

[157] E. W. Dijkstra, "A note on two problems in connexion with graphs," *Numerische Mathematik*, vol. 1, no. 1, pp. 269–271, 1959.

[158] M. L. Fredman and R. E. Tarjan, "Fibonacci heaps and their uses in improved network optimization algorithms," *Journal of the Association for computing Machinery*, vol. 34, pp. 596–615, July 1987.

[159] F. D. Rango, F. Guerriero, and P. Fazio, "Link-stability and energy aware routing protocol in distributed wireless networks," *IEEE Transactions on Parallel and Distributed Systems*, vol. 23, no. 4, pp. 713–726, 2012.

[160] W. C. Tan, S. K. Bose, and T.-H. Cheng, "Power and mobility aware routing in wireless ad hoc networks," *IET Communications*, vol. 6, no. 11, pp. 1425–1437, 2012.

[161] A. A. Jeng and R.-H. Jan, "Adaptive topology control for mobile ad hoc networks," *IEEE Transactions on Parallel and Distributed Systems*, vol. 22, no. 12, pp. 1953–1960, 2011.

[162] G. Ferrari and O. K. Tonguz, "Impact of mobility on the BER performance of ad hoc wireless networks," *IEEE Transactions on Vehicular Technology*, vol. 56, no. 1, pp. 271–286, 2007.

[163] S. L. Correia, J. Celestino, and O. Cherkaoui, "Mobility-aware ant colony optimization routing for vehicular ad hoc networks," in *2011 IEEE Wireless Communications and Networking Conference (WCNC 2011)*, (Quintana-Roo, Mexico), pp. 1125–1130, 28-31 March 2011.

[164] H. Wang, X. Zhang, F. Nait-Abdesselam, and A. Khokhar, "Cross-layer optimized MAC to support multihop QoS routing for wireless sensor networks," *IEEE Transactions on Vehicular Technology*, vol. 59, no. 5, pp. 2556–2563, 2010.

[165] M. Cheng, Q. Ye, and L. Cai, "Cross-layer schemes for reducing delay in multihop wireless networks," *IEEE Transactions on Wireless Communications*, vol. 12, no. 2, pp. 928–937, 2013.

[166] E. Altman, A. P. Azad, T. Basar, and F. D. Pellegrini, "Combined optimal control of activation and transmission in delay-tolerant networks," *IEEE/ACM Transactions on Networking*, vol. 21, no. 2, pp. 482–494, 2013.

[167] H. Li, Y. Cheng, C. Zhou, and W. H. Zhuang, "Routing metrics for minimizing end-to-end delay in multi-radio multi-channel wireless networks," 2012.

[168] G. A. Shah, W. Liang, and O. B. Akan, "Cross-layer framework for QoS support in wireless multimedia sensor networks," *IEEE Transactions on Multimedia*, vol. 14, no. 5, pp. 1442–1455, 2012.

[169] X. Wang, J. J. Garcia-Luna-Aceves, and H. R. Sadjadpour, "Understanding the interaction between packet forwarding and channel access in multihop wireless networks," *IEEE Transactions on Mobile Computing*, vol. 11, no. 4, pp. 679–691, 2012.

Index

Author Index